IntechOpen

Sedimentation Engineering

Edited by Ata Amini

SEDIMENTATION ENGINEERING

Edited by **Ata Amini**

Sedimentation Engineering
http://dx.doi.org/10.5772/intechopen.68509
Edited by Ata Amini

Contributors

Sailesh Chitrakar, Hari Prasad Neopane, Ole Gunnar Dahlhaug, Lidia Kim, Gabriela Geanina Vasile, Bogdan Stanescu, Adriana Cuciureanu, Alina-Maria Muresan, Nicolae Ionut Cristea, Alexandre Santos-Ferreira, Cláudia Santos, Toan Vu Duc, Mai Tra Ngo, Bruno Moreira, Fábio Arouca, João Jorge Damasceno, Emilio Ramírez Juidías, Fahmi Hidayat, Pitojo Tri Juwono, Agus Suharyanto, Alwafi Pujiraharjo, Djoko Legono, Dian Sisinggih, David Neil, Marise Garcia Batlle, Manuel Navarrete, Prince Suka Momta, Ata Amini

Notice

Statements and opinions expressed in the chapters are these of the individual contributors and not necessarily those of the editors or publisher. No responsibility is accepted for the accuracy of information contained in the published chapters. The publisher assumes no responsibility for any damage or injury to persons or property arising out of the use of any materials, instructions, methods or ideas contained in the book.

We are IntechOpen,
the first native scientific
publisher of Open Access books

3,400+
Open access books available

109,000+
International authors and editors

115M+
Downloads

151
Countries delivered to

Our authors are among the
Top 1%
most cited scientists

12.2%
Contributors from top 500 universities

CLARIVATE ANALYTICS
BOOK CITATION INDEX
INDEXED

WEB OF SCIENCE™

Selection of our books indexed in the Book Citation Index
in Web of Science™ Core Collection (BKCI)

Interested in publishing with us?
Contact book.department@intechopen.com

Meet the editor

Dr. Ata Amini is an Associate Professor of water resource engineering in Kurdistan Agricultural and Natural Resources Research and Education Center, AREEO, Sanandaj, Iran. He completed his doctorate at the University Putra Malaysia in 2009. In recent years, he has been in charge of many research projects and supervised many master and PhD students in the field of water engineering. He is also the author of 3 books and 2 book chapters. He has devoted his academic career to study the integrated water resource management, river engineering, sediment, scouring and watershed managements. Dr. Ata Amini has more than 20 years of teaching experience and has published many academic papers and final research reports.

Contents

Preface

Sedimentary processes are a real complex concern and result from the interaction between deep processes that are still imperfectly understood. Poor understanding of the dynamics of river, marshes, offshores, harbor estuaries and reservoir caused unsustainability of human economic and social hazards. In this regard, the influence of sectoral plans and ignorance of integrated managements of human interventions are noticeable. Many questions remain unanswered and sedimentary flux quantification and qualification are still a challenge in science. Investigating the nature and scope of sedimentation problems and the socio-economic and environmental impacts of sediment have reached global importance. Therefore, *Sedimentation Engineering* is a book that could assist with the implementation of integrated management policy.

This book is intended for engineers and researchers with basic background and knowledge in sediment transport. Theories, measurements, modeling, practice updates, sediment quality and impact assessment of man-made structures are the main topics of the book. It brings together multiple disciplines to understand and help resolve problems of sedimentation. The outcomes of researches and analysis of processes governing land erosion and sedimentation across varied climatic regions have been pointed. The relation and interaction of these processes with ecosystem dynamics, taking place in a watershed or a waterbody, are presented in this book.

The book contains 10 chapters under two sections, which is a collection of many case studies provided by international spectrum of researchers from a number of countries. The sections were formed by grouping together chapters that are related. The first section focuses on sedimentation processes with the aim of providing concepts of sedimentation and shows its impacts on environments and a few water bodies. Since sediments are considered as a source of pollutant in aquatic ecosystem, the second section of the book points out the physico-chemical analyses of sedimentation. The effects of contaminated sediment on water bodies and soils to improve remedial actions are presented in Section 2. Each chapter is self-contained, with an individual title, summary, concise and well-structured research content and a list of references. Obviously, for convenience of readers, we tried to use a similar chapter structure. However, each chapter may have its own power of presentation. Thus, the readers can read the entire book and individual sections or pick any chapter and read it on its own.

This book is beneficial for water resource managers, environmental and agricultural professionals, policymakers, researchers, students and experts belonging to a wide range of disciplines such as geography, modeling, land planning and marine policy. The editor allocated adequate time for evaluating and in preparing the chapters in close association with the authors and for final proof reading and checking in cooperation with the publishing process

manager. The editor would like to thank all the authors for their effort and excellent collaboration in the preparation and editing of the chapters. Furthermore, I wish to greatly appreciate Ms. Maja Bozicevic for her editorial assistance in the preparation of the chapters. It is hoped that this book reassures more activities in improving our thoughts and knowledge in order for us to achieve an integrated management of sediment.

Dr. Ata Amini, Associate Prof
Kurdistan Agricultural and Natural Resources Research and Education Center, AREEO
Sanandaj, Iran

Sedimentation Concepts

Introductory Chapter: Sustainable Development and Sediment Engineering

Ata Amini

Additional information is available at the end of the chapter

http://dx.doi.org/10.5772/intechopen.74683

1. Sediment

Due to their importance to social growth, environmental and economic issues, surface erosion, sedimentation, scour, and deposition have been investigated by engineers and geologists for centuries. Solid fragments of naturally occurring organic or inorganic materials with a particle size of less than 2 mm are named fine sediment, which is broken down by the processes of weathering and erosion. The fine sediment generally includes sand, silt, and clay particles. Particles greater than 2 mm are categorized as coarse sediments which includes gravel, cobble, and boulders. These materials become detached from the rocks and are transported to a deposition site such as streambeds and lakes by the action of water, ice, wind, and force of gravity. In this process, sediments may be affected by cementation, consolidation, solution, or biological action. The physical and biological characteristics of stream systems are influenced by sedimentation. Apart from human activity, the level of deposited and suspended sediments in each stream depends on climate, geology, and terrestrial characteristics of a stream's watershed. The process of erosion is natural, while the human activities can greatly intensify the process of erosion and sediment transportation [1]. In the function of watershed or aquatic ecosystems, sediment plays vital role and can has a positive or negative effect on stakeholders and biota.

2. Human effects on sedimentation

Surface erosion from watersheds and bank erosion along the river caused sedimentation in all water bodies. As a result of earth-forming developments, for instance climate, glaciations, weathering, and geologic events, some characteristics of a basin such as slope, soil

composition, elevation, and size have formed throughout centuries. The contributions of these characteristics are different in each watershed. However, in a watershed, there is a historic adaption between the livelihood of the aquatic life and the amount and characteristics of the sediment of stream system. Management at the watershed scale is a main challenge facing existing and coming generations. Many of the environment ecosystems are being dishonored or being used in an unsustainably manner [2]. Degradation of waterways in a watershed was intensified a result of human activities which aims to convert the home-grown vegetation to land uses related to agriculture and urbanization. These changes increasingly disturb the local hydrological cycle creating problems with stream flows, erosion, and sedimentation [3]. Apart from land use change, river canalization, water pumping, inter basin water transfer, logging, road construction, gravel mining, and mega hydraulic structures like dams are commonly considered unnatural contributors to sedimentation [4]. As common human activities, agricultural land development and urbanization within a stream's watershed often increases excessive quantities of sediment to water ways. In addition, the stream habitats and water quality are influenced by human activities. Excessive sediment inputs from the disturbed lands reduce water quality in watersheds. **Figure 1** shows agricultural land development in a steep hill in KhorKoreh watershed, Kurdistan Iran, destroying the land cover and making it more erodible.

In contrary, for runoff and sediment storage purposes, numerous watershed practices are currently being implemented, which improved the hydrologic conditions in watersheds [1]. To increase water infiltration and to decrease runoff and sediment flow into streams and water bodies, structural measures such as the construction of check dams and nonstructural management such as biological treatment have been practiced worldwide [1]. However, to measure the effectiveness of these activities, consistent assessments are essential. In many cases, the misconducting of man-made structures intensifies the watershed erosion. **Figure 2** shows the downstream of a stilling basin of a constructed check dam in Kurdistan, Iran. The dimensions of the stilling basin are too small to diminish the flow velocity, and the accelerated

Figure 1. Agricultural land development as a common human activity caused surplus sedimentation.

Figure 2. Misconducting of a check dam on a water way.

flow degrade stream condition washed out the stream bed, which caused bed deformation passing through stream bed.

3. Sustainable development and sedimentation

Understanding the aspects and principles governing the river processes is essential for engineers. An unquestionable method to shorten the useful life of hydraulic structures like lakes, reservoirs, and wetlands is sedimentation. In line with sustainable development and integrated water resources managements (IWRM), all the aspects of environment, social, and economic issues must be considered in the planning, design, construction, and operation of any water project. Even, for current projects, evaluation methods should be developed and applied to reassess their advantages considering the principle of IWRM. Ecosystem restoration and waterway recreation are considered, by researchers and engineering, as a way to attain sustainable development [5]. In recent years, to restore a river's environment, many existing hydraulic structures were modified or redesigned [5]. Accordingly, some of the hydraulic structures may need to be decommissioned. Reasons for withdrawing include, structure security and safety, legal and economic liability, and environmental considerations. A sedimentation management method for reducing watershed erosion to reduce sediment inflow and sluicing sediment from hydraulic structures is a way to increase useful life of constructed structures. Engineering design and construction of hydraulic structures, without considering a river as a dynamic system, and taking IWRM principles into consideration may not serve the basic functions of rivers.

4. Sedimentation engineering

Sedimentation engineering involves sediment issues in the development, use, and conservation of water and land resources. The guidance to theoreticians and practitioners' worldwide, concerns the hydraulics of sediment transport in fluvial systems. In fact, sedimentation engineering is an effort to relate the mechanics of sediment transport in waterways and by turbidity

flows to the morphodynamics of reservoir and lake sedimentation, with the development of fluvial deltas [6]. The gravity force from the differences in density between particles and the fluid are the main cause for sedimentation of particles. In flowing water, the sediment particles, because of the gravitational forces and the upward-acting lifting forces induced by the flow, remain suspended. For particles denser then water, the gravity forces is dominant in comparison with the upward-acting lifting forces and the particles fall through standing water. Sediment entrainment and transport maintenance are two fundamental independent processes of bed material movements. Numerous methods to estimate and evaluate the mechanisms' quantity and effects of both suspended and bed sediment loads are presented by sediment engineers. Apart from increasing sediment loads in watersheds, water bodies, and industrial, the contemned sediments are the challenges that affect the environments. Contaminated sediment may exist in streams, rivers, wetlands, lakes, along ocean margins, harbors, reservoirs, or in other water bodies. The contaminants may have man-made or natural sources like many metals and some organic compounds. Principles of the cleanup process are complex at sediment sites and sites with soil or ground water contamination. As noted above, in recent years, refreshing urban areas and returning land and water bodies to creative uses have become increasingly important. In these efforts, protecting or re-establishing a natural riparian corridor along the stream is considered as the most proper ecological option.

To the achievement of river engineering design, actions, and maintenance, our considerate of the dynamic stability between amount of sediment loads in a stream and sediment source from upstream is important. In sedimentation engineering, theories of erosion, sediment transport, and deposition are considered to alter the knowledge about human interaction with environment to diminish the inappropriate effects of projects on environments. To simulate and predict sedimentation processes in a basin, a systematic method based on reliable theories can be used. For such reasons, numerous models are presented and accessible for engineers to be used for analyzing sedimentation problems in various watersheds, waterways, and waterbodies. However, several of the complicate aspects and principles of sedimentation are yet to be understood, and they remain among the challenging subjects for upcoming investigations.

Author details

Ata Amini

Address all correspondence to: a.amini@areeo.ir

Kurdistan Agricultural and Natural Resources Research and Education Center, AREEO, Sanandaj, Iran

References

[1] Amini A, Taheri P, Javan M, Saghafian B. Evaluating the impacts of watershed management on runoff storage and peak flow in Gav-Darreh Watershed, Kurdistan, Iran. Arabian Journal of Geosciences. 2014;**7**(8):3271-3279. DOI: 10.1007/s12517-013-0950-1

[2] MEA (Millennium Ecosystem Assessment). Ecosystems and Human Wellbeing: Synthesis. Washington: Islands; 2006

[3] Amini A, Mohamad TA, Halim G, Bujang H, Azlan A, Akib S. Impacts of land use change on streamflow generation in Damansara Watershed, Malaysia. Arabian Journal of Science and Engineering. 2011;**36**:713. DOI: 10.1007/s13369-011-0075-3

[4] Amini A, Zareie S, Taheri P, Yusof KW, Mustafa MR. Drought Analysis and Water Resources Management Inspection in Euphrates—Tigris Basin, River Basin Management. Rijeka, Croatia: InTech; 2016. DOI: 10.5772/63148

[5] USBR. Erosion and Sedimentation Manual. Denver, Colorado, USA: U.S. Department of the Interior Bureau of Reclamation; 2006. 1028p

[6] García Marcelo H. Sediment Transport and Morphodynamics. USA: ASCE Publication; 2013. DOI: 10.1061/9780784408148.ch02

A Review on Sediment Erosion Challenges in Hydraulic Turbines

Sailesh Chitrakar, Hari Prasad Neopane and
Ole Gunnar Dahlhaug

Additional information is available at the end of the chapter

Abstract

Sediment constitutes several mineral compositions depending upon the geological formation and geography. In many of the rivers in Himalayas and Andes, Quartz is found as a main constituent (more than 50%), along with feldspar and other hard minerals. These particles have hardness more than 5 Moh's scale, which is capable to erode turbine components. In hydraulic turbines, flow is highly turbulent and unsteady, which can aggravate the erosion problems. Depending upon the nature of the flow, different components of turbines are eroded with different mechanisms. This chapter will provide a review on how various flow phenomena is responsible for particular types of erosion in turbines and their potential consequences. Some examples of the effect in existing power plants will be shown. This chapter will also discuss about some preventive measures that have been proposed and implemented to reduce the impact of the sediment particles in hydraulic machineries.

Keywords: sediment, erosion, Francis, Pelton, flow, turbine

1. Introduction

Hydropower is one of the cleanest forms of energy and has been used in many countries as a principle source of electricity. However, it has been reported that two-third of the world's feasible hydropower resources are still undeveloped. Out of these potential resources, more than 55% lies in Asia alone [1]. Despite the future prospects in hydropower development in this region, the geological problem seems to be a major obstacle. It has been studied that out of 20 billion tons of global sediment flux from rivers to the oceans per year, around 6 billion tons is contributed by Asian rivers, particularly from Indian subcontinent [2]. The problem of sediment handling, maintenance and operation of the power plants has become a serious issue.

The study of wear and erosion in general applications is found to be abundantly studied in literature. However, there are only few literatures related to erosion problems in hydraulic machineries. Brekke [3] reported that the hydraulic machineries working in the range of high Reynolds number, between 10^6 and 10^8 will normally be exposed to micro erosion, secondary flow vortex erosion and acceleration erosion. There have also been several endeavors made to predict and quantify erosion rates. The most general expression for erosion as studied by Truscott [4] was erosion $\propto$ (velocity)^n. This relation is an indication that higher velocity will increase the erosion because of higher turbulence. Apart from velocity, erosion is also a function of the shape, size and material of the particles hitting the turbine surfaces. Some more factors affecting the turbine's wear are explained in Section 2.

This chapter focuses specifically on the erosion of Pelton and Francis turbines. A detailed investigation of the eroded components of these turbines has shown that turbines erode depending upon the particular types of flow phenomena in particular regions. It has been explained that the secondary flow and sediment erosion in turbines are simultaneous in nature [5], which means that one phenomenon aggravates another. In most of the cases, the condition gets worse because of the cavitation induced after the surfaces are eroded. The combined effect of erosion, cavitation and secondary flow affects the turbine's performance drastically, causing the efficiency loss, damage and fatigue problems. Different mechanisms of flow in Francis and Pelton turbines inducing different types of erosion are explained in Sections 3 and 4.

Section 5 of this chapter explains some recent studies that have been done in the field of erosion in guide vanes of Francis turbines. Sediment particles wear the surface out of the clearance gap, which results in the leakage flow through the gap. This leakage flow mixes with the main flow, causing disturbances in the form of a vortex to downstream turbine components. This concept is one of the examples of the two-way effect between erosion and secondary flow. This section also explains some possibilities of minimizing the leakage flow by changing the guide vane profiles.

2. Wear and erosion

Erosion can be classified under one of the various forms of wear. According to the standard of ASTM 640-88, wear is defined as "damage to a solid surface, generally involving progressive loss of material, due to relative motion between that surface and a contacting substance or substances." Hence, the major cause of wear and energy dissipation is friction and it is estimated that one-third of the world's energy resources in present use is needed to overcome friction in one form or another [6]. The classification of the wear, in recent years have taken a very broad concept, compared to 1950s, when only adhesive, abrasive, surface fatigue and corrosion were considered as the types of wear [7]. The addition of erosion by solid particle and droplet impact were done by Bhusan [8]. The wear rate, which is the rate of material removal, depends upon the geometry of the interacting surfaces, types of interaction, material properties, load and surface pressure, surrounding temperature, humidity, atmosphere, surface properties and relative velocities between interacting surfaces [9].

Erosive wear or erosion is one form of wear caused by the impacts of solid or liquid particles on a solid surface. The flow medium contains particles that possess enough kinetic energy to damage metallic surface. The mechanism of the erosive wear is quite similar to the abrasive wear, but in the case of the abrasive wear, the eroding agent is much bigger in size and the angle of impingement is lower. The erosive wear on the other hand, is accompanied with relatively small particles with several number of wear mechanisms. These mechanisms are differentiated based on the impingement angle, size, shape and speed of the particles and mechanical properties of the base material. Stachowiak and Batchelor [6] have discussed seven different possible mechanisms for solid particle erosion, including abrasive erosion, surface fatigue, brittle fracture, ductile deformation, surface melting, macroscopic erosion and atomic erosion. In the case of hydraulic machinery, the first four mechanisms out of the seven are applicable, as shown in **Figure 1**. A low angle of impingement is favorable for the abrasive wear, as the particles are drawn across the surface after the impact. Similarly, if the speed is low, the stresses at impact are insufficient for plastic deformation or brittle fracture, which induces surface fatigue depending upon the endurance limit of the base material. If the shape of the eroding particle is blunt or spherical, the plastic deformation is more likely to occur, whereas, if the particles are sharp, the cutting or abrasive wear is more common. It is seen that for the ductile mode, the maximum erosive wear is found close to an angle of 30° whereas, for the brittle mode, the maximum erosive wear is found at around 90° impingement angle [6]. **Figure 2** shows the rotation of a particle due to the velocity profile near a boundary layer. When the particle is bigger than the boundary layer, it experiences different velocities along its height, causing it to rotate. Because of the irregular shape of the particle, the rotating movement enhances the abrasive wear.

A detailed survey on abrasive wear in hydraulic machinery was done by Truscott [4]. This study consisted of some of the critical findings related to the factors affecting wear that were
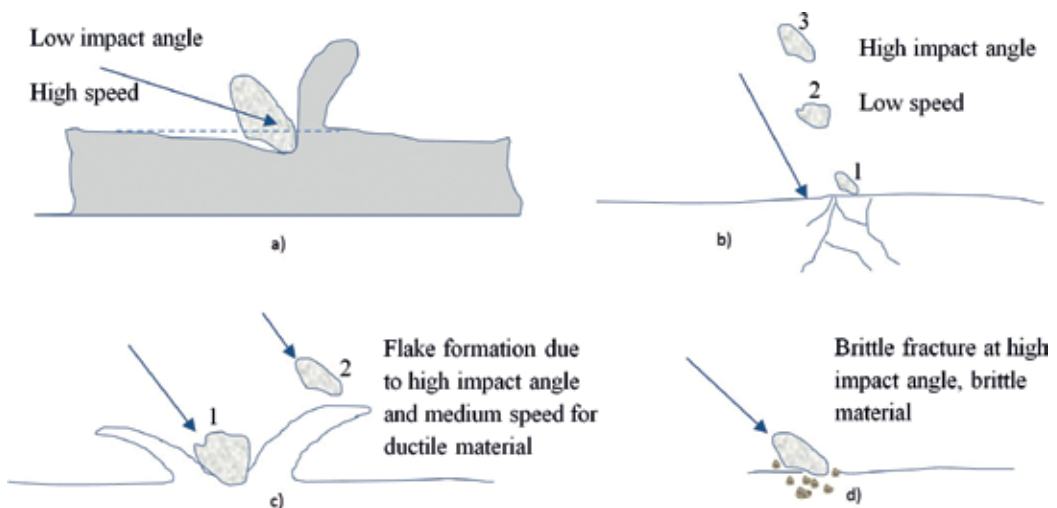
Figure 1. Various forms of erosive wear mechanisms: (a) abrasive/cutting erosion; (b) fatigue erosion; (c) plastic deformation; and (d) brittle fracture [6].
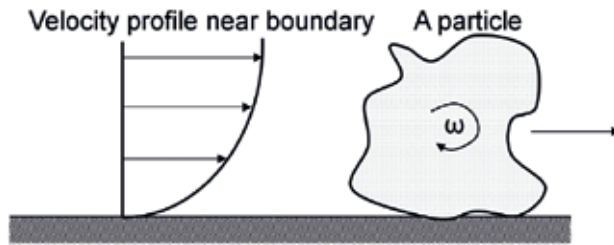
Figure 2. Rotation of a particle in a boundary layer.

studied in several works since 1950s. Brekke [3] characterized sand erosion in turbo-machines in three categories: (i) micro erosion, where fine particles with grain size less than 60 μm strikes the turbine surfaces with high velocity, (ii) secondary flow vortex erosion, caused by obstacles in the flow field or secondary flow in the corners of conduits and (iii) acceleration erosion, where acceleration of particles normal to the flow direction separates the particles from the flow direction and collide with the surface.

The basic factors affecting wear of hydraulic machines are (i) the properties of the solid particles (sand) like hardness, size, shape, relative density and concentration, (ii) properties of the eroded material like composition, structure and hardness and (iii) the operating condition like flow-speed, temperature and impact angle. Laboratory tests conducted by Wellinger and Stauffer, according to Truscott [4] show that for metals in general, wear increases rapidly once the particle hardness exceeds that of the metal for both scouring and impact abrasion. While most literature [10] state that in general, the absolute wear rate increases with grain size and sharpness, Wellinger and Worster, according to Truscott [4] state that wear is directly proportional to size for sliding abrasion, but is independent of size for direct impact. Wellinger also shows the effect of particle shape, with angular grains causing about twice the wear as compared to the round ones. Although the particle shapes are described qualitatively such as round, angular and semi-round, the actual shapes of particles are complex and cannot be quantified in simple mathematical terms. In the case of river sedimentation, concentration of particles is expressed in terms of parts per million (ppm), which is equivalent to milligram/liter or kilogram of particles in 1000 m^3 of water. It is mostly accepted that the wear increases with the concentration of particles [11]. Similarly, the increase in the temperature of the operating condition softens the material and hence the erosion rate increases. The conveying medium such as air, water or oil also plays a significant role on erosion rate depending upon their density, viscosity, nature of the flow (laminar or turbulent) and microscopic properties. Stachowiak and Batchelor [6] show that small amount of lubricant in the liquid medium reduces erosion rate due to restriction in the change in material properties during particle impingement.

Velocity of the fluid carrying particle and impingement angle are characteristics which affect wear significantly. The expression for the relation between erosion and velocity is often quoted as erosion $\propto$ (velocity)^n, where n depends on the material and operating conditions. This value is mostly taken to be 3, but Truscott [4] reported different value of this exponent, for instance 1.4 for steel St37 to 4.6 for rubber. The dependency of erosion rate on the impingement angles show contrasting results in many studies. While Bhusan [8] showed no erosion up to certain

low impingement angles, Stachowiak and Batchelor [6] have shown erosion rates at even zero degree impingement. According to IEC 62364, the hydro-abrasive erosion depth in a Francis turbine can be estimated by using following equation [12]:

$$S = \frac{W^{3.4} \times PL \times K_m \times K_f}{RS^p} \qquad (1)$$

where PL (particle load) is the integral of the modified particle concentration over time:

$$PL = \int_0^T C(t) \times K_{size}(t) \times K_{shape}(t) \times K_{hardness}(t) \mathrm{d}t \qquad (2)$$

W is the characteristic velocity. In the case of guide vanes, it is the flow through unit divided by the minimum flow area at the guide vane apparatus at best efficiency point.

$W_{gv} = \frac{Q}{\alpha \times Z_0 \times B_0}$, Q is the discharge, α is the average shortest distance between adjacent guide vanes. Z_0 is the total number of guide vanes in a turbine and B_0 is the height of the distributor in a turbine. In the case of runner, it is the relative velocity between the water and the runner at best efficiency point.

$W_{run} = \sqrt{u_2^2 + c_2^2}$, $u_2 = n \times \pi \times D$, $c_2 = \frac{Q \times 4}{\pi \times D^2}$.

K_m is the material factor, which characterizes how the hydro-abrasive erosion relates to the material properties of the base material.

K_f is the flow coefficient $\left[\frac{\mathrm{mm} \times \mathrm{s}^{3.4}}{\mathrm{kg} \times \mathrm{h} \times \mathrm{m}^a} \right]$, which characterizes how the hydro-abrasive erosion relates to the water flow around each component.

RS is the turbine reference size (m), which is the reference diameter (blade low pressure section diameter at the band) for the case of Francis turbines.

p is the value of the exponent, which is 0.25 for guide vanes, facing plates and runner inlet, whereas 0.75 for labyrinth seals and runner outlet.

C is the concentration of particles ($\mathrm{kg/m^3}$).

K_{size} is the size factor (median particle size d50 (mm)), K_{shape} is the shape factor (round = 1, sub-angular = 1.5 and angular = 2) and $K_{hardness}$ is the hardness factor (fraction of par0ticles harder than Mohs 4.5 for stainless steel).

The erosion resistance of a material is seen to depend upon the material hardness and the impingement angle. The difference in the erosion resistance for two impingement angles can be seen in **Figure 3** [6]. Some materials such as cobalt have a very good erosion resistance at low impingement angle but the resistance decreases severely once the impingement angle is high. The formation of the martensites results in the improved hardenability and erosion resistance except at low impingement angles and in the case of low allow steels, the ferritic phase with sufficient spheroidal carbide to induce strengthening is very effective against erosion wear. The erosion resistance of austenitic steels (21Cr4Ni) strengthened with nitrogen was seen to be higher than a martensitic steels (13Cr4Ni) due to the distribution of hard carbides in the matrix of stabilized austenite [13].
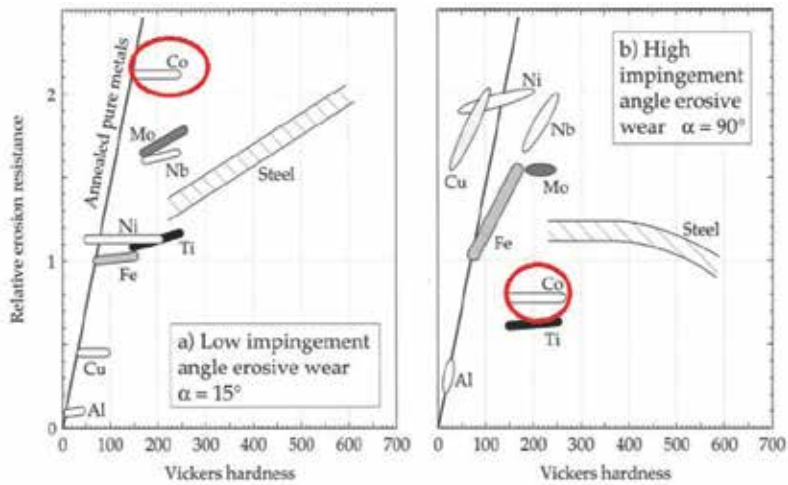
Figure 3. Erosive wear for materials with different impingement angles [6].

Some materials such as ceramics are recommended for applications where the working temperature is high. However, these materials are brittle and might result in the brittle fracture. In the case of hydro turbines, the prevention of the erosion is also done by applying coating on the surfaces of the vulnerable regions. The most common type of the coating is the tungsten-carbide (WC-Co), that uses 86–88% WC and 6–13% Co [14]. These coatings have excellent hardness, with better adhesion and large toughness.

3. Erosion in Pelton turbines

In the case of Pelton turbine, all the hydraulic energy of water is converted into kinetic energy before runner inlet. Because of the high head application of Pelton turbines, the velocity of water in the jets is usually higher than 100 m/s. Since velocity is the dominant factor for erosion (erosion $\propto$ velocity^3), the rise in velocity make the flow more turbulent, increasing the erosion rate. Brekke [3] has classified the erosion of Pelton turbine into four parts: (i) inlet and valve, (ii) nozzles, (iii) runner and (iv) wheel pit. Out of these components, nozzle system and runner are mostly vulnerable to erosion. In the nozzle, a strong turbulent effect occurs on the needle surface due to very high velocity at the nozzle outlet and the needle surface. In Chilime Hydropower Plant (2 × 11 MW, gross head: 350 m), average erosion in the needle tip during the maintenance was found to be around 0.3 mm [15]. In this region, the average quartz particle in the sand is more than 75%.

Some eroded components of Pelton turbines are shown in **Figure 4**. **Figure 4a** is the runner bucket of Khimti HPP. It shows that most of the erosion in this bucket is inside the bucket surface. However, in **Figure 4b**, a more severe case has been shown, where erosion is predominant in surface as well as in splitter. In **Figure 4c**, formation of ripple and grooves ahead of the webs are seen, which are explained later. In **Figure 4d**, the effect of both erosion and cavitation is seen.
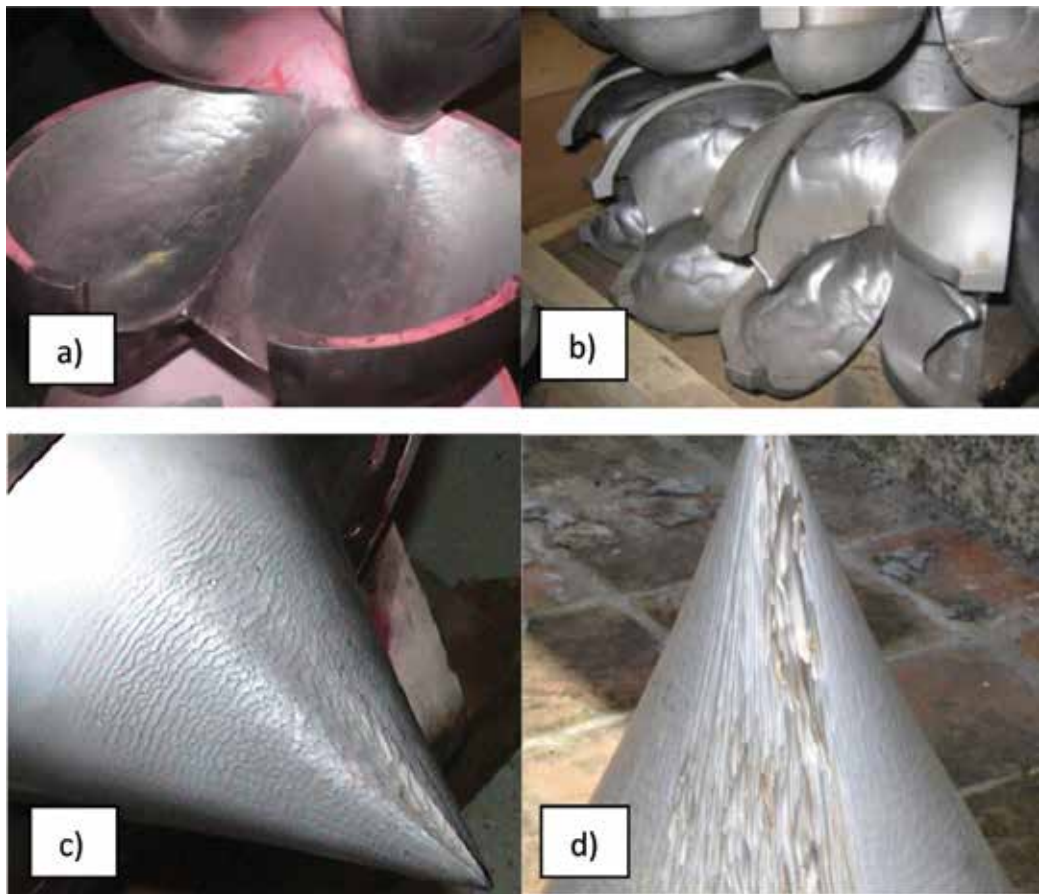
Figure 4. Erosion in Pelton turbines: (a) Khimti HPP [16], (b) Rangjung HPP [16], (c) Khimti HPP [9], (d) Chilime HPP [15].

3.1. Erosion of the nozzle system

The erosion pattern and intensity on the nozzle system depends on the operating condition. In the case of full opening of the needle, the mean velocity increases along the surface of needle due to gradual contraction of the fluid passage. This decreases the pressure on force towards the needle tip. Although the velocity is maximum towards the tip, the force at this point is minimum, which reduces the intensity of the erosion in this region. The erosion pattern is formed as ripples with circular grooves when viewed in axial direction (shown in **Figure 4c**). In the case of partial opening, the contraction of the fluid passage increases further, which reduces the pressure to such an extent that it can give rise to cavitation (shown in **Figure 4d**). In this case, a combined effect of erosion and cavitation can be seen on the needle surface. In the case of Khimti Hydropower Plant (5 × 12 MW, gross head: 684 m), two distinct grooves were seen ahead of the two webs to support needle guide to the vortices from the trailing edges of the webs [9].

The mechanism for the formation of the ripple pattern during erosion has not been specifically explained for hydraulic turbines. One explanation is the micro-roughness in the surface

of the needle forming a turbulent boundary layer with eddies that erode the surface with both fine sediment and cavitation. Another explanation is the formation of Kelvin-Helmholtz vortex due to the velocity gradient between the interface of water and air. **Figure 5** explains the erosion types in the case of full and partial opening of needles as explained earlier. Apart from the needles, the outer ring of the nozzle also faces similar erosion problems. In summary, the nozzle system in Pelton turbines is one of the most eroded components due to a highly turbulent flow. The erosion intensity aggravates during the part load operations due to the combined effect of erosion and cavitation. It has also been explained that the erosion challenges in the nozzle system cannot be solved by a hydraulic design, but can be minimized by using hard material for turbine nozzle as well as its coating.

3.2. Erosion of the runner

It was analytically explained that the acceleration normal to the bucket of the Pelton turbine can reach up to 100,000 m/s^2 [3] At such a high acceleration, the sand particles separate from the flow and collide on the bucket surface. It has been shown that the erosion in the bucket is sensitive to its curvature (R). The location and types of erosion have been classified according to the size of the sand particles [9]. The coarse particles most likely hit the bucket inlet, eroding the surfaces around splitter. Fine particles glide along with water and strike on the outlet surface. It was also seen that the damages in the splitter and entrance lip were severe due to direct hitting of the particles. The erosion on the surface of the bucket on the other hand, was seen like a hammering effect. It has also been explained that the efficiency loss in Pelton turbines is primarily due to the erosion of the entrance lip. **Figure 6** explains the particle distribution inside the bucket and the erosion patterns due to different sizes of materials hitting the bucket.
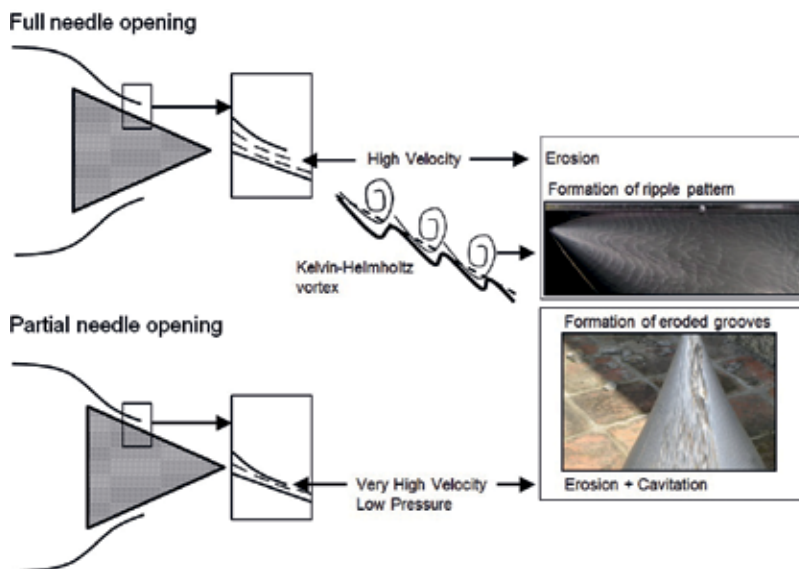
Figure 5. Erosion mechanisms in full and partial needle openings.
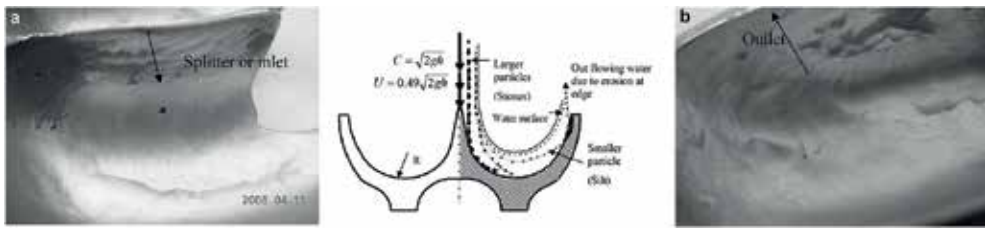
Figure 6. Erosion distribution at inlet and outlet of the bucket [9, 17].

Another experimental study also showed that the coarse particles with high velocity have tendency to move with jet and hit the splitter blade causing erosion due to shearing action of the sand on the surface [17]. The smaller particles on the other hand are flown out of the jet causing erosion on the depth and outlet of the bucket. The splitter tip was found to be eroded by plastic deformation and indentation whereas the depth of the bucket by plastic deformation and plowing.

Figure 7 shows pictures of eroded buckets from Andhi Khola Power Plant (5.1 MW) in Nepal. Erosion of such intensity causes the drop in efficiency of the turbine significantly. In a largely sediment affected power plants like these, the turbines are repaired on a regular basis. The efficiency loss due to erosion in Pelton turbines can be estimated from the graph shown in the **Figure 7**. Compared with the repaired runner, the efficiency drop in the non-repaired one is more than 10% for part load operations.

Based on these illustrations, it can be concluded that the fine sand particles mostly erode the nozzle system and coarse particles mostly affect the buckets. The erosion in the bucket due to fine particles is towards the outlet end, which is due to the separation of the particles at high acceleration. The coarse particles are not easily detached from the water stream, which on the direct impact with the bucket, can damage the splitter and region around it. Although the minimization of the erosion in Pelton turbines depend mostly on the material and types of coating used, some hydraulic design preferences can be used. They are: (i) using large radius of curvature in the location where the flow direction changes, (ii) using low number of jets and (iii) using large radius of the bucket and the nozzle. It has also been found [18] that an increase of D/B, that is, the ratio of pitch circle diameter and bucket width and/or decrease of specific speed enhances erosion.
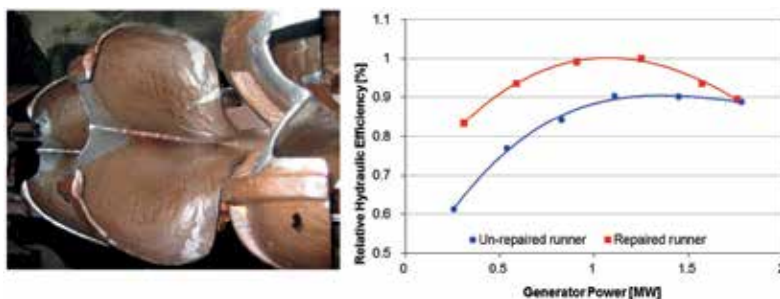
Figure 7. Eroded bucket in Andhi Khola power plant and efficiency drop due to erosion.

4. Erosion in Francis turbines

Francis turbines are also one of the seriously affected turbines due to sand erosion. Brekke [3] has classified the erosion in several components of this turbines which includes (i) the inlet valve system, (ii) the spiral casing, (iii) the pressure relief and/or by pass system, (iv) the guide vane system, (v) the runner and runner seals, (vi) the draft tube and (vii) the shaft seal. In Francis turbines, the highest absolute velocity is found to be at the guide vane outlet. It is the region where the maximum hydraulic energy of water is converted into kinetic energy, producing highly unsteady flow. The velocity distribution inside Francis turbine operating in best efficiency point is shown in **Figure 8a**. It shows that before the flow reaches the inlet of the runner, about 50% of the potential energy is converted into kinetic energy. The kinetic energy increases from about 10% to about 50% from guide vanes inlet to the runner inlet for a high head Francis turbine. This infers that the flow should contain very high acceleration inside the guide vane. Such high acceleration results in secondary flow, aggravating the erosion problems in case of sediment carrying fluid. The erosion removes the material away from the surface, causing more disturbances in the flow. **Figure 8b** shows an example (Lio Power Plant, 45 MW) of efficiency drop due to increase in the clearance gap from erosion [19]. The guide vane span in this case is 230 mm, and only by increasing the clearance gap by 1 mm (~0.5%), the efficiency drops by about 2%. Similarly, highest relative velocity in Francis turbines is found at the runner outlet. This causes erosion at the runner outlet due to high turbulence. The minimization of erosion in Francis turbines, unlike Pelton turbine, significantly depends on the hydraulic design of the vanes other than the turbine material and coating. It can be found from literatures that several investigations have been carried out so far to minimize the erosion by changing the blade angle distribution of the runner blades [20–22].

4.1. Erosion in the stay vanes

In stay vanes, the erosion occurs due to turbulences formed due to high velocity. **Figure 9** shows the eroded surface of a stay vane at Jhimruk HPP. Although the velocity in stay vanes
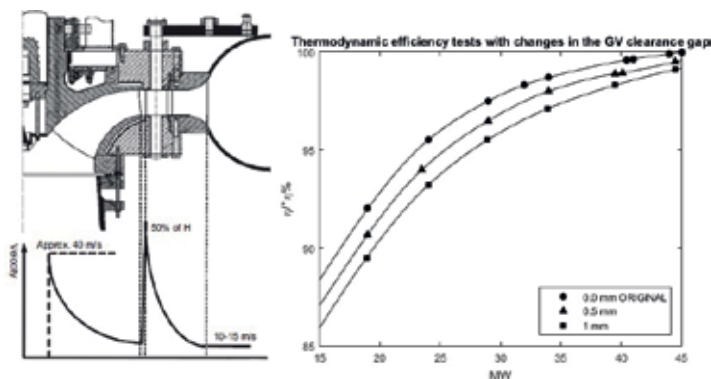
Figure 8. (a) Velocity distribution inside Francis turbine [23] and (b) loss in efficiency due to clearance gap in guide vanes (adapted from [19]).

Figure 9. Erosion in stay vanes at Jhimruk HPP.

is less than in guide vanes and runner, the detached material from this region after erosion travels downstream, which causes more severe impact on the turbine.

4.2. Erosion in the guide vanes

In guide vanes, the erosion can be classified into four types, based on the flow conditions. They are:

1. *Turbulence erosion*: fine particles can erode the outlet of the guide vane due to high velocity, especially towards the suction side. At this region, the Reynolds number is in the order of 10^8, which is under highly turbulent regime. At such a high turbulence, erosion can be severe on guide vane surfaces as well as on facing plates.

2. *Secondary flow*: guide vanes are accompanied with complex nature of the flow, which gives rise to several forms of vortices. In this case, secondary flow is referring to the accumulation of flow in the corner between facing plates and guide vanes, which give rise to horse-shoe vortex. These vortices increases the size of the gap, which brings more consequences as discussed in the next category.

3. *Leakage erosion*: guide vanes are accompanied with a small clearance gap at both ends to adjust the opening angle based on various operating conditions. In the case of sediment affected power plants, the hard fine particles mixed in water erode the connecting ends due to horse-shoe vortices. This erosion together with the head cover deflection due to water pressure increases the size of the gap. Due to the adjacent pressure and suction sides in guide vane, the flow passes through the gap from high pressure side to low pressure or suction side. At high acceleration, when the sediment particles enter in to the gap, it further causes abrasion on the guide vane ends and facing plates. This leakage flow disturbs the main flow in the suction side, which can be observed in the form of a vortex filament.

4. *Acceleration erosion*: the rotation of the water in front of the runner creates acceleration normal to the streamlines, which separates the coarse sand particles from the flow. This impacts the steel surface, which could lead to catastrophic destruction in the guide vane surfaces.

4.3. Erosion in the runner

In runner, the erosion can be classified into four types:

1. *Turbulence erosion*: in the runner, the highest relative velocity occurs at the outlet region. This increases the turbulence erosion due to fine sand particles.

2. *Acceleration erosion*: the highest acceleration is found close to the blade inlet. As discussed in the erosion categories of guide vanes, due to acceleration normal to the streamlines, the coarse sand particles are detached from the flow, which causes erosion of both guide vane and runner inlet surfaces.

3. *Erosion due to incorrect stagnation angle*: the inlet region is sensitive to incorrect pressure distribution and large difference in pressure between pressure and suction sides. The stagnation angle at inlet of the runner may change depending on different guide vane opening angles. It is also seen that the leakage flow through the clearance gap of guide vane mixes with the main flow in suction side, which forms vortex filament that hits the runner blade near hub and shroud. This vortex pushes the stagnation angle, which not only erodes the corners, but also induces cavitation.

4. *Cross flow erosion:* in some cases, cross flow from hub to shroud caused by incorrect blade leaning also increases horseshoe vortex in the blade roots. This may create sand erosion grooves at the blade inlet similar to guide vanes.

4.4. Erosion in the labyrinth sealing

The clearance between the stationary and rotating parts in labyrinth seals is between 0.5 and 1.5 mm depending upon the size of the turbine [3]. The erosion is severe in this region due to a strong turbulence in the flow. **Figure 10** shows the efficiency of Jhimruk HPP in an interval of 2 months. The total hydraulic efficiency loss after erosion in wet season is around 5%. At the same time, the leakage loss through the labyrinths was measured. It can be seen that the total loss due to leakage is between 2 and 4%. Hence, it can be inferred that the losses contributed by the leakage due to erosion of labyrinth seals is significant.
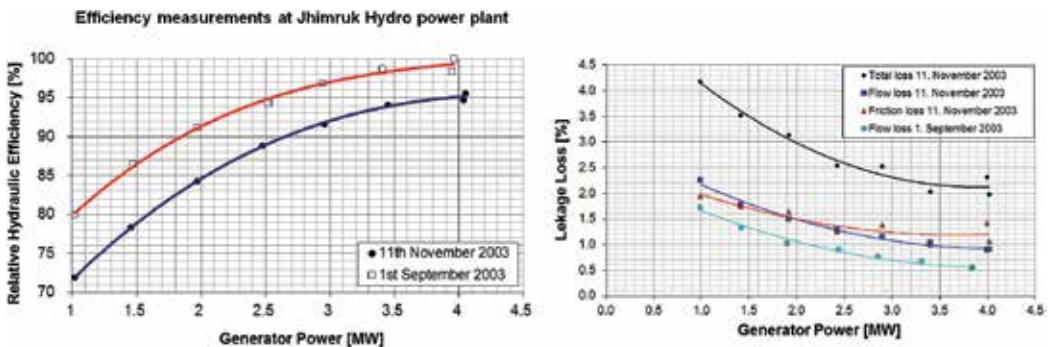
Figure 10. Efficiency measurements at Jhimruk HPP and losses from the leakage through labyrinth seal.

The erosion due to sediment particles not only causes the efficiency loss of the turbine, but also intensifies cavitation. Although the regions of cavitation and erosion is different, as shown in **Figure 11**, sometimes the eroded surface can also enforce pressure gradients in a localized regions, causing a cavitating pressure. Cavitation results in the formation of sharp edges.

Figure 12 shows some eroded components of Francis turbines. From these figures, it can be seen that the erosion in Francis turbine is predominant in particular places. The erosion depends on the nature of the flow in that location. In **Figure 12a**, erosion is shown at the outlet of the runner. It is the region where the flow leaves the runner with high relative velocity. Due to high turbulences, erosion occurs due to turbulence, as explained above. In **Figure 12b**, runner inlet towards the shroud end is seen to be more eroded than other places. This could be due to the incorrect stagnation angle driven by leakage flow through the guide vane's clearance gap. In **Figure 12c** abrasion is occurring at the guide vane ends due to leakage flow. The connecting shafts are also heavily eroded due to flow separation towards the trailing side of the shaft. In **Figure 12d** eroded grooves are formed on the facing plates due to horseshoe vortices. The grooves are formed within the range of some angles towards full GV opening. Hence, it can be inferred that these vortices affect the GV during full flow operation, for example, in the monsoon period, when the concentration of sediment in the flow is high.

Apart from using hard coatings, erosion in Francis turbines can be minimized by using new design philosophies for the design of the turbine blades. The design of runner blades follow complicated algorithms in both axial and radial directions. The blade angle distribution is maintained in such a way that maximum amount of hydraulic energy is converted into kinetic energy in the first half of the blade. However, it is found that the erosion in the blade is sensitive to the blade angle distribution, and by slightly modifying this parameter, the erosion can be minimized significantly [19]. The new design philosophy would reduce the relative velocity at the outlet, which could also affect the efficiency of the runner. However, the most optimized design in terms of erosion and efficiency can be chosen so that the new design can compensate the loss from the losses incurred due to erosion of blades in a period of time.

Similarly, for the design of the guide vanes, it is found that the change in the guide vane's hydrofoil profiles could minimize the erosion in runner and guide vanes at some operating conditions [24]. The hydrofoils are usually standard profiles such as NACA. For zero angle of attack, which is the case for best efficiency, the lift force is zero in a straight passage for profiles symmetrical around the chord. However, due to the circumferential orientation of
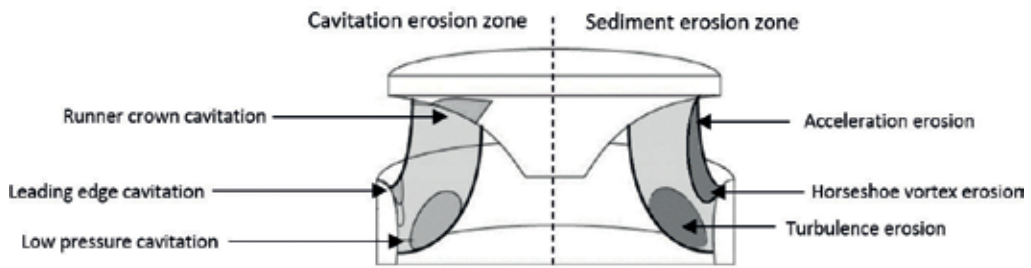
Figure 11. Cavitation and sediment erosion prone zones in Francis runner [5].
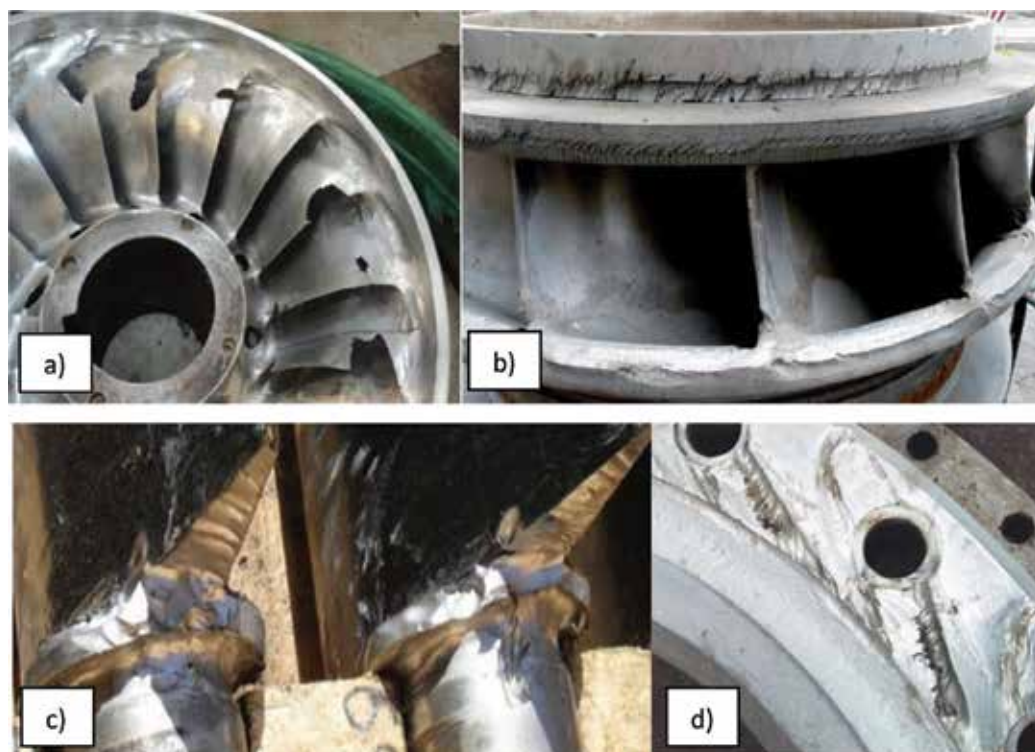
Figure 12. Erosion in Francis turbines at (a) runner outlet, Jhimruk HPP, (b) runner inlet, Cahua HPP, (c) guide vane faces, middle Marsyangdi HPP, (d) facing plates, Jhimruk HPP.

the guide vanes, pressure and suction sides are developed at a same chord-wise position. As a result, when the clearance gap grows in size, the flow from pressure side is driven into suction side. The leakage flow can be minimized by using an asymmetric profile, such that the resultant lift force in zero angle of attack is compensated by the orientation of the guide vanes.

5. Coating techniques and maintenance

The most common hydro-abrasive erosion resistant coating materials in hydraulic machines is thermal sprayed tungsten carbide cobalt chromium, WC-CoCr [12]. These coatings have a Vikers' hardness of 900–1200 HV at 0.3 kg loading [25], which is harder than feldspar (Mohs' hardness 6) and similar hardness as quartz (Mohs' hardness 7). Although it was difficult to apply coating on the surfaces of small and medium sized Francis runners, with recent technologies and use of robots, it has become possible to coat them completely. According to IEC 62364, coatings might initially result in reduction of the efficiency due to increased roughness, but can maintain a higher efficiency compared to the uncoated turbine over time. **Figure 13** shows an example of a coating applied on Francis turbine runner and its effect after 1 year of operation.
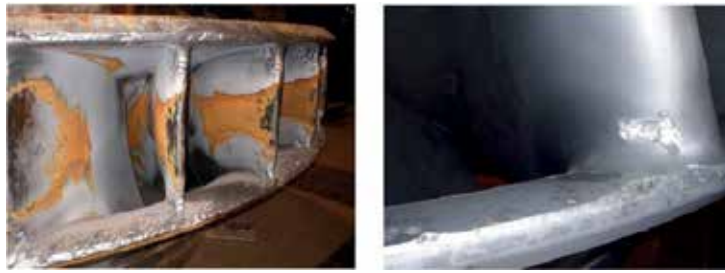
Figure 13. Francis turbines at Nathpa Jhakri HPP in India, without and with coating, both after 1 year of operation [28].

A new production method was developed for Cahua HPP by applying a tungsten carbide based coating to Francis turbine runners and guide vanes [26]. The coated turbine increased the energy production by about 50% compared to the energy generated by the uncoated turbine during the same time period.

However, most of the hydro-abrasive erosion resistant coatings are not effective against cavitation. A high intensity implosion of cavity might locally destroy the coatings. In addition, the dimensional tolerances of the coatings have to be considered before applying the right coating. Hard-coatings are also sensitive to impacts of larger particles, such as gravels and stones. Since the thickness of the coating is around 300–500 μm, it could also hinder the detention of potential cracks in the base material [27].

An effective maintenance strategy must be implemented to get maximum output from a power plant. Frequent maintenance is required to run the turbines with good condition. Although power plants contain spare turbine parts, the downtimes during assembly and disassembly adds to the total cost, due to losses in electricity generation. Hence, design of turbines for easy dismantling, maintenance procedure and overhaul time is being continuously optimized for best production. These days, power plants employ pit stop maintenance for making the maintenance actions more efficient, saving both time and money. This philosophy implies more focus on preparation, planning, follow-up and evaluation than during shutdown maintenance.

IEC 62364 gives some criteria to determine the overhaul time due to hydro-abrasive erosion. Some parameters are listed below:

1. When the efficiency has deteriorated to an extent that it is economically beneficial to restore the unit to its design efficiency.

2. Water outflow through balancing pipes from the head cover indicating erosion of labyrinth seal.

3. Increase in the axial thrust indicating erosion of labyrinth seal.

4. The time taken by the unit to stop after the guide vanes are closed and the inlet valve are kept open, indicating erosion of the guide vanes and covers.

5. Pressure in the spiral casing with closed inlet valve and opened bypass, indicating erosion of the guide vanes and covers.

6. For internal inspection, if runner blade outlet is eroded more than two-thirds of its thickness (for large turbines) or completely abraded (for small turbines), clearance of the runner labyrinth is more than doubled and for coated surface, if the area of coating removed exceeds 5–10% of the total coated area.

6. Some recent findings related to erosion in guide vanes and its consequent effects

As discussed in the previous section, guide vanes are accompanied with highly turbulent flow, which results in a number of unsteady flow phenomena. When sediment particles travel with these unsteady flows, it causes erosion with various mechanisms. Some recent studies have focused on the clearance gaps of guide vanes and how the leakage flow through the gap is affecting the performance of the turbine [29–31]. This section provides a summary of the important findings, which were obtained from these studies.

Guide vanes are connected to shafts which can rotate about its axis so that the closing and opening according to different flow and load conditions are possible. A small dry clearance is present between guide vanes and facing plates to enable movement of the vanes. The leakage losses due to such a small clearance gap can be neglected. However, due to head cover deflection and constant impact of the sand particles, the size of the clearance gap increases. Inside the clearance gap, the flow is driven from high pressure side to low pressure side, disturbing the primary flow in the low pressure or suction side. This leakage flow occurs with a very high acceleration inside the gap, which creates rotational flow component after mixing with the main flow. As a result, vortex filaments are developed downstream at both ends, which eventually hit the runner blades. **Figure 14** shows a guide vane cascade including these mechanisms. These vortices tend to hit the runner inlet towards hub and shroud. Moreover, these vortices also change the stagnation angle at runner inlet towards the edges. Vortex carrying sediments along with improper stagnation angle can have a combined effect of sediment and cavitation erosion. An example of such an effect was shown in **Figure 12b**.

Recently, a one GV cascade rig was built in Waterpower Laboratory of Norwegian University of Science and Technology to study the effect of increasing clearance gap in the flow. The rig consisted of a 1:1 scale guide vane corresponding to a turbine with specific speed of 0.086 and clearance gap on one end. The rig covered angular position of 30°, which is 1/12th of the size of the turbine in angular direction. The cascade's walls were optimized so that the velocity field around the GV gives a close estimation of the actual flow in real turbines. The velocity field around the GV was measured using PIV technique by tracking the particles over a 2D laser sheet flashed at different span locations. Similarly, pressure measurements were taken at points along the surface of the GV.
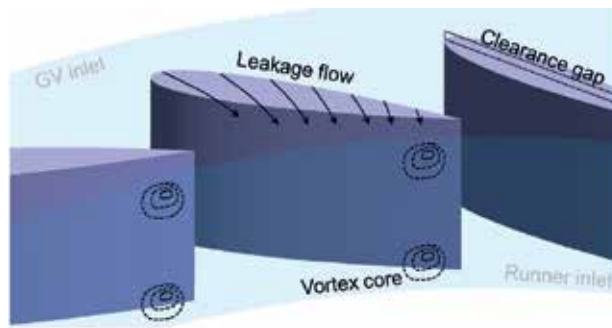
Figure 14. Leakage flow and vortex core through clearance gap.

The rig was used to test several GV profiles of same thickness and chord length, including the reference NACA0012. It was seen that the highest pressure difference between the GV surfaces for the reference design is equivalent to 20% of the net hydraulic head acting on the turbine, and it occurs around 75% of the GV chord. The leakage flow through the clearance gap depends directly on this pressure difference, as the velocity component normal to the chord increases with the similar trend. It is estimated that for a clearance gap of 2 mm (~2% of the span height), the total cross-wise leakage flow is more than 1% of the total flow. Higher leakage produces higher intensity of the vortices, which aggravates efficiency, erosion and structural integrity of the turbine.

It was seen from the experiment that the pressure difference and consequently, the leakage flow can be reduced by using asymmetrical guide vanes in the designed opening angle. **Figure 15** shows the velocity contour in the clearance gap plane taken from PIV in the rig, for three different GV profiles. In the case of NACA0012, the result is significantly affected by cavitation. The intensity of the cavitating vortex is very high, which causes several reflections of the laser sheet inside the plane, producing disturbances in the post-processed contour. However, the intensity of this disturbance is seen (and also heard during the measurement) to be reduced for the asymmetrical profiles. In the case of NACA2412, the vortex originates
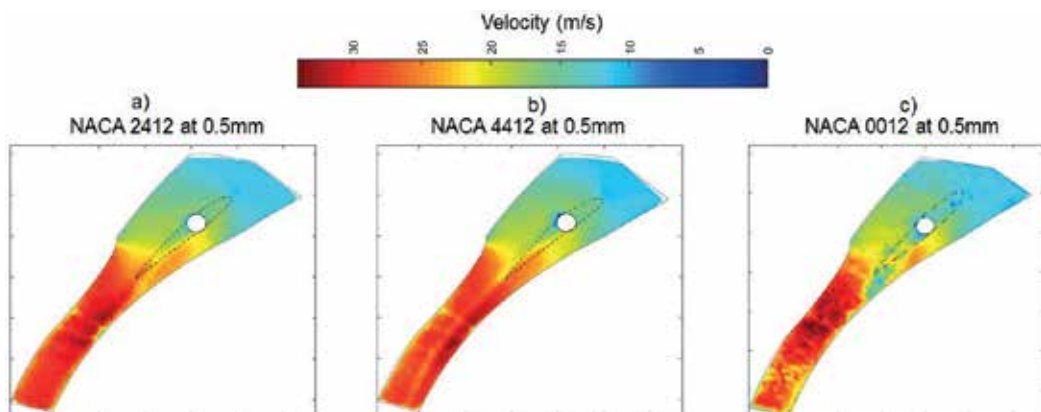
Figure 15. Velocity contours inside the clearance gap from PIV measurement [26].

from the leakage flow and disappears after moving few centimeters downstream of the GV's trailing edge. In the case of NACA4412, the vortex follows straighter path (like the wakes from GV boundary), which infers no cross-flow through the gap. However, the vortex does not disappear and it can be seen up to the end of the rig. It can be explained that the vortices in NACA2412 and NACA0012 have changed their planes while moving downstream. As the image was taken one plane at a time, the out-of-plane movement of the vortices was not captured. The intensity of the vortex in NACA4412 is relatively less, which decreases the rotational velocity component, preventing the out-of-plane movement.

Although the results in the designed opening angle showed reduced leakage flow in NACA4412, some recent results have shown that there could be some negative leakage flow at full load operation. The consequences could be more severe in terms of the erosion, because turbines operate in full load condition during wet season, when the concentration of the sediments in water is maximum. Hence, an intermediate profile between NACA0012 and NACA4412 (e.g., NACA2412) can be one of the optimum solutions, considering all the operating points.

7. Conclusion

Sediment erosion is of the inevitable challenges in the operation of power plants of many countries. Erosion depends on several factors, including materials of the turbine, as well as shape, size and mineral contents of sand. However, because of the highly unsteady flow in turbines, velocity of the fluid plays one of the most important roles for erosion. Depending upon the type of flow phenomena, the components of turbines are eroded at particular locations with particular mechanisms. This chapter explained some erosion mechanisms in Pelton turbine's nozzle systems and buckets and Francis turbine's guide vanes and runner. Some recent findings related to the flow phenomena inside the clearance gap of guide vanes were discussed. The future turbines operating in sediment affected power plants should consider the particles and their erosion potential during the design phase. The repair and maintenance and efficiency loss after erosion imposes heavy loss of capital along with the premature failure of turbines compared to their estimated life expectancy. In order to have reliable investments for hydropower development in a country, the challenges of sediment erosion in turbines need to be addressed with a sustainable solution.

Author details

Sailesh Chitrakar[1]* , Hari Prasad Neopane[1] and Ole Gunnar Dahlhaug[2]

*Address all correspondence to: sailesh@ku.edu.np

1 Kathmandu University, Nepal

2 Norwegian University of Science and Technology, Norway

References

[1] Edenhofer O, Pichs Madruga R, Sokona Y, P. United Nations Environment, O. World Meteorological, C. Intergovernmental Panel on Climate, et al. Renewable Energy Sources and Climate Change Mitigation: Special Report of the Intergovernmental Panel on Climate Change. New York: Cambridge University Press; 2012

[2] Milliman JD, Meade RH. World-wide delivery of river sediments to the oceans. Journal of Geology. 1983;**91**:1-21

[3] H. Brekke, Design of hydraulic machinery working in sand laden water, in Abrasive erosion and corrosion of hydraulic machinery, Imperial College Press, London, pp. 155-81, 2002

[4] Truscott G. A literature survey on abrasive wear in hydraulic machinery. Wear. 1971; **20**(1):29-50

[5] Chitrakar S, Neopane HP, Dahlhaug OG. Study of the simultaneous effects of secondary flow and sediment erosion in Francis turbines. Renewable Energy. 2016;**97**:881-891

[6] Stachowiak GW. and Batchelor AW. Engineering Tribology, 3rd ed., Butterworth – Heinemann, Elsevier, 2006

[7] Burwell JT Jr. Survey of possible wear mechanisms. Wear. 1957;**1**(2):119-141

[8] Bhusan B. Introduction to Tribology. New York: John Wiley & Sons; 2002

[9] Thapa B. Sand erosion in hydraulic machinery [PhD Thesis]. 2004

[10] Bergeron P, Similarity conditions for erosion caused by liquids carrying solids in suspension, Application to centrifugal pump impellers, in La Houille Blanche, 5 (Spec. No. 2) B.H.R.A. translation T 408, pp. 716-729, 1950

[11] Bak E. Construction materials and testing results of the wear of pumps for transporting solid media. In: Biuletyn Glownego Instytuta Gornictwa, B.H.R.A. translation available; 1966

[12] IEC, Hydraulic machines. Guide for dealing with hydro-abrasive erosion in Kaplan, Francis, and Pelton turbines, BS EN 62364:2013

[13] Chauhan AK, Goel DB, and Prakash S, Erosion behavior of hydro turbine steels, Bulletin of Materials Science, vol. 31, no. 2, pp. 115-120, 2007

[14] Price T, Probert D. Harnessing hydropwer: A practical guide. Applied Energy. 1997; **57**(2/3):175-251

[15] Bajracharya TR, Acharya B, Joshi CB, Saini RP, Dahlhaug OG. Sand erosion of Pelton turbine nozzles and buckets: A case study of Chilime hydropower plant. Wear. 2008;**264**:177-184

[16] Neopane HP, Dahlhaug OG, Cervantes M. Sediment erosion in hydraulic turbines, Global Journal of Researches in Engineering Mechanical and Mechanics Engineering, vol. 11, issue 6, pp. 17-26, 2011

[17] Padhy MK, Saini RP. Effect of size and concentration of silt particles on erosion of Pelton turbine buckets. Energy. 2009;**34**:1477-1483

[18] Rai AK, Kumar A, Staubli T. Forces acting on particles in a Pelton bucket and similarity considerations for erosion. IOP Conference Series: Earth and Environmental Science. 2016;**49**

[19] Brekke H. The influence from the guide vane clearance gap on efficiency and scale effect for Francis turbines. In: 14th IAHR Symposium, Section on Hydraulic Machinery Equipment and Cavitation; Trondheim. 1988

[20] Thapa BS, Thapa B, Eltvik M, Gjosater K, Dahlhaug O. Optimizing runner blade profile of Francis turbine to minimize sediment erosion. In: 26th IAHR Symposium on Hydraulic Machinery and Systems. 2012

[21] Eltvik M. Sediment erosion in Francis turbines [PhD Thesis]. 2013

[22] Chitrakar S, Cervantes M, Thapa BS. Fully coupled FSI analysis of Francis turbines exposed to sediment erosion. International Journal of Fluid Machinery and Systems (IJFMS). 2014;**7**(3):101-109

[23] Thapa BS, Dahlhaug OG, Thapa B. Sediment erosion in hydro turbines and its effect on the flow around guide vanes of Francis turbine. Renewable and Sustainable Energy Reviews. 2014;**49**:1100-1113

[24] Chitrakar S, Thapa BS, Dahlhaug OG, Neopane HP. Numerical and experimental study of the leakage flow in guide vanes with different hydrofoils. Journal of Computational Design and Engineering. 2017

[25] Winkler K, Dekumbis R, Uppal A. Coating minimizes operational losses at Nathpa Jhakri in India, Hydro Review Worldwide. **19**(1), 2011

[26] Dahlhaug OG, Skåre PE, Mossing V, Gutierrez A. Erosion resistant coatings for Francis runners and guide vanes. International Journal of Hydropower and Dams. **17**(2):109-112

[27] Felix D. Experimental investigation on suspended sediment, hydro-abrasive erosion and efficiency reductions of coated Pelton turbines [PhD Thesis], 2017

[28] Andritz Hydro, Solutions against Hydro-Abrasive Erosion – Optimized Design and SXH™ Coating, 2015

[29] Thapa BS, Trivedi C, Dahlhaug OG. Design and Development of Guide Vane Cascade for a Low Speed Number Francis Turbine, Journal of Hydrodynamics, Ser. B, vol. 28, issue 4, pp. 676-689, 2016

[30] Thapa BS, Dahlhaug OG, Thapa B. Sediment erosion induced leakage flow from guide vane clearance gap in a low specific speed Francis turbine. Renewable Energy. 2017;**107**: 253-261

[31] Chitrakar S, Neopane HP, Dahlhaug OG. PIV investigation of the leakage flow through clearance gaps in cambered hydrofoils. Journal of Fluids Engineering. 2017;**139**:091201

Chapter 3

Sedimentation and Erosion in Harbor Estuaries

Alexandre M.G. Santos Ferreira and

Cláudia S.N. Santos

Abstract

Harbors, whenever possible, are established in estuaries to take advantage of the existing natural safety and protection conditions. To keep harbors in a safe and usable way, periodic dredging works are carried out. The expansion of harbor's activities and the growth of maritime traffic may lead to changes in the harbor's layout or to improvements of navigation channels and basin depths. Such design adjustments entail changes in estuarine hydrodynamics, and therefore the usual dredging rates are subject to alteration, namely, tending to increase. It is then important to assess the influence of the harbor's new layout on the solid transport pattern and how its effects can be minimized, aiming the reduction of economic and environmental impacts. Within this context, in this chapter estuary hydrodynamics and sedimentation-erosion patterns are summarized. Also, the modeling methodology for planning and management of dredging works which uses geo-processing automatic GIS environment, developed by the Portuguese harbor authority, is presented. Finally, the case study of harbor of Portimão is also described showing the implementation of the referred methodology.

Keywords: erosion, sedimentation, layout, hydrodynamics, dredging

1. Introduction

Sedimentation and erosion patterns and rates in estuaries rely on the interaction of multiple conditions and so are generally complex. However, in a brief and simplified overview, when a system is in equilibrium, there is neither sedimentation nor erosion; when, at local conditions, the flow velocity is not strong enough, there will be accretion; and, if the flow velocity is too strong, there will be erosion. In the case of an environment alteration (e.g. due to natural

causes, as a heavy storm, or due to human intervention, as the construction of a dock), a change in hydrodynamics and, consequently, in the sediment-erosion pattern will occur [1].

Sediment transport processes are subject to the influence of site conditions as the geological and geotechnical characteristics of the estuary basin bed and of the existing suspended sediments. So a good knowledge on sediment geotechnical properties (i.e. granulometry, mineralogy, resistance to erosion,) is important as they define the hydrodynamic velocity for which sedimentation occurs [2] due to the distinct dynamics of transport, and even interactions, between cohesive sediments (mud) and of non-cohesive sediments (sand) [1].

Depending on harbor emplacement, sediment movement is also controlled by the river flow and tidal and wave conditions [3]. When considering harbors located in estuarine areas, particularly in the terminal section where the tide occurs, the tide plays a more important role in solid transport patterns than the river flow itself. Nevertheless, a major factor in this situation is the estuary's tidal prism, which is the volume of water exchanged between mean high tide and mean low tide or the volume of water leaving an estuary at ebb tide. The available tidal prism is so dependent on the geometry of the basin in terms of surface area and mean water depth and also the tidal range, the frictional forces and, to a lesser extent, freshwater inflow. Therefore, the larger the tidal prism related to the river flow, the more determinant for the sedimentation and erosion processes, in the estuary, is the tide and tide flow.

Hence, to better understand estuarine sediment dynamics, it is relevant to study the existing topography, through reliable surveys performed, at adequate detail and scale, for each case location. The obtained data allows hydrographic modeling in order to relate hydrography with hydrodynamics and thus attain the referred knowledge.

Estuarine locations, although provide natural safety and protection conditions to the establishment of harbors and other facilities, are prone to natural filling caused by the settlement of sediments. Consequently, periodic dredging is required to maintain navigation channels and harbors in a safe and usable way. Moreover, given the natural trend of harbor activities expansion, dredging works are also needed to improve the design depth for larger vessels access, to build new wharfs and piers, or to improve existing harbors or other facilities [1]. As stated above, changes to harbor layout entail changes in estuarine hydrodynamics; hence the dredging need rates are subject to alteration, namely, tending to increase. So, it is important, when planning harbor new layout design, to include methods to minimize hydrodynamics changes and to reduce dredging volumes.

Although dredging operations are essential, these have a significant economic impact, not only during the construction phase but also along the operation phase, due to maintenance works. In fact, in small harbors, it corresponds to almost 75% of all maintenance costs [4]. Moreover, dredging activities can also have adverse environmental impacts, either within the dredge area or the deposition site, as fine-grained fraction of sediment resuspension (increasing the turbidity of water), nutrients and pollutants dispersion, water column contamination, or ecosystem degradation (e.g. by burying the biological habitats). So, potential environmental effects and risks are imperative to ascertain and well manage through the implementation of adjusted containing or remedial measures.

The referred economic and environmental impacts of dredging works highlight the impor-
tance of an accurate knowledge of sediment transport patterns, namely, the identification
of sediment deposition and erosion areas and also of the areas in which there is a balance.
Regular hydrographical surveys can allow the determination of the sedimentation rate [4]
and are considered as a key procedure for dredging design optimization.

Taking into account the referred goals of efficiency improvement, cost reduction and envi-
ronment protection, the use of management models is considered a valuable method to
support harbor management and design (or new design) decisions. This approach allows
to adequately manage the dredged material, in operation phase, with its use (e.g. beach nour-
ishment) or its safe disposal. As well, in design phase, the hydrodynamic modeling enables to
achieve a better balance in erosion and sedimentation rates, throughout optimized technical
choices. The aimed performance improvement intends to minimize the dredging volumes,
keeping the sediments within the system but, at the same time, keeping the waterways of the
harbor in a safe mode for the vessels that use it.

This chapter presents a planning and management model of dredging using the geo-pro-
cessing automatic GIS environment developed by the Portuguese harbor authority, which is
intended to be an accessible and efficient tool to support technical options in dredging design.
Additionally, the particular case of harbor of Portimão, where the referred methodology was
implemented, is discussed. The present hydrodynamic situation of the estuary is character-
ized, using a tidal model and considering average flows of the river. Then, taking into account
the plans for the harbor expansion, the hydrodynamic modeling of the new layout is pre-
sented. Using as a reference the current situation, a method to analyze the influence that the
planned works will introduce into the estuarine hydrodynamics and, consequently, in the
pattern of sediment deposition and erosion is also summarized.

2. Methodology

In estuarine locations, dredging activities are a required procedure both in harbor design and,
during operation stage, in harbor management. However, from economic and environmental
standpoints, dredging can also cause adverse effects related to the sediment removal from the
basin bottom and also related to the management of the dredged material that are important
to control. The referred impacts result from changes in local hydrodynamics and as conse-
quence in the existing sedimentation-erosion patterns and rates.

An adequate management system that keeps the harbor in a safe and usable way, but also that
controls the dredging impacts, reducing to a minimum the dredged volumes and disposing
them, if possible and useful, within the system is so aimed.

In order to achieve those goals, it is essential to have a comprehensive knowledge of the pres-
ent situation (reference situation) in terms of accretion and erosion areas and the typology
(grain size) of the sediments within those areas. This data is attained through the combined
analysis of local hydrography and hydrodynamics, as well as local geology and geotechnical

characteristics. As a result, predictive models can be established, and better technical choices concerning harbor design or management are then possible.

Therefore, a set of procedures were established to aid and simplify both the planning of harbor dredging and of the disposal of the dredged materials. Some guidelines are then proposed to be followed [3–5]:

- Analysis of the granulometry of sediments in the harbor area of the estuary
- Analysis of the maximum velocities of tidal flow and its comparison with average tide and living waters flow velocities
- Comparison of the sediment size with the maximum velocities of tide
- The use of automatic geo-processing
- The use of this information in harbor dredging planning, including the definition for dredged material

2.1. Physicochemical model development

Aiming an optimized dredging project management tool, the Portuguese harbor authority has developed and implemented a model of planning and management of dredging using the geo-processing automatic GIS environment which is next presented. Taking into account geo-referenced detailed hydrographical surveys and physicochemical analyses of the sediment, the referred model:

- Identifies the spatial distribution of zones where erosion and sedimentation occur
- Relates them with the existing types and concentrations of contaminants (if any)

allowing then the zoning of the area to be dredged.

The developed analysis system is based on a conceptual model of morph-dynamic and multi-temporal sediment distribution in port areas, automating the production of maps [6].

Through the conversion of different data formats, the proposed model is able to:

  i. Generate surfaces of different particle sizes by using interpolation methods.

 ii. Zone the dredging area.

iii. Assess the areas and volumes of eroded and deposited sediments considering four distinct particle classes: pebble, sand, silt and clay [4].

This system was implemented by applying Model Builder software ArcGIS ® (ESRI), and it consists of a set of tools that operate sequentially in the calculation of the various components of the model.

Firstly, **Figure 1**, five modules (defined as M1–M5) were implemented, each with specific processes to build automatic digital maps with the relevant information allowing [4–7]:

- M1—conversion of CAD entities into vector entities (GIS shapefile).

- M2—development of digital terrain models from bathymetry (DTM), tin and raster.

- M3—interpolation of particle sizes, deterministic method IDW.

- M4—preliminary zoning of sediments of harbor areas.

- M5—calculation of areas and volumes of erosion and deposition for subsequent dredging planning.

So, the integration of the flow field pattern and tides, using finite element method (FEM), with size distributions in estuarine sediments (determined with MAZD), identifying their source, allows then to divide the harbor area in main areas, according to the same sediment typology, for dredging purposes.
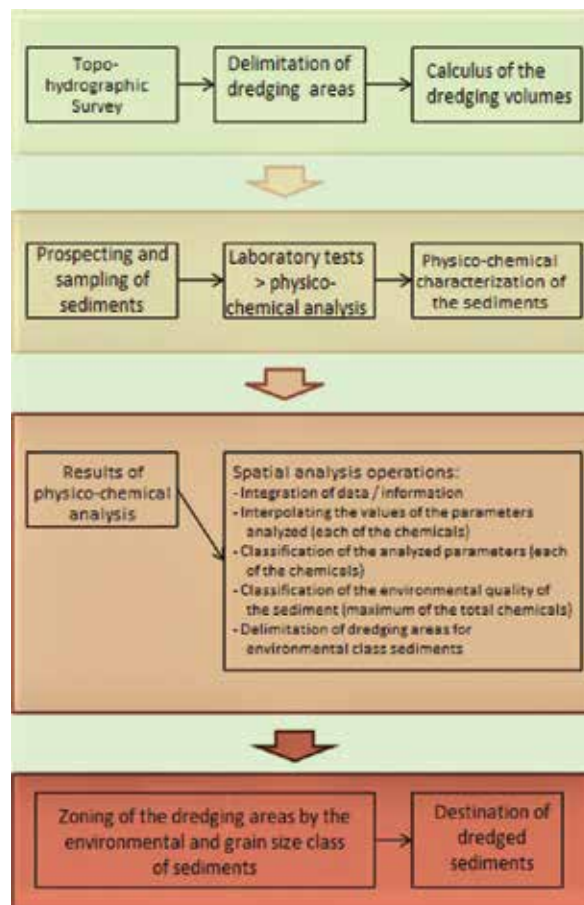
Figure 1. Flow chart of the developed procedure of physicochemical characterization for sediment dredging management in harbors.

2.2. Zoning (M4)

Following the physicochemical characterization and analysis of the sediments and taking into account the obtained results, the proposed methodology aims the identification of areas of erosion and deposition of materials.

In the reference situation for the case study, the identification was made using tools of geographic information systems, namely, 3D Analyst and ArcGIS Spatial Analyst. The zoning of the estuary area according to the grain size of the sediments was then established.

2.3. Hydrodynamics

According to the applied methodology, the determination of the maximum velocities of the ebb tide in each of the study zones must be performed, for the reference situation. Later, the determination of the maximum velocities of ebb tide, for the new layout, must also be carried out.

2.4. Sedimentation and erosion (M5)

The following step of the stated method is comprised by the identification of the areas where sedimentation and erosion occur and also where a balance between both states takes place, using the different digital terrain modules obtained from bathymetry in different years.

For each study area, the maximum velocities of the ebb tide are related with the erosion or sedimentation status verified.

2.5. Simulation for layout changes

By the integration of the gathered results from the reference situation and the new layout, it is aimed in this stage to foresee the changes in erosion and sedimentation patterns, comparing the flow changes in both situations. So, the areas in which erosion and sedimentation are likely to increase, or to maintain a probable balance, are then identified, estimating the variation in yearly volume dredging.

Finally, according to the results, an eventual consideration of alternative solutions to dredging can be studied.

3. Case study: harbor of Portimão

In this chapter, the hydrodynamics of the Arade estuary is analyzed considering the area of port interest (Port of Portimão), studying the present situation of deposition and erosion of sediments, relating them, based on the detailed information about the model [8].

The port of Portimão presents the best natural conditions on the southern coast of Portugal. The area under port jurisdiction runs from the mouth of the River Arade to the Roman bridge

in Silves, 13 km upstream. At present, the port area only encompasses the frontier stretch of the city of Portimão, and it can be seen that, upstream of the first Arade Bridge, the river can only be used by small tourist boats and in certain places only at high tide. Two breakwaters protect the entrance to the port, with a minimum of 200 m wide, followed by a 150 m wide navigation channel, which extends to the commercial wharf and the fishing port [9]. The W and E quays have lengths of 820 m and 680 m, respectively. In the wide front, there is a circular and maneuvering basin. On the right bank, from the inlet upstream, first there is Portimão Marina; then the Navy Pier, with a length of about 200 m; and the Terminal of Passengers and General Cargo, about 340 m long; further upstream, in a lower depth zone, there are other docks and berths for recreational craft. The fishing port is located on the left bank, with mooring wharves, a shipyard and a supply pier. The port of Portimão is used for trade, cruising, fishing and recreation. There is a weekly ferry link to Madeira and the Canary Islands.

The modeling of the estuary of the River Arade includes the west coastal zone up to Ponta da Piedade, west of Lagos and the east coastal zone till near Vilamoura. Given the referred coast extension, it was intended to ensure that the tide conditions that were taken into account at the entrance of the bar would be free of undesired influences from the boundary conditions.

Regarding the study area towards the inland, the river Arade was considered as far as the Roman bridge of Silves, in an extension of 13 km, and the Odelouca stream to a section about 14 km upstream from the mouth of the Arade. This way, it was intended to obtain, in the area under study—Arade estuary between the Portimão road bridge and the bar—the most representative situation possible.

It was considered that hydrodynamic conditions are determined almost exclusively by the effect of the tide, since the influence of the river flow is very small, given the regularization imposed by the built dam upstream; it was assumed for the river flow the value of 10 m^3/s. Upstream of the model limit, the roman bridge of Silves, the volume of the tide prism is very small, due to both the small widths of the channels of the water lines and the high levels of the bottoms.

For the hydrodynamic modeling, the RMA2 model, with the SMS interface, was used. The mesh of finite elements used for the reference situation is presented in **Figures 2** and **3**. For the future layout, the mesh and the boundary conditions were modified considering the future hydrography, according to what each work planned, the respective geometry and the limit of analysis.

To calibrate the model in the reference situation, three points were taken into account, respectively, upstream of the railway bridge in Mexilhoeira Grande, at the junction of the Odelouca River with the Arade River, and downstream of the Roman Bridge in Silves, as referenced in **Figure 4**. The observations available for the calibration of the model, considering the free surface of the flow, took place during a tide cycle. Besides the points used for the calibration of the model, **Figure 4** shows the points used for the overall analysis of the results and also for the detailed analyses.

The variables obtained in the calibration of the model were used in the future layout model, with minor adjustments to eliminate instabilities of convergence of the iterations.
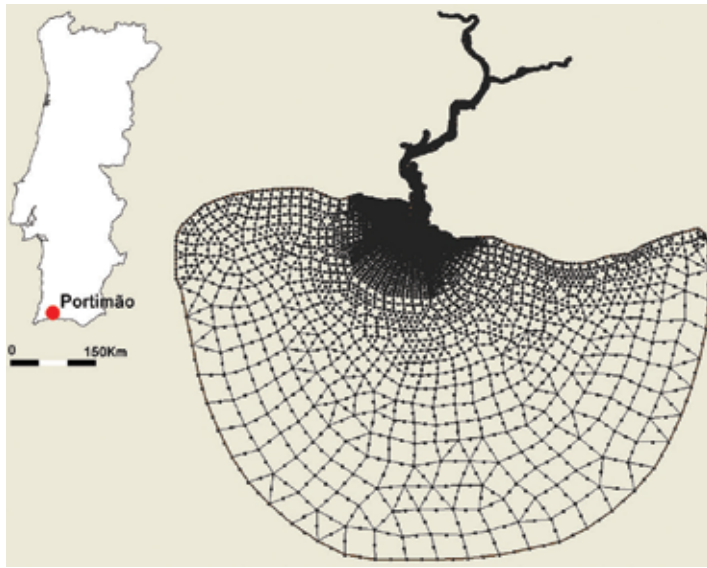
Figure 2. Finite element mesh of the case study and the harbor location.
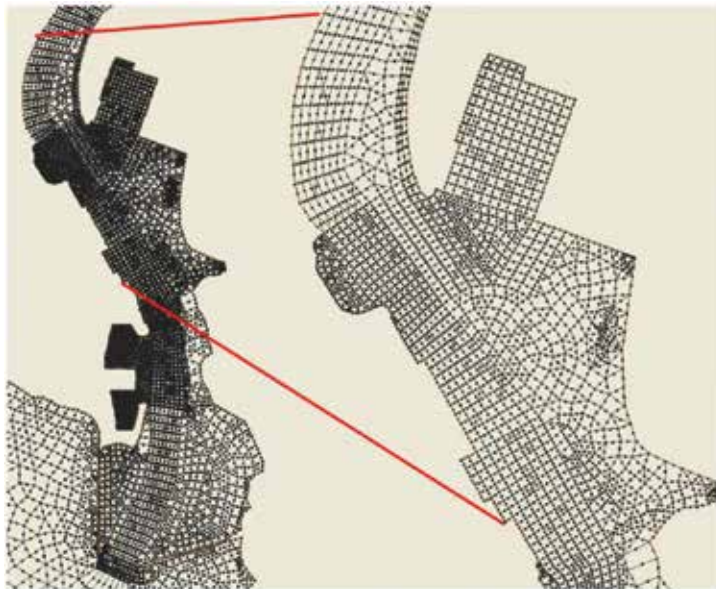
Figure 3. Details of the mesh in the estuary of the Arade River: the estuary and the zone that comprises the Dock of San Francisco, the fishing port, the commercial wharf and the Navy Pier and the maneuvering basin.

The flow rate considered for both situations (reference situation and future layout) was 5 m^3/s in the Arade River and 5 m^3/s in the Odelouca stream. In fact, the average current flow rate at the Portimão road bridge is estimated at about 10 m^3/s. For the calibration, and taking into account the flow rates verified on the day of the field readings, a flow rate of 0.5 m^3/s was used for each of the streams.
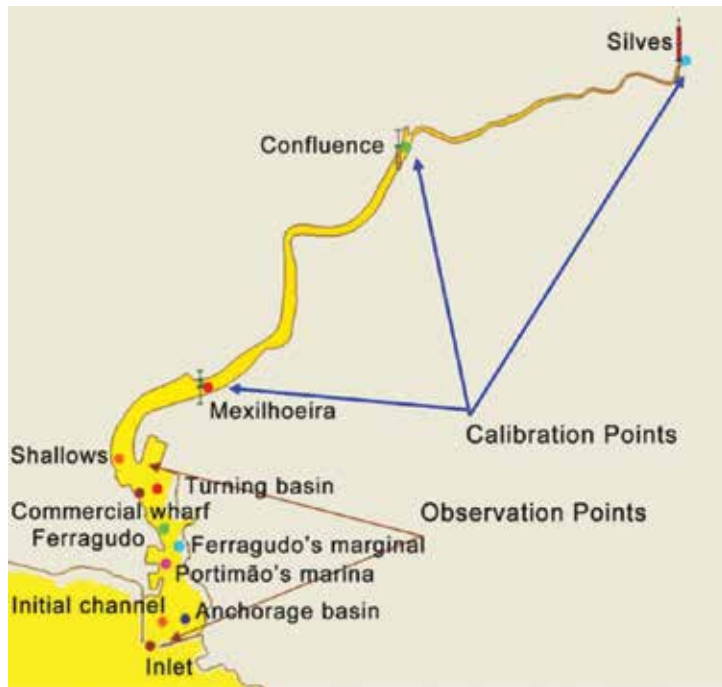
Figure 4. Calibration points and observation points, for comparison of results.
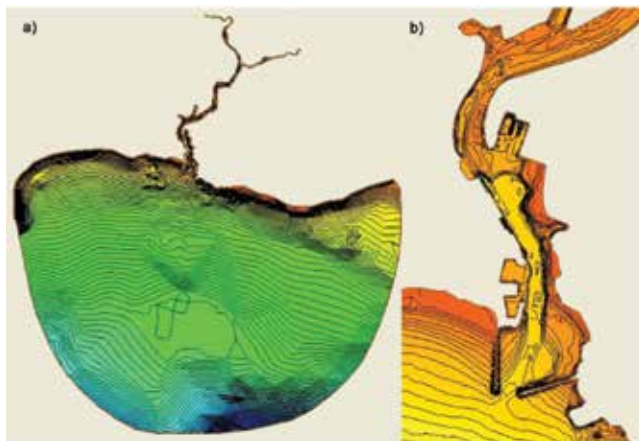
Figure 5. (a) Topo-hydrography considered for the reference situation and (b) detail of the estuary.

In **Figure 5**, the topo-hydrography regarded in the hydrodynamic analysis is presented in a very schematic way, and it was based on the surveys carried out in 2003. For the future layout simulation, this hydrography was modified according to the various reviewed works. This way, the velocity and the water heights at each point were obtained. The interventions planned for the port will not have a significant influence on the hydrodynamics upstream the Portimão road bridge, as there will be no changes in that reach.
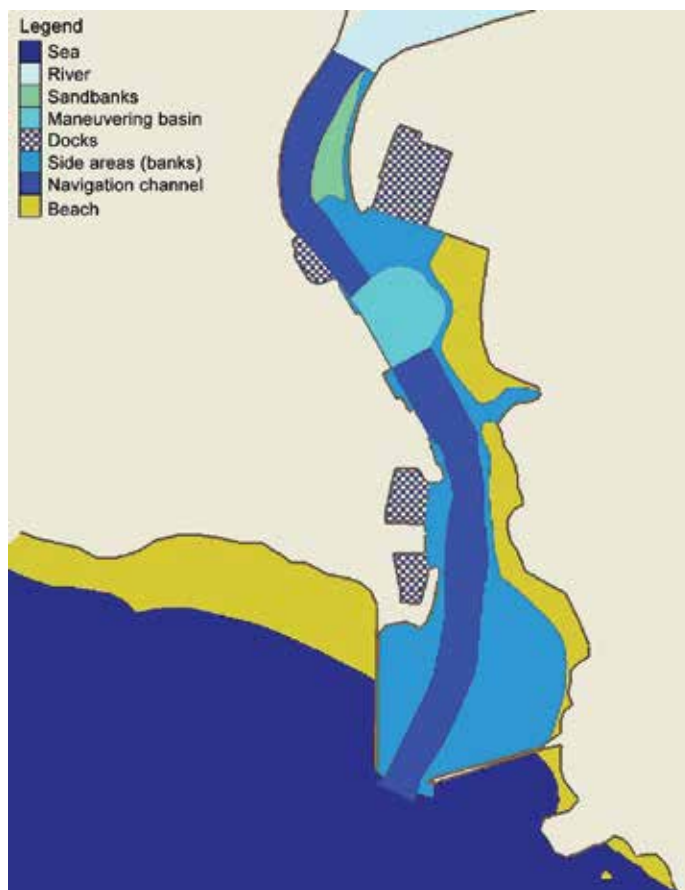
Figure 6. Materials (different roughness) considered in the analysis, in the section between the road bridge and immediately downstream of the bar.

Consequently, the "overall" analysis of the results to be achieved will focus only on the section between the Portimão road bridge and the inlet, and so four areas were analyzed in detail: commercial quay and maneuvering basin, Ferragudo channel and Ferragudo bank, the first section of the navigation channel and the inlet. Some considerations are also done about the sandbank channel, upstream the commercial quay. Several zones were considered in the modeling, corresponding to different "materials" and their corresponding roughness, in the RMA2 model, which are represented in **Figure 6**. In fact, the hydrodynamic conditions within the several docks are substantially different from those observed, for example, along the navigation channel.

3.1. Zoning (M4)

Considering the sampling and grain size analysis performed, and considering the fine alternations of thinner and coarser sediments, typical in this type of environment, as well as the various strata, it was decided to divide the estuary into three zones (**Figure 7**):

- Upstream, between the road bridge and the downstream part of the maneuvering basin, as a zone of fine sediments

- Downstream of the former and to the southern end of the Portimão Marina, as an area of medium sediments

- To the south of the previous one, and to the bar, as a zone of coarse sediments

It is considered that the occurrence of erosion and sedimentation in the mooring area, and the coarser sediments, is more related to the swell of SW, than to the currents caused by the tide.

In this zoning, "fine sediments" include materials ranging from fine sand to mud, including silts; in "medium sediments" fine to medium sand, with some silt, are included; the "coarse sediments" include coarse to medium sand.

Figure 7 shows the proposed zoning for sediments, which will serve as a basis for the subsequent analysis of the possible acceleration of erosion or sedimentation trends.
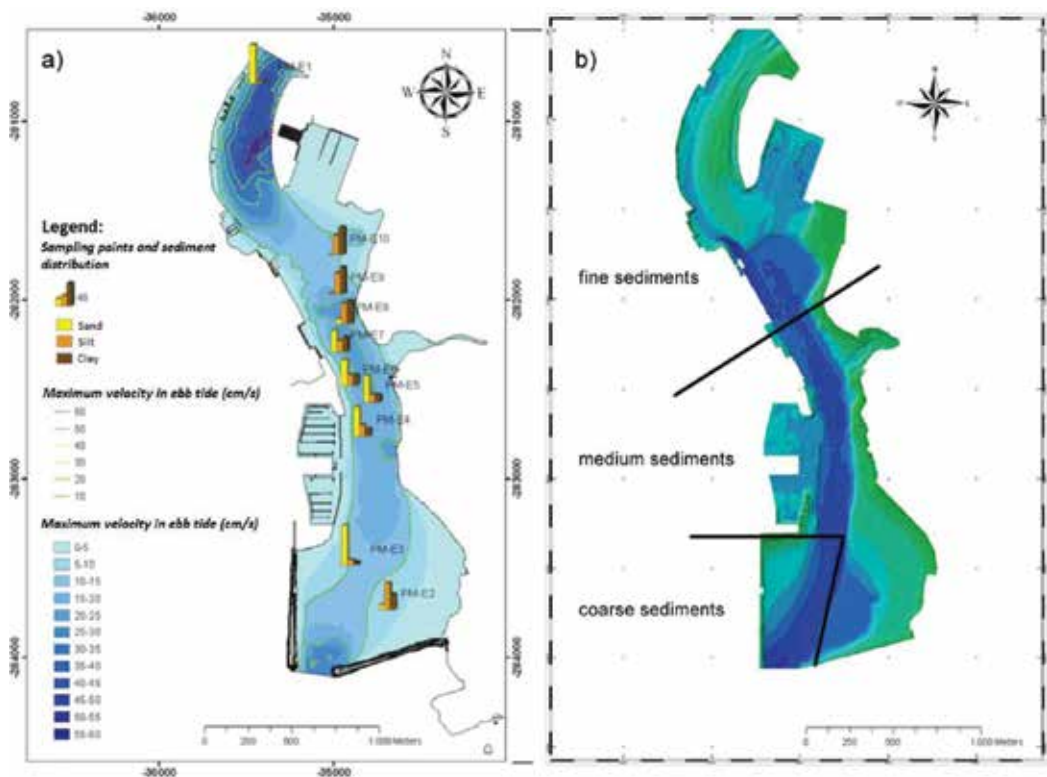
Figure 7. (a) Sampling points and grain size distribution; (b) simplified zoning of the estuary.

3.2. Hydrodynamics

The reference situation corresponds to the current situation of the port of Portimão, as in 2010; however, the hydrography of the survey of 2003 was used since it is still representative.

For performed modeling, and for all subsequent modeling, the tide of 27 February 2002 (**Figure 8**) was considered for representing a tidal wave, as it corresponds to the obtention of the field values for the calibration of the model. The tide used has a flood level of 3.69 m ZH and a low sea level of 0.30 m ZH.

All the modeling was carried out for a period of 65 hours, i.e. more than five complete cycles of flood and ebb tide. In this way, the aim was to stabilize the obtained results, since, in general, and in the application of the RMA2 model, the two or three first cycles show variations before reaching stabilization. The period considered for analysis, both in this modeling and in the following models, was the between 48 and 62.3 hours of simulation.

Figures 9–11 show some of the results that are considered more relevant for the reference situation. As expected, in this case, there is a delay of almost 1 hour between the peak velocity in the bar and the channel in front of the central zone of Portimão, near the sandbank. There is also a substantial reduction in flow velocity in front of the S. Francisco dock, due to the widening of the flow channel due to the entrance to the fishing port, the S. Francisco dock, and the maneuvering basin. There is also a significant reduction in velocity on the initial section of the channel and in the mooring area, due to the widening of the flow section in that area.
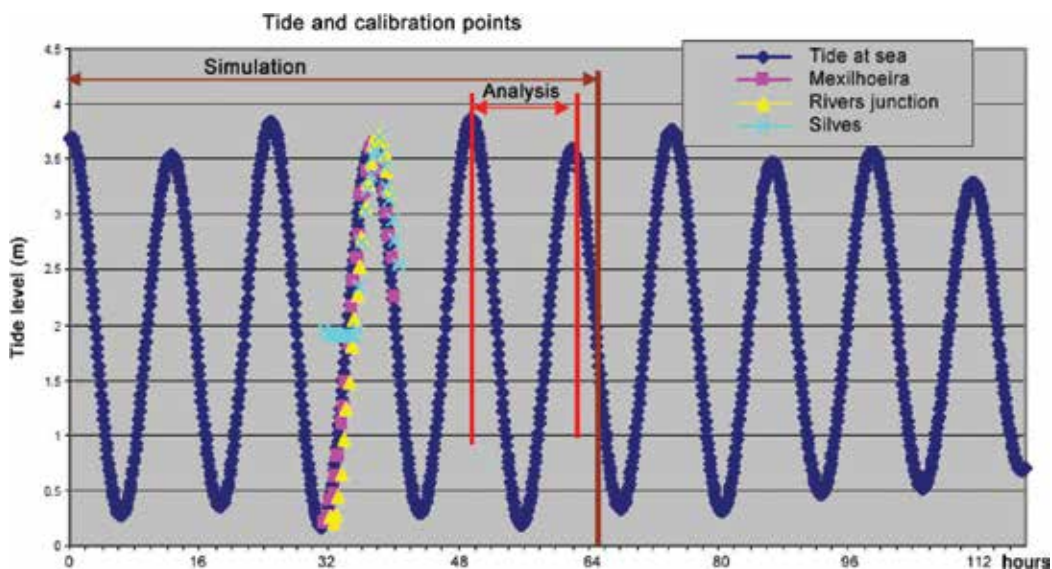
Figure 8. Tide used in the modeling, including the 27th of February (calibration data) and the period used in the analysis.

Figure 9. Reference situation. Results obtained during ebb flow: (a) 50, (b) 51, (c) 53 and (d) 55 hours.
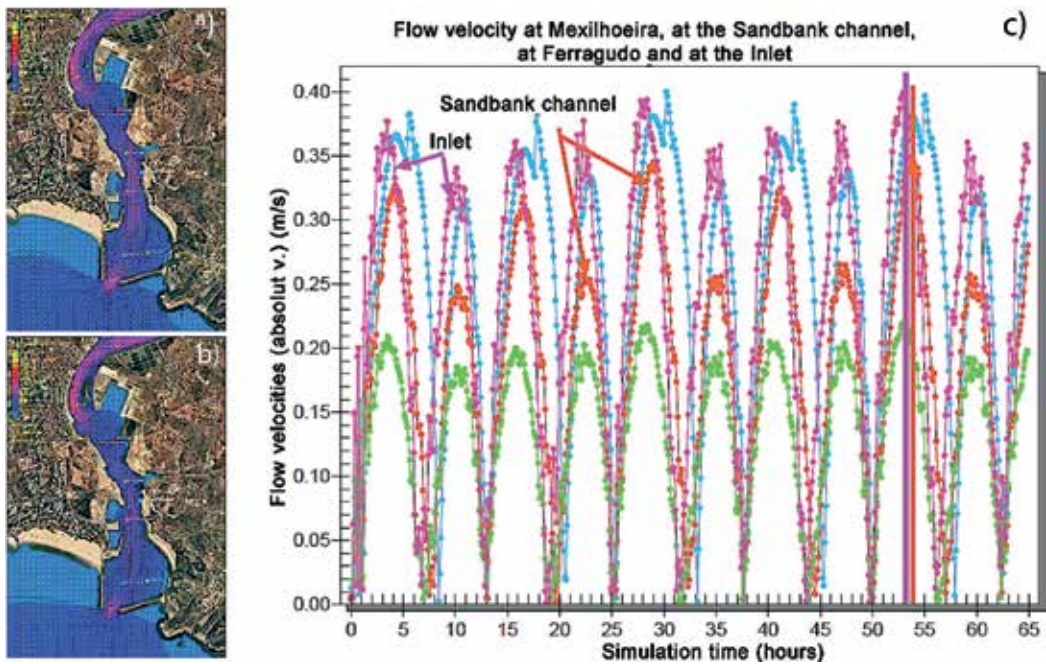
Figure 10. Reference situation. Flow at (a) 53 and (b) 54 hours; (c) delay between the peak of velocity in the ebb tide in the bar and in the channel near the sandbank.

3.3. Sedimentation and erosion

The determination of the areas currently subject to sediment deposition or erosion was done following the methodology explained in Section 2, using the 3D Analyst and the Spatial Analyst tools of ESRI geographic information software. The 2000 and 2003 surveys of the

Figure 11. Reference situation. Results obtained during flood flow: (a) 58, (b) 59, (c) 60 and (d) 61 hours.

entire port of Portimão were used. These two surveys allow a good understanding of the erosion sedimentation procedure, as there were no full dredging works in the meantime, only local dredging works.

The application of this model, simple to apply on geo-referenced surveys, allows to determine the locations where the depth has lowered (deposition of material), or risen (erosion of sediments), and to assess the value of these variations, by analyzing the difference on the assessed depths of two hydrographic surveys separated by a certain time interval.

With the application of 3D Analyst and Spatial Analyst to the two surveys of 2000 and 2003, the results, represented graphically in **Figure 12**, were obtained.
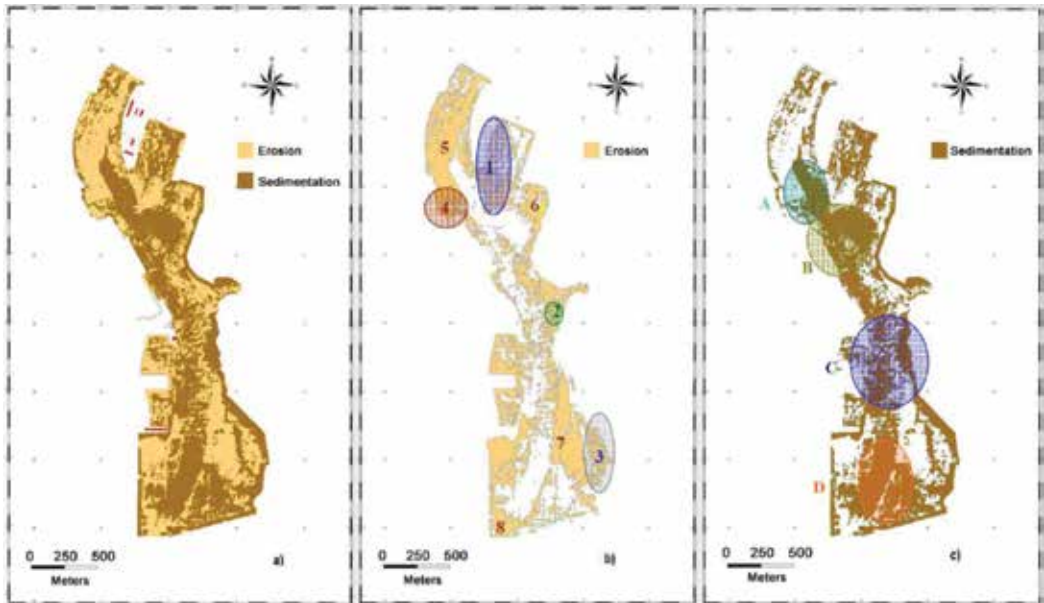
Figure 12. Results of the application of modules M1 to M5 to the surveys of 2000 and 2003: (a) overall results, (b) erosion and (c) sedimentation areas.

The two situations of erosion and sediment deposition will be analyzed separately.

Firstly the areas where erosion occurs (which are presented in **Figure 12b**) will be analyzed. In particular, eight distinct locations deserve careful consideration, as follows.

Starting in zone 1, which corresponds to the fishing port, it is important to notice that a maintenance dredging was carried out in 2001, since this zone, and especially the port entrance and the area next to the haul ramp of the shipyards, was very much silted. Therefore, erosion did really not occur here but rather maintenance dredging. In the remaining areas of this fishing port, the alternation between eroded and silted areas, always of very small values, corresponds to the mooring area of the boats, and to the areas under the piers, and indicates that there was practically no sediment erosion or sedimentation.

The zone 2, which appears in this analysis as strongly eroded, was in fact subject to a local dredging, so, contrary to the obtained results, this is a zone of strong deposition of sediments; on the other hand, the section upstream of this zone, also at the mouth of the Ferragudo River, is, in fact, an area of high erosion. This is, moreover, an area which is important to analyze with particular attention, since it is probable that the planned works will have there an important influence.

In zone 3, the regional departments of environment undertook beach nourishment activities, by placing sands as a coastal reinforcement. According to the empirical experience, confirmed in the present case, the sand that was deposited in this beach was dragged to the mooring area by the effect of the SW waves, so, throughout the tidal range in this zone, there was an erosion of all the material deposited there. Above the level of variation of the tide, there was deposition of sand.

Zone 4 corresponds to São Francisco Dock. In this zone, in the period between the two general surveys, the works of establishment of the referred dock were concluded. Thus, there was no erosion here—it is likely that relatively high silting will occur—but rather a dredging for the establishment of the referred port infrastructure.

The section upstream of the San Francisco Dock and the fishing port and downstream from the road bridge defines the zone 5. Within this area, the erosion is very small, and there is also a small sedimentation under the quay bridges and at the downstream end of the sandbank.

Zone 6 is a muddy, sandy-muddy zone, with a general elevation between low tide and full tide, and is thus under water and out of water in all tide cycles. This zone toggles between erosion and deposition of sediments but always with a very low value, being almost in balance in the current situation.

Zone 7 is usually a zone of erosion, a tendency that was increased after the construction of the Marina of Portimão, on the right bank of the Arade River, with the consequent narrowing of the channel. The sediments eroded in this Zone will generally be deposited in the mooring area.

Zone 8 corresponds to the inlet, and the erosion observed there, of the order of 10 cm, is not significant and may be linked to periodic phenomena of storms and, consequently, higher flow speeds in the inlet. It can be considered that this area is almost in equilibrium.

Regarding some of the areas where apparently sedimentation occurs, such as the fishing port, the sediment deposition trend has already been discussed above and related to the observed erosions.

As for the four areas where sedimentation occurs, referred as zones A–D and referenced in **Figure 12c**, these have the greatest interest for port management.

Zone A corresponds to the downstream end of the existing sandbank in front of the central zone of Portimão and is located where the channel widens, with consequent slowing of the flow velocity which results in a reduction of the capacity of solid transport of the river. One of the planned works in the new layout is the dredging of the referred sandbank. There will be an increase of the tide prism, but as the flow section increases, it is not sure if the flow velocity will decrease; as it is possible that there will be a reduction in erosion in the area of the current sandbank, it is important to analyze this area regarding the eventual hydrodynamic change. So, a careful analysis of foreseeable speed variations will be carried out.

Zone B, corresponding to the commercial wharf and the maneuvering basin, is the widest zone in this section of the estuary, where, therefore, the flow velocities decrease, as well as the transportation capacity of the flow, with significant rate of sedimentation.

Zone C is a particularly sensitive zone. In fact, the alternation of the erosion and deposition zones, which are always of small thickness, suggests that the system is close to equilibrium in the navigation channel within this Zone. However, there is a marked deposition both at the entrance to Portimão's marina, on the right bank, and along the left bank of sand, which will be dredged to carry out the planned arrangement of the Ferragudo marginal. Thus, the width of the channel in this section will increase, and it is necessary to carefully analyze what will happen with the flow velocities, especially in the area of the navigation channel.

The zone D, corresponding to the first section of the navigation channel, and the mooring area, is subject to heavy siltation since it is the widest area of the estuary, and that is downstream of areas of substantial erosion, namely, zones 3 and 7.

The histogram (**Figure 13**) shows the distribution of erosion and sedimentation from 2000 to 2003, using ArcGis Space Analyst. Almost all of the values are between −1 m (erosion) and +1 m (sedimentation). Values outside this range correspond, in fact, to one-off dredging interventions or landfill works. Even in the −1 to +1 m interval, part of the values was caused either by dredging or by land filling.

A more detailed analysis of the results is shown in **Figures 14** and **15**. **Figure 14** presents the same results of **Figure 15b** and **c** but superimposed on the hydrography of 2003.

The direct comparison of the two situations, on the section of the navigation channel between the commercial dock and the Marina de Portimão, shows a mixing of the deposition and sedimentation areas. Considering **Figure 14**, where the section in reference is presented in more detail, both the erosions and the settlements have an absolute value inferior to 0.5 m throughout the zone. The analysis of the right-hand side of this same figure suggests that, in general, this absolute value for erosions and sedimentation is, in fact, less than 0.20 m. It also suggests that an interchange occurs at short distance (distances of the order of the metre) between erosion and sedimentation, with the exception of the river bank areas, where, in fact,
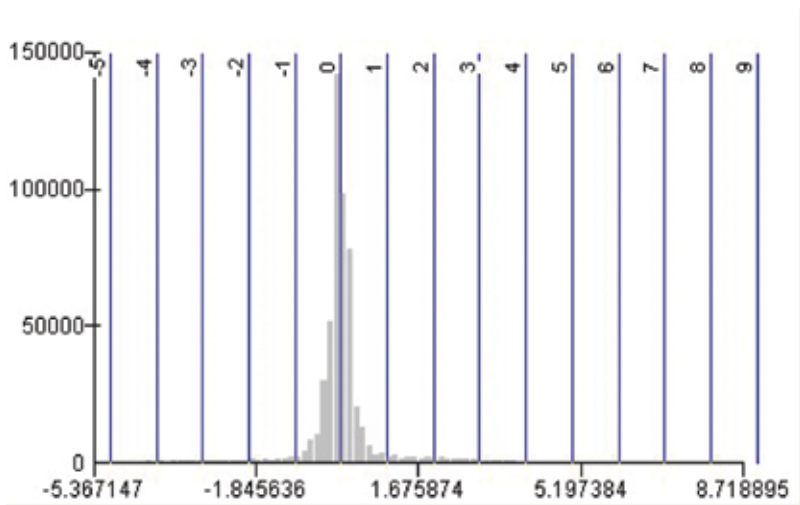
Figure 13. Distribution histogram for the thickness of erosion and sedimentation.
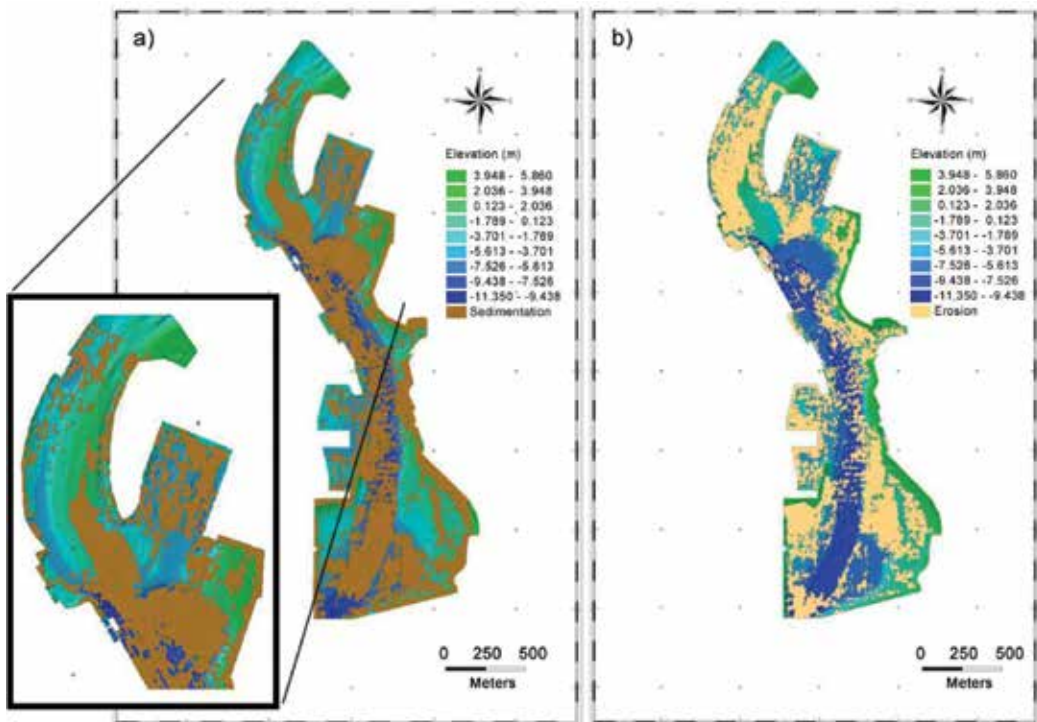
Figure 14. (a) Sedimentation areas on the 2003 hydrography and (b) Erosion.

only sedimentation is observed, with a value between 0.20 and 0.50 m. Thus in this section of the channel, a relative stability is observed, and the described sedimentation and erosion pattern is due to sediment drift in the bottom of the canal, caused by the tide, as well as the propellers of the vessels.
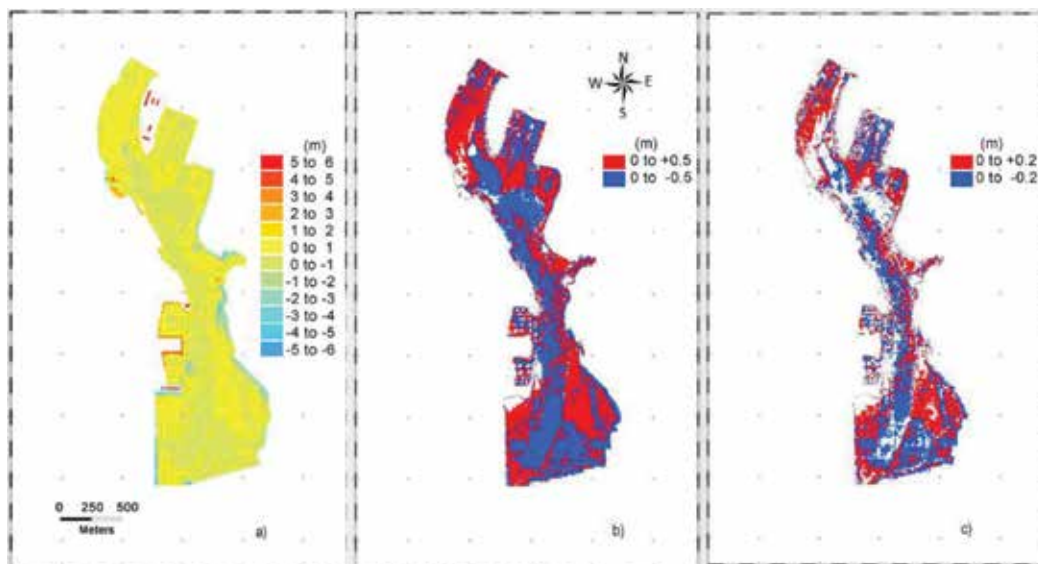
Figure 15. (a) Total erosions and sedimentations, 1 m intervals, (b) erosions from 0 to −0.5 m and sedimentations from 0 to +0.5 m, (c) erosions from 0 to −0.20 m and sedimentations from 0 to +0.20 m.

Another area that deserves a careful analysis is the one that constitutes the section, limited upstream by the road bridge and downstream by the south end of the maneuvering basin. The observation of **Figure 14** shows that there is a high erosion rate in the channel, but not in the sandbank, probably due to the small channel width between the shallows in front of the shipyards and the central zone of Portimão, where higher flow speeds are verified.

Downstream, with the widening of the flow section, the velocities decrease, and a strong sedimentation of 0.50 m in the canal and in the maneuver basin is observed. That is to say, the sandbank is moving downstream, which is a serious problem for the management of the port. It is necessary to consider the complete removal of this sandbank or at least a dredging intervention that would establish a balance, without sedimentation or erosion, in the sandbank section.

As can be seen from **Figure 15**, in the navigation channel and the anchoring area at the southern end of the estuary, most of the erosions and sedimentations are of the order of 0.20 m; however, in some localized areas, higher values are observed. But in the navigation channel, throughout this section, the sedimentation is always on the order of 0.50 m.

In the bar itself, erosions reach, for this same period of 3 years, values of 0.50 m.

3.4. Simulation for layout changes

After the calibration of the model for the reference situation, it was applied to the new layout, changing accordingly the topography and hydrography of the harbor. The new layout

includes a new marina, the reshaping of the river bank downstream Ferragudo and the deepening of the navigation channel in order to allow larger ships.

Regarding the sandbank area, a dredging level of −1 m ZH was considered. However this value is not yet final. In the analysis of the obtained results, it will be discussed which would be the most advantageous level for dredging, from the hydrodynamic point of view. **Figures 16–18** present some relevant results obtained for the whole harbor.
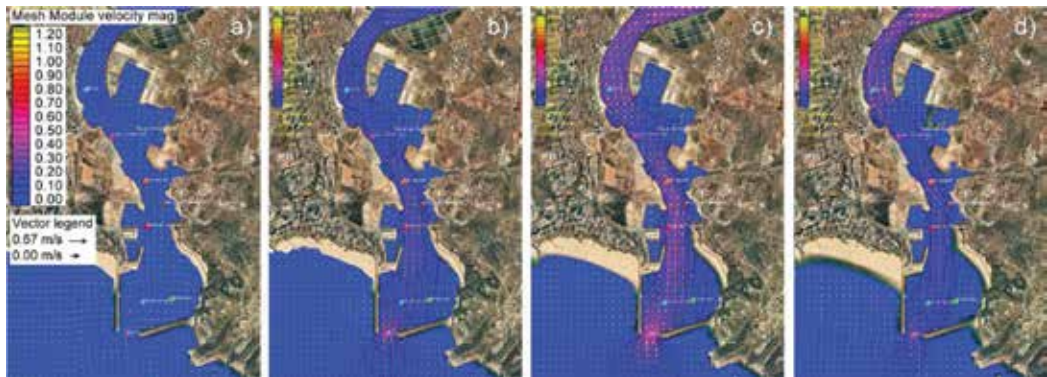
Figure 16. Modeling with the new layout. Results for ebb tide: (a) 50, (b) 51, (c) 53 and (d) 55 hours (see **Figure 12**).
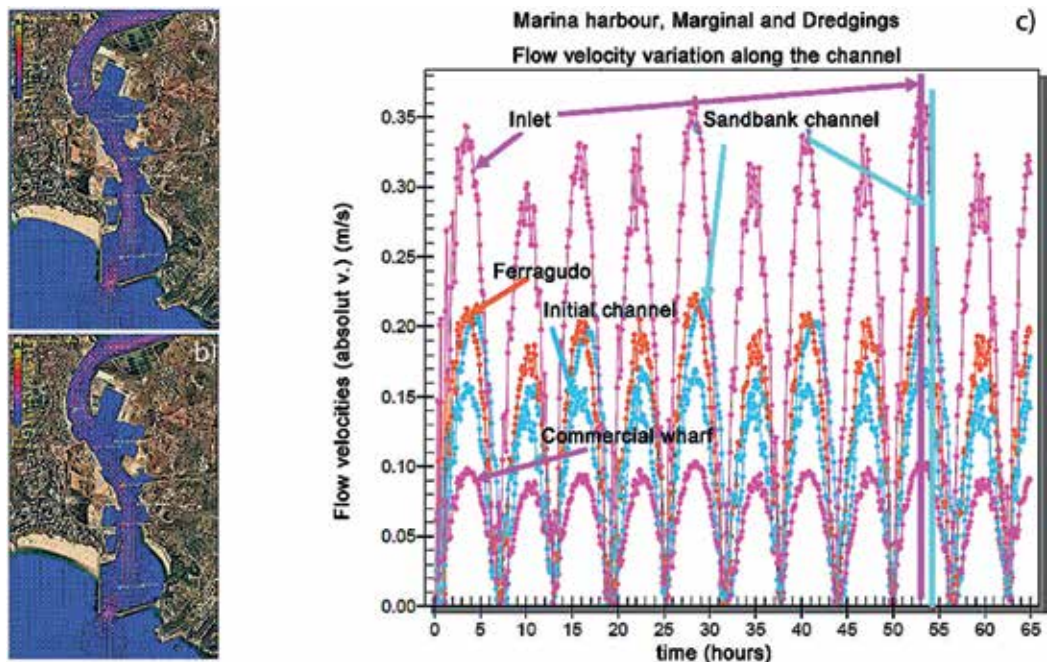
Figure 17. Modeling with the new layout. The delay of the peak velocity in ebb tide (c), between the harbor inlet and the sandbank (a) 53 and (b) 54 hours.

Figure 18. Modeling with the new layout. Results for the flood tide: (a) 58, (b) 59, (c) 60 and (d) 61 hours.

4. Results

According to the mineralogy and grain size of sediments, the longshore transport of sediments only affects this estuary near the inlet, more precisely in the mooring area, due to SW waves. In this particular case study, the longshore transport and the waves have no significant
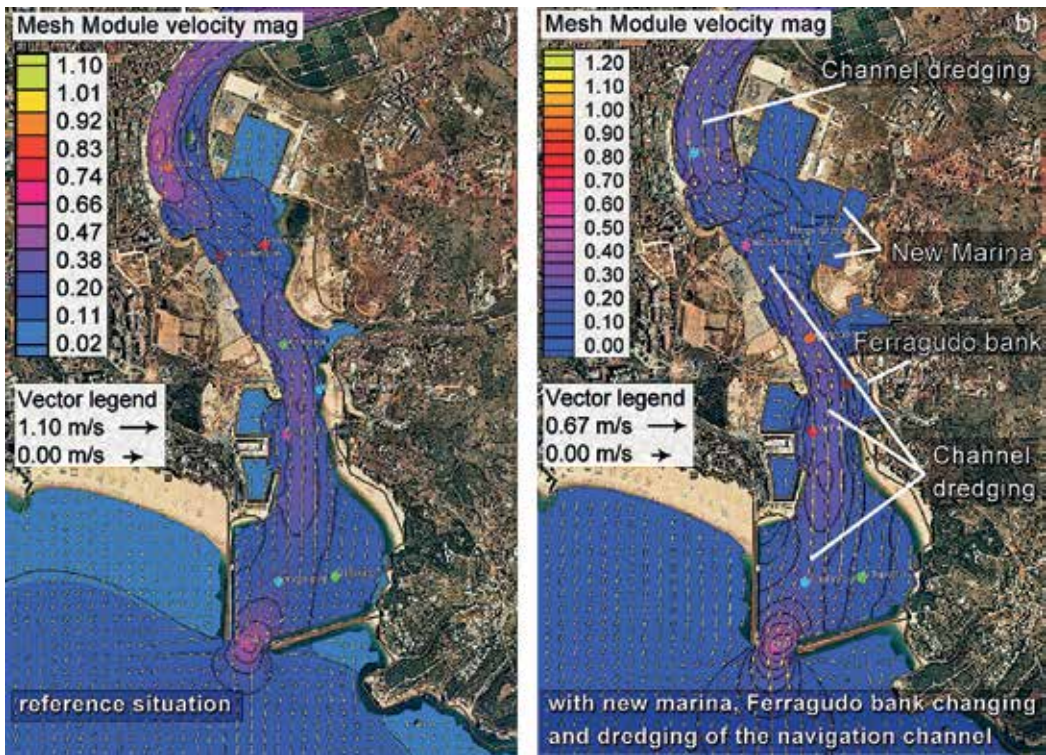
Figure 19. The estuary, in the peak of ebb tide (53 hours), (a) for the reference situation and (b) for the new layout simulation.

effect in the main part of the estuary, and so the referred influences were not considered in this analysis. However, taking into account the new layout, **Figure 19**, it can be observed that the construction of the new marina affects the main flow in the channel leading it to the right bank, downstream of the commercial wharf.

The new shape for the Ferragudo river bank will increase the flow velocity near the left margin. Also the flow, as being diverted by the promontory of the castle of S. João towards the right bank, will increase the velocity near the entrance of the Marina of Portimão; moreover, there is an flow velocity increase, upstream of the São Francisco dock, in the area of the sandbank, due to its dredging to −1 m. The planned dredging will have a significant influence on the flow in the sandbank area, where the flow will be more evenly distributed over the whole width, with a significant reduction of the maximum speed that occurred in the reference situation in the channel near the right bank of the river (**Figure 20**).

In front of the commercial wharf, and the new marina, is located the maneuvering basin of the harbor; as a consequence of the increase in the ships draft that is aimed, and also due to the construction of the new marina, this area will be dredged, and so it will present a larger water section. As it can be seen from the velocity variation from the reference situation, there will be a still significant decrease in the velocity in this area.

As for the maneuvering basin, **Figure 21**, there is also a clear reduction of the velocity; the peak velocity values obtained for the ebb tide were 0.076 m/s and for the flood tide 0.063 m/s.
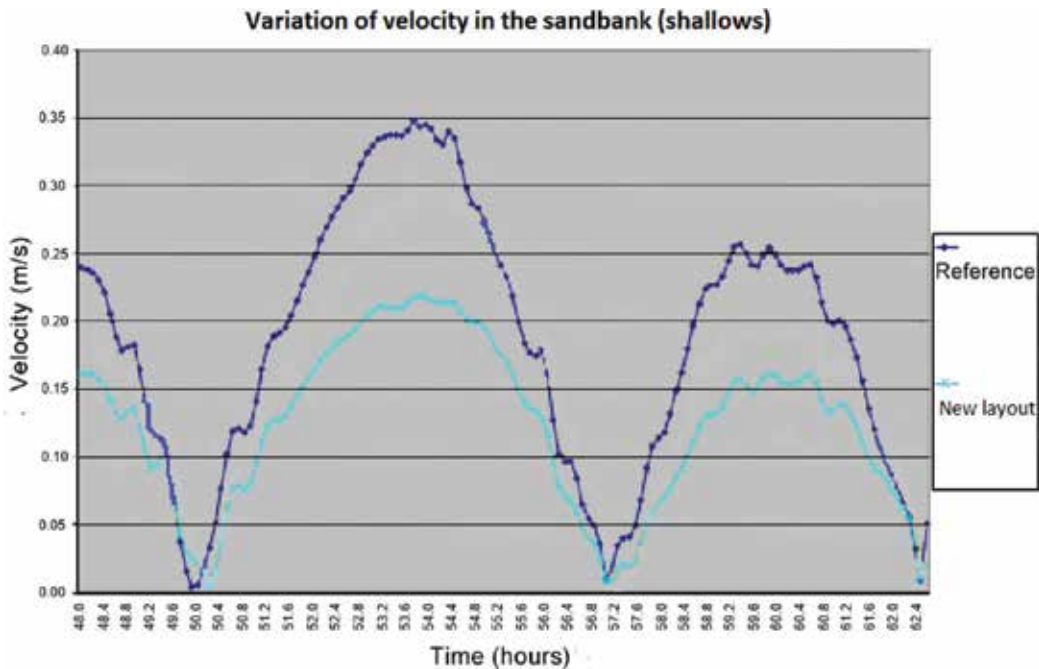
Figure 20. Upstream of the study area, in the sandbank in front of the town, the dredging of that sandbank will reduce significantly the velocities (velocity in absolute value).
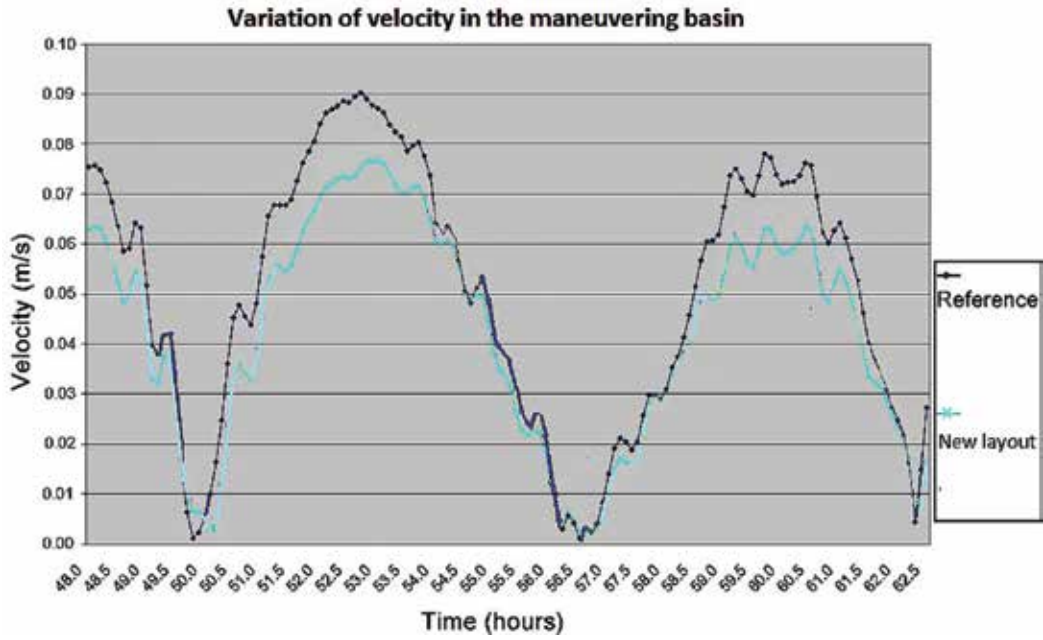
Figure 21. It can be seen from the velocity variation that there will be a still significant decrease in the velocity in this area (velocity in absolute value) and so an increased sedimentation.
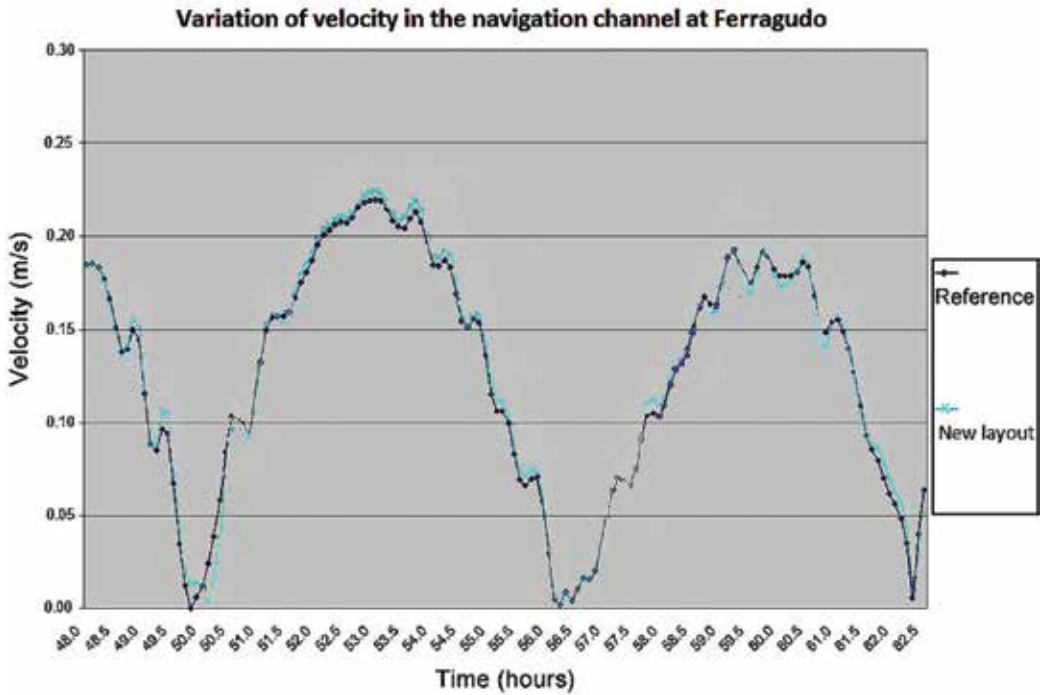
Figure 22. In front of Ferragudo, the velocity is almost unchanged (velocity in absolute value).
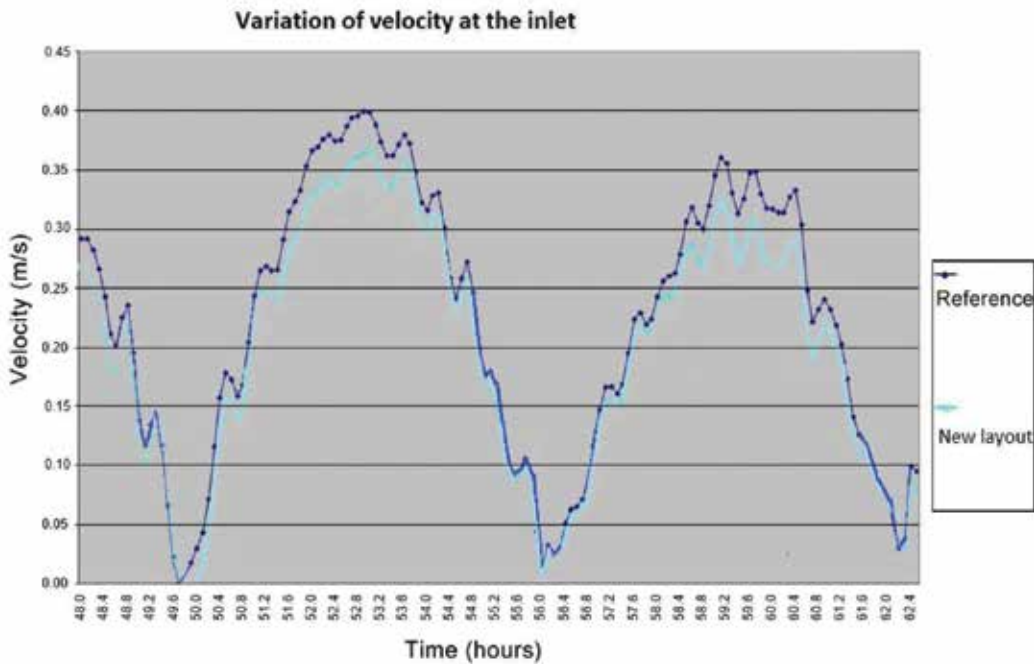
Figure 23. At the inlet the velocity will decrease slightly (velocity in absolute value).

The navigation channel, in front of Ferragudo, **Figure 22**, presents almost no velocity variation from the reference situation to the final layout situation. This is due to contrary effects of the various interventions planned for the harbor: on one hand, the dredging of the channel will increase the section flow and, so, decrease the velocity, and on the other hand, the works upstream, marina, sandbank, by example, will increase the tide prism upstream this analysis point and so increase the velocity. The referred effects, opposite to each other, cause almost no variation in velocity.

After the planned work completion, the predicted peak velocity of the ebb in the inlet is 0.36 m/s. In the flood, the peak velocity, which in the reference situation was 0.36 m/s, will then change, with the three interventions performed, to 0.32 m/s (**Figure 23**). So, at the inlet the velocity will decrease slightly, and so an increase in sedimentation and consequently of dredging should be expected.

Analyzed situation	Ebb maximum velocity (m/s)			
	Sandbank	Maneuvering Basin	Ferragudo	Inlet
Reference situation	0.350	0.090	0.220	0.400
New layout	0.220	0.077	0.225	0.365

Notes: ▇ Ref. situation erosion zone; ▇ Ref. situation limited erosion zone; ▇ Ref. situation equilibrium zone; ▇ Ref. situation sedimentation zone.

Table 1. Result summary.

Table 1 presents, for the four reference sections above mentioned, the ebb maximum velocity in the reference situation and in the simulation considering the new layout. It presents also, for the reference situation, if each zone presents erosion and sedimentation or is in equilibrium.

5. Conclusions

As stated, harbors are, whenever possible, established in estuaries to take advantage of the existing natural safety and protection conditions. But to keep harbors in a safe and usable way, periodic dredging works are carried out. The expansion of harbor's activities and the growth of maritime traffic may lead to changes in the harbor's layout or to improvements of navigation channels and basins depths. Such adjustments entail changes in estuarine hydro-dynamics, and therefore the usual dredging rates are subject to alteration, namely, tending to increase. It is then important to assess the influence of a harbor's new layout on the solid transport pattern and how its effects can be minimized, aiming the reduction of economic and environmental impacts. Within this context, in this chapter estuary hydrodynamics and sedimentation-erosion patterns were summarized. Also, the modeling methodology for planning and management of dredging works which uses geo-processing automatic GIS environment, developed by the Portuguese harbor authority, was presented. Finally, the case study of harbor of Portimão was also described showing the implementation of the referred methodology.

The method presented to estimate erosion and deposition ratings, and so allowing to plan dredging works, has proven its usefulness and proved to be of easy implementation. In the case study presented, it allowed to identify the areas where the hydrodynamic changes will likely increase sedimentation and also where no change or an increase of erosion should be expected. Lower velocities will mean higher depositions and, accordingly, a greater volume to dredge. Anyway its application must be careful, as it is important, besides the use of adequate topographic surveys, to know where, in the time period of those topographic surveys, dredging works were carried on, as well as the volumes dredged.

Also the hydrodynamic pattern of the harbor is of the uttermost importance, mainly when a changing in the harbor layout is planned, in order to forecast the changing in the erosion deposition rates in the different harbor zones.

Author details

Alexandre M.G. Santos Ferreira* and Cláudia S.N. Santos

*Address all correspondence to: sferreira@dgrm.mam.gov.pt

DGRM, Directorate-General for Natural Resources, Safety and Maritime Services Lisbon, Portugal

References

[1] Santos Ferreira AMG, Trigo Teixeira AA. As novas infraestruturas portuárias no estuário do Arade: influência prevista na hidrodinâmica estuarina. In: Proceedings of the 6th Jornadas Portuguesas de Engenharia Costeira e Portuária, 8 and 9 Oct 2009, Funchal, Portugal, 16 p (in Portuguese)

[2] Silva APF, Santos-Ferreira A, Dias E. Análise multitemporal e morfodinâmica no estuário do Arade com geoprocessamento automático. In: Proceedings of the 1st Jornadas Hidrográficas, IH, 21 and 22 Jun 2010, Lisbon. pp. 251-254 (in Portuguese)

[3] Trigo Teixeira AA, Santos Ferreira AMG. Erosão e sedimentação no estuário do rade. Interpretação da evolução com consideração da hidrodinâmica estuarina. In: Proceedings of the 1st Jornadas Hidrográficas, IH, 21 and 22 Jun 2010, Lisbon. pp. 255-258 (in Portuguese)

[4] Santos-Ferreira A, Dias E, Trigo Teixeira AA, Silva APF. Análise morfodinâmica por geo-processamento automático: aplicação ao planeamento de dragagens no porto de Portimão. In: Proceedings 6th Congresso Planeamento e Gestão de Zonas Costeiras de Países de expressão portuguesa, 4-8 Apr 2011, Boavista Island, Cape Verde. 14 p (in Portuguese)

[5] Dias E. Utilização de um Sistema de Informação Geográfica na Caracterização de Áreas de Dragagem [thesis]. ISEGI, UNL, Lisboa (Portugal). 2005. 150 p. (in Portuguese)

[6] Santos-Ferreira A, Dias E, Silva APF, Santos C, Cabral M. Dredging of Vila do Conde harbor, Portugal – Contamination of sediments. In: Proceedings 8th International

[7] Santos-Ferreira A, da Silva APF, Dias E. Harbor geotechnics: The case of the Portuguese small Harbor. In: Proceedings of GeoHubei International Conference 2014 – Sustainable Civil Infrastructures: Innovative Technologies and Materials, Yichang, Hubei, China, 20-22 Jul 2014. Application of Nanotechnology in Pavements, Geological Disasters, and Foundation Settlement Control Technology, GSP 244. 2014. pp. 78-85 (© ASCE 2014)

[8] Santos Ferreira AMG. Impacte do Plano do Porto de Portimão na Hidrodinâmica do Estuário do Arade [thesis]. IST – University of Lisbon; 2006. 145 p (in Portuguese)

[9] Weinholtz MB. Estudo da Situação do Troço Terminal do Rio Arade a Jusante das Pontes e Zona marítima Frontal após a Conclusão da Primeira Fase das Obras Portuárias. Lisbon: Direcção-Geral de Portos; 1985 (in Portuguese)

Sedimentary Processes and Sedimentation in the Shallow Offshore, Eastern Niger Delta, Gulf of Guinea

Prince Suka Momta

Additional information is available at the end of the chapter

Abstract

The Cretaceous Afikpo sedimentary Basin in Southeastern Nigeria contains rocks of fluvial, deltaic and shallow marine origin. This study examines the role of sedimentary processes in sediment distribution in the various geologic environments. The outcrop sections and the Afikpo River were studied by visual observation and photographing of important features during a field mapping exercise. Well log data from the Niger Delta Basin were also used to infer depositional environments based on gamma ray log motifs. These outcrop sections consist of fluvial, deltaic and shallow marine sediments that occurred as braids, point-bars, mouth-bars and beach/regressive bars. Braids and point-bar deposits also occurred within the recent Afikpo River channel, a major conduit transporting sediments to the offshore area of eastern Niger Delta. Sandstone outcrops showing a mouth-bar architecture occurred at Akpoha Town east of Afikpo Town, with a shallow marine sequence at Amasiri area, west of Afikpo Town. The Amasiri sandstone is a massive outcrop with large lateral extent covering more than 8 kilometers. Gamma ray log trends observed on well log from offshore area in the eastern Niger Delta indicated deposits of fluvial, deltaic and shallow marine origin.

Keywords: Afikpo Basin, cross river, fluvial, sedimentation, Niger delta, shallow offshore

1. Introduction

The Gulf of Guinea has recently received tremendous attention from both the oil companies and the academia for several decades due to increasing hydrocarbon discoveries in the region. To maximize production from offshore reservoirs, there is the need to properly understand the processes of sedimentation and the consequent depositional architecture of facies and their distribution within the marine realm. The two major rivers (Niger and Benue rivers) in Nigeria

are of significance in the distribution of sediments in the east and western offshore area of the country. The Niger River is active and supplies sediments toward the western part of the Niger Delta, whereas, the Benue River concentrates sedimentation in the eastern offshore (**Figure 1**) area. There are subsurface evidences of the occurrence of ancient river channels and canyons that served as conduits for transporting sediments from the continent to the Gulf of Guinea [1]. These sedimentation processes are still active today and sediments keep building out along the shores and on the continental shelf of the Niger Delta. We will look at the outcrop evidence of fluvial and marine sandstones at Afikpo Town, and trace the course of the Cross River from Afikpo (**Figure 2**) to the coastal town of Calabar where presently these sediments are deposited into the estuaries and open marine environments. The subsurface occurrence of shallow marine facies will serve as analogue to the outcrop exposures of marine sandstones in the Afikpo basin. The eastern offshore of the Niger Delta occurs within few kilometers away from the active volcanic line of the Cameroun Mountain. The geomorphic features and surface processes in this region are of interest to most researchers and enables the paleo-reconstruction of subsurface sediments of Tortonian age in the offshore area. The adjacent highland areas consisting of the Precambrian basement of the Oban Massif, Obudu Plateau and the Cameroun Mountain form the sources of weathered sediments that are transported through the Great Kwa and Calabar Rivers to the offshore area south of Calabar Town, South Eastern Nigeria [2]. These rocks are weathered, highly fractured, foliated, and exposed by stream channels cutting through them [2]. They from the major provenance of sediments deposited within the shallow to deep offshore through submarine canyons. In this paper, we will consider a major tributary

Figure 1. Map of Africa showing the location of Afikpo town and the Cross River flowing south-ward into the Gulf of Guinea.

Figure 2. The river configuration within Afikpo town, SE Nigeria.

of the Benue River, the Afikpo-Cross River, which transport sediments from the hinterland in eastern Nigeria to the eastern offshore area of the Niger Delta. We will discuss the continental, deltaic and shallow marine processes, sediments and their responses from both outcrop and subsurface data. A consideration of the subsurface architecture of shallow marine sediments from the eastern part of the Tertiary Niger Delta sedimentary basin will also be made. The study and understanding of sedimentary processes and their responses have serious economic, environmental and mineral exploration significance.

2. Sedimentation processes

Generally, there are two major rivers in Nigeria that run through the country with several tributaries. They are; the Niger and Benue rivers. The Niger river empties into the Atlantic Ocean in the south- western axis of Nigeria, whereas the Benue River in the southeastern part. These rivers supply sediments to the Gulf of Guinea. The active river system controlled by climate and topographic landscapes accounts for sediment distribution within the continent and offshore areas. Along the stream and river channels there are serious mining of these sediments used for construction purposes. Generally, sites for sand deposition fall into three main categories: 1. the alluvial fan province which is an area proximal to the base of mountains and high-altitude rock outcrops which serve as the major sources of high sediment supply to the rivers. These outcrops include; the weathered Cretaceous rocks of Afikpo Basin and other basement rocks from Obudu Plateau, the Oban Massif and the Cameroun Mountain 2. channelized braided stream sediments and associated overbanks, and, 3. meandering stream province

that finally discharges into the open sea. The alluvial fan sediments occurred in the hinterland proximal to the Afikpo Basin sedimentary rock outcrops and the basement rocks of the Oban Massif. The Afikpo-Calabar River south-east of Afikpo Town in the South-eastern part of Nigeria possesses high sediment loads that account for the braids deposited within the channel in this area. This area is highly prone to river bank erosion that claims parts of adjacent farmlands (**Figure 3**). This river maintains a straight course from Afikpo area through Adim town to Etono where the river meanders in the south-west direction as it flows towards Iyakpan. The general trend of the river from Afikpo to Calabar is in the NE-SW direction.

2.1. Braided stream

Braided stream sediments occur within Afikpo Town in both ancient outcrop section and within the recent Afikpo-Calabar River course (**Figure 4**). The formation of braids usually occurred in areas proximal to sediment provenance with high sediment supply and stream gradient. The channel within this region possesses steep gradient with variations in stream discharge' eroding the river banks at Ndibe Beach (**Figure 3**) and adjacent lands along the entire river course. The river channel is constantly expanding due to this erosion and has exceeded 100 m in width within Ndibe Beach (**Figure 3**). The region generally possesses uneven topography due to tectonism and differential weathering of the basement rock along the river channel [2]. The Cretaceous sandstone outcrop in the Afikpo Basin revealed this multi-story braided sediments stacking into about eight braids (**Figure 4**). These braided stream deposits reflect high sediment supply within the stream channel, great proportions of suspended and bedload load sediments which are the main controlling factors on the development of the ancient river that transported the sediments. Fluvial sediments are widespread in outcrop exposures in Afikpo Town and the various stream sedimentary features at various points along the channel are obvious in the outcrop sections in the area.

2.2. Meandering channels

There are more than seven major meandering loops along this river from Afikpo to Calabar Area (**Figure 5**). The degree of meandering along this river course increases downstream as it

Figure 3. Ndibe Beach, Afikpo-Cross River area: latitude N05°50′30.4″; longitude E-007°56′55.6″; elevation is 17 m. The width of the river is more than 100 m. The banks of the river in this area is prone to constant erosion.
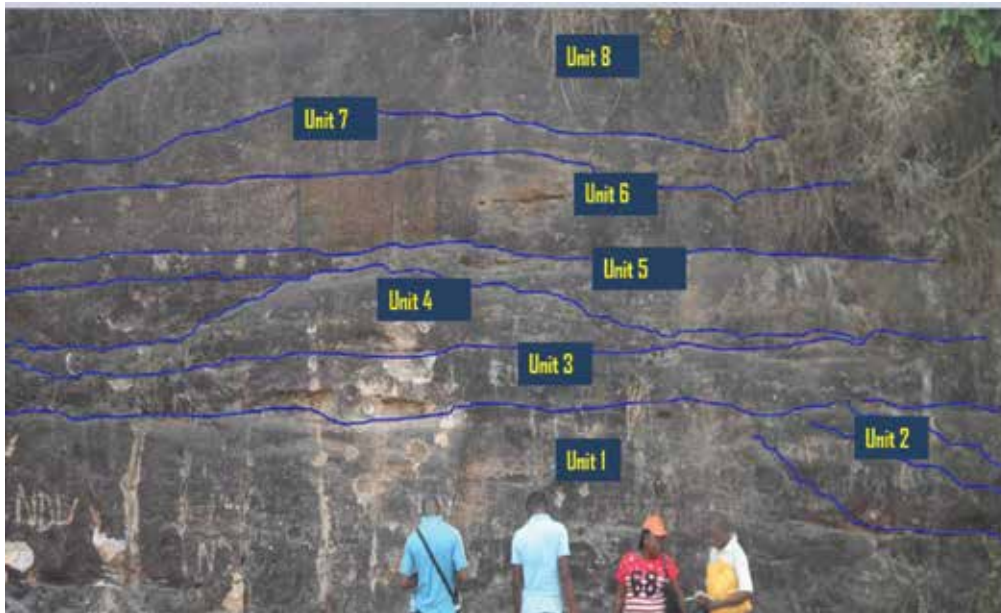
Figure 4. Stacked multi-story braided channel deposit at MacGregor Hill, Afikpo, SE Nigeria.

approaches Calabar area in the Niger Delta (**Figure 5**). This river and its tributaries forms the major sediment transporting conduit to the offshore area in the south-eastern Niger Delta and to the Gulf of Guinea. Site for more sediment accumulation within the meandering system is the point bar characterized by poorly sorted, coarse to very coarse-grained sands with gravels deposited in the deeper parts of the meander belt by a slow-moving water along the curve (**Figure 6**). It grades upward into a very fine grained well-sorted sediment from the deeper part of the channel towards the shallow section with reduced current flow. The amount of suspended sediments guaranteed the deposition of fine grained sands along the meandering curve prompting a swift transition from braided deposition to a meandering configuration. The areas experiencing high degree of meandering along the river course include; south of Afikpo Town, Etono area, Iyakpan, Itu and Ayadeghe with waning energy as it approaches Calabar Town where the river empties into the open sea to deposit its sediments. These sediments are moved oceanward into the Gulf of Guinea through canyon. Some are distributed within the shores by waves, longshore currents and other marine energy fluxes to form beaches as can be seen in Ibeno Beach south of Eket Town in Akwa Ibom State, west of Calabar Town. The ancient river deposits within the shallow offshore in the eastern Niger Delta have been identified from subsurface data [3].

2.3. Deltaic deposits

The marine portion of the outcrops in Afikpo marks a transition from a more fluvially influenced sedimentation to a deltaic process. This is evident in the isolated lobes of sandstone outcrops that occur within Akpoha area west of Afikpo Town (**Figure 7**). It may possibly be a
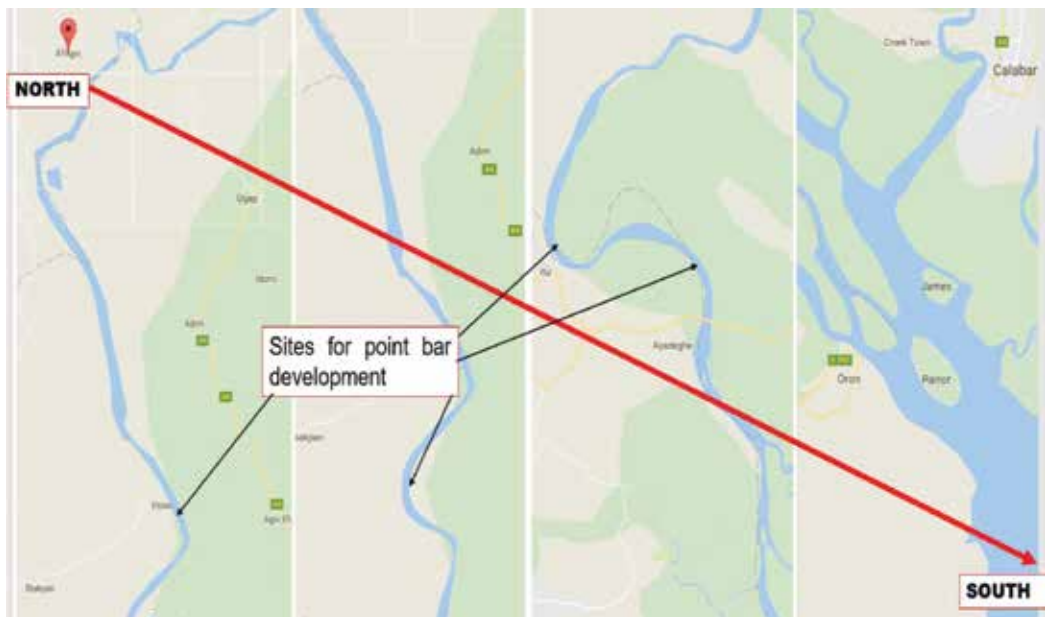
Figure 5. Meandering points along the river course from Afikpo town to Calabar. The degree of meandering increases in the south-east direction as the river approaches the sea.

Figure 6. Meandering channel deposit: Fining upward point bar channel deposits showing lag base with very coarse grained, pebbles and gravels (cretaceous sandstone of Afikpo Basin, south-eastern Nigeria).

mouth-bar deposit that occurred towards the end of a distributary channel. It consists of two facies units: a massive planar bed overlying a mega trough cross-beds facies of between 250 and 300 cm thick (**Figure 7**). The sandstone is underlain by mudstones and shale portraying a coarsening upward sequence in grain size typical of a deltaic environment. A shoreface shallow marine section is observed in the Cretaceous age Amasiri sandstone (Afikpo Basin) showing a large lateral extent of more than 8 km with thickness greater than 100 m (**Figure 8a** and **b**).

Figure 7. Massive planar beds underlain by cross-bedded sandstone (250–300 cm thick). The sandstone is underlain by marine shale—Deltaic environment.

Figure 8. (a) Regressive barrier bars (Amasiri, Afikpo Basin, SE Nigeria). Thickness: over 100 m; width: 3 m; length: (more than 8 km). These regressive bars are underlain by marine shales, (b) shallow marine regressive Amasiri sandstone in Afikpo Basin, SE Nigeria. It is laterally extensive and runs parallel to paleo-coastline. The thickness is above 70 m, more than 3 m in width. N05°53′09.9″; longitude E-007°52′15.4″. Elevation is 67.8 m.

3. Subsurface sedimentary analogue of eastern offshore Niger Delta

Stratigraphically, the Niger Delta Basin has three formations. They include; Akata Formation, a prodelta marine shale which is the basal unit; the Agbada Formation, a paralic sequence of

shale and sandstone beds occurring in almost equal proportions, which forms the hydrocarbon habitat in the basin, and finally the youngest continental Benin Formation comprising of loose fluvial sands and gravels [4–10]. There are four unique Members that occur within the Agbada Formation in the eastern offshore Niger Delta. They include; the Qua Iboe Shale, Biafra Member, the Rubble Bed, and the D-1 Sand [3]. The Qua Iboe Shale (QIS) is identified on well log as the first continuous shale interval that occurred towards the base of the continental Benin Formation. The well data used for this study were taken from an oilfield located in the shallow offshore area in the eastern part of the Niger Delta sedimentary basin. The location is about 4 km away from the Calabar Town, just at the mouth of the major estuary where most sediments from the continent are deposited and consequently transported to the deep sea in the Gulf of Guinea.

Studies of modern sedimentary environments revealed that vertical profiles of grain size from a specific environment have certain log characteristics [11–14]. For instance, prograding deltas and barrier bars deposit display an upward-coarsening grain size profiles (**Figure 9**). Three prominent trends identified on well log that helped to delineate the various depositional settings are: coarsening upward trend representing deltaic facies (**Figure 10**, number 4).; fining upward trend showing transgressive facies (**Figure 10**, number 1 and 5), boxcar gamma ray log motif of regressive barrier bar/beach deposits (**Figure 10**, number 2 and 3).
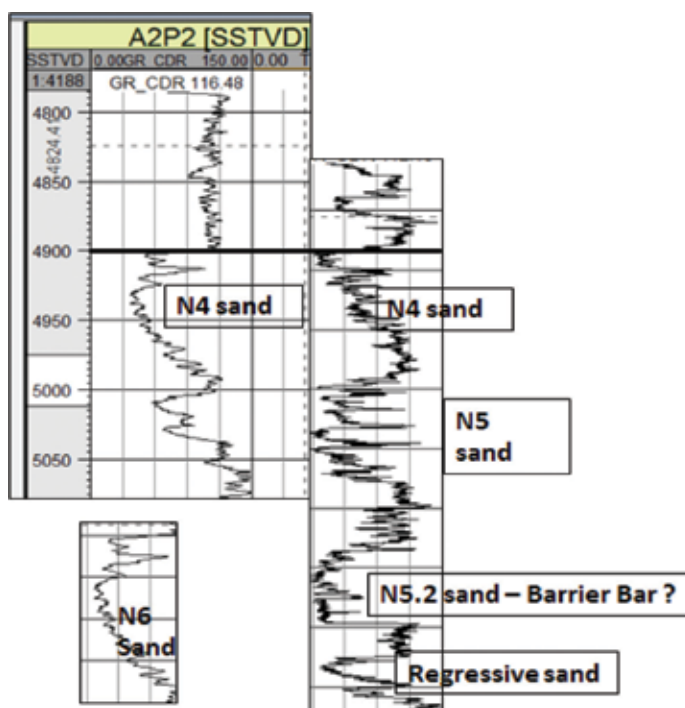
Figure 9. Electrofacies patterns showing some distinct depositional environments.
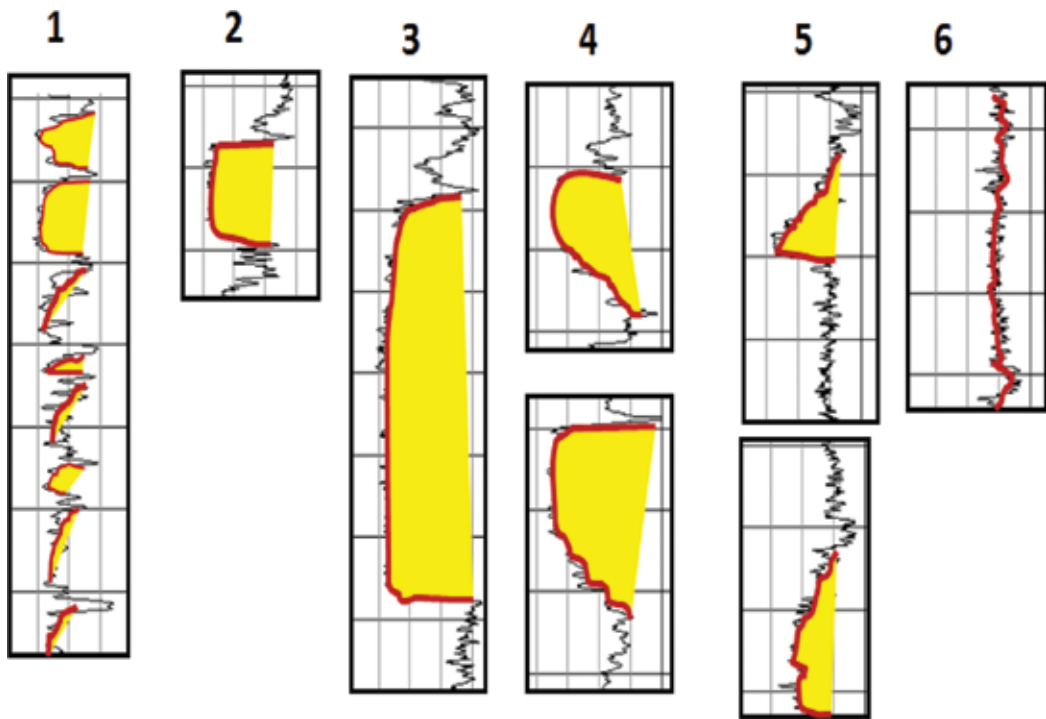
Figure 10. Specific gamma ray log trends in the study area.

3.1. Gamma ray log facies description

Seven main gamma-ray log characteristics (**Figure 11**) have been established using gamma-ray log trends; (1) spiky or mixed (2) blocky and coarsening-upward (3) blocky and fining-upward (4) coarsening upward (5) fining upward (6) erratic and (7) blocky [3]. The log facies descriptions below are used to infer genetically related environments. The gamma-ray electrofacies patterns represent environments that range from deltaic front to shallow marine setting.

Electrofacies 1: This facies is characterized by spiky or mixed gamma ray log signature, which may represent middle or lower deltaic plain environment (**Figure 11**).

Electrofacies 2: This facies consists of both a blocky pattern in association with a coarsening-upward trend. The repeated blocky pattern may represent amalgamated fluvial (distributary) or estuarine channels, whereas coarsening upward shows seaward progradation of continental sediments (**Figure 11**).

Electrofacies 3: This unit has a sharp lower contact with a weak fining upward trend at the upper boundary displaying a blocky shape typical of distributary channel or tidally influenced delta (**Figure 11**) [3].

Electrofacies 4: This unit displayed a spiky and coarsening upward gamma ray log motif that may represents a prograding deltaic or a delta front facies (**Figure 11**) [3]. The environments
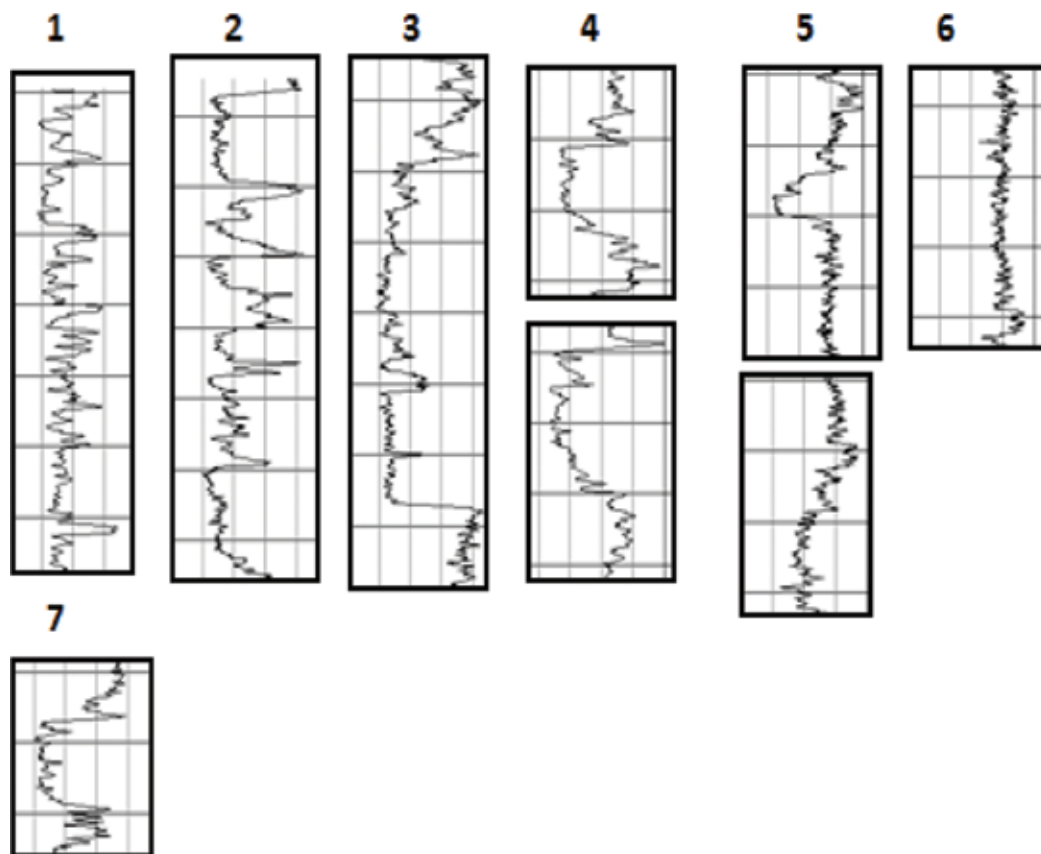
Figure 11. Gamma ray log motifs in association.

depicted by this trend could be shoreface, tidal or mouth bar. By the methods reported in [15], the environments of coarsening upward successions can be classified into three general categories: (1) prograding submarine fans (2) regressive barrier bars, and (3) prograding deltas or crevasse splays [3]. Prograding submarine fans and regressive barrier bars are commonly associated with glauconite and shell debris [3, 11, 15, 16]. Glauconite debris occurred in all the samples from about 1800 ft. in all the wells, consequently, there is the possibility of the first two environments (regressive barrier bars or prograding submarine fans) occurring in the field. Deductively, the paleoenvironments of funnel shape facies can be attributed to shallow marine and deltaic front environments. One of the major difference between a prograding delta and a crevasse splay is the scale of deposition; the scope of a prograding delta is comparatively large. The work of [11, 15], shows that environments of funnel-shaped successions with the presence of carbonaceous detritus may be depicted a prograding delta or a crevasse splay [3]. The average thickness of the thin funnel-shaped successions in this work is less than 800 cm, which suggests that the paleoenvironment could be a crevasse splay associated with a deltaic channel. A scale of less than 800 cm is comparatively small to be classified as a prograding delta [3].

Electrofacies 5: The unit characteristically displayed sharp lower contact with a gradational upper boundary (**Figure 11**). It is a transgressive unit. The bell-shaped succession usually occurs in three types of environments: tidal channels, turbidite fills and fluvial or deltaic channels. Tidal channels and turbidite fills also commonly include glauconite and shell debris [16]. The only bell-shaped successions with carbonaceous detritus are deposited in environments of fluvial or deltaic channels [11].

Electrofacies 6: This is erratic in nature. It may represent a lower deltaic plain to shallow marine shelf deposits.

Electrofacies 7: The electrofacies of this unit shows sharp upper and lower contact (blocky) [3]. The thickness of the boxcar gamma ray log motifs in all the studied intervals is less than 25 m [3]. Mudlog report indicates that the lithologies of these sections are mostly sandstones (off white to creamy white, gray in part, translucent to transparent, very fine to fine, occasionally medium grained, sub-rounded to rounded, sub-spherical, primarily calcareous cement, argillaceous in part poorly to moderately sorted [3], very good porosity and permeability) (**Table 1**) [3]. In the Yowi field, the boxcar shaped gamma-ray log occurred in all the wells with average thickness of 58 ft. in well A2P2 between the intervals of 3357–3412 ft., 5286–5344 ft., 5750–5813 ft., 6047–6110 ft. and 6848–6903 ft. Carbonaceous matter, mica and glauconitic materials are also present in the successions (**Table 1**). The presence of glauconite depicts a marine environment, whereas mica and carbonaceous detritus showed that the sediments were deposited within the shallow marine/coastal realm.

3.2. Depositional environments

Sedimentary deposits identified using well log motifs helped in reconstructing sediments that were deposited within the open sea and reworked to confer the various architecture and

Reservoir interval	Core description	Remarks
5018–5021	Sandstone: Light to medium brown, friable, clear, translucent, light brown, quartz grains, very fine, slightly silty, sub rounded to rounded, well sorted, glauconitic, carbonaceous speckles, micaceous, good porosity and permeability. Oil Shows: Very light brown oil stain, very dull yellow fluorescence, weak diffuse white cut fluorescence, no residue, faint Hydrocarbon odor.	A regressive bar
5027–5033	Silty Sandstone: Light to medium gray, friable, clear, translucent, Lower part of opaque, quartz grains, very fine, silty in part, with thin Siltstone laminae, sub rounded to rounded, well sorted, micaceous, glauconitic, carbonaceous speckles, traces of pyrite, moderate to good porosity and permeability. Oil Shows: Very light brown oil stain, moderate yellow white fluorescence, slow streaming to weak diffuse white cut fluorescence, no residue, faint hydrocarbon odor.	Lower part of a regressive bar
5042–5045 Well A2P2, N5.2 sand	Sandstone: Medium to dark brown oil saturated sandstone, clear, translucent, medium brown, friable to loose quartz grains, very fine to fine, predominantly very fine, sub rounded to rounded, very well sorted, excellent porosity and permeability, micaceous, trace glauconite, trace carbonaceous speckles. Oil Shows: Medium brown oil stain, intense bright yellow fluorescence, instant blooming milky white cut fluorescence, light brown residue. Very strong hydrocarbon odor.	Top of 5.2 sand, a regressive bar

Table 1. Ditch-cutting description of rock samples [3].

configurations of the deposits [3, 17]. Well log correlation revealed sand bodies displaying lateral continuity across the field (**Figures 12** and **13**). The Qua Iboe Shale (QIS) forms a key stratigraphic marker across the field that delimits the marine sediments from the continental deposits. The top and base of key sand units are used for correlation base on gamma ray trends (**Figure 12**). Each depositional stack (parasequence) is unique to guide sand body correlation thereby complementing the traditional lithostratigraphic correlation. High gamma ray (with a cut-off of 75 ^{0}API value and above) corresponding to the shale base line indicates shale lithology. In the sequence of the various major environments, there is swift transition from fluvial to marine. The fluvial section occurred at the top of the Qua Iboe Shale which demarcated the continental sediments from the marine section (**Figure 13**). The marginal marine segment comprises of the coastal plain sands, whereas delta front sandstones occurred within the shallow marine realm (**Figure 13**). The delta front sandstone is characterized by thicker, cleaner and more shale-free sandstones than the coastal plain sands (**Figure 13**).

From the perspective of facies models, layer-caked shore-parallel facies have been assumed to form homogenous, uniform reservoirs with high production capacities. Wave-influenced coastline
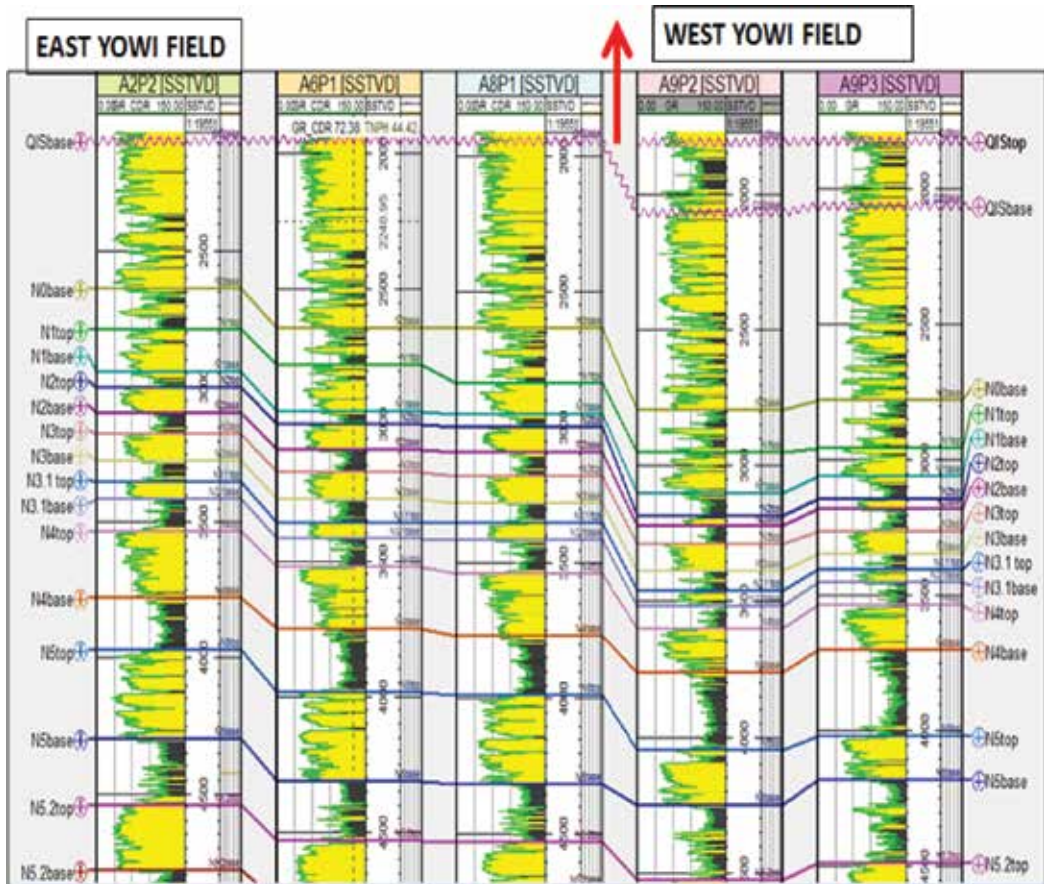
Figure 12. E-W Litho-correlation of key sand bodies across the field.
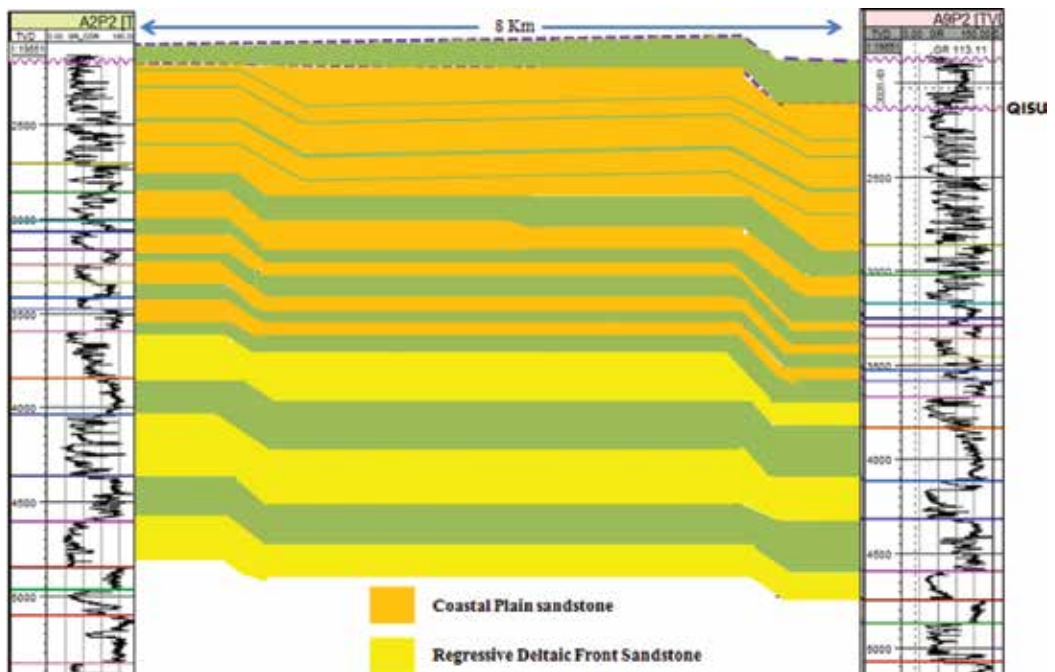
Figure 13. E-W correlation showing increasing shale thickness towards the west (A9P2) and increasing thickness of coastal plain/deltaic front sandstones towards the east.

deposits possess distinct facies with homogenous beach and shoreface sands accumulating on the updrift side of the river mouth with significantly more heterogeneous facies on the downdrift side. The heterogeneous unit is noticed towards the lower parts of the reservoirs (N4, N5, and N5.2) in wells A2P2 and A9P2 (**Figure 9**). The thick shale segments within each sequence are interpreted to be shelf or deep marine deposits.

3.2.1. Fluvial sediments

The well log signature of the continental fluvial environment of the Benin sand shows a jagged log motif, a typical characteristic of siliciclastic fluvial environment [3]. It occurred above the top of Qua Iboe Shale Member (QISM) at 1850 ft. (**Figure 13**) [3]. Different subenvironments that occurred within the Benin Formation include; braided stream, channel fills, flood plain, meandering channels, point-bar, etc. [3]. For example, sand beds that indicate meandering channel system consist of an alternation of fining-upward (**Figure 11**), channel fills and mud dominated floodplain deposits [3]. Braided fluvial systems are often composed of amalgamated channel fills, which confer a blocky pattern to the well logs [3]. In contrast, other types of rivers, including fine grained meandering or flashy ephemeral, produce a more irregular, jagged type of motif on well logs (**Figure 11**, number 1) [3]. Relatively thin-bedded (±m scale) coarsening-upward sand units may also occur in fluvial successions relative to crevasse splays in a low-energy and confined meandering system [3, 18]. The ditch cutting description for the sandy section shows sand dominated by Quartz grains (**Table 1**) after [3].

3.2.2. Deltaic and shallow marine sediments

The deltaic front environment is highly unstable due to the variety of processes operating within this realm. A combination of marine and fluvial influences account for the depositional styles within the marginal marine. Studies on modern sedimentary environments revealed that vertical profiles of grain size from a specific environment have certain log characteristics [3, 11]. Hence, prograding deltas and barrier bar deposits have coarsening upward grain size trends (**Figure 12**, number 4) [3, 19]. Gamma ray motifs with a bell-shape reflects a gradual vertical transition from shale to sandstone, whereas an upward increase in sand-size is indicative of a gradual change in the energy level of the depositional milieu, and no unique SP-curve pattern is representative of any specific depositional environment [12]. However, when these patterns are integrated with the presence or absence of glauconite and/or carbonaceous detritus from cuttings, a more meaningful and reliable interpretation emerges [20]. The presence of glauconite is observed in ditch-cutting samples from studied wells in the field at about 1800 ft., which is the base of Benin Formation and the beginning of the marine sequence. The highest occurrence of glauconite is reported at 2005 ft. It has been consistently recorded from the uppermost part of the Agbada sand sequence down hole, signifying a more marine influence than fluvial or deltaic. The associated environments based on log shapes and the presence of glauconite within this interval in the study area include [3]; beach, barrier foot, offshore/regressive bars, and shoreface deposits.

4. Conclusions

The Cretaecous exposure in Afikpo Basin South Eastern Nigeria comprises of sediments of fluvial, deltaic and marine origin. Ancient fluvial deposits in the area contains both braided stream and point bar channel sedimentary units. These deposits are also observed in the recent fluvial process that is continuously transporting sediments from the highland into the open sea in the offshore of the eastern Niger Delta through the Afikpo-Cross River. This has significant implications for paleo-environmental reconstruction of the subsurface formations of the Niger Delta. Subsurface data from an offshore field south of Calabar Town revealed the architecture of sediments probably of fluvial, deltaic and marine origin.

The overall stacking pattern of these sedimentary units as reconstructed from gamma ray log within the Agbada section shows a coarsening upward succession. This is typical of a deltaic and shallow marine depositional setting. Within the Agbada sequence in the field, stacked regressive sand occurred between 2000 and 3300 ft., and may indicate rapid sedimentation and progradation on adjacent shelf (**Figure 9**). This interval contains stacked highstand parasequence sets. The generalized subsurface depositional model for this field will show different environments affected by variety of processes ranging from wave action, long shore currents, tidal action and fluvial process, [3]. These sediments were derived from the continent and deposited within the shallow marine environment through distributary channels. The sediments upon arrival within the shores are reworked by wave action to form beach ridges/dunes [3]. Longshore currents reworked the sediments into longitudinal bars [3] running parallel to coastline. Subaqueous migration of regressive sands forms the offshore

bars. Most of the log facies units displaying erratic/fining upward motifs are representatives of tidal events. The ancient and recent sediments identified in the area form the major sources of sand used for construction purposes. Some essential minerals are also concentrated in these sedimentary units. In the subsurface, the sediments form reservoirs for hydrocarbon accumulation.

Acknowledgements

Conflict of interest

The author declares that no conflict of interest exists.

Author details

Prince Suka Momta

Address all correspondence to: princemomta@yahoo.com

Exploration Department, Belemaoil Producing Limited, Port Harcourt, Nigeria

References

[1] Petters SW. An ancient submarine canyon in the Oligocene-Miocene of the western Niger Delta. Sedimentology. 1984;**31**:805-810. DOI: 10.1111/j.1365-3091. 1984.tb00887

[2] Momta PS, Essien NU. The geology and structural evolution of the Aningeje Metasediment in the lower part of the Oban massif, SE Nigeria. Journal of Geography, Environment and Earth Science International. 2015, 2016;**4**(1):1-16. DOI: 10.9734/JGEESI/2016/19888 ISSN: 2454-7352

[3] Momta PS, Odigi MI. Reconstruction of the depositional setting of Tortonian sediments in the Yowi field, shallow offshore Niger Delta, using Wireline logs. American Journal of Geoscience. 2015, Science Publication (under review)

[4] Short KC, Stauble AJ. Outline geology of the Niger Delta. American Association of Petroleum Geologists Bulletin. 1967;**51**:761-779

[5] Reijers TJA, Petters SW, Nwajide CS. The Niger Delta Basin. In: Selley RC, editor. African Basins. Sedimentary Basins of the World. Vol. 3. Amsterdam: Elsevier; 1997. pp. 145-168

[6] Allen JRL. Sediments of the modern Niger Delta: A summary and review. In: Morgan JR, Shaver RH, editors. Deltaic Sedimentation. Soc. Econ. Paleontologists and Mineralogists, Spec. Publ.15, Tulsa, Okla. 1970. pp. 138-151

[7] Evamy DDJ, Haremboure P, Kamerling WA, Knaap F, Molloy A, Rowlands MH. Hydrocarbon habitat of the tertiary Niger Delta. American Association of Petroleum Geologists Bulletin. 1978;**62**:1-39

[8] Ejedawe JE. Patterns of incidence of oil reserves in Niger Delta basin. American Association of Petroleum Geologists Bulletin. 1981;**65**:1574-1585

[9] Doust H, Omatsola E (1990). Niger Delta. In: Edwards JD, Santogrossi PA (Eds.), Divergent/Passive Margin Basins American Association of Petroleum Geologists Memoir, vol. 48, pp. 201-238

[10] Reijers TJA. Stratigraphy and sedimentology of the Niger Delta. Geologos. 2011;**17**(3): 133-162

[11] Selley RC. Elements of Petroleum Geology. New York: W. H. Freeman and Company; 1985. p. 448

[12] Amajor LC, Agbaire DW. Depositional history of the reservoir sandstones, Akpor and Apara oilfields, eastern Niger Delta, Nigeria. Journal of Petroleum Geology. October 1989; **12**(4):453-464

[13] Chow JJ, Ming-Chung L, Fuh SC. Geophysical well log study on the Paleoenvironment of the hydrocarbon producing zones in the Erchungchi formation, Hsinyin, SW Taiwan. TAO. 2005, August 2005;**16**(3):531-545

[14] Asquith GB, Gibson CR. Basic well log analysis for geologists: AAPG, Methods in Exploration Series No. 3; 1982. 216 p

[15] Selley RC. Elements of Petroleum Geology. Imperial College, London United Kingdom: Department of Geology; 1998. pp. 37-145

[16] Nelson CS, James NP. Marine cements in mid-tertiary cool-water shelf limestones of New Zealand and southern Australia. Sedimentology. 2000;**47**:609-629

[17] Momta PS, Odigi MI. Geobody architecture and petroleum potential of the Yowi field, offshore eastern Niger Delta, Nigeria. American Journal of Geosciences. 2015. DOI: 10.3844/ajgsp2015

[18] Catuneanu, O. (2006). Principles of sequence stratigraphy. Elsevier, the Netherlands: pp. 89-159

[19] Momta PS, Omoboh JO, Odigi MI. Sedimentology and depositional environment of D2 sand in part of greater Ughelli Depobelt, onshore Niger Delta, Nigeria. American Journal of Engineering and Applied Sciences. 2015;**8**(4). DOI: 10.3844/ajeassp.2015.556.566

[20] Selley RC. Concept and methods of subsurface facies analysis Cont. Edu. Course; 1978

Sedimentation Processes in the Tinto and Odiel Salt Marshes in Huelva, Spain

Emilio Ramírez-Juidías

Abstract

Global warming is a key factor to take into account when a study is conducted on tidal wetlands. Both Odiel and Tinto salt marshes are the major wetlands in Andalusia (Spain). From the mid-1950s to date, the land use changes (LUC) have caused a great landscape alteration that along with the effects of climatic variables and sea wave energy have given rise to a hard impact on the environment. The advent of new image processing procedures and use of high-resolution images from satellites gave precise patterns of erosion. In this work, a new method patented by the author is presented and used to obtain the total cubic meters of eroded soil in both salt marshes. Moreover, the different factors that begin this phenomenon as well as the influence of intertidal processes are discussed. The results show how the greater integration of remote sensing and geographical information systems (GIS) technologies, with regression model, was most useful to describe, analyze and predict the volumetric change process in both salt marshes.

Keywords: eroded soil, salt marshes, south of Iberian Peninsula, remote sensing, high-resolution images

1. Introduction

According to [1], marshes are ecosystems that tend to go away as a result of silting process. Nonetheless, human beings have accelerated this process giving rise to loss of its surface. Several researchers, such as [2, 3], think that marshes are possibly a type of ecosystem that has experimented important alteration by anthropic action. Indeed, the present estimates [3–5] specify that the European marsh areas have decreased by about 80%.

Though both ecosystem processes and their implications for the future mitigation of land degradation have been taken into account in different field researches around the world, it is

difficult to extrapolate findings from field studies at patch scale in other areas [6]. Although satellite platforms may bring out the solution of this problem, the use of high-resolution images obtained by satellites has a significant advantage because it allows us to depict all the physical features of the marshes, which are often insufficiently reflected in classical contour lines mapping [3, 7], thereby supplying the spatial information needed to study the relationships between climate variables and soil erosion at marshes-scale analyses.

In both Tinto salt marshes and Odiel salt marshes, the residence times of sediments in their respective river systems are long with much intermediate storage of eroded material, as is common to most large river systems around the world, for example, as occurs in Chile [8], while on the other hand, increased storage of sediments can result in substantial changes to Tinto and Odiel river's physical form as well as their ecological health. This last aspect is key as a result of the importance of Tinto river to the study of life in extreme conditions.

A further consequence of long residence times in rivers, and in accordance with [3, 4, 8], is that the major historical changes will influence river behavior for many decades to come. Likewise, it is essential for us to obtain and evaluate the trajectory of response to global historical change, being the temporal scale of analysis of great relevance to predict the relationship the net response of sediment to the distribution of floods over many years.

Up to now, in most of the remote sensing studies, researchers have made an effort to approach soil loss and its erosion processes solely through mapping changes in canopy and vegetal abundance, or LUC in general sense, and even with different methods capable of deriving state variables based on the reflectance characteristics of soils [6] and/or the characteristics of the vegetable canopy, while, on the other hand, though the use of high-resolution images can be considered novel, the ratio of published manuscripts is much greater, perhaps, it can be due to the massive potential of these images in the distinct techniques used in remote sensing.

The quantification of erosion processes through high-resolution techniques, scientific procedures based on previous-generation iterative processes, with the help of ground work, can make available for use new required insights to predict the total volume of eroded soil not only in any wetland but also elsewhere in the world. However, when the area is compound for a complex network of catchments and/or aquifers, it is necessary to use high-resolution orthophotography. A possible solution is the use of new image treatment techniques [9], which are nowadays accepted by all researchers around the world. In this sense, the main aim of this work would be to obtain the prediction of mean erosion in the study area (Tinto and Odiel salt marshes). In order to achieve that goal, it will be necessary to obtain, firstly, the prediction of volumetric change processes, which is a required secondary objective.

2. Research methods

2.1. Study area

Both Tinto and Odiel salt marshes, with a total area of 32,867,946.31 m^2 and 7185×10^4 m^2, respectively, are located in the province of Huelva (southwest of the Iberian Peninsula), associated with both Tinto and Odiel river mouths, respectively (**Figure 1**).
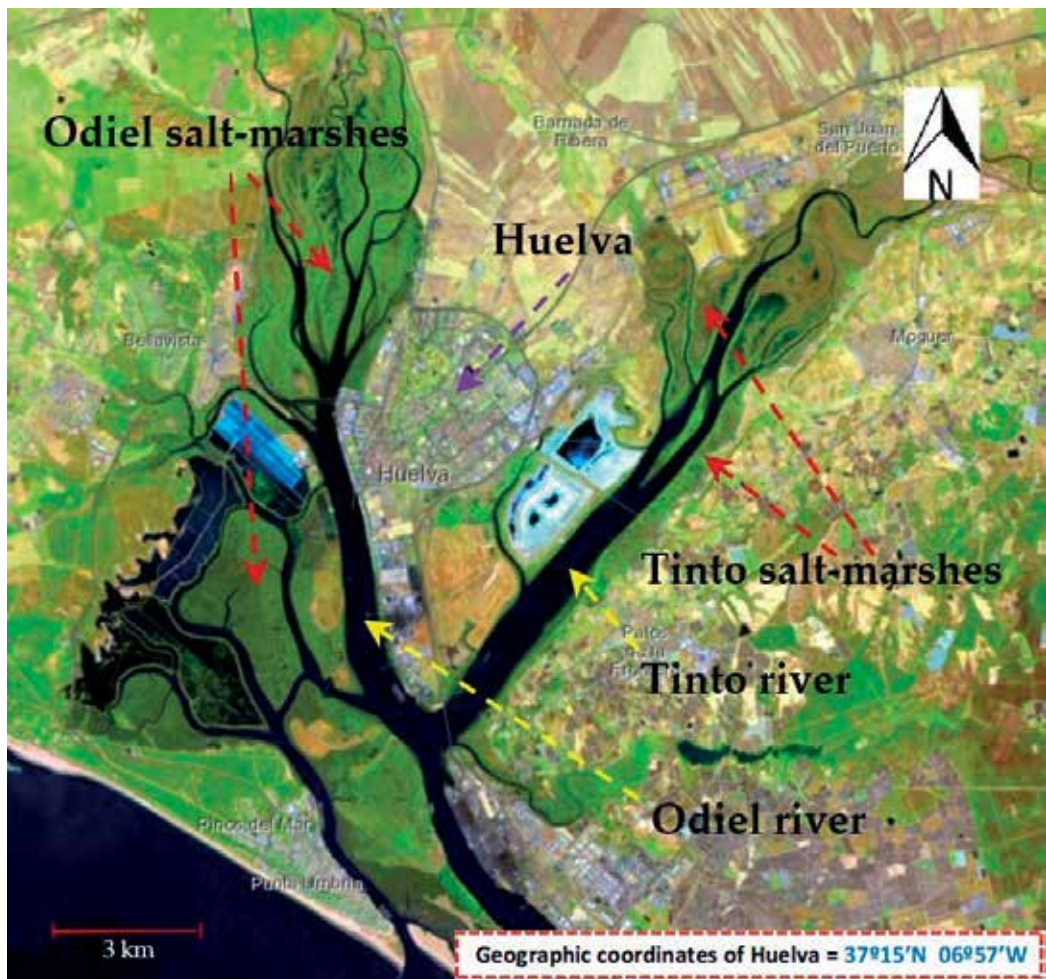
Figure 1. Location of study area (Landsat 8, bands 652).

In accordance with [4], the area is integrated in a complex system of estuaries of recent sedimentation affected, in their genesis, by the level of changes in the Earth's crust [10]. All sets are surrounded by tertiary formations of yellow silt and Miocene marls, Pliocene sands and marls, and remains of a Pleistocene erosive glacis. In the study area, both sedimentation and erosion processes are given simultaneously, influenced by a variation in space and time, creating a lot of seasonal or long-lasting physiographic characteristics giving rise to an appreciable diversity of habitats. The tidal movement is the key conditioning factor in shaping of these ecosystems.

On the one hand, Odiel salt marshes are composed of a set of islands crossed by numerous natural pipes. They are divided into the north marsh, comprising the Occidental, Central and La Yegua islands, and the south marsh, constituted by Bacuta, De Enmedio and Saltés islands. Moreover, Tinto salt marshes consist of a well-preserved tidal marsh area and another area, Dehesa de Alquería, where both woods and dry-land crops are predominant. The part of dry land located in the North is composed of clayey soils on which both native and migratory birds breed.

In the environment, the anthropic influence is very high. The raw sewage and solid waste from the Tartessos' Industrial Park (nearby to Tinto salt marshes) pour into the area. In the West is located the solid waste landfill of Huelva, where abounds discharges of debris due to the existence of the brownfield site. The vulnerability of the Tinto salt marshes area is variable (16% very high, 49% high, 34% moderate, 1% low) as a consequence of the risk of threat.

On the other hand, the area offers a Mediterranean maritime climate, with an insolation rate very high in comparison with North of the Iberian Peninsula. The decrease in the temperature in the winter season is responsible for the increase in the rainfall, while in the summer season, the temperature can reach up to 44°C (Tinto salt marshes) and 40°C (Odiel salt marshes), respectively. The average annual rainfall is 483.922 mm (Tinto salt marshes) and 506.6 mm (Odiel salt marshes), respectively, concentrated in the months of December and January, presenting, likewise, a dry season with deficient water balance between May and September [3, 4].

2.2. Methodology

For this study, a total of 24 control points (12 at Tinto salt marshes and 12 at Odiel salt marshes) were distributed throughout the study area (**Figure 2**), each of which was georeferenced in the ETRS-89 system.

In June 2017, the acquisition of images of both marshes were initiated using an Unmanned Aerial Vehicle (UAV) equipped with a radar system. During the low tide, along with the radar and RGB images were taken panchromatic images of 0.5 m resolution (Pléiades) collected from the AIRBUS DEFENSE & SPACE platform, from which data necessary for the study of the physical
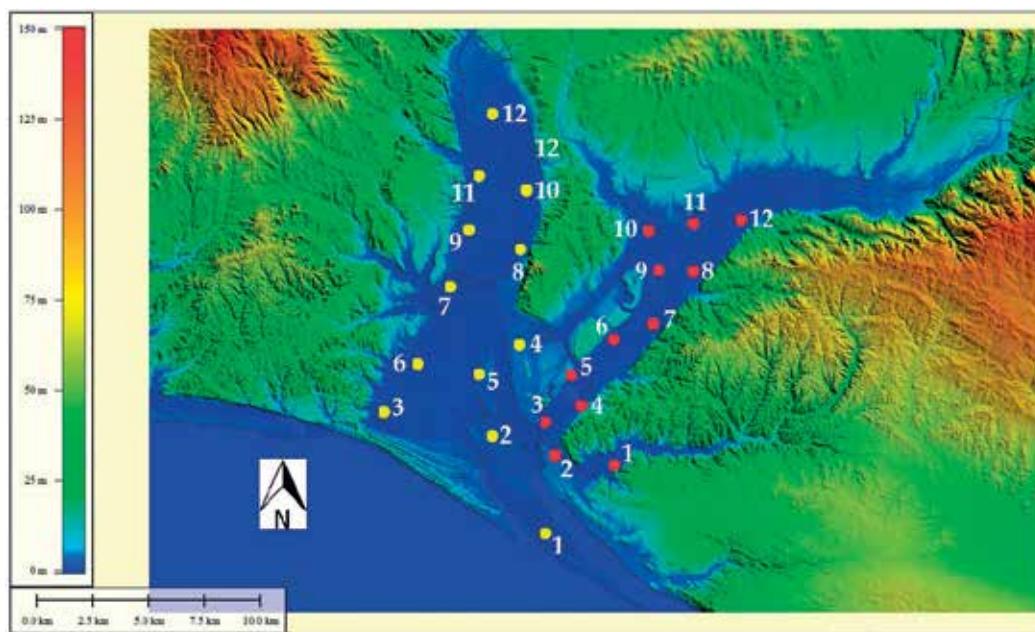
Figure 2. Distribution of control points (yellow points = Odiel salt marshes; red points = Tinto salt marshes) in the study area.
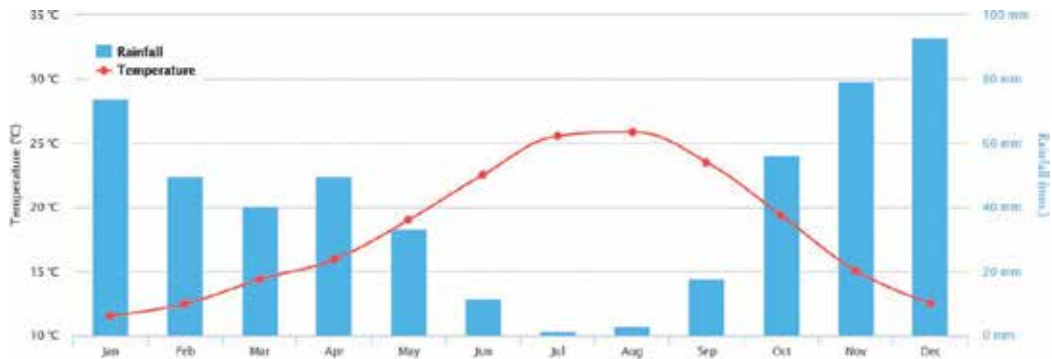
Figure 3. Average monthly temperature and rainfall for the period from 1901 to 2012.

characteristics of the marshlands was extracted), for the period from January 2016 to June 2017, and obtained in July 2017 (three high-resolution images were obtained per month since January 2016 to June 2017 in the study area), helped to adequate characterize the study area.

With a view to obtain the total cubic meters of eroded soil in the area under study, all the collected images were orthorectified by means of respective digital elevation model (DEM) of 25 m (of the year 1992–1999 and of 3 m of vertical precision) and 10 m (of the year 2001–2002, corresponding to LIDAR data with a dimension accuracy from the range of 0.15 to 0.30 m) resolution. The images obtained by the drone were orthorectified based on the DEM finished in the second half of July 2017, at 1.5 cm/pixel resolution, solved from the data captured by the radar sensor. All DEMs were complemented with selected control points in order to be able to calculate the total volume from iterative processes [11]. In the same way, the data treatment based on iterative processes was employed in order to obtain the average depth of the water in the study area, which was necessary to obtain the data on the soil eroded in the natural reserve.

According to [4], an exhaustive literature review was conducted in order to determine the potential existence of a rainfall record that covered a sufficiently broad time to obtain results, discussion and conclusions consequent with this study. From this point of view, the rainfall data were analyzed based on data provided by [12], which is necessary for the prediction of rainfall in the study area from 1982 to 2012 based on the correlation between the weather data from the nearby locations. A first approximation to climatic data is shown in **Figure 3**.

3. Results and discussion

3.1. Results

3.1.1. Land use changes

Both Tinto and Odiel salt marshes have undergone a major transformation due to an increase in the area dedicated to tourist activities. Based on [13] and by considering the LUCs between

1956 and 2007 in the altered areas, a significant growth was seen in these marshes as a result of the expansion of the urban fabric in coastal areas due to an increase in the tourism rate in the study area.

Crop evolution has been varied, while arable land has remained stable in terms of land area; the extent of another land uses, such as forestation has enormously decreased by 60% between 1956 and 2007. In the meantime, the area under irrigation has been aided by technological advances, giving rise to a huge area increase rate between 1956 and 2007.

Though there was a slight increase in Odiel salt marshes area in 2007, as a consequence of the increase in aquaculture, nature reserve total area was about 9% smaller compared to the existing area in 1956.

In order to be able to visualize the changes that occurred between 1982 and 2012, and in relation to rainfall data mainly, maps of detected changes were obtained in the study area from 1975 to 1990 (**Figure 4**), from 1990 to 2000 (**Figure 5**), from 2000 to 2005 (**Figure 6**) and from 2005 to 2012 (**Figure 7**). All maps were obtained by the difference between the NDVI values of images corresponding to the end date and start date of each time period.

In **Figures 4–7**, most areas are gray, indicating no change because each pixel has comparatively equal value in start date and the end date. Areas that show up green had more vigorous vegetation in the initial date, while areas that show up in magenta were brighter in the end date (meaning more vigorous vegetation on this date).

3.1.2. Prediction of volumetric change processes

Based on [3, 4, 7], and after having analyzed all the available data, a progressive decrease was detected in the surface water in the study area as a consequence of the dry period to which the area is subjected.

Afterward, and using the software Ilwis GIS, an analysis was conducted [7] between the average DEMs of each natural area (Tinto and Odiel salt marshes) and the climatic peculiarities of

Figure 4. Detected changes in study area between 1975 and 1990.
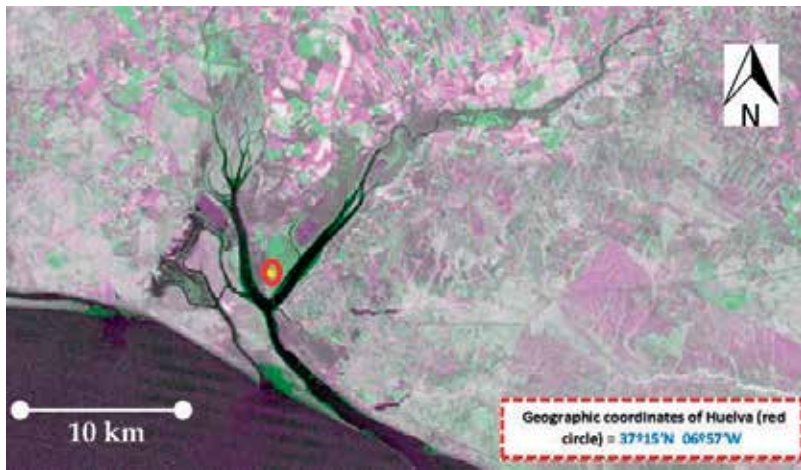
Figure 5. Detected changes in study area between 1990 and 2000.

Figure 6. Detected changes in study area between 2000 and 2005.

the area in order to obtain the prediction of the average cubic meters of flooded area in terms of the DEM used and salt marsh (Tinto or Odiel) taken into account (**Table 1**).

The estimated depth (**Table 2**), in each salt marsh, was obtained through iterative processes using a total of 1500 random sample points selected in the Pléiades images, a necessity to identify the eroded soil in both the Tinto and Odiel salt marshes.

As can be seen in **Table 1**, significant relationships were observed between the volume of water and the Tinto salt marsh surface, not becoming part of the model, the estimated depth (contrariwise, in Odiel salt marshes, estimated depth plays an important role in the model).

After having made the volumetric prediction of the Tinto and Odiel marshes, and based on the data of precipitation and on the topographical characteristics of the area of study, it was

Figure 7. Detected changes in study area between 2005 and 2012.

Average DEM in:	Equation	Significance
Tinto salt marshes	$y = -8.490 + 1.627 \cdot Sr = 0.98 \ R^2 = 0.913$ (1)	≤0.001
Odiel salt marshes	$y = -18.269 + 2.059 \cdot S - 4.208 \cdot EDr = 0.957 \ R^2 = 0.936$ (2)	≤0.001

"y" is the volume obtained in each marsh in hm³, "S" is the estimated area occupied by the volume in km², and "ED" is the estimated depth in meters.

Table 1. Prediction of average flood volume based on the average DEM used in each marsh.

Control point no.	Estimated depth (m) for each salt marsh	
	Tinto salt marshes	Odiel salt marshes
1	0.16	0.40
2	0.35	2.97
3	1.51	3.04
4	1.94	3.08
5	2.74	3.08
6	3.00	3.10
7	3.07	3.19
8	3.10	3.22
9	3.11	3.24
10	3.21	3.35
11	3.23	3.37
12	3.30	3.91

Table 2. Estimated depth per control point based on the average DEM used in each salt marsh.

found that the total area of the Tinto marshes, 32,867,946.31 m^2, corresponded to a flood volume of 48.35 × 10^6 m^3, while the total area of the Odiel marshes, 7185 × 10^4 m^2, corresponded to a flood volume of 110.28 × 10^6 m^3. **Figure 8** shows the graph equivalent to the estimated surface area of both Tinto marshes and Odiel marshes, while in **Figure 9**, the graph of estimated volume in study area can be observed.

Furthermore, an analysis of the variance of a factor for correlated samples was conducted for the estimated depth variable (this analysis has been done after taking into account only the values shown in **Table 2**) and in terms of the average DEM used in each marsh. These results are shown in **Table 3**.

As can be seen in **Table 3**, there are significant differences ($p \leq 0.05$) between the estimated depth in both the marshes, which was expected based on the particular conditions of the Tinto marshes. Similarly, we must consider the level of anthropic pressure at the Odiel marshes as another factor of great importance.

3.1.3. Prediction of mean erosion in Tinto and Odiel salt marshes

The transport of sediments was obtained using the procedure patented by [9], whose results are shown in **Figure 10** (considering that both marshes are unique natural systems). In **Figure 10**, sediment transport is simulated for the period between 1982 and 2012, based on the sediment characteristics, precipitation and temperature existing in each marsh. It is very important to specify that these results are based on an algorithm that is dependent on the superficial shape factor existing in study area.
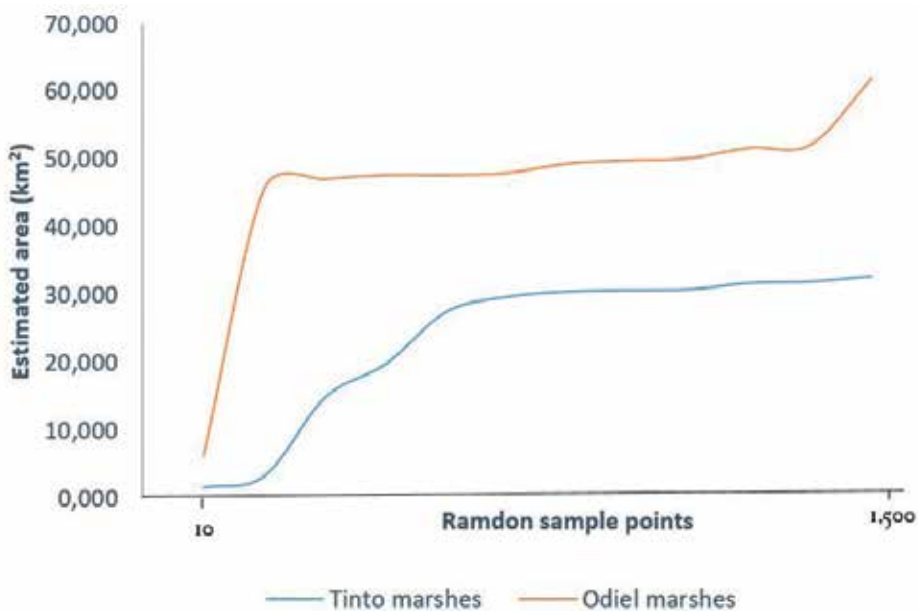
Figure 8. Estimated surface area by random sample points "1500 in total selected with Ilwis GIS".
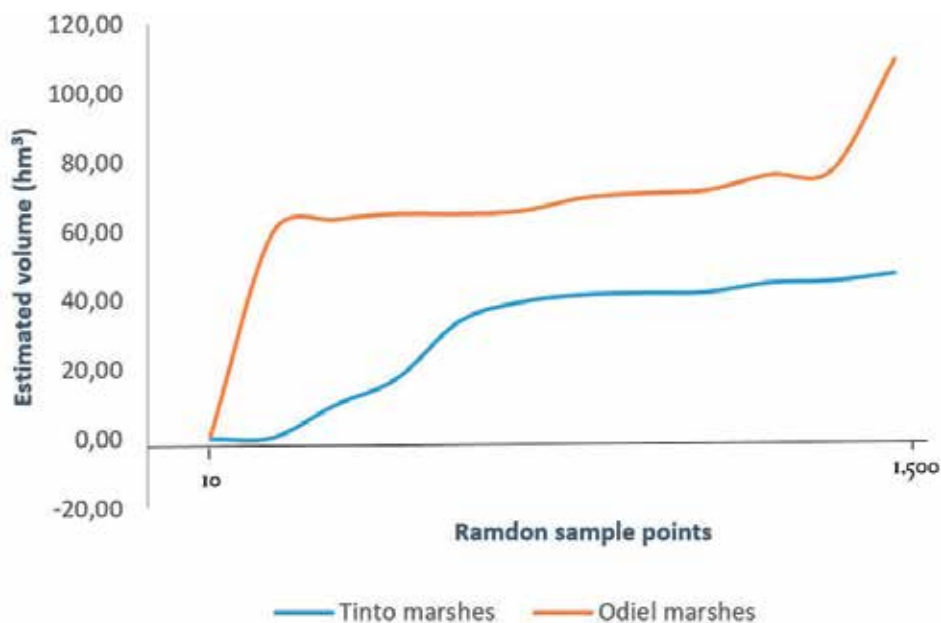
Figure 9. Estimated volume by random sample points "1500 in total selected with Ilwis GIS".

	SS	df	MS	F	P
Treatment (between groups)	2.178	1	2.178	7.06	0.022303
Error	3.3946	11	0.3086		
Block (DEMs)	18.917	11			
Total	24.4896	23			

SS = sum of squares; df = degrees of freedom; MS = mean squared; F = value of the test statistic; P = significance.

Table 3. Summary of the analysis of the variance (ANOVA) for the estimated depth variable.

Based on **Figure 10**, and with the purpose of correctly visualizing the areas affected by the sedimentary transport in the study area, a simulation was carried out, using the patented algorithm by [9], corresponding to the levels of ±0.05 m (**Figure 11**) and ±0.1 m (**Figure 12**) of the eroded soil. As can be observed in both the figures, the main changes started in the western area.

In respect of Tinto salt marshes, it is important to specify that dynamics of the process of eroding divides these marshes into two zones. Firstly, the Southward zone has 0.20 m (mean value) of the total erosion, industrial activities being responsible for the erosion increase [3]. Secondly, the Northward area, with 0.10 m of the total erosion (mean value), and with the existence of the Tartessos' Industrial Park, presents a great problem related to the dumping of raw sewage and solid waste, which gives rise to the increasing vulnerability of the area.
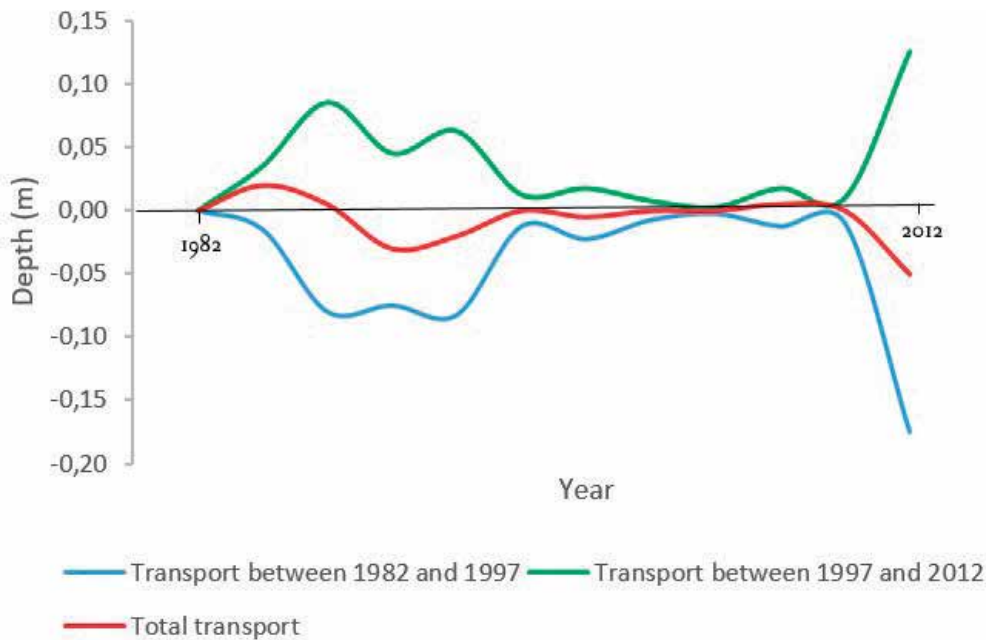
Figure 10. Variation of the depth in both the salt marshes in terms of average sediment transport from 1982 to 2012.
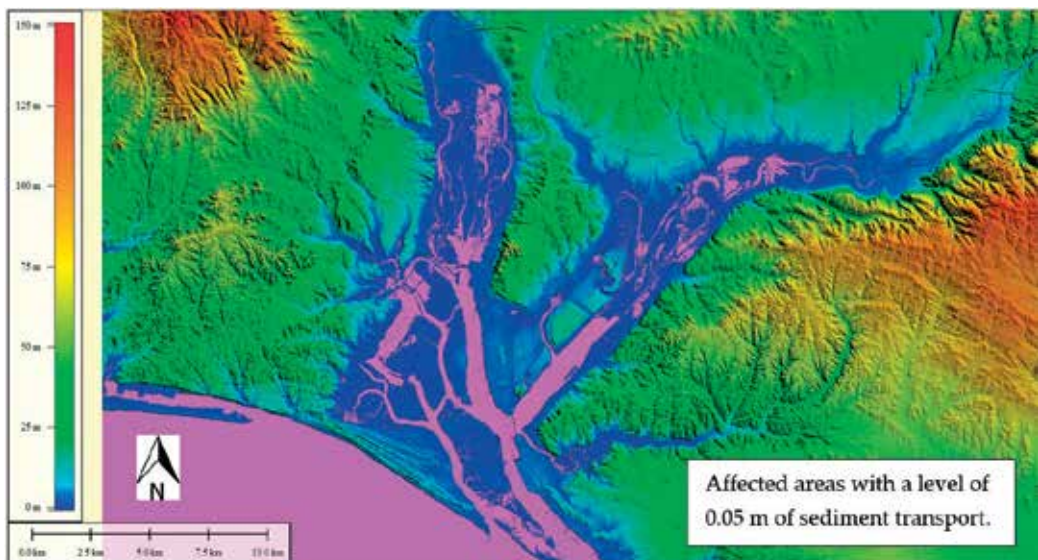
Figure 11. Eroded soil affected with a level of 0.05 m of sediment transport (in magenta).

3.2. Discussion

According to [14], one of the main causes of the rise of the tidal level in the study area, as well as its speed and drag force, is the wind speed (from 30 to 50 km/h). This fact is very important, since in the present work, it has been possible to verify that the maximum levels of sedimentary
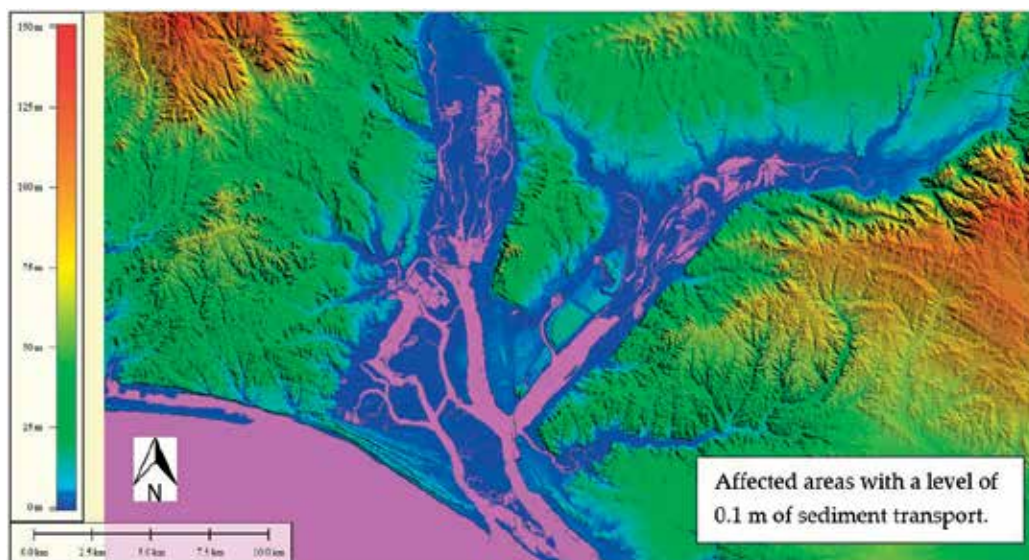
Figure 12. Eroded soil affected with a level of 0.1 m of sediment transport (in magenta).

transport present a direct correlation with the wind speed (always in the direction toward the Iberian Peninsula). Part of the LUCs that occur in the study area depend on this effect.

In relation to the transport of sediments, one aspect that needs to be taken into account is the construction of the Juan Carlos I breakwater, which interrupts the natural flow of sediments in the study area and gives rise to the fact that the marine currents carry these sediments toward Isla Cristina salt marshes [7], which causes an over silting-up in this natural area.

On the other hand, although the predictions of tides made by the Hydrographic Institute of the Spanish Navy for the ports are calculated with an accuracy of 1 cm in height, and 1 min in time, [14] showed that there are significant differences between the theoretical predictions and the real ones recorded by the tide gauge of the Port Authority of Huelva. This converts Eqs. (1) and (2) in an important prediction instrument, especially as a consequence of both the non-dependence of tide predictions and its high probability of success with reality.

Although this is the first time that predictive models have been obtained from the study area as a whole, it is important to specify that these could be used in other tidal-marshes independent of the South of the Iberian Peninsula, although correcting the results obtained with the prevailing climatic variables in each area.

4. Conclusions

Both the marshes existing at the study area experience an annual filling process coinciding with the months of highest rainfall and a water loss focused during the summery period. Comparing the occupied volume by water between 1975 and 2012, a slight decrease of the

annual water volume coming into these salt marshes was observed, which is related to the global warming in the study area.

The results obtained in the present study agree with those carried out by [3, 4, 7, 14] in distinct wetlands, so it can be deduced that the methodology patented by [9] has been validated, and it is completely safe and reliable.

According to [7], both remote sensing throughout UAV and satellite remote sensing of surface water fluxes and storages in wetlands is an immature but rapidly growing field. This research showed that combined remote sensing and GIS approach was very successful in visualizing the differences in salt marshes levels existing in the study area throughout the analysis period (1975–2012). In addition, Pléiades data were found to be very suitable for this analysis. Although hitherto Landsat data have been utilized for different types of remote sensing applications, other important platforms (Sentinel or SPOT) cannot be forgotten, whose resolution is better than Landsat in the majority of its bands.

The results show that high-resolution imagery can be used to visualize water-level variations as a result of changes in climatic variables. This may be required to create a public awareness about socio-ecologic problems caused by global warming.

Acknowledgements

Conflict of interest

The author declares that there is no conflict of interest.

Notes/Thanks/Other declarations

The author thanks the JZP company for the data collection carried out with the drone.

Author details

Emilio Ramírez-Juidías

Address all correspondence to: erjuidias@us.es

University of Seville, Seville, Spain

References

[1] Análisis P-GM. de los trabajos publicados en revistas y congresos nacionales en relación con humedales españoles durante el period 1989-1999. In: VII Simposio de Hidrología; 1-2 June 2001, Murcia. Murcia: Asociación Española de Hidrólogos; 2001. pp. 31-45

[2] González-bernáldez F. Los Paisajes del Agua: Terminología Popular de Humedales. 1st ed. Reyero Editores, Madrid; 1992. 257 p

[3] Ramírez-Juidías E. Study of erosion processes in the Tinto salt-marshes with remote sensing images. Advances in Image and Video Processing. 2014;**2**(4):39-52. DOI: 10.14738/aivp.24.417

[4] Ramírez Juidías E, Justicia Segovia M, Madueño Luna A. New method to predict the volumetric changes in the Odiel marshes (Huelva, Spain). Lecture Notes in Engineering and Computer Science. 2013;**2**:1335-1339

[5] Custodio E. Aguas subterráneas y humedales. In: VII Simposio de Hidrología; 1-2 June 2001; Murcia. Murcia: Asociación Española de Hidrólogos; 2001. pp. 3-30

[6] Hill J, Schütt B. Mapping complex patterns of erosion and stability in dry Mediterranean ecosystems. Remote Sensing of Environment. 2000;**74**(3):557-569. DOI: 10.1016/S0034-4257(00)00146-2

[7] Ramírez-Juidías E, Víquez-Urraco F, Noguero-Hernández D. Sedimentary processes in the Isla Cristina salt-marshes: Geomorphological changes of landscape. Ocean & Coastal Management. 2017;**143**:148-153. DOI: 10.1016/j.ocecoaman.2016.11.007

[8] Soto MV, Märker M, Paz Castro C, Rodolfi G. Análisis integrado de las condiciones de amenaza natural en el medio ambiente costero semiárido de Chile. La Serena, Coquimbo. Boletín de la Asociación de Geógrafos Españoles. 2015;**67**:213-231

[9] Ramírez-Juidías E, Pozo-Morales L, Galán-Ortiz L. Procedimiento para la Obtención de una Imagen Teledetectada a Partir de Fotografía Universidad de Sevilla, Spain. Patent No. ES253778B2 (with extension to International Patent No. PCT-WO2014198974 [Internet]. 2015. Available from: http://consultas2.oepm.es/InvenesWeb/detalle?referencia=P201300573 [Accessed: Nov 10, 2017]

[10] Castellanos EM, Nieva FJ, Luque CJ, Figueroa ME. Modelo annual de la dinámica sedimentaria en una marisma mareal mediterránea. Cuaternario y Geomorfología. 1998;**12**(3-4):69-76

[11] Matgen P, Schumann G, henry JB, Hoffmann L, Pfister L. Integration of SAR-derived river inundations areas, high-precision topographic data and a river flow model toward near real-time flood management. International Journal of Applied Earth Observation and Geoinformation. 2007;**9**(3):247-263. DOI: 10.1016/j.jag.2006.03.003

[12] Global Climate Monitor [Internet]. 2017. Available from: http://www.globalclimatemonitor.org/# [Accessed: Nov 5, 2017]

[13] Government of Andalusia. Medio Siglo de Cambios en la Evolución de Usos del Suelo en Andalucía 1956-2007 [Internet]. 2011. Available from: http://www.juntadeandalucia. es/medioambiente/portal_web/servicios_generales/doc_tecnicos/2011/evolucion_usos_ suelo/cambios_usos_suelo.pdf [Accessed: Nov 12, 2017]

[14] Cáceres-Benavides F. Bases Técnicas para el Control de Mosquitos en la Costa de Huelva [Internet]. 2002. Available from: http://fondosdigitales.us.es/tesis/tesis/1145/bases-tecni- cas-para-el-control-de-mosquitos-de-la-costa-de-huelva/ [Accessed: Nov 5, 2017]

Sediment Management of Reservoirs in Volcanic Area: Case of Wlingi and Lodoyo Reservoirs in Indonesia

Fahmi Hidayat, Pitojo T. Juwono, Agus Suharyanto,
Alwafi Pujiraharjo, Djoko Legono,
Dian Sisinggih and David Neil

Additional information is available at the end of the chapter

Abstract

Volcanoes erupt in many parts of the world, producing abundant sediment that is rapidly delivered to deposition sites. Where a reservoir is located near an active volcano, the sedimentation will be very severe. Wlingi and Lodoyo reservoirs are severely affected by eruptions of Kelud volcano, one of the most active volcanoes in Indonesia. After the February 2014 eruption, the capacity of Wlingi and Lodoyo reservoirs decreased dramatically to 2.20 million cubic meter (Mm^3) and 1.33 Mm^3, respectively, just 46 and 49% of their pre-eruption capacities and 19.42 and 26.60% of their initial capacities. To cope with the extreme sedimentation problems in Wlingi and Lodoyo reservoirs, diverse sediment management strategies have been applied in these reservoirs and their catchments. Construction of many on-stream sediment control facilities (sabo works) and a sediment bypass channel has reduced sediment inflow to the reservoirs. Removal of deposited sediment by dredging and hydraulic flushing in Wlingi and Lodoyo reservoirs has also resulted in storage capacity recovery. These measures are an integral part of the Mt. Kelud Volcanic Disaster Mitigation Plan.

Keywords: reservoir, sediment management, volcanic area, Wlingi and Lodoyo

1. Introduction

Volcanoes erupt in many parts of the world, from ocean ridges to the center of continents, producing tremendous sediment that is rapidly delivered to sites of deposition. Yearly sediment fluxes from basins affected by volcanic eruptions commonly range from 10^3 to 10^6

mega-grams (Mg)/km^2 that can be considered as the greatest sediment producer on Earth [1]. Prolonged tremendous sediment transport after a volcanic eruption can cause environmental and socioeconomic damage equaling or exceeding that caused directly by an eruption [2]. If volcanic sediment fluxes are ultimately trapped by dams in a river system, severe sedimentation may take place in its reservoir.

Reservoir sedimentation occurs when sediment carried by a river flowing into a reservoir is trapped by a dam and deposited in the reservoir upstream of the dam. The sediment carried by the inflowing river is deposited in a reservoir because the water slows after entering it, reducing its capacity to transport the sediment. Such deposits consume reservoir storage space that was originally intended for water storage, thereby impeding the intended function of the dam and reservoir, i.e., adversely affecting hydropower generation and reducing the reliability of domestic and irrigation water supplies and flood management systems.

Where the reservoir is located near an active volcano, the sedimentation will be very severe. Effective measures to mitigate reservoir sedimentation in a volcanic area include measures to manage sediment inflows during periods of high sediment yield to minimize trapping in reservoirs, removal of sediment already deposited in reservoirs using a variety of techniques, and measures to reduce sediment yield from the area affected by the eruption of the volcano upstream of reservoir. These measures should be an integral part of the volcanic disaster mitigation plan. This chapter discusses the importance of reservoir sediment management in a volcanic area by examining the case of Wlingi and Lodoyo reservoirs which are located near Kelud Volcano, one of the most active volcanoes in Indonesia.

2. Reservoir sedimentation management

Sustainable reservoir sedimentation management is vitally important for preserving reservoir storage space and minimizing long-term maintenance costs. There are three main strategies for reservoir sedimentation management as follows: (1) strategy to reduce sediment inflow from upstream area, (2) strategy to pass sediment through or around the impoundment to minimize sediment trapping effect, and (3) strategy to recover, increase, or reallocate storage or to modify intake or other structures, after sediment has been deposited in the reservoir [3], as summarized in **Table 1**.

3. The eruptions of Kelud volcano in the Brantas River basin, Indonesia

Across Indonesia's 13,677 islands, there has been a volcanic eruption, on average, every year for the past 1000 years. These eruptions have resulted in more than 175,000 deaths and also caused numerous debris flows [4] with significant implications for landscape characteristics, soils, hydrological processes, and human societies. Kelud volcano (1724 m), located in the

Strategy	Description
Reduce sediment inflow from upstream	1. Erosion control to reduce sediment yield
	2. Upstream trapping by check dams, etc.
Route sediment around or through reservoir	3. Bypass sediment to pass sediment around the storage zone by constructing sediment bypass tunnel or channel, etc.
	4. Sediment pass-through to route sediment through the impounded reach by venting turbidity currents or reservoir drawdown
Recover, increase, or reallocate reservoir volume	5. Flushing to scour out deposited sediment in reservoir
	6. Dredging to remove sediment by mechanical means
	7. Dry excavation to remove sediment by earthmoving equipment
	8. Increase storage by raising the dam or constructing additional storage reservoirs
	9. Modify structures to avoid areas of sediment deposition by modifying intakes or other structures
	10. Redistribute sediments to manipulate water levels to deposit sediment in areas of the pool where impacts are reduced
	11. Reallocate available storage to distribute sedimentation impacts among the beneficial uses to maximize the utility of the remaining volume

Table 1. Classification of reservoir sediment management strategies [3].

center of the Brantas River basin at $112^0 18.5'$E and $7^0 56'$S, about 38 km west of Malang City, 35 km east of Kediri City, and 24 km north of Blitar City, is portion of the Sunda volcanic arc system that is linked to the subduction of the Australian plate. Kelud volcano is an andesitic stratovolcano with a complex structure which primarily includes two avalanche calderas, of which one is exposed to the south and the other to the west [5]. **Figure 1** depicts the location of Kelud volcano, Wlingi and Lodoyo reservoirs in the Brantas River basin, East Java, Indonesia.

The morphology of Kelud volcano includes the formation of a deep crater lake, which stores up to 10 million cubic meters (Mm^3) of rainwater. Stored water in the crater of Kelud volcano (see **Figure 2** showing Kelud volcano's crater with the lake in 2005) was the main mover at each eruption, water mixing with the ejecta to produce hazardous hot debris flows. The primary lahars generally flow down the slopes of the western half of the Kelud volcanic area through dissected torrents discharging from the crater area and afterward form abundant deposits on the lower slopes. Those erupted materials deposited on Kelud volcano's slopes are the major source of the hazardous secondary lahars which are usually mobilized by subsequent heavy rains after the eruptions. The eruptions of Kelud volcano affect large area of about 2003 km^2 and cover the catchment area of the Konto, Serinjing, Ngobo, Sukorejo, Petungkobong, Badak, Abab, Putih, Jari, and Lekso Rivers, entirely tributaries of the Brantas River, the longest river in east part of Java.

Historical eruptions of Kelud volcano are well known because they have caused catastrophic outpouring of the crater lake and formation of "primary" (eruption-triggered) lahars. Kelud volcano's 1000 AD eruption is the oldest in the historical record of eruptions for the entire
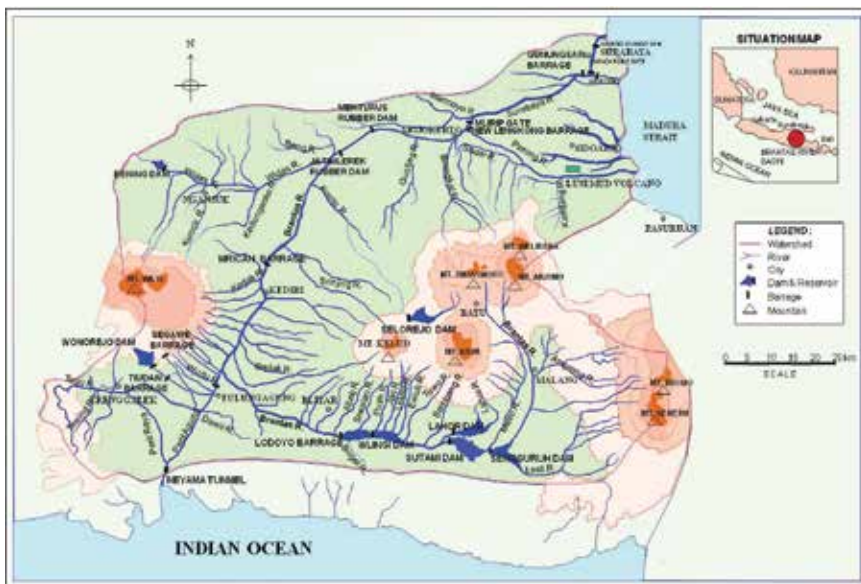
Figure 1. Location of Kelud volcano, Wlingi and Lodoyo reservoirs in the Brantas River Basin, East Java, Indonesia.

Indonesian archipelago. In the recent past, eruptions occurred in 1901, 1919, 1951, 1966, 1990, 2007, and 2014. **Table 2** summarizes the chronology of Kelud volcano's activities in historical time. These eruptions were generally similar, characterized by very short durations. Explosive activity typically started with a phreatomagmatic outburst followed by a short plinian eruption with convective columns reaching an altitude of more than 10 km. These eruptions produced devastating lahars, pyroclastic surges and flows, as well as ash fall deposits.

In May 1919, Kelud volcano erupted, ejected 38.5 Mm^3 of hot lahar, and claimed 5110 lives. After this eruption, a series of drainage tunnels were constructed during the period 1923–1927 through the west rim of the crater lake to decrease the lake water to 1.8 Mm^3, lowering the lake water level by 50 m. The August 1951 eruption produced only minor destruction with total volcanic product estimated at 192 Mm^3 based on point depth surveys of the ash deposits. Kelud volcano erupted again in April 1966, producing an estimated 90 Mm^3 of volcanic materials [6].

The 10 February 1990 eruption began at 11:41 local time (GMT + 7 hours) with a series of phreatic explosions [5]. The eruption resulted in large volumes of volcanic ash spreading over the south to west slopes of Kelud volcano, with deposition in villages, paddy fields, and plantations within a 20–30 km radius. The 1990 eruption produced about 125 Mm^3 of tephra as a combination of fall, flow, and surge and devastated the summit area within 1–5 km from the crater rim. Subsequently, the potential lahar yield (the ash deposits which could form lahar flows) was estimated through field investigation as 57.3 Mm^3. The 2007 eruption of Kelud volcano produced no significant volume of ejecta but created a lava dome which rose through the center of the crater lake atop the volcano. The lava dome expanded to 250 m diameter and

Figure 2. The evolution of Kelud volcano's crater with the lake in 2005 (top, left), the formation of lava dome in 2007 (top-right), the crater before eruption in 2013 (middle- left), the crater after eruption in 2014 (middle-right), and the eruption of Kelud volcano in February 2014 (bottom). Historical eruptions of Kelud volcano are well known, because they have caused catastrophic outpouring of the crater lake and formation of "primary" (eruption-triggered) lahars. Kelud volcano's 1000 AD eruption is the oldest in the historical record of eruptions for the entire Indonesian archipelago. In the recent past, eruptions occurred in 1901, 1919, 1951, 1966, 1990, 2007, and 2014. These eruptions were generally similar, characterized by very short durations. Explosive activity typically started with a phreatomagmatic outburst followed by a short plinian eruption with convective columns reaching an altitude of more than 10 km. These eruptions produced devastating lahars, pyroclastic surges and flows, as well as ash fall deposits.

120 m high and cracked open, and lava began oozing into the surrounding water. **Figure 2** depicts the evolution of Kelud Volcano's crater with the lake in 2005 until the eruption in February 2014 which destroyed the lava dome inside the crater.

Date	Year	Comments
	1000	Reported ash falls
	1311	Reported casualties
	1334	Reported ash falls and lahars
	1376	Explosive, lava dome formed,; reported casualties
	1385	
	1395	
	1411	
	1451	
	1462	
	1481	
	1548	
	1586	About 10,000 casualties
	1641	
Jul-20	1716	Reported casualties
May-01	1752	
Jan-10	1771	Reported ash falls
	1776	
	1785	
Jun-05	1811	Reported ash falls
	1825	Reported casualties
October 11, 14, 18, 25	1826	Strong detonations: glowing avalanche, summit area destroyed; post-eruption lahar
	1835	Reported casualties
	1848	
May-16	1851	
Jan-24	1864	
January 3-4	1901	
May 22-23	1919	Reported casualties
May-20	1920	5110 casualties
Dec 6-12	1951	Formation of lava dome
Aug-31	1966	Destruction of the 1920 lava dome; seven casualties
Apr-24	1990	211 casualties
Feb-10	2007	32 casualties, post-eruption lahar; embryonic lava dome
November 3-4	2014	Formation of lava dome
Feb-13		Destruction of the 2007 lava dome

Table 2. The chronology of Kelud volcano's activities in historical time, based on Bourdier et al. [12] and Hidayat et al. [13].

The most current eruption of Kelud volcano occurred on 13 February 2014. Satellites detected the eruption plume at 11:09 p.m. local time (16,09 UTC). At 12:30 a.m. (17.30 UTC), an image from the Visible Infrared Imaging Radiometer Suite (VIIRS) on the Suomi NPP satellite indicated an ash plume reaching above a lighter-colored cloud deck [7]. CALIPSO satellite data revealed that a rapidly rising portion of the plume ejected material up to an altitude exceeding 26 km, well into the tropical stratosphere [8]. The eruption sent an enormous plume of ash drifting west across Java island and over the Indian Ocean. By 9 hours after the initial eruption, the center of the plume top had drifted 600 km westward [9]. Ash plumes rose to an altitude of 17 km and caused ash fall in areas to the NE, NW, W, and elsewhere as far as Pacitan, East Java (133 km WSW); Kulon Progo, Yogyakarta (236 km W); Temanggung, Central Java (240 km WNW); and Banyuwangi, East Java (228 km E) [8]. A 18 February 2014 satellite image shows that the lava dome was destroyed during the February 2014 eruption and significant ash was deposited on the slopes and in the river channels around Kelud volcano. The lava dome with estimated volume of about 20 Mm^3 was extruded into the crater lake at the summit during the eruption in November 2007 [10], continuing to extrude through the crater lake until growth ceased in March 2008. During the 2007 eruption, nearly all the lake water was vaporized as the lava dome grew to a diameter of 400 m, a height of 260 m, and a volume of 35 Mm^3 [11].

4. Sedimentation problem in Wlingi and Lodoyo reservoirs

Wlingi dam and Lodoyo barrage are located in the Brantas River basin, in the east of Java Island, Indonesia. Wlingi dam, with a catchment area of 2890 km^2, is located on the southern slope of Kelud volcano in the upstream reach of the Brantas River basin and approximately 30 km downstream of Sutami dam. Lodoyo barrage is located approximately 7 km downstream of Wlingi dam. Wlingi dam was completed in 1979 for the purpose of peak demand hydropower generation (54 MW), irrigation water supply (12,687 ha irrigation area), and flood control. Lodoyo barrage is located 7.9 km downstream of Wlingi dam. Construction of Lodoyo barrage, the second stage of the Wlingi Raya Project, started in 1978 and was completed in 1980. The function of Lodoyo barrage is for hydropower generation (4.7 MW) and flood control.

Wlingi and Lodoyo reservoirs are very small with capacity to inflow (C/I) ratios of about 0.007 and 0.001, respectively. Following its completion in November 1979, the gross storage volume of Wlingi reservoir was 24.00 Mm^3, and the effective storage volume was 5.20 Mm^3 between the high-water level (HWL) of 163.50 m and the low-water level (LWL) of 162.00 m, while the gross storage volume of Lodoyo reservoir at the time of its completion in December 1980 was 5.20 Mm^3, and the effective storage volume was 5.00 Mm^3 between the HWL of 136.00 m and the LWL of 125.50 m.

The sedimentation in Wlingi and Lodoyo reservoirs is mainly caused by sediment inflow from the areas most affected by ejecta from eruptions of Kelud volcano, one of the most active volcanoes in Indonesia. Sedimentation in Wlingi reservoir is affected by sediment-laden

floods from the major tributaries to the Brantas River, i.e., the Putih, Jari, and Lekso Rivers, which drain the southern slopes of Kelud volcano. **Figure 3** depicts sediment deposits on the southern slopes of Kelud volcano and the upstream of the Lekso River just after the eruption in February 2014. Sedimentation in Lodoyo reservoir is caused by sediment outflow from Wlingi reservoir (66%), and the rest is largely from tributary streams draining the slopes of Kelud volcano and the southern catchment area. Longitudinal bed profile changes of Wlingi and Lodoyo reservoirs and aerial views of both reservoirs taken by a drone showing sediment deposition in the reservoirs during sediment flushing on 25–26 March 2016 can be seen in **Figures 4** and **5**, respectively.

Figure 3. Sediment deposits on the southern slopes of Kelud volcano on 23 April 2014 (top), sediment deposition in the upstream of the Lekso River on 23 April 2014 (middle), and debris flow in the Lekso River on 22 April 2014 (bottom).
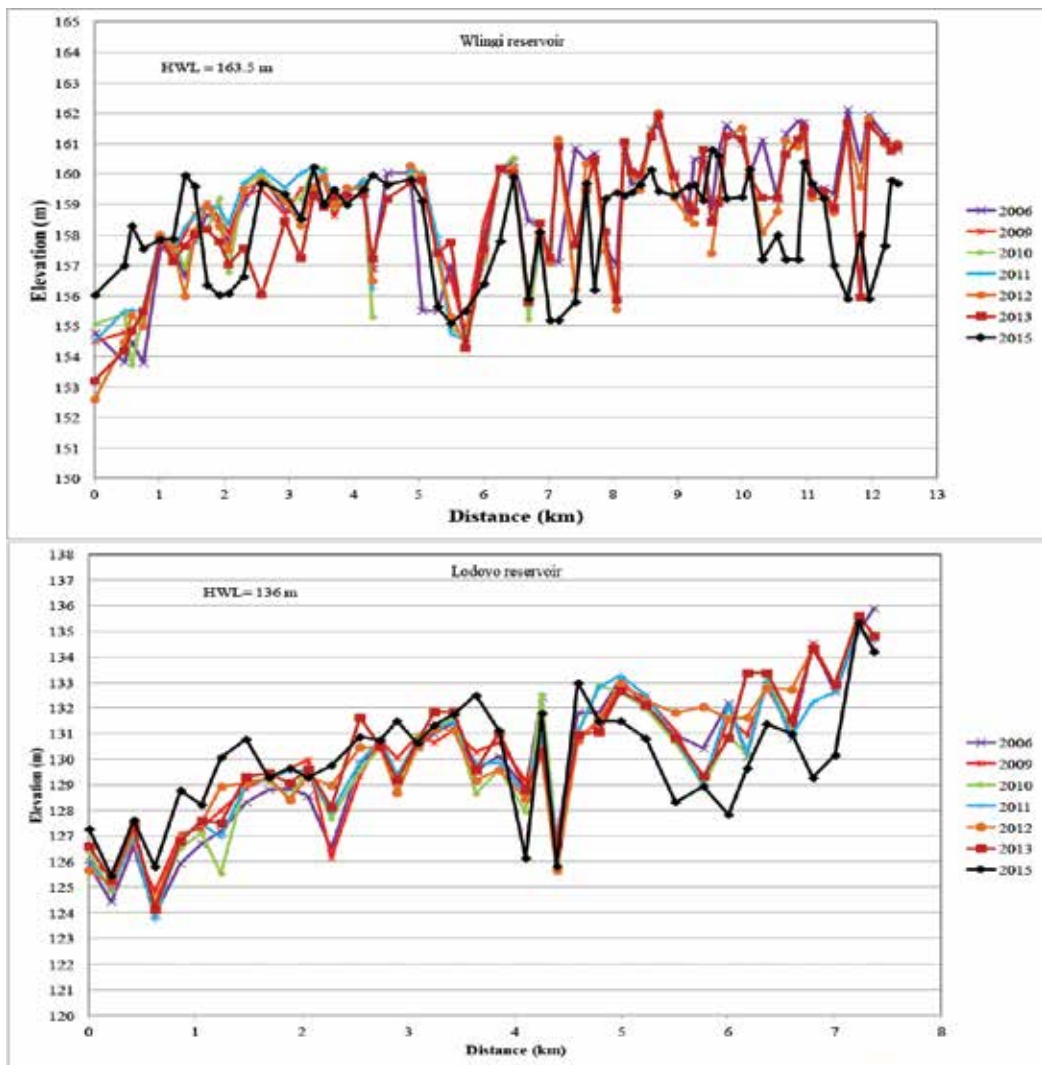
Figure 4. Longitudinal bed profile changes of Wlingi (top) and Lodoyo (bottom) reservoirs.

The sedimentation rate in Wlingi reservoir has been very rapid, with annual average sediment deposition from its completion in 1979 to January 1990 (before the eruption on 10 February 1990) of about 1.49 Mm³. The sedimentation rate increased over the 1977–1988 period, from 1.14 Mm³/year in 1977–1982 to 1.29 Mm³/year in 1982–1985 and 1.65 Mm³/year for the 1985–1988 period. This increase in yield rate is attributed to sediment outflow from lahar pockets and sabo check dams, which had mostly filled to capacity by the 1990 eruption of Kelud volcano. In the period of 1977 to January 1990, shortly before the February

Figure 5. Aerial views of Wlingi (left) and Lodoyo (right) reservoirs taken by a drone showing sediment deposition in the reservoirs during sediment flushing on 25–26 March 2016.

1990 eruption of Kelud volcano, the gross capacity had decreased to 4.6 Mm^3 (19.16% of the initial volume), and the effective storage decreased to 2.20 Mm^3, 42.31% of the initial volume [14].

The total sediment deposited in Wlingi reservoir from its construction in 1977 to immediately prior to the 1990 eruption is estimated at 19.40 Mm^3. Sediment inflow from the area between Sutami dam and Wlingi dam (catchment area, 430 km^2) which was not affected by Kelud volcano during the survey period is estimated at 0.43 Mm^3/year, 5.59 Mm^3 over the 13-year

Survey years	Gross storage		Effective storage		Dead storage	
	Volume (Mm^3)	Percentage (%)	Volume (Mm^3)	Percentage (%)	Volume (Mm^3)	Percentage (%)
1977	24.00	100.00	5.20	100.00	18.80	100.00
1982	18.32	76.33	NA	NA	NA	NA
1985	14.44	60.17	NA	NA	NA	NA
1988	9.50	39.58	NA	NA	NA	NA
Jan 1990	4.60	19.16	2.20	42.31	2.40	12.77
Eruption of Kelud volcano in February 1990						
March 1990	1.60	6.67	NA	NA	NA	NA
1995	4.94	20.58	1.59	30.58	3.35	17.82
2004	4.41	18.38	2.01	38.65	2.41	12.82
2009	4.38	18.25	2.01	38.65	2.37	12.61
2013	4.83	20.13	2.01	38.65	2.82	15.00
Eruption of Kelud volcano in February 2014						
2015	2.20	9.17	1.01	19.42	1.19	6.33

Note: NA = not available.

Table 3. Storage capacity change in Wlingi reservoir.
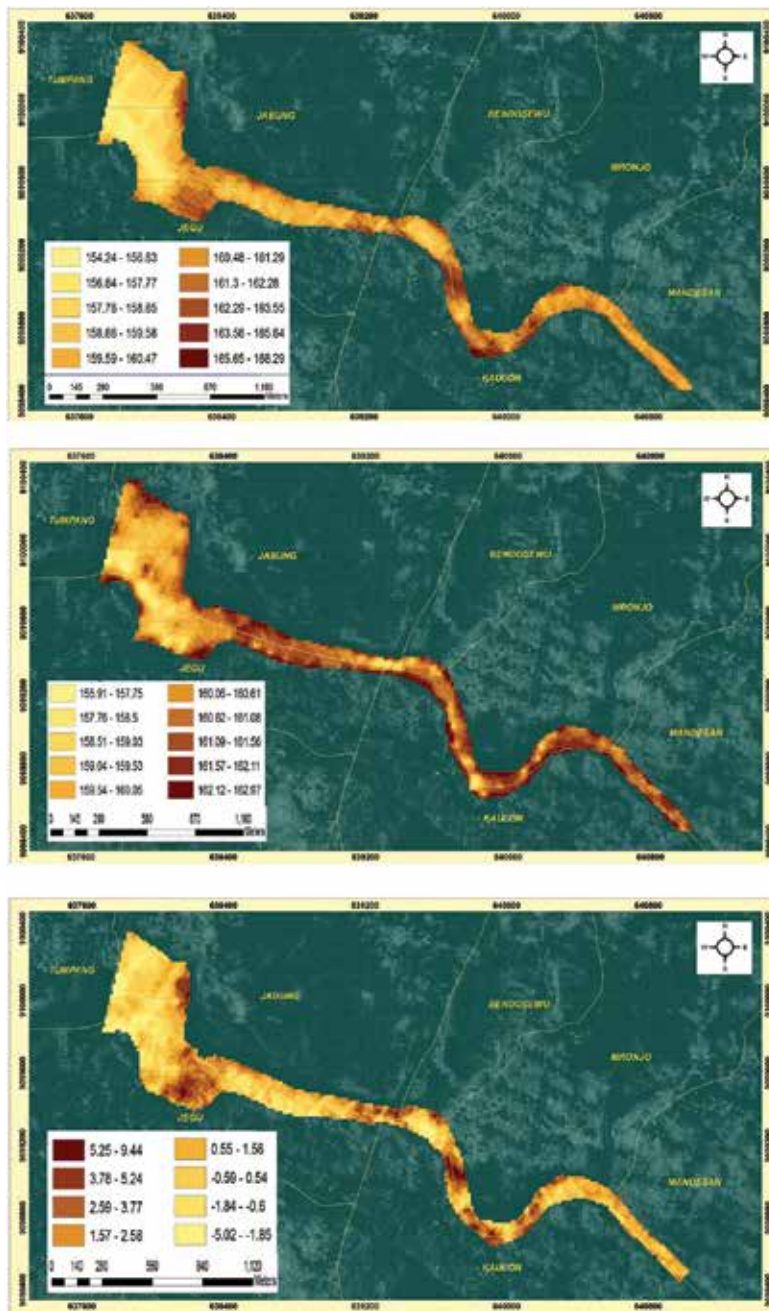
Figure 6. Bed elevation from March 2013 bathymetric survey in Wlingi reservoir (top), May 2015 bathymetric survey in Wlingi reservoir (middle), and measurement of bed evolution in Wlingi reservoir: difference between March 2013 and May 2015 bathymetries (bottom).

period. Thus, net sediment inflow from the tributaries (Putih, Jari, and Lekso) carrying ejecta from Kelud volcano over that period is estimated at 13.81 Mm³, which corresponds to an average sediment inflow rate of 1.06 Mm³/year.

After the eruption of Kelud volcano on 10 February 1990, Wlingi reservoir completely filled with sediment. According to the 1995 survey by Jasa Tirta I Public Corporation (PJT-1), the River Basin Management Agency of Brantas River basin, the gross storage and effective storage of Wlingi reservoir were then 4.94 and 1.59 Mm^3, respectively [13]. As a result of the continuous removal works, the effective storage capacity of Wlingi reservoir in 2013 recovered to 2.01 Mm^3, which corresponds to 38.65% of the designed effective storage capacity of 5.2 Mm^3. Changes in surveyed storage capacity since 1990 are significantly affected by the sediment removal works. Kelud volcano erupted again on 13 February 2014. The reservoir capacity survey in May 2015 indicates that the gross storage and effective storage capacities of Wlingi reservoir were decreased to 2.20 and 1.01 Mm^3, respectively [14]. **Table 3** summarizes storage capacity change in Wlingi reservoir from 1977 to 2015. Bed elevations from March 2013 and May 2015 bathymetric survey in Wlingi reservoir can be seen in **Figure 6**.

The rate of storage capacity decline in Lodoyo reservoir is, like Wlingi reservoir, very high. After the eruption of Kelud volcano in February 1990, when Wlingi reservoir completely filled with sediment and the trapping efficiency of Wlingi dam was very low, sediment outflow from Wlingi reservoir deposited in Lodoyo reservoir. According to the 1996 survey by PJT-1, the gross storage capacity of Lodoyo reservoir was 2.35 Mm^3, 45.19% of the initial volume. In 2013, the effective storage capacity of Lodoyo reservoir was reduced to 2.72 Mm^3, despite the implementation of flushing activities from 1999 and dredging from 2003. This represents 52.31% of the designed effective storage capacity of 5.20 Mm^3. Largely as a result of the 2014 eruption, storage capacity in Lodoyo reservoir decreased by about 50% between the surveys of 2013 and 2015. The reservoir capacity survey in May 2015 indicates that the

Survey years	Gross storage		Effective storage		Dead storage	
	Volume (Mm³)	Percentage (%)	Volume (Mm³)	Percentage (%)	Volume (Mm³)	Percentage (%)
1980	5.20	100.00	5.00	100.00	0.20	100.00
Eruption of Kelud volcano in February 1990						
1990	3.69	70.96	3.69	73.80	0.00	0.00
1993	2.84	54.62	2.84	56.80	0.00	0.00
1996	2.35	45.19	2.35	47.00	0.00	0.00
2003	2.03	39.04	1.86	37.20	0.17	85.00
2006	2.73	52.50	2.73	54.60	0.00	0.00
2009	2.67	51.35	2.67	53.40	0.00	0.00
2011	2.65	50.96	2.65	53.00	0.00	0.00
2013	2.72	52.31	2.72	54.40	0.00	0.00
Eruption of Kelud volcano in February 2014						
2015	1.33	25.78	1.33	26.60	0.00	0.00

Table 4. Storage capacity change in Lodoyo reservoir.
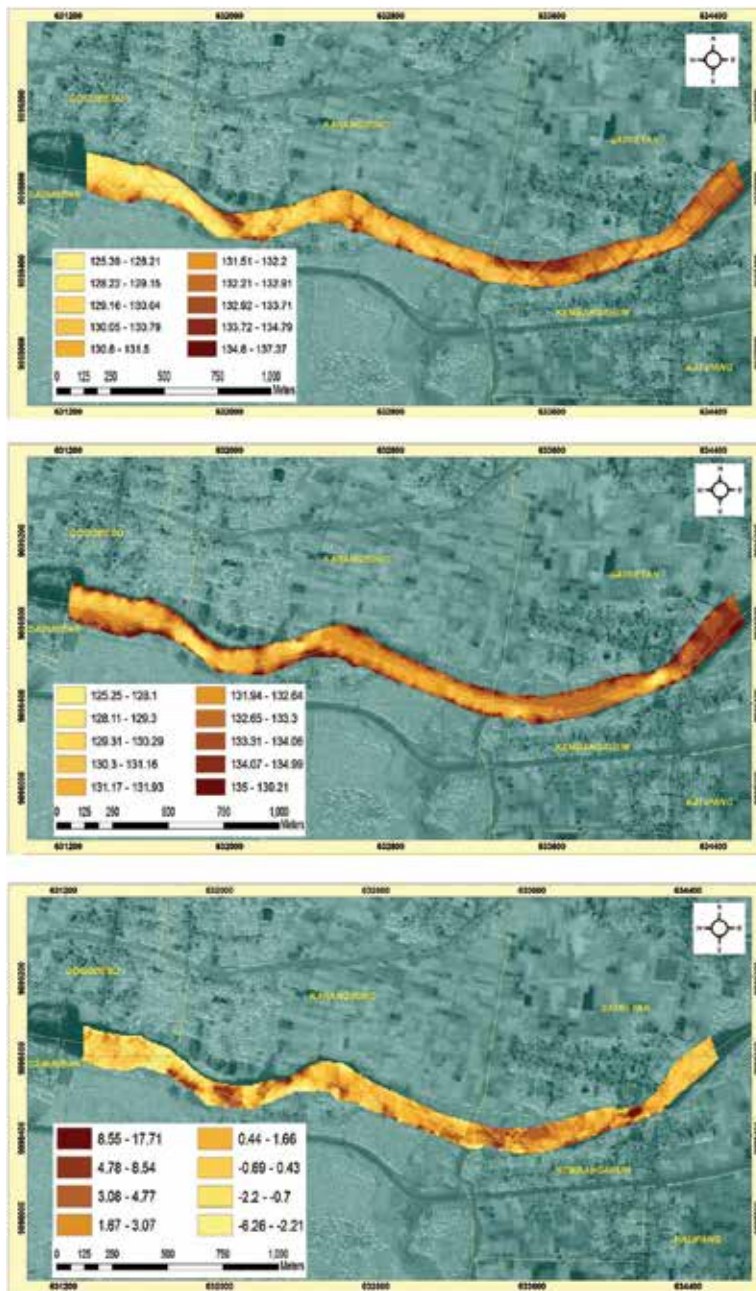
Figure 7. Bed elevation from March 2013 bathymetric survey in Lodoyo reservoir (top), May 2015 bathymetric survey in Lodoyo reservoir (middle), and measurement of bed evolution in Lodoyo reservoir: difference between March 2013 and May 2015 bathymetries (bottom).

effective storage capacity of Lodoyo reservoir was decreased to 1.33 Mm^3 [14]. **Table 4** summarizes storage capacity change in Lodoyo reservoir from 1980 to 2015. Bed elevations from March 2013 and May 2015 bathymetric survey in Wlingi reservoir can be seen in **Figure 7**.

5. Sedimentation management in Wlingi and Lodoyo reservoirs

5.1. Sabo works

Sabo is a Japanese term referring to intensive erosion and sediment control works, particularly in mountainous landscapes. The Sabo Plan in the Brantas River basin was formulated to control sediment and debris flows caused by mobilization of volcanic ash and mud by intensive rains in order to prevent and mitigate disasters [14]. The Sabo Plan targets mountain slope and river channel areas at high risk of debris flows and volcanic hazards. It was formulated by assessing both natural phenomena and socioeconomic conditions in order to ensure safety, quality of life, and socioeconomic development. The Sabo Plan in the Brantas River basin consists of two parts, i.e., the Sediment Control Plan and the Mt. Kelud Volcanic Disaster Mitigation Plan.

The Sediment Control Plan for control of debris flows was formulated using a combination of structural measures and nonstructural measures. The structural measures proposed included construction of 142 sediment control facilities consisting of 134 check dams (61 open-type check dams and 73 closed-type check dams) and 8 closed-type consolidation dams. The urgent works, including construction of five check dams on the upper reach of the Brantas River, one sediment settlement pond upstream of Sengguruh reservoir, one check dam, and two consolidation dams on the Lesti River, were completed in 2008 [15].

The second part of the Sabo Plan in the Brantas River basin is the Mt. Kelud Volcanic Disaster Mitigation Plan comprising: (1) volcanic sediment control plan against rainfall, secondary lahar (debris flow and mudflow), and (2) volcanic sediment control plan against volcanic eruption, primary lahar (nuee ardente, pyroclastic flow, volcanic ash fall, primary lahar with crater water). The Mt. Kelud Volcanic Disaster Mitigation Plan proposes construction of 145 sediment control facilities consisting of 49 check dams (11 open-type check dams and 38 closed-type check dams), 76 consolidation dams (16 open-type consolidation dams and 60 closed-type consolidation dams), and 20 sand pockets. Urgent works included the rehabilitation of one consolidation dam on the Semut River and two check dams on the Badak River, the construction of three check dams and two consolidation dams on the Lekso River, and the construction of a bypass channel. These urgent works were completed in 2011 under the support of the government of Japan [15]. **Figure 8** depicts the check dams in the Lekso River in Kelud volcanic area.

5.2. Bypass channels

The other countermeasure to control debris flow in the area affected by Kelud volcano is the construction of sediment bypass channels. To prevent the Putih River's lahar sediments from entering Wlingi reservoir, the sediment-laden flow of the Putih River was diverted to the Siwalan River by a bypass channel of about 3.32 km length. This first part of sediment bypass channel in Kelud volcanic area was completed in 1991. The bypass channel reduced sedimentation in Wlingi reservoir but shifted it downstream to Lodoyo reservoir. An extension of the bypass channel from the Siwalan River to the Brantas downstream of Lodoyo barrage was completed in 2008 (**Figure 9**). This is the second part of bypass channel development in Kelud

Figure 8. Check dams in Kelud volcanic area.
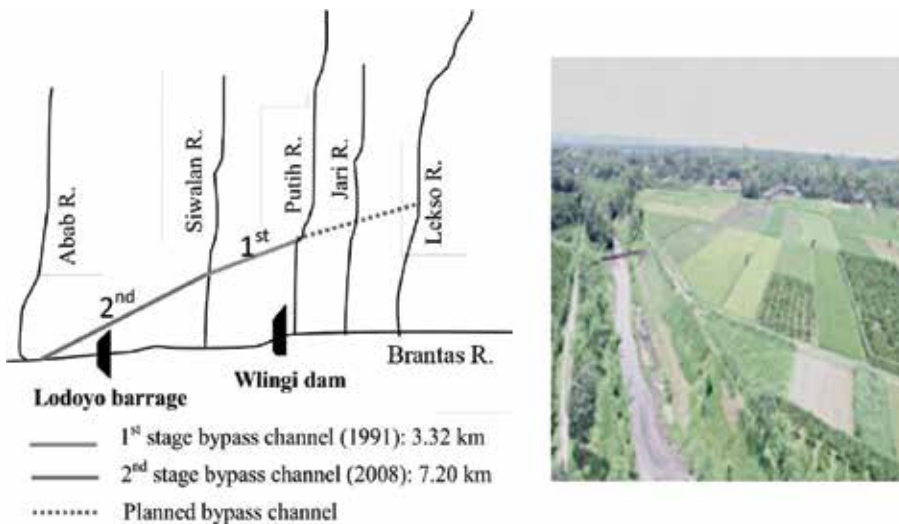
Figure 9. The bypass channel scheme in Kelud volcanic area (left) and photograph showing the bypass channel next to agriculture field.

volcanic area. The completed bypass channel and lower extension is 7.2 km long and 20 m wide, with an average flow depth of 3 m, and includes a side spillway in the Gondang River, 9 drain outlets, and 20 groundsills. The bypass channel extension was also conducted under the support of the government of Japan [15].

Diversion of sediment inflows from the Wlingi and Lodoyo reservoirs by sediment bypass channels is a part of long-term countermeasure program of the Mt. Kelud Volcanic Disaster Mitigation Plan that needs further development by constructing full diversions of both the lower and the upper parts of relevant lahar streams such as the Jari and Lekso Rivers. Sediment flows from the Putih River and the other rivers that drain from Kelud volcanic area to Lodoyo reservoir are diverted to below the reservoir by the existing bypass channel. At the moment, this channel does not divert sediment from the Lekso and Jari Rivers which flow into Wlingi reservoir. Full diversion of the lower parts of these lahar streams by construction of a bypass channel to connect with the existing channel from the Putih River to the Siwalan

River warrants urgent consideration. In addition, full diversion of the upper parts of the lahar streams with a second bypass channel obviously would further reduce reservoir sedimentation in Wlingi and Lodoyo reservoirs drastically. The design criteria for the proposed full diversion of lower and upper lahar streams, such as hydrology, sediment characteristics, and channel hydraulics, require careful survey, investigation, and design. A monitoring program to obtain baseline hydrological and water quality data for these streams should be developed and implemented as soon as possible. The potential problem for the development of the inclusive sediment bypass channel in Kelud volcanic area is primarily related to land acquisition.

5.3. Dredging, dry excavation, and flushing

While sabo facilities and sediment bypass channels are important measures to reduce sediment input from the slopes and channels of Kelud volcano, other measures are required to manage the sediment not trapped or bypassed by these facilities, as well as the 2.52 Mm^3 annual average (1996–2015) sediment inflow to Wlingi reservoir from the upper Brantas River catchment. To that end, sediment deposited in Wlingi and Lodoyo reservoirs is continuously removed by dredging, dry excavation, and flushing in order to recover their storage volume. About 12.52 Mm^3 of sediment have been removed from Wlingi and Lodoyo reservoirs by dredging operations since 1988. Currently, due to limited availability of disposal sites adjacent to Wlingi dam, dredged sediment is also discharged to the river downstream of the dam. **Figure 10** depicts sediment dredging works in Wlingi and Lodoyo reservoirs.

The other measure used to recover the storage volume of Wlingi and Lodoyo reservoirs is flushing operation. The sediment flushing operation in Wlingi and Lodoyo reservoirs is generally conducted during the rainy season by fully opening the spillway gates to empty both reservoirs. Flushing operations commenced in August 1990, 6 months after the 1990 eruption, and have been conducted occasionally since then when there is sufficient water. **Figure 11** depicts the high-flow velocities that entrain and transport large volumes of sediment from the reservoirs to the river downstream during sediment flushing in the Wlingi and Lodoyo reservoirs. About 15.11 Mm^3 of sediment has been removed from both reservoirs by flushing since August 1990. Sediment flushing has proven to be an effective and economical measure to recover the

Figure 10. Sediment dredging works in Wlingi reservoir (left) and Lodoyo reservoir (right).

Figure 11. Sediment flushing through spillway gates in Wlingi reservoir (left) and Lodoyo reservoir (right) on 29–31 March 2013.

reservoirs' storage capacity. **Figure 12** shows ratio of total water volume and flushed sediment volume of sediment flushing operations in Wlingi and Lodoyo reservoirs from 1990 to 2016.

The sediment flushing in Wlingi and Lodoyo reservoirs is very effective to remove deposited sediment, same as sediment flushing operations in other cascade reservoirs in the world such as in Verbois and Chancy-Pougny reservoirs on the Rhone River in Europe [16] and Dashidaira and Unazuki reservoirs on the Kurobe River in Japan [17, 18]. The efficiency of sediment flushing operation in Wlingi and Lodoyo cascade reservoirs in 2016 was 0.042, almost three times the efficiency of sediment flushing operation in 2009 [19]. This improved flushing efficiency is largely a result of the very large volume of deposited sediment in both reservoirs after the eruption of Kelud volcano in February 2014. The efficiency of sediment flushing operation in Wlingi and Lodoyo reservoirs in 2016 is higher than reported for cascade reservoirs elsewhere
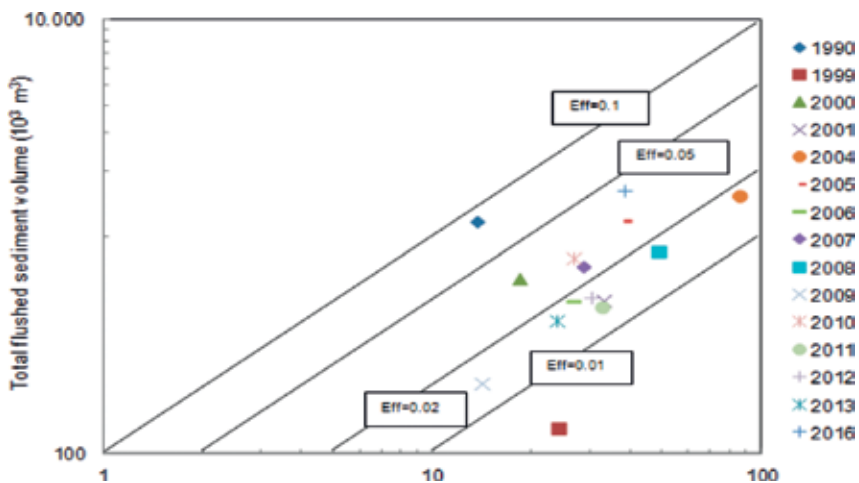
Figure 12. Total water volume and flushed sediment volume of sediment flushing operations in Wlingi and Lodoyo reservoirs (1990–2016).

in the world. In Dashidaira and Unazuki reservoirs, the flushing efficiency calculated from the water consumption including the discharge during drawdown and the sediment volume flushed out is about 0.02 [20]. In four hydropower reservoirs in the Italian central Alps, i.e., Cancano, Valgrosina, Sernio, and Madesimo, sediment flushing efficiency varied between 0.001 and 0.006. This parameter was also calculated as the ratio between the volume of evacuated sediment and the corresponding volume of water employed in the controlled sediment flushing operations (CSFO) including water for dilution [21].

Flushing discharges extreme sediment loads with very limited volumes of water, commonly producing aquatic environmental impacts in downstream area including very low dissolved oxygen (DO) and very high sediment concentrations that interfere with the function of gills in fish, smother stream benthos, reduce visibility and light penetration, and have channel morphological impacts such as infilling of pools and clogging of river gravels with fine sediment, thereby eliminating spawning sites and destroying habitat of vulnerable species [22]. In Wlingi and Lodoyo reservoirs, sediment flushing has caused impacts to river environment and water quality downstream of the reservoirs mainly due to very high concentrations of suspended solids. Currently this impact is not considered adequately, because it is only significant for several days during the flushing operation. However, sediment flushing from reservoirs is not so feasible at many sites worldwide because there have caused severe impacts on the downstream aquatic environment, principally where heavy deposition or high concentration of suspended solids affects the habitat and survival of fish and other wildlife species. In this respect, short periods of high-intensity, high sediment concentration flushing are particularly problematic. Therefore time of flushing operation should be long enough to mitigate the extreme adverse influences of sediment flushing if the higher volume of water needed is available [23]. By adding more clear water to have dilution effect during flushing operation, high peak suspended sediment concentrations may be reduced, diminishing negative ecological impacts [24]. Sediment flushing operation in Wlingi and Lodoyo reservoirs should be supported by additional water available from Sutami and Wonorejo reservoirs upstream to provide the dilution effect and should be timed to coincide with natural high-flow events.

Greater attention has been paid to the environmental effects of sediment flushing in Europe since the flushing of Genissiat reservoir on the Rhone River in France produced severe damage to the downstream fishery due to insufficient water being available from the upstream reservoirs in Switzerland in 1965 and 1978 [23]. Since then, reservoir operations for flushing have been subject to regulatory limits on downstream sediment loads or concentrations, which have to be taken into account in the detailed planning of every flushing operation. For example, in Switzerland, it is stipulated that the mean suspended sediment concentration (SSC) during flushing operation should not exceed 10 mg/L at the reservoirs in crystalline areas and 70 mg/L at the reservoirs in noncrystalline areas and the peak SSC should be in the range 1–10 g/L except one river with 70 g/L [25]. While in France, it is specified that maximum SSC should not exceed 10 g/L during flushing operation [25]. In order to fulfill the environmental regulations, the flushing operation at Genissiat reservoir has been performed in concert with Verbois and Chancy-Pougny dams in Switzerland since 1978 [26]. Thus to control the environmental effects of sediment flushing operations in Wlingi and Lodoyo reservoirs, it is necessary to regulate and monitor the SSC during flushing and take it into account in the detailed planning of the flushing operations.

6. Conclusion

Wlingi and Lodoyo reservoirs are severely affected by eruptions of Kelud volcano, one of the most active volcanoes in Indonesia. Before the February 2014 eruption of Kelud volcano, following the eruptions in 1990 and 2007, the capacity of Wlingi reservoir was, by 2013, restored to 4.83 Mm^3, which corresponds to 20.1% of the initial capacity of 24.00 Mm^3. Similarly, the capacity of Lodoyo reservoir was restored to 2.72 Mm^3, which corresponds to 52.3% of the initial capacity of 5.20 Mm^3. However, after the February 2014 eruption, the capacity of Wlingi and Lodoyo reservoirs decreased dramatically to 2.20 and 1.33 Mm^3, respectively, just 46% and 49% of their pre-eruption capacities and 19.42 and 26.60% of their initial capacities. To cope with the extreme sedimentation problems in Wlingi and Lodoyo reservoirs, diverse sediment management strategies have been applied in these reservoirs and their catchments. Construction of many on-stream sediment control facilities (sabo works) and a sediment bypass channel has reduced sediment inflow to the reservoirs. Removal of deposited sediment by dredging and hydraulic flushing in Wlingi and Lodoyo reservoirs has also resulted in storage capacity recovery. The sedimentation problems in Wlingi and Lodoyo reservoirs are affected by recurrent volcanic activity of Kelud volcano. Consequently, sediment management strategies for both reservoirs require constant maintenance and recurrent operations, evaluation, and improvement in order to achieve sustainable use of the reservoirs for their diverse design purposes, while minimizing downstream environmental and economic effects of the management interventions.

Acknowledgements

Author details

Fahmi Hidayat[1,2]*, Pitojo T. Juwono[3], Agus Suharyanto[1], Alwafi Pujiraharjo[1], Djoko Legono[4], Dian Sisinggih[3] and David Neil[5]

*Address all correspondence to: hidayat.f@jasatirta1.net

1 Civil Engineering Department, Brawijaya University, Malang, Indonesia

2 Jasa Tirta I Public Corporation, Indonesia

3 Water Resources Engineering Department, Brawijaya University, Malang, Indonesia

4 Department of Civil and Environmental Engineering, Universitas Gadjah Mada, Indonesia

5 Centre for Advanced Research on Global Change, Hanoi University of Natural Resources and Environment (HUNRE), Vietnam

References

[1]   Milliman JD, Syvitski JPM. Geomorphic/tectonic control of sediment discharge to the ocean; the importance of small mountainous rivers. Journal of Geology. 1992;**100**:525-525

[2]   Mercado RA, Bertram J, Lacsamana T, Pineda GL. Socioeconomic impacts of the mount Pinatubo eruption. In: Newhall CG, Punonbayan RS, editors. Fire and Mud: Eruptions and Lahars of Mount Pinatubo, Philippines. Quezon City: Philippine Institute of Volcanology and Seismology/Seattle: University of Washington Press; 1996. pp. 1063-1070

[3]   Morris L, G. Sediment management and sustainable use of reservoirs. In: Wang LK, Yang CT, editors. Modern Water Resources Engineering. New York, USA: Humana Press; 2014

[4]   Jakob M, Hungr O. Debris-Flow Hazard and Related Phenomena. Chichester, UK: Praxis Publishing Ltd; 2005

[5]   Lesage P, Surono. Seismic precursors of the February 10, 1990 eruption of Kelut volcano, Jawa. Journal of Volcanology and Geothermal Research. 1995;**65**:135-146

[6]   Soetojo et al. Kelut Volcano Volcanic Debris Control Project. Government of Indonesia: Directorate General of Water Resources Development, Ministry of Public Works and Power; 1969

[7]   NASA. Indonesia's Mount Kelud Erupts. 2014. Available from: http://earthobservatory. nasa.gov/IOTD/view.php?id=83144 [Accessed: August 27, 2016]

[8]   Global Volcanism Program. Report on Kelud (Indonesia). 2014. In: Wunderman R, editor. Bulletin of the Global Volcanism Network, 39:2. Smithsonian Institution. Available from: 10.5479/si.GVP.BGVN201402-263280

[9]   Tanaka LH, Iguchi M, Nakada S. Numerical solutions of volcanic ash plume dispersal from Mt. Kelud in Indonesia on February 13, 2014. Journal of Disaster Research. 2016;**11**(1):31-42

[10]   Iguchi M, Surono, Nishimura T, Hendrasto M, Rosadi U, Ohkura T, Triastuty H, Basuki A, Loeqman A, Maryanto S, Ishihara M, Yoshimoto K, Nakada S, Hokanishi N. Methods for eruption prediction and hazard evaluation at Indonesian volcanoes. Journal of Disaster Research. 2012;**7**(1):26-36

[11]   Bélizal ED, Lavigne F, Gaillard JC, Grancher D, Pratomo I, Komorowski I. The 2007 eruption of Kelut volcano (East Java, Indonesia): Phenomenology, crisis management and social response. Geomorphology. 2010;**136**:165-175

[12]   Bourdier JL, Pratomo I, Thouret JC, Boudon G, Vincen PM. Observations, stratigraphy and eruptive processes of the 1990 eruption of Kelut volcano, Indonesia. Journal of Volcanology and Geothermal Research. 1997;**79**:181-203

[13]   Hidayat F, Juwono PT, Suharyanto A, Pujiraharjo A, Sisinggih D, Legono D. Sedimentation in rivers and reservoirs following the eruptions of Kelut volcano, Indonesia. In: Wieprecht S, Haun S, Weber K, Noack M, Terheiden K, editors. River Sedimentation. Leiden, the Netherlands: CRC Press/Balkema; 2017

[14]   Hidayat F, Juwono PT, Suharyanto A, Pujiraharjo A, Legono D, Sisinggih D, Neil D, Fujita M, Sumi T. Assessment of sedimentation in Wlingi and Lodoyo reservoirs: A secondary

disaster following the 2014 eruption of Mt. Kelud, Indonesia. Journal of Disaster Research. 2017;**12**(3):617-630

[15] Nippon Koei Co., Ltd. and Associates. Completion Report on Overall Consulting Services for Water Resources Existing Facilities Rehabilitation and Capacity Improvement Project. Government of Indonesia: Directorate General of Water Resources Development, Ministry of Public Works; 2012

[16] Bollaert EFR, Diouf S, Zanasco JL, Barras J. Sequential flushing of Verbois and Chancy-Pougny reservoirs (Geneva, Switzerland). In: Schleiss AJ, De Cesare G, Franca MJ, Pfister M, editors. Reservoir Sedimentation. Leiden, the Netherlands: CRC Press/Balkema; 2014

[17] Sumi T. Sediment flushing efficiency and selection of environmentally compatible reservoir sediment management measures. In: International Symposium on Sediment Management and Dams, 2nd EADC Symposium; Yokohama, Japan; 2005

[18] Sumi T. Evaluation of efficiency of reservoir sediment flushing in Kurobe River. In Fourth International Conference on Scour and Erosion; Tokyo, Japan. 2008. pp. 5-7

[19] Hidayat F, Juwono PT, Suharyanto A, Pujiraharjo A, Sisinggih D, Legono D. 2017. Assessment of efficiency and environmental impact of sediment flushing from Wlingi and Lodoyo cascade reservoirs, Indonesia. In: E-proceedings of the 37th IAHR World Congress, August 13-18, 2017; Kuala Lumpur, Malaysia

[20] Kantoush SA, Sumi T, Suzuki M, Murasaki M. Impacts of sediment flushing on channel evolution and morphological processes: Case study of the Kurobe River, Japan. In: Dittrich, Koll, Aberle, Geisenhainer, editors. River Flow 2010. Bundesanstalt für Wasserbau 2010. ISBN 978-3-939230-00-7

[21] Brignoli ML, Quadroni S, Crosa G, Gentili G, Batalla RJ. Experiences of controlled sediment flushing from four alpine reservoirs. In: Wieprecht S, Haun S, Weber K, Noack M, Terheiden K, editors. River Sedimentation. Leiden, the Netherlands: CRC Press/Balkema; 2017

[22] Annandale GW, Gregory LM, Pravin Karki. Extending the Life of Reservoirs: Sustainable Sediment Management for Dams and Run-of-River Hydropower. Directions in Development. Washington, DC: World Bank; 2016. DOI: 10.1596/978-1-4648-0838-8. License: Creative Commons Attribution CC BY 3.0 IGO

[23] Liu J, Minami S, Otsuki H, Liu B, Ashida K. Environmental impacts of coordinated sediment flushing. Journal of Hydraulic Research. 2004;**42**(5):461-472. DOI: 10.1080/00221686.2004.9641216

[24] Sumi T, Nakamura SY, Hayashi K. The Effect of Sediment Flushing and Environmental Mitigation Measures in the Kurobe River. In: 23rd ICOLD Congress; 2009

[25] Staub E. Effects of sediment flashing on fish and invertebrates in Swiss Alpine rivers. In: International Workshop and Symposium on Reservoir Sedimentation Management; October; Toyama, Japan. 2000. pp. 109-118

[26] Habara S, Suzuki N, Tokito Y, Asaka M. The Measures for the Sediment at the Dam Reservoirs in Europe. Tokyo: Water Resources Environment Technology Center; 2001

Analysis of Relationships Between Permeability, Pressure on the Solids, and Porosity for Calcium Carbonate

Bruno Arantes Moreira,
Fábio De Oliveira Arouca and
João Jorge Ribeiro Damasceno

Additional information is available at the end of the chapter

Abstract

This study aims to evaluate the constitutive equations for pressure on the solids and permeability of porous media consisting of calcium carbonates with different degrees of polydispersity. The constitutive relations are intended to assist in the modeling and simulation of sedimentation operations when theory of mixtures of continuum mechanics is used. In this work, a porous media was obtained after the complete sedimentation of aqueous suspensions of calcium carbonate. The gamma-ray attenuation technique was used, which allowed the realization of measurements of the distribution of porosity in the sediment before and after liquid percolation. The experimental results showed a considerable degree of compressibility for calcium carbonates, and significant deviations from the Kozeny-Carman correlation when the carbonates were used to express permeability. Therefore, the use of the incompressibility hypothesis for this solid in equations that model sedimentation may not be a viable consideration. Overall, this study provides relevant information about sedimentation for situations in which the formation of compressible sediments occurs.

Keywords: constitutive equations, permeability, porosity, pressure on the solids, sedimentation

1. Introduction

The sedimentation phenomenon has a great importance in several processes related to the chemical and mining industry. For this reason, the behavior of particles settling in a fluid has been widely studied over the years in both Newtonian fluids [1–6] and non-Newtonian fluids [7–13].

The first study to evaluate the sedimentation theoretically was proposed by Kynch [14]. In the Kynch model, the descending interface is not described mathematically, being necessary to obtain it empirically. The upward interface is provided by way of lines (or curves) of equi-concentration.

Thus, the theory only describes the propagation of waves of the same concentration that propagates from the bottom of the base to the clarified interface. Four distinct regions are verified during the sedimentation process according to Kynch's theory (**Figure 1**):

	Region of clarified liquid (volumetric solids concentration is zero, $\varepsilon_s=0$)
	Region where the sedimentation rate is constant and the solids concentration remains equal to the initial concentration of the suspension ($\varepsilon_s=\varepsilon_{s0}$).
	Region where sedimentation rate is decreasing and the concentration varies da from initial solid concentration (ε_{s0}) up to the maximum solids concentration (ε_{sm}).
	Region of incompressible sediment, in which settling velocity of particles is zero and solid concentration is equal to the maximum solids concentration ($\varepsilon_s=\varepsilon_{sm}$).

Figure 1. Description of the batch sedimentation phenomenon according to Kynch's theory.

Several studies in the literature mention that Kynch's model describes reasonably well the sedimentation that forms sediments with a low degree of compressibility, such as non-flocculated mineral particles [15]. For situations where solid-fluid separation causes the forma-tion of compressible sediments, the theory is not indicated to describe sedimentation.

The accommodation of the solid materials is related to the existing forces on the particles that are not taken into account in the mathematical modeling developed by Kynch [14].

In order to describe the phenomenon in a way that is closer to reality, it is verified that the modeling developed by Kynch has been modified. Thus, the equation of the motion (associ-ated with the force balance of the particle) has been included into the modeling of the

sedimentation phenomenon [5–7, 16]. An example of modeling that includes the balance of particle forces is the theory of mixtures of continuum mechanics.

The theory of mixtures of continuum mechanics has been used successfully in describing solid-fluid separation systems. Such theory has been indicated even in situation where the formation of compressible porous media occurs (as it usually occurs in sedimentation and filtration operations) [5, 6].

The application of theory of mixtures of continuum mechanics is confronted with the difficulty in obtaining the constitutive equation of pressure on the solids, $P(\varepsilon_s)$, and permeability of porous media, $k(\varepsilon_s)$. Generally, constitutive equations are empirically determined and express the relationships between porosity, pressure on the solids, and permeability of the porous matrixes.

The functions, $P(\varepsilon_s)$ and $k(\varepsilon_s)$, when used in the mathematical modeling of the phenomenon, associate the compression effects to the porous medium, representing the thickening and filtration processes in a more reliable way with the physical reality [17–20].

Despite the importance and the several techniques available in the literature for determination of constitutive equations, many works adopt the porous media as incompressible like simplifying assumption, and the minority solve numerically the problem of thickening and filtration with the formation of compressible porous media [18].

In this context, this study aims to evaluate the relationships between porosity, permeability, and stresses in solids, $P(\varepsilon_s)$ and $k(\varepsilon_s)$, for porous media composed of carbonates. The methodology used in this study (gamma-ray attenuation technique) avoids using compression-permeability cells through densification presses, reaching reliable results for $P(\varepsilon_s)$ and $k(\varepsilon_s)$ even at low pressures.

Moreover, the permeability results, $k(\varepsilon_s)$, determined experimentally were compared with the values estimated by the classical Kozeny-Carman correlation for porous media with different degrees of size and polydispersity.

2. Theoretical analysis

In the theory of mixtures of continuum mechanics, the equations of continuity and motion for each constituent of the mixture must be used. For the case of one-dimensional flow through the porous media, the numbers of scalar available equations to study the problem are two continuity (Eqs. (1) and (2)) and two motion equations (Eqs. (3) and (4)):

$$\frac{\partial\left(\rho_f \varepsilon_f\right)}{\partial t} + \nabla \cdot \left(\rho_f \varepsilon_f \boldsymbol{v}_f\right) = 0. \tag{1}$$

$$\frac{\partial(\rho_s \varepsilon_s)}{\partial t} + \nabla \cdot (\rho_s \varepsilon_s \boldsymbol{v}_s) = 0. \tag{2}$$

$$\rho_f \varepsilon_f \left[\frac{\partial v_f}{\partial t} + (\nabla v_f) v_f \right] = \nabla \cdot T_f - m + \rho_f g \tag{3}$$

$$\rho_s \varepsilon_s \left[\frac{\partial v_s}{\partial t} + (\nabla v_s) v_s \right] = \nabla \cdot T_s - m + \left(\rho_s - \rho_f \right) \varepsilon_s g. \tag{4}$$

where ε_f is the local porosity of the suspension; ε_s is the local volumetric concentration of solids; ρ_f and ρ_s are, respectively, the fluid and solid densities; v_s and v_f are, respectively, the interstitial velocities of the solid and fluid; m represents the resistive force that the fluid exerts on the solid matrix; g is the local gravity; and T_f and T_s are, respectively, the stresses exerted on the fluid phase and on the solid phase.

From the analysis of Eqs. (1)–(4), it can be seen that the number of variables to be measured are seven (two concentrations, two velocities, two stresses, and a resistive force). Thus, another three equations are required to nullify the number of degrees of freedom and making system of equations solvable.

Considering that the sum of the volume fraction of solids and fluid is equivalent to 1 ($\varepsilon_s + \varepsilon_f = 1$), then it is necessary to determine only two constitutive equations to make the system of equations solvable: one for stress in solids (T_s) and other for the resistive force.

2.1. Stress on the solids

For the resolution of the system, it is necessary to adopt constitutive hypotheses related to the tension on the solid (T_s) and for the resistive force (m).

d'Ávila [21] developed a constitutive theory considering the solid-fluid system as an isotropic medium. The authors indicate that the stress tensor may be represented as follows:

$$T_i = -piI - T_i'' \tag{5}$$

where pi and T_i'' are, respectively, the pressure (the arbitrary tensor) and the extra stress (constitutive part of the tensor). The term T_i'' represents the dynamic part of the stress tensor, and the term piI is the static part, being I the identity tensor.

The majority of studies in the literature suggest the dependence of pressure on the solids as an exclusive function of the porosity of the system:

$$T_i(\varepsilon_f) = -P_i(\varepsilon_f)I. \tag{6}$$

An example of such expressions can be enunciated by the model proposed by Arouca [6]:

$$P(\varepsilon_s) = a\varepsilon_s{}^b \tag{7}$$

where a and b are model parameters.

2.2. The resistive force

The representation of the resistive force vector is another necessary condition to make determined the system formed by the equations of continuity and motion for the solid and the fluid. For the case of one-dimensional slow flow in porous media, the resistive force can be represented by Darcy's law:

$$m = \frac{\mu \varepsilon_f}{k(\varepsilon_f)} \left(v_s - v_f \right) \tag{8}$$

where k is the permeability of the porous medium and μ is the viscosity of the fluid.

There are models in the literature that describe the relationship between permeability and porosity from the empirical determination of its parameters. An example of such expressions can be enunciated the model proposed by Tiller and Leu [22]:

$$k(\varepsilon_s) = k_0 \left(\frac{\varepsilon_s}{\varepsilon_{sc}} \right)^{-\eta} \tag{9}$$

where k_0, ε_{sc}, and η are parameters of the model.

The correlations in literature that express the permeability as a function of porosity allows obtaining constitutive equation $k(\varepsilon_s)$ without the experimental determination. An example of such correlation is the Kozeny-Carman (Eq. (10)). Such correlations allow correlating the permeability with the properties of the particles and the porosity of the medium:

$$k = \frac{\left(D_p \varphi \right)^2 \varepsilon_f{}^3}{180 \left(1 - \varepsilon_f \right)^2} \tag{10}$$

where φ is the sphericity of the particle and d_p is the diameter of the sphere of the same volume of the particle.

Endo et al. [23] proposed an equation that relates the porosity with the permeability, contemplating the effects of form, and polydispersity of the particulate material:

However the use of the equation of Endo et al. [23] requires particle sizes to follow the lognormal distribution. In addition, there is in some cases a certain difficulty to estimate some of the parameter of equation-like factor form. For this reason, it is often necessary to empirically obtain the relationships between permeability and porosity.

The experimental determination of constitutive equations, $k(\varepsilon_s)$ and $P(\varepsilon_s)$, that govern dimensional percolation fluids through porous media with low porosity can be made with the aid of compression-permeability cells through presses densification tests [24, 25].

However, according Tiller et al. [26], the use of compression-permeability cells at low stresses may lead to considerable errors in the characterization of porous media. According to the authors, the porosity distribution in the porous matrix as homogeneous must be considered

as simplifying assumption. This situation is not achieved when performing tests at low pressures, because the uniformity of concentration in the sample is not achieved.

Furthermore, the lowest stress applied in porous medium by a compression-permeability cell is often above the tension in which the filter cake and the sediments are submitted in filtration and thickening operation.

In this context, Damasceno [5] developed a methodology that has been successfully used by some studies in the literature [17–20] to assess the relationships between porosity, stress in solids, and permeability of porous media. This technique was used in this study and avoids using compression-permeability cells through densification presses, reaching reliable results at low pressures.

3. Material and methods

In this study, samples of calcium carbonate (designed as calcium carbonate A and calcium carbonate B) were used as suspended particles in aqueous continuous phase.

The granulometric analyses of the materials (calcium carbonate A and calcium carbonate B) were obtained using the particle size analyzer Malvern Mastersizer Microplus MAF 5001®. **Figure 1** represents the cumulative distribution obtained for the carbonates used in this study.

As can be seen in **Figure 2**, the samples of calcium carbonate B have a larger range of particle size distribution, that is, such material can be considered more polydisperse than calcium carbonate A.

In **Table 1**, the volumetric particle diameters corresponding to 10% ($D_{0.1}$), 50% ($D_{0.5}$) and 90% ($D_{0.9}$) of the cumulative distribution (diameter cutting) along with the Sauter mean diameter ($D_{3,2}$) are shown.

The density of solids was determined by helium pycnometry. The results are shown in **Table 2**.

3.1. Experimental methodology

The methodology proposed Damasceno [5] to determine the relationship between porosity, stress in solids, and permeability can be established from the following considerations and simplifying assumptions:

a.   The flow through the porous medium is slow and steady one dimensional (z direction).

b.   Darcy's law represents the resistive force.

c.   Tension in solids is an exclusive function of local porosity.

d.   The terms of the inertial equation of motion for the constituent solid are negligible.

Under these conditions, the equations of continuity for the fluid and the solid phase (Eqs. (1) and (2)) and the equation of motion for the solid (Eq. (4)) reduce to

$$\frac{d}{dz}\left(\varepsilon_s \boldsymbol{v_s}\right) = 0 \tag{11}$$

$$\frac{d}{dz}\left(\varepsilon_f \boldsymbol{v_f}\right) = 0 \tag{12}$$
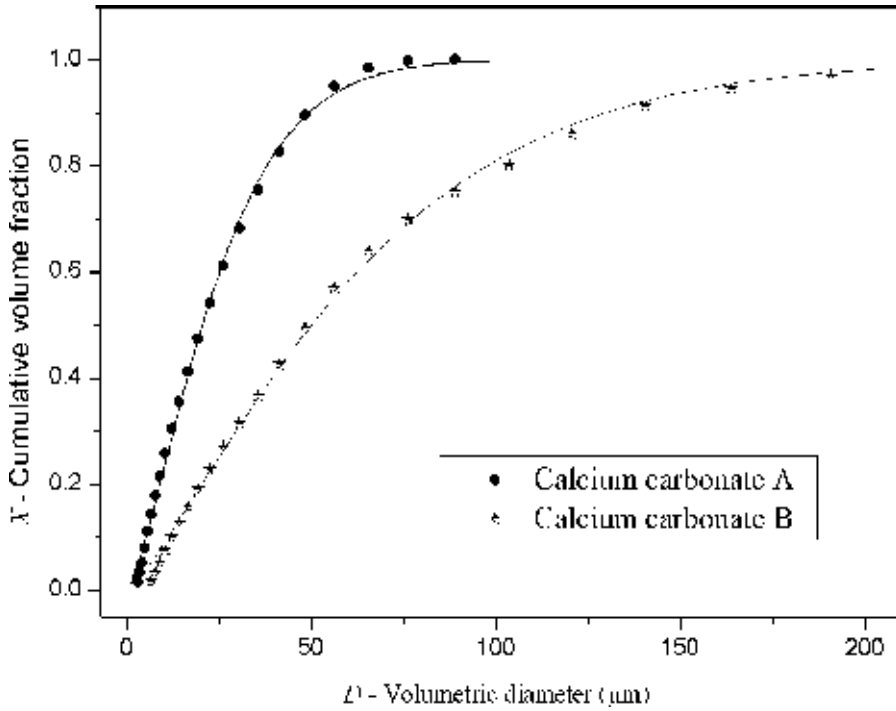
Figure 2. Cumulative distribution of the material solids.

Solid	$D_{0.1}$ (μm)	$D_{0.5}$ (μm)	$D_{0.9}$ (μm)	$D_{3.2}$ (μm)
Calcium carbonate A	5.39	20.48	48.80	12.84
Calcium carbonate B	12.11	48.73	134.71	29.73

Table 1. Volumetric particle diameters.

Solid	Density (g/cm^3)
Calcium carbonate A	2.84
Calcium carbonate B	2.81

Table 2. Density of calcium carbonate.

$$\frac{dP_s}{dz} = \frac{\mu \varepsilon_f}{k(\varepsilon_f)} \left(v_f - v_s\right) + \left(\rho_s - \rho_f\right)\varepsilon_s g \tag{13}$$

Integrating Eqs. (11) and (12) takes the relationships shown below:

$$\varepsilon_s v_s = q_s \tag{14}$$

$$\varepsilon_f v_f = q_f \tag{15}$$

Substituting Eqs. (14) and (15) in (13):

$$\frac{dP_s(\varepsilon_f)}{dz} = \frac{\mu \varepsilon_f}{k(\varepsilon_f)} \left(\frac{q_f}{\varepsilon_f} - \frac{q_s}{\varepsilon_s}\right) + \left(\rho_s - \rho_f\right)\varepsilon_s g \tag{16}$$

The functions $P_s(\varepsilon_s)$ and $k(\varepsilon_s)$ are, respectively, called constitutive equations for pressure on the solids and permeability of porous media.

The experimental determination of constitutive equations for $P_s(\varepsilon_s)$ and $k(\varepsilon_s)$ can be done by using Eq. (16) and by establishing at least two different situations of the concentration distribution in the sediment and the superficial velocity of the solid (q_s) and the liquid (q_f) [5–7].

The first experiment can be idealized in a static porous media, in which the superficial velocity of solid and liquid is null ($q_f = q_s = 0$). For this condition, and with the motion equation for the solid constituent, the expression that relates the stress in solids and porosity of the porous media is given by

$$P_s = \left(\rho_s - \rho_f\right)g \int_0^L \varepsilon_s dz \tag{17}$$

where "z" is the axis reference measured from the top of the sediment height "L."

By establishing the function $P(\varepsilon_s)$, a second experiment can be designed to determine the permeability of the porous media. The sediment formed inside the test tube undergoes an accommodation process, which was characterized for a new configuration of the porous matrix, resulting from the slow liquid percolation through the porous media. With such conditions, Eq. (16) can be rewritten as

$$k = \frac{\mu q_f}{\frac{dP_s}{d\varepsilon_f}\frac{d\varepsilon_f}{dz} - (\rho_s - \rho_f)\varepsilon_s g} \tag{18}$$

In this study, the characterization of a static porous media was obtained after the complete sedimentation of aqueous suspensions of calcium carbonate. For this, the system was allowed to stand for 48 hours to stabilize the porous matrix. Then, the flow control valve was opened, and the sediment obtained a new particle accommodation due to the percolation of the liquid in the system.

A porous sintered copper plate was used to prevent the passage of solids and to promote the percolation of the liquid, which resulted in the new stability condition. With the concentration profile established along the height of the column before and after percolation of the liquid, the stress in solids and permeability of the porous medium were determined, from Eqs. (17) and (18). The volumetric concentration of the suspension at the beginning of the tests was $\varepsilon_{s0} = 12\%$.

3.2. The gamma-ray attenuation technique

The use of nondestructive techniques for the analysis of porous media is a very reliable alternative when simple sampling cannot be used as it interferes in the configuration and stability of the system. In this study the concentration profile in the sediment was determined based on the count of radiation pulses emitted by the radioisotope americium-241.

The technique used is based on the number of photons reaching the radiation detector scintillation. The radiation is converted into electrical pulses which are then amplified and quantified. The experimental system used to determine the solid concentration was composed of a source of gamma rays, collimators, radiation detection equipment, a test tube in which the suspension of the solid under study was placed, and a device to promote the vertical displacement of the test tube, enabling to study the sedimentation process in several positions (**Figure 3**).
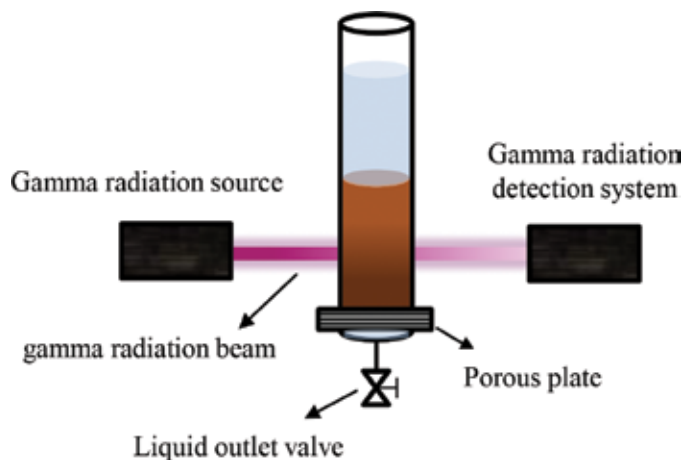
Figure 3. Experimental apparatus.

The variation of the intensity of a collimated beam of monoenergetic gamma rays passing through a physical medium can be determined by the equation of Lambert. For the particular case where the mean that focuses the radiation is suspended and solid-liquid state as a reference solution without suspended solids, this equation takes the following form [27]:

$$\ln\left(\frac{I_0}{I}\right) = \beta\varepsilon_s \qquad (19)$$

where I is the intensity of the beam after passing through the physical medium and I_0 is the intensity of beam passing through a reference condition.

The intensity of the beam after passage through the physical medium must be corrected by the time resolution of the system or dead time from the following equation:

$$R = \frac{I}{1 - \tau I} \qquad (20)$$

in which R is the corrected counting from the number of pulses that pass through the physical medium and τ is the resolution time of the system. Thus, Eq. (19) becomes

$$\ln\left(\frac{R_0}{R}\right) = \beta\varepsilon_s \qquad (21)$$

being the corrected counting R_0 the number of pulses of radiation passing through the measuring cylinder (without solids concentration).

The application of Eq. (21) is made from calibration tests to estimate the parameter β. Identifying the local solid concentration using the gamma-ray attenuation technique was possible by determining the specific calibration curve for the solids for each particular suspension of calcium carbonate.

4. Results

Obtaining the distribution of solid concentration in the sediment before to percolation of liquid, it was possible using Eq. (16) to determine the pressure on the solids as function of solid concentration (**Figure 4**).

Analyzing **Figure 4**, it can be observed that the carbonates presented variation in the porosity at different pressures, indicating, in this way, a considerable degree of compressibility. Thus, the use of the incompressibility hypothesis for carbonates in equations that model sedimentation may not be a viable consideration.

Moreover, the results showed that the calcium carbonate B was more compressible than calcium carbonate A. This fact can be explained because particulate materials with a higher degree of polydispersity when subjected to a given pressure deform more easily due to smaller particles that accommodate themselves in the interstices of the larger particles.

In **Figure 4**, the curve representing the function, $P(\varepsilon_s)$, was adjusted by estimating the parameters of Eq. (7). The estimated parameters of the model (a, b) are shown in **Table 3**.
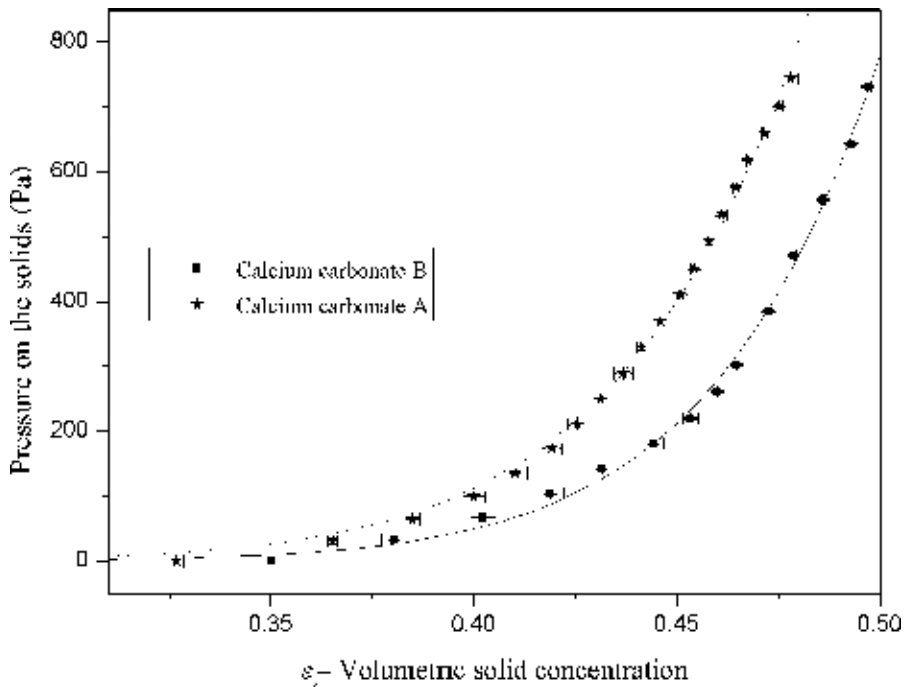
Figure 4. Pressure on the solids as a function of the solid concentration in the sediment.

Solid	a (Pa)	b
Calcium carbonate A	2.20×10^6	10.79
Calcium carbonate B	4.12×106	12.37

Table 3. Parameters of the model for pressure on the solids.

There is an absence in the literature of expressions that allow expressing the relationship between the pressure on the solids and porosity, without the necessity of empirical determination. For this reason, the gamma-ray attenuation technique appears as a viable alternative, especially in situations where the use of denser presses is not indicated, i.e., low pressures.

4.1. Determination of constitutive equation for permeability of porous medium

Obtaining the solid concentration profile in the sediment before and after the percolation of liquid, it was possible with Eq. (17) to determine the permeability of the porous medium as function volumetric concentration of solids (**Figure 5**).

In **Figure 5**, it is observed that the decrease in porosity results in the reduction in permeability of the porous matrix. The permeability may be understood as a measure of the facility of a
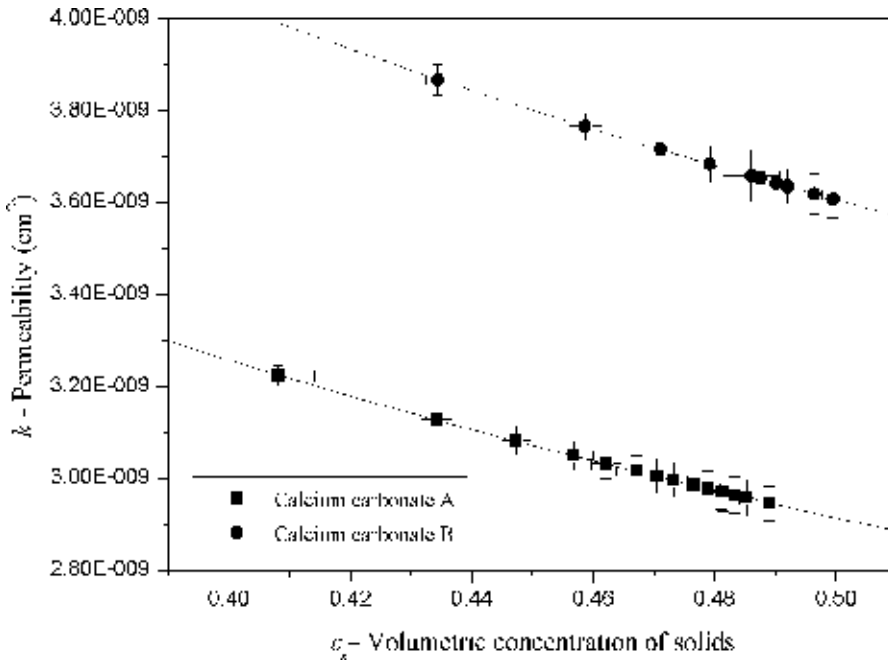
Figure 5. Permeability as function of volumetric concentration of solids in the sediment.

flowing fluid in a medium. Therefore, with the reduction of the volume of voids (smaller porosity), the reduction in the permeability of the medium occurs.

As can also be seen in **Figure 5**, the results showed that calcium carbonate A had the permeability-porosity curve below the calcium carbonate B. This can be explained because particulate materials, which have smaller sizes, form porous media less permeable.

In **Figure 5** the curve representing the function $k(\varepsilon_s)$ was adjusted by the classical model proposed by Tiller and Leu [22]:

$$k(\varepsilon_s) = k_0 \left(\frac{\varepsilon_s}{\varepsilon_{sc}}\right)^{-\eta} \tag{22}$$

The estimated parameters of the model (k_0, ε_{sc} and η) are shown in **Table 4**:

The experimental results shown in **Figure 5** were compared with the values estimated by the Kozeny-Carman correlation (**Figure 6**).

As can be observed in **Figure 6**, the experimental values and the estimated values by Kozeny-Carman correlation showed that the reduction in particle size resulted in a decrease in the permeability curve.

It can also be seen in **Figure 6** that the theoretical results predicted by the Kozeny-Carman correlation underestimated the experimental values for both studied carbonates.

Solid	k_0 (cm^2)	ε_s	η
Calcium carbonate A	7.28.10-9	0.08	0.5
Calcium carbonate B	8.50.10-9	0.09	0.5

Table 4. Parameters of the tiller and Leu [5] model.
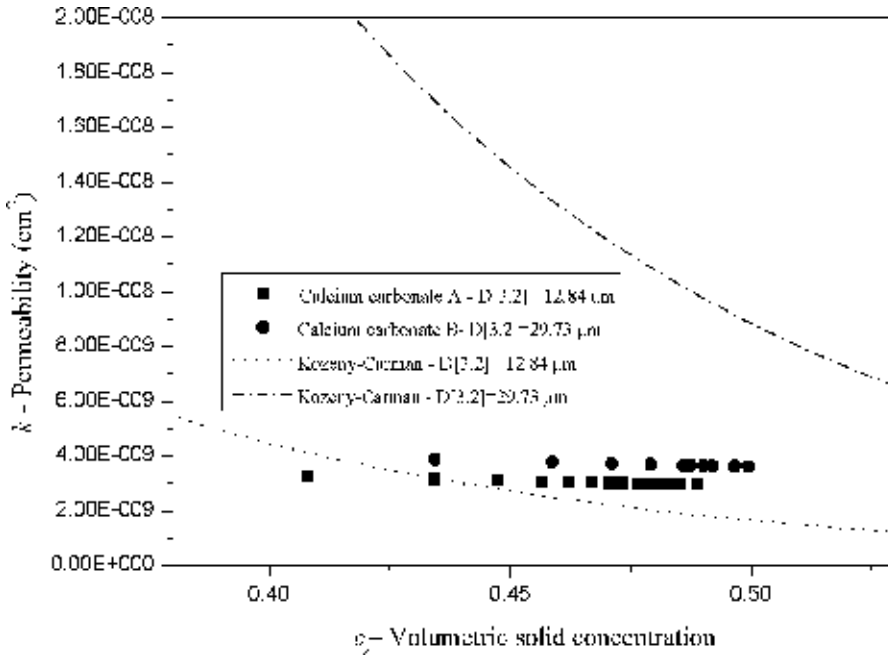
Figure 6. Comparison between the experimentally results with the values estimated by the Kozeny-Carman correlation.

This difference verified in **Figure 6** can be explained because the Kozeny-Carman correlation was proposed based in monodisperse materials and therefore includes only the effects of size and shape.

As the Kozeny-Carman correlation does not contemplate the polydispersion effects; it can be considered that this parameter increased the experimental values of the permeability-porosity relationship, causing the observed deviations.

5. Conclusions

In this study, the theory of mixtures of continuum mechanics was described as an interesting alternative for the theoretical description of sedimentation. The constitutive equations for pressure on the solids and for permeability of porous media that constitute the system of mathematical equations were determined experimentally for carbonates.

The gamma-ray attenuation technique using americium-241 proved to be satisfactory to determine the porosity of porous media composed of carbonate, as well as to determine the relationships of pressure on the solids and permeability.

The increase of the carbonate size distribution range caused the increase of the compressibility of the porous medium, indicating in this way a relation between the polydispersity of the particulate material and the compressibility of the porous matrices.

The theoretical values predicted by the Kozeny-Carman correlation for the relationships between permeability and porosity underestimated the experimental values. The deviations were quite significant for both studied carbonates, demonstrating that such correlation should be used with careful for polydisperse materials.

Acknowledgements

Author details

Bruno Arantes Moreira[1]*, Fábio De Oliveira Arouca[2] and João Jorge Ribeiro Damasceno[2]

*Address all correspondence to: brunomoreira@utfpr.edu.br

1 Federal Technological University of Paraná, Academic Department of Chemical Engineering, Linha Santa Bárbara, s/n—Campus Francisco Beltrão, Francisco Beltrão, PR, Brazil

2 Federal University of Uberlândia, Faculty of Chemical Engineering, Uberlandia, MG, Brazil

References

[1] Bürger R, Concha F, Tiller FM. Applications of the phenomenological theory to several published experimental cases of sedimentation processes. Chemical Engineering Journal. 2000;**80**(1-3):105-117. DOI: 10.1016/S1383-5866(00)00090-3

[2] Bürger R, Donat R, Mulet P, Veja CA. On the implementation of WENO schemes for a class of polydisperse sedimentation models. Journal of Computational Physics 2011;**230**:2322-2344. DOI: http://dx.doi.org/10.1080/00207160.2015.1075985

[3] Bürger R, Tory EM. On upper rarefaction waves in batch settling. Powder Technology. 2000;**108**:74-87. DOI: 10.1016/S0032-5910(99)00257-0

[4] Moreira BA, Arouca FO, Damasceno JJR. Analysis of solid concentration profiles in batch sedimentation tests using viscous Newtonian fluids. Materials Science Forum. 2014;**802**: 209-214. DOI: 10.4028/www.scientific.net/MSF.802.209

[5] Damasceno JJR. Uma Contribuição ao Estudo do Espessamento Contínuo. [thesis]. Instituto Alberto Luiz Coimbra de Pós-Graduação e Pesquisa de Engenharia—Rio de Janeiro, Brasil: Universidade Federal do Rio de Janeiro; 1992

[6] Arouca FO. Uma Contribuição ao Estudo da Sedimentação Gravitacional em Batelada. [thesis]. Uberlândia-MG, Brazil: Universidade Federal de Uberlândia; 2007

[7] Moreira BA. Estudo da sedimentação em suspensões de fluidos com características reológicas pseudoplásticas [thesis]. Uberlândia-MG, Brazil: Universidade Federal de Uberlândia; 2014

[8] Moreira BA, Arouca FO, Damasceno JJR. Analysis of suspension sedimentation in fluids with rheological shear-thinning properties and thixotropic effects. Powder Technology. 2017;**308**:290-297. DOI: 10.1016/j.powtec.2016.12.034

[9] Allen E, Uhlherr PHT. Nonhomogeneous sedimentation in viscoelastic fluids. Journal of Rheology. 1989;**22**:627-638. DOI: 10.1122/1.550030

[10] Bobroff S, Phillips RJ. Nuclear magnetic resonance imaging investigation of sedimentation of concentrated suspensions in non-Newtonian fluids. Journal of Rheology. 1998;**42**:1419-1436. DOI: 10.1122/1.550895

[11] Daugan S, Talini L, Herzhaft B, Peysson Y, Allain C. Sedimentation of suspensions in shear-thinning fluids. Oil & Gas Science and Technology. 2004;**59**:71-80. DOI: 10.2516/ogst:2004007

[12] Philips RJ. Structural instability in the sedimentation of particulate suspensions through viscoelastic fluids. Journal of Non-Newtonian Fluid Mechanics. 2010;**165**:479-488. DOI: 10.1016/j.jnnfm.2010.02.003

[13] Moreira BA, Netto LG, Faria REA, Arouca FO, Damasceno JJR. Rheological behavior of xanthan gum solutions to estimate the settling velocity of particles during stops drilling operation. Materials Science Forum. 2012;**727-728**:1872-1877. DOI: 10.4028/www.scientific.net/MSF.727-728.1872

[14] Kynch GJ. A theory of sedimentation. Transactions of the Faraday Society. 1952;**48**:166-176. DOI: 10.1039/TF9524800166

[15] Bustos MC, Concha F, Bürger R, Tory EM. Sedimentation and thickening—Phenomenological foundation and mathematical theory. Kluwer Academic Publishers; 1999

[16] Bürger R, Concha F. Mathematical model and numerical simulation of settling of flocculated suspensions. International Journal of Multiphase Flow. 1998;**24**:1005-1023. DOI: 10.1016/S0301-9322(98)00026-3

[17] Arouca FO. Obtenção experimental das Equações Constitutivas para o Espessamento e Filtração Utilizando Técnica de Atenuação de Radiações de Altas Energias [dissertation]. Uberlândia, MG, Brazil: Universidade Federal de Uberlândia; 2003

[18] Moreira BA, Oliveira H Jr, Arouca FO, Damasceno J Jr. Analysis of the compressibility of sediments in batch settling tests using Newtonian and non-Newtonian fluids. Materials Science Forum. 2014;**802**:280-284. DOI: 10.4028/www.scientific.net/MSF.802.280

[19] Oliveira H Jr, Moreira BA, Damasceno JJR, Arouca FO. Obtaining constitutive equations for thickening and filtration non-Newtonian fluids. Materials Science Forum. 2014;**802**: 274-279. DOI: 10.4028/www.scientific.net/MSF.802.274

[20] Moreira BA, Arouca FO, Damasceno JJR. Avaliação da permeabilidade de meios porosos constituídos por carbonato de cálcio utilizado como agente obturante em processos de perfuração de poços de petróleo. Exacta, São Paulo. 2012;**10**(3):341-348. DOI: 10.5585/ Exacta.v10n3.3908

[21] d'Ávilla JS. Um modelo matemático para a sedimentação. [thesis]. Rio de Janeiro-RJ, Brazil: Universidade Federal do Rio de Janeiro—COPPE/UFRJ; 1978

[22] Tiller FM, Leu W. Basic data fitting in filtration. Journal of the Chinese Institute of Engineers. 1980;**1**:61-70

[23] Endo Y, Chen D, Pui DYH. Effects of particle polydispersity and shape factor during dust cake loading on air filters. Powder Technology. 1998;**98**:241-249. DOI: 10.1016/S0032-5910 (98)00063-1

[24] Grace HP. Resistance and compressibility of filter cake. Chemical Engineering Progress. 1953;**49**:303-318

[25] Ruth BF. Correlation filtration theory with industrial practice. Industrial & Engineering Chemistry. 1946;**38**(6):564-571

[26] Tiller FM, Haynes S Jr, Lu W. The role of porosity in filtration VII—Effect of side-wall friction in compression—Permeability cells. AIChE Journal. 1972;**18**:13-20. DOI: 10.1002/ aic.690180104

[27] Gardner RP, Ely RL Jr. Radioisotope Measurement Applications in Engineering. New York, EUA: Reinhold Publishing Corporation; 1967

Sediment Contamination

Contamination of Selected Persistent Organic Pollutants (POPs) in Sediment of Some Areas in Vietnam

Vu Duc Toan and Ngo Tra Mai

Additional information is available at the end of the chapter

Abstract

This chapter evaluates the contamination of selected persistent organic pollutants (S-POPs) in the sediment of some typical areas in Vietnam. S-POPs are composed of dichlorodiphenyltrichloroethanes (DDTs), hexachlorocyclohexanes (HCHs), polychlorinated biphenyl (PCBs), and polybrominated diphenyl ethers (PBDEs). The collected data and analyzed results indicated the wide occurrence of significant S-POPs residues in studied areas. The main sources of S-POPs are discussed by using composition analyses and diagnostic ratios of S-POPs indicator. Ecotoxicological risk of S-POPs is assessed. The obtained results have contributed to the assessment of S-POPs fate in the environmental sediment in Vietnam.

Keywords: sediment, persistent organic pollutants, residues, ecological risk assessment

1. Introduction

Persistent organic pollutants (POPs) have low solubility in water and dissolve well in non-polar solvents. Therefore, when penetrating into the river, POPs tend to accumulate in creatures in the river (such as fish, shellfish…), suspended solids, and sediment. In sediment, most POPs accumulate in organic phases and persist for a long time. A part of POPs is transformed through chemical reactions, decomposed, and diffused back into the rivers. Flowing from the river to the sea, POPs are transmitted along with suspended solids and creatures. POPs distribution in the river water-sediment is a continuous process, which is considered to be important for detailed valuation in studies about POPs in the environment; it can be simulated using the modeling method.

Studies about POPs residue in sediment are mostly about the surface layer. The selected depths of sampling in the surface layer vary depending on the viewpoint of research groups in the world (usually 2, 3, and 10 cm in depth). Several studies also evaluate POPs residue according to depth and carry analysis for numerous segments (which can be tens of centimeters, depending on the substance in POP group and characteristics of the waste source). However, in many cases, it is very difficult to compare the obtained results of studies because of the difference in the quantity of POPs used for analysis. For example, total polychlorinated biphenyl (PCB) residue can consist of 6, 7, 10, or 13 PCBs congeners, depending on the research conditions of standard substances, equipment, procedures, and capability of the research group. Still, within its research conditions and obtained results, each study about POPs residue in sediment contributes to the overall picture of POPs in the environment.

Among POPs, dichlorodiphenyltrichloro-ethane (DDTs), hexachlorocyclohexane (HCHs), polychlorinated biphenyl (PCBs), and polybrominated diphenyl ethers (PBDEs) are found in sediment from big cities to remote areas. This chapter will focus on contamination status, composition analyses, and ecological risk assessment of these selected POPs (S-POPs).

2. PCBs in sediment in Vietnam

2.1. General characteristics of PCBs

PCBs are industrial products, which constitute a global environmental health hazard of solely anthropogenic origin. Theoretically, there are 209 PCB isomers and congeners with 1–10 chlorine atoms attached to the biphenyl molecule.

The term "PCBs homolog" is used to refer to all PCBs with the same number of chlorines. Homolog with different substitution patterns is referred to as isomer. The numbering system for the PCBs is shown above. Positions 2, 2′, 6, and 6′ are called ortho positions, positions 3, 3′, 5, and 5′ are called meta positions, and positions 4 and 4′ are called para positions. The benzene rings can rotate around the bond connecting them. The two extreme configurations are planar and the nonplanar in which the benzene rings are at a 90° angle to each other [1]. The benzene rings of non-ortho substituted PCBs, as well as monoortho substituted PCBs, may assume a planar configuration and are referred to as planar or coplanar congeners. The PCBs congeners are arranged in ascending numerical order using a numbering system that follow the IUPAC rules.

2.2. Contamination status of PCBs

Monitoring surveys of PCBs residue in sediment have been conducted during the early 1994s. In the northern Vietnam, PCBs were found in environmental sediment of Thaibinh province (Ba Lat Estuary, coast lines of Thai Binh province), Quangninh province (Halong Bay), and Hanoi city (Set, Kim Nguu, CauBay River, Yen So Lake). PCBs penetrated into the estuaries, urban rivers, lakes, and coastal areas. High PCB concentrations were found in sediment of Kim Nguu River (328 ng/g) and Yen So Lake of Hanoi city (384 ng/g) in 2006 [2]. Hoai et al. [2]

reported that the sediment levels of PCBs measured in their study in 2006 revealed a clear increase compared to 0.79–40 ng/g (mean 13 ng/g) in 1997 and 15–120 ng/g (mean 45 ng/g) in 1999 [3, 4]. Until 2015, sediment levels of PCBs decreased compared to 31.72–167.32 ng/g [5]. Toan et al. reported that the main source of contamination in Hanoi city could originate from the dielectric oil used in old hanging transformers and capacitors [6]. From such equipment, PCBs could penetrate into the environment by re-filling of dielectric oil, mechanical damage, electrical accident, and fire. Statistics until 2006 show that the total amount of dielectric oil containing PCBs in the entire country is approximately 19,000 tons [7]. This clearly indicates a huge contamination source of PCBs in the environment in Vietnam. In central Vietnam, PCBs were found in the environmental sediment of Hue city (Phu Da, A Luoi, and Tam Giang-Cau Hai Lagoon), Quy Nhon city (Thi Nai Lagoon). PCBs penetrated into the lagoons and canals near paddy fields or municipal sewage at low levels (<25 ng/g). In southern Vietnam, PCBs were also found in Mekong River Delta (Tra Vinh), Can Tho city, and Hochiminh city. PCBs were distributed in wide spaces such as drainage from rice fields, rivers near ferry harbors, river near the mouth of Mekong, shrimp farming areas, and canals in the densely populated areas. Highest PCBs concentrations were found in sediment of Saigon River, Hochiminh city (590.5 ng/g) [8]. According to typical data about PCB residues in sediment in Vietnam in **Table 1**, we can draw a number of general conclusions about studies of PCB residues in sediment in Vietnam (**Figures 1** and **2**):

- Within 23 years (1994–2016), about 143 typical sediment samples in several areas of Vietnam were analyzed. Obtained results had a great effort to show the PCB residues level in a number of studied areas. However, the database of PCBs is still limited and further assessment is required in the future.

- Studies about total PCBs are quantified according to various PCBs standards. Several studies do not report the depth of sediment sampling, and the component of total PCBs is not the same (total PCBs can be the sum of 6, 7, 22, 53, 93, or even more than 100 PCBs isomers and congeners). Therefore, the comparisons of total PCBs of different studies are relative and are not precise. This calls for a unified standard about PCBs research for application and further study in the future. We recommend that the researchers can analyze only six indicator congeners (PCB 28, 52, 101, 138, 180). After, the sum of six PCBs can be multiplied by five relatively to get the value of total PCBs. This recommendation is in good agreement with Kohler et al. [16].

- Published studies about PCBs in sediment only provide an initial evaluation about the residue in a point in time without assessments about the time trend variation or in-depth studies about the consequences of PCBs residue in the studied areas. These problems can be additional research directions for PCBs in Vietnam in the future.

2.3. Composition analyses of PCBs

Concerning the PCB congeners, PCBs could be detected from tri-CB to octa-CB in the collected sediment samples. The mean percentages of six selected PCB indicators in the collected sediment samples from several studies (**Table 1**) followed the order PCB138 > PCB153 > PCB101 > PCB52 > PCB180 > PCB28. This order can be explained by physical and chemical properties of PCBs.
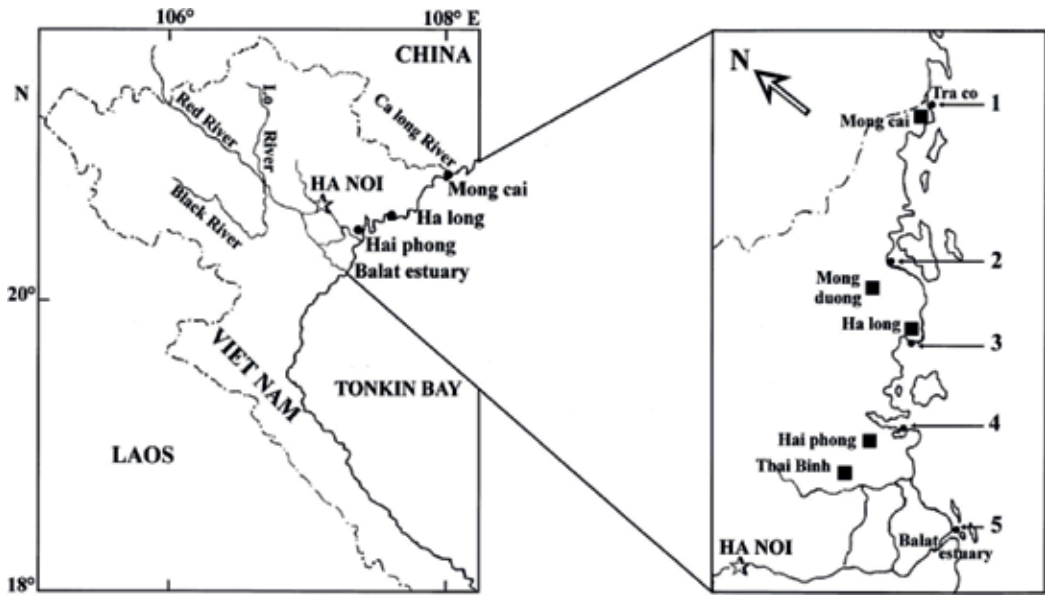
Figure 1. The five sampling stations along the coast of northern Vietnam [3].
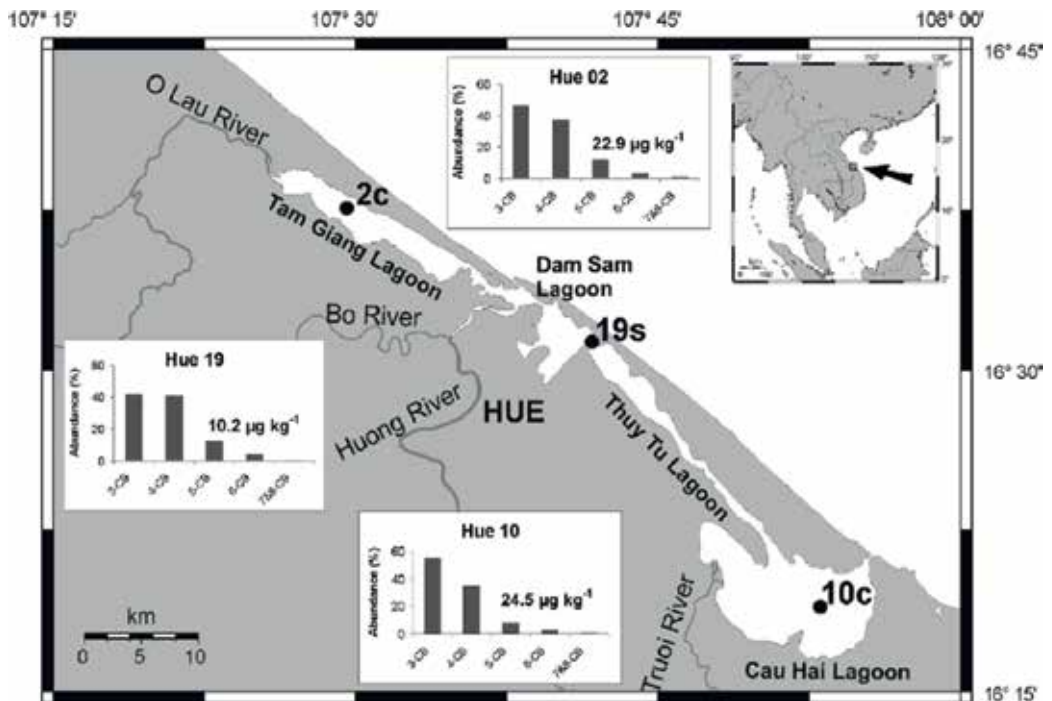
Figure 2. The sampling stations along the Tam Giang-Cau Hai Lagoon, Central Vietnam [12].

According to Toan et al., lightly chlorinated PCBs are less persistent, have lower log K_{ow}, and are more volatile than heavily chlorinated PCBs. Therefore, heavily chlorinated PCBs are more accumulative in the sediment, whereas lightly chlorinated PCBs are degraded and volatilized faster [6].

Location	Year of sampling	Number of samples	Depth of sampling (cm)	Component of analyzed PCBs/PCBs standards	Total PCBs (ng/g)	Reference	Remark
A. Northern Vietnam							
Ba Lat Estuary, coast lines of Thai Binh province	1995/1996	1	0–5	Aroclor 1254, Aroclor 1260[b]	1.1/0.7[a]	[9]	Sediment, intertidal mudflat areas
	2003–2004	10	–[c]	8, 18, 28, 29, 44, 52, 66, 87, 101, 105, 110, 118, 128, 138, 153, 170, 180, 187, 195, 200, 206, 209	0.04–0.26	[10]	Sediment, intertidal mudflat areas
Ha Long Bay, Quang Ninh province	1997	1	0–5	Aroclor 1254, Aroclor 1260	11	[9]	Marine sediment
	1998	1	–	Aroclor 1254, Aroclor 1260	37	[4]	Estuary sediment
	2003–2004	16	–	8, 18, 28, 29, 44, 52, 66, 87, 101, 105, 110, 118, 128, 138, 153, 170, 180, 187, 195, 200, 206, 209	0.11–10.1	[10]	Surface sediment
Nhue River, suburb of Hanoi city	1997	2	0–5	Aroclor 1254, Aroclor 1260	1.7 (0.97–2.51)[d]	[3]	Sediment, canal, densely populated
	1997	1	0–5	Aroclor 1254, Aroclor 1260	0.74	[3]	Sediment, canal, rural area
	2006	2	–	28, 52, 101, 118, 138, 153, 180	22–153	[2]	Sediment, river
Set River, Hanoi city	2006	2	–	28, 52, 101, 118, 138, 153, 180	36–139	[2]	Sediment, river
Kim Nguu River, Hanoi city	2006	2	–	28, 52, 101, 118, 138, 153, 180	237–328	[2]	Sediment, river
Yen So Lake, Hanoi city	2006	6	–	28, 52, 101, 118, 138, 153, 180	20–384	[2]	Sediment, lake
CauBay River, Hanoi city	2015	10	–	4, 5, 6, 7, 8, 9, 10, 12, 13, 15, 16, 17, 19, 21, 22, 26, 28, 31, 32, 37, 41, 42, 44, 45, 47, 48, 49, 52, 53, 56, 60, 61, 64, 66, 70, 71, 74, 77, 81, 83, 84, 85, 86, 87, 89, 91, 92, 95, 99, 100, 101, 105, 110, 114, 118, 119, 123, 126, 128, 131, 132, 135, 138, 144, 149, 153, 156, 157, 163, 167, 169, 170, 171, 172, 174, 180, 189, 194, 199, 200, 202, 205, 206, 207	31.72–167.32	[5]	Sediment, river
B. Central Vietnam							
Phu Da, Hue city	1990	1	No data	KC-300, KC-400, KC-500, KC-600[e]	0.65	[11]	Sediment, near paddy field

Location	Year of sampling	Number of samples	Depth of sampling (cm)	Component of analyzed PCBs/PCBs standards	Total PCBs (ng/g)	Reference	Remark
A Luoi, Hue city	1990	1	No data	KC-300, KC-400, KC-500, KC-600	0.18	[11]	Sediment, municipal sewage
Tam Giang, Hue city	2002	10	0–2; 2–4; 8–10; 20–23; 23–26; 32–35; 38–41; 47–50	53 congener (no data in detail)	2.03–24.7	[12]	Sediment, Tam Giang-Cau Hai Lagoon
Thi Nai Lagoon, Quy Nhon city	2010	18	–	11, 16, 19, 18, 17, 24, 27, 16, 32, 34, 29, 26, 25, 31, 28, 20, 33, 22, 20, 45, 46, 52, 49, 47, 48, 44, 42, 59, 41, 64, 71, 40, 67, 63, 74, 70, 66, 56, 60, 104, 93, 95, 91, 92, 84, 90, 101, 99, 97, 87, 115, 85, 110, 82, 107, 123, 118, 105, 136, 151, 135, 144, 147, 149, 146, 153, 132, 141, 138, 164, 158, 128, 167, 156, 157, 169, 13, 179, 176, 178, 187, 183, 174, 177, 171, 172, 180, 193, 170, 190, 199, 196, 203, 194, 208, 209	0.47–6.40	[13]	Surficial sediment, lagoon
C. Southern Vietnam							
Tra Vinh, Mekong River Delta	1998	1	–	44, 49, 52, 101, 105, 118, 128, 138, 149, 153, 170, 180, 200	0.985	[14]	Sediment, canal
Can Tho city, Mekong River delta	2003–2004	4	No data	KC-300, KC-400, KC-500, KC-600	1.8 (0.12–3.7)	[11]	Sediment, canals in Cantho city
Hau River, Mekong River delta	2003–2004	7	No data	KC-300, KC-400, KC-500, KC-600	0.21 (0.12–0.54)	[11]	Sediment, river
Saigon River, Hochiminh city	2004	5	No data	No data	81	[15]	Canals, densely populated areas
	1996	11	–	28, 52, 101, 138, 153, 180	N.D – 590.5[f]	[8]	Canals, densely populated areas

[a]Dry season/rainy season.
[b]PCB mixture from the US; Aroclor 1254 and Aroclor 1260 contain more than 100 PCBs isomers and congeners.
[c]Not reported.
[d]Mean (range).
[e]PCB mixture from Japan. KC-300, KC-400, KC-500, and KC-600 contain more than 100 PCBs isomers and congeners.
[f]Not detected.

Table 1. Concentrations of PCBs (ng/g) in sediment from Vietnam.

Another explanation could be related to the compositions of PCB mixtures that probably escaped from the dielectric oil. Up to April 1998, 48.3% of the total quantity of dielectric oils in Vietnam was imported from the Soviet Union. Japan and China contributed with smaller percentages of 7.5 and 3.6%, respectively [6, 17]. According to Falandysz et al., the percentages of PCB138, PCB153, PCB101 (along with PCB90), PCB52, PCB180, and PCB28 (along with PCB31) in Sovol (trade name of Soviet Union dielectric oil) were 11.4, 7.0, 6.5, 3.6, 0.4, and 0.8%, respectively [18]. It seems that the predominance of heavily chlorinated PCBs, PCB138, and PCB153, still remained when they penetrated the sediment. In general, low percentages of lightly chlorinated PCBs and a high percentage of heavily chlorinated PCBs in the analyzed sediment samples reflect their long-time release **Figure 3** [6].

2.4. Ecological risk assessment of PCBs

To evaluate the ecotoxicological significance of PCBs contamination, total PCBs in collected sediments were compared with the NOAA sediment quality guideline (SQG) [19]. This guideline specifies the "effects range low" (ERL) and the "effects range median" (ERM). The ERL represents the chemical concentration below which an adverse effect would rarely be observed. The ERM represents the concentration above which adverse effect would frequently occur [20]. Only total PCBs of sediment samples in two big cities (Hanoi and Ho Chi Minh cities) exceeded ERM levels (ERM of total PCBs is 180 ng/g). The other sediment samples listed in **Table 1** that were collected from the estuaries, coastal areas, lagoons, canals near paddy field or municipal sewage, drainage from rice fields, rivers near ferry harbors, river near the mouth of Mekong, shrimp-farming areas, were lower than ERL levels (ERL of total PCBs is 22.7 ng/g). This finding raises the concern on PCBs impact in the two big cities of Vietnam. Thus, further investigation is required in Hanoi and Hochiminh cities to assess possible toxic effects on human health and ecological system.
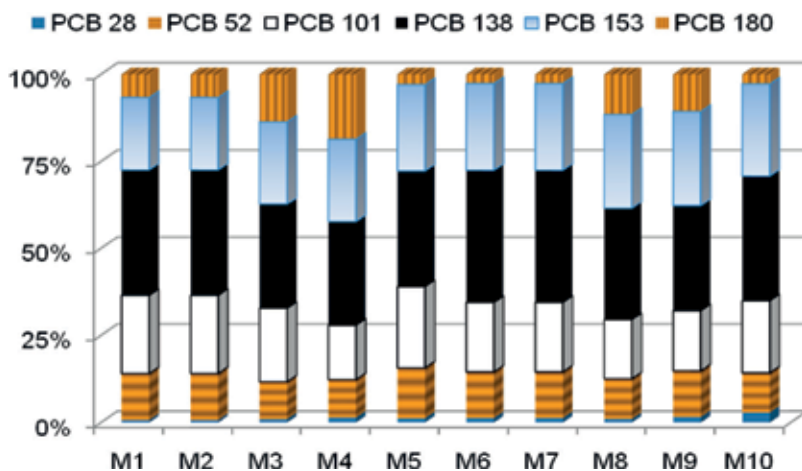
Figure 3. Mean percentages of PCB congeners in sediment samples in CauBay River [5].

3. PBDEs in sediment in Vietnam

3.1. General characteristics of PBDEs

Polybrominated diphenyl ethers (PBDEs) are used commercially as additives in plastics and textiles, building materials, carpets, and vehicles and aircraft with half-lives in the order of 2–10 years. In computers, these compounds are commonly used in printed circuit boards, components such as connectors, cables, plastic covers, and parts of keyboards and monitors. Theoretically, there are 209 PBDEs isomers and congeners with 1–10 bromine atoms attached to the biphenyl molecule.

PBDEs are highly resistant to heat, light, oxidizing, and reducing compounds. Thus, PBDEs are extremely persistent when released into the environment. The use of PBDEs has increased over the last 30 years with production estimated to be about 3000–5000 tons in Europe. Deca-BDE is the largest mix on the market and makes up over 80% of the total PBDE production, whereas penta-BDE and octa-BDE products constitute about 12 and 6%, respectively, of the total PBDE production [21]. The presence of high levels of these compounds in samples from remote areas suggests that they may now have been distributed worldwide as a result of long-range atmospheric transport. PBDEs have been associated with endocrine disruption, neurotoxicity, and cancer. Sediments are major sinks for these contaminants in aquatic environments, and their study is an important step in mapping possible pollution sources and exposure pathways that facilitate PBDE bioavailability to sediment-dwelling organisms [21].

3.2. Contamination status of PBDEs

From the north to the south of Vietnam, PBDEs was found in environmental sediment of Hanoi city (CauBay river), Quy Nhon city (Thi Nai Lagoon), Hochiminh city (canals), and Saigon-Dongnai River. PBDEs penetrated in the environmental sediment of rivers, lagoon urban canals, urban sewer systems, and estuary. Data about PBDE residue in sediment in these areas of Vietnam are presented in **Table 2**.

A number of general conclusions can be drawn from studies about PBDE in Vietnam:

- At present, there is a lack of studies about PBDE in Vietnam. In three representative studies presented in **Table 2**, the numbers of samples and research areas are not enough to represent PBDE residue in sediment in Vietnam. Published studies do not report the depth of sampling. There are also different viewpoints about the total PBDE value. Components of total PBDE can be the sum of 7, 9, or 11 PBDEs. Therefore, it is difficult to compare research results.

- Published studies about PBDE in sediment are mainly about initial evaluation of residue in a point in time. There is no assessment about the change in trend or in-depth research about the consequences of PBDE residue in the studied areas. Further studies about PBDE residue and its impact on the environment are necessary.

When compared with other regions in the world, the residues of total PBDEs in Hanoi and Hochiminh are lower than those in Dianchi lake, China and and higher than residues found in Hongfeng and Chenghai lake, China [23].

Location	Year of sampling	Number of samples	Depth of sampling (cm)	Component of analyzed PBDEs	Concentration PBDEs (ng/g)	Reference	Remark
A. Northern Vietnam							
CauBay River, Hanoi city	2014	10	–[a]	28, 47, 99, 100, 153, 154, 209	15.39–25.64	[21]	Sediment, river
B. Central Vietnam							
Thi Nai lagoon, Quy Nhon city	2010	18	–	17, 28, 47, 66, 100, 99, 85, 153, 183	N.D – 9.62[b]	[13]	Surficial sediment, lagoon
C. Southern Vietnam							
Hochiminh city canals	2004	5	0–5	28, 47, 99, 100, 153, 154, 183, 196, 197, 206, 207	54.5–119	[22]	Urban sediment, sewer system
Hochiminh city canals	2004	6	0–5	28, 47, 99, 100, 153, 154, 183, 196, 197, 206, 207	<0.2–10.63	[22]	Sub-urban sediments
Saigon-Dongnai estuary	2004	3	0–5	28, 47, 99, 100, 153, 154, 183, 196, 197, 206, 207	<0.02–0.065	[22]	Estuary sediment

[a]Not reported.
[b]Not detected.

Table 2. Concentrations of PBDEs (ng/g) in sediment from Vietnam.

3.3. Composition analyses of PBDEs

Concerning the composition analyses, PBDEs congeners could be detected from tri-BDE to deca-BDE in the collected sediment samples (**Table 2**). BDE-209 was a predominant congener in sediment samples. In the past, BDE-209 is the largest mix on the market and makes up over 8% of the total PBDE production, whereas penta-BDE and octa-BDE products constitute about 12 and 6%, respectively, of the total PBDE production [24]. This is one of important factors to explain the predominance of BDE-209.

The mean percentages of six PBDEs indicators in the collected sediment samples followed the order: BDE-47 > BDE-99 > BDE-100 > BDE-154 > BDE-153 > BDE-27. This order is in agreement with chemical properties of PBDEs as well as the percentages of PBDEs in the commercial mixtures.

3.4. Ecological risk assessment of PBDEs

It has been suggested that PBDEs biomagnified as they move along a food web. In addition, PBDEs can inhibit growth in colonies of algae as well as depress the reproduction of zooplankton. Based on the toxicity data of benthic organisms, the multiple species have no observed effect on the concentrations of ΣPBDEs which is 3.1 mg/kg of sediment

[21, 25]. Most of the collected sediment samples in **Table 2** had residues of PBDEs lower than 3.1 mg/kg. However, the values of PBDEs in the urban canals and urban sewer system of Hochiminh city are very high (maximal 119 ng/g). Due to the propensity of PBDEs to highly accumulate in various compartments of wildlife and human food webs, further evaluation of ecological risk assessment in Hochiminh city should be undertaken as a high priority.

4. DDT and HCH in sediment in Vietnam

4.1. General characteristics of DDTs and HCHs

4.1.1. General characteristics of DDTs

Chemical formula of DDT is $C_{14}H_9C_{15}$. Technical DDT is prepared by the Bayer condensation of chlorobenzene with trichloroacetaldehyde in oleum (fuming sulfuric acid), and the reaction is carried out with an excess of chlorobenzene (recommended molar ratio 3:1). Technical grade DDT is composed of up to 14 chemical compounds of which only 65–80% is the active ingredient, *p,p'*-DDT and included 15–21% of the nearly inactive *o,p'*-DDT. DDT is transformed by metabolism or by degradation in the environment [26]. The most common metabolites are DDE (1,1-dichloro-2,2-*bis*(*p*-chlorophenyl)ethylene) and DDD (1,1-dichloro-2,2-*bis*(*p*-chlorophenyl) ethane), which usually are found together with DDT in environmental samples. Thus, actually, people and animal are poisoned by these compounds at the same time. Each compound has three isomers and their primary isomers are *p,p'*-DDT; *p,p'*-DDE; *p,p'*-DDD [26]. Total concentration of DDTs can be evaluated by the sum of *p,p'*-DDT; *o,p'*-DDT; *p,p'*-DDE; *o,p'*-DDE; *p,p'*-DDD, and *o,p'*-DDD.

4.1.2. General characteristics of HCHs

1,2,3,4,5,6-Hexachlorocyclohexane (HCH), also called benzene hexachloride (BHC), is an organochlorine insecticide used throughout the world. HCH is available in two formulations: technical HCH and lindane. A total of eight HCH isomers have been identified in technical HCH. However, only the γ-HCH, α-HCH, β-HCH, and δ-HCH and ε-HCH isomers are stable, and these are the ones commonly identified in technical formulations [26]. Generally, technical HCH consists of approximately 60–70% α-HCH, 5–12% β-HCH, 10–15% γ-HCH, 6–10% δ-HCH, and 3–4% ε-HCH. Lindane contains more than 90% of γ-HCH, but lindane used in many countries is almost pure γ-HCH [27]. Total concentration HCH can be evaluated by the sum of ϒ-HCH, α-HCH, β-HCH, and δ-HCH.

4.2. Contamination status of DDT and HCH

Data about DDT and HCH residues in sediment in Vietnam are relatively adequate, including sediment in freshwater, brackish water, and seawater. There are research results about DDT and HCH in sediment from 1994 up to now (**Table 3**). According to data in **Table 3**,

Location	Year of sampling	Number of samples	Depth of sampling (cm)	Component of analyzed DDTs; HCHs	Concentration DDTs; HCHs (ng/g)	Reference	Remark
A. Northern Vietnam							
Diem Dien Estuary, Thai Binh coast lines	1995/1996	1	0–5	*p,p'*-DDT; *p,p'*-DDE; *p,p'*-DDD; Υ-HCH, α-HCH, β-HCH, δ-HCH	6.2; 0.36	[3]	Sediment, intertidal mudflat areas
Ha Long Bay	1997	1	0–5	*p,p'*-DDT; *p,p'*-DDE; *p,p'*-DDD; Υ-HCH, α-HCH, β-HCH, δ-HCH	7.2; 1.8	[3]	Marine sediment
	1998	1	–[a]	*p,p'*-DDT; *p,p'*-DDE; *p,p'*-DDD; Υ-HCH, α-HCH, β-HCH, δ-HCH	28; 6.1	[4]	Estuary sediment
	2003–2004	16	–	*p,p'*-DDT; *o,p'*-DDT; *p,p'*-DDE; *o,p'*-DDE; *p,p'*-DDD; *o,p'*-DDD; Υ-HCH, α-HCH, β-HCH, δ-HCH	1.60–274; N.D[b] – 0.85	[3]	Surface sediment
Set River, Hanoi city	2006	2	–	*p,p'*-DDT; *o,p'*-DDT; *p,p'*-DDE; *o,p'*-DDE; *p,p'*-DDD; *o,p'*-DDD; Υ-HCH, α-HCH, β-HCH, δ-HCH	215–680; <0.2	[2]	Sediment, river
Kim Nguu River, Hanoi city	2006	2	–	*p,p'*-DDT; *o,p'*-DDT; *p,p'*-DDE; *o,p'*-DDE; *p,p'*-DDD; *o,p'*-DDD; Υ-HCH, α-HCH, β-HCH, δ-HCH	82–1100; <0.2–17	[2]	Sediment, river
Yen So Lake, Hanoi city	2006	6	–	*p,p'*-DDT; *o,p'*-DDT; *p,p'*-DDE; *o,p'*-DDE; *p,p'*-DDD; *o,p'*-DDD; Υ-HCH, α-HCH, β-HCH, δ-HCH	17–109; <0.2–36	[2]	Sediment, lake
CauBay River, Hanoi city	2012	10	–	*p,p'*-DDT; *p,p'*-DDE; *p,p'*-DDD; Υ-HCH, α-HCH, β-HCH, δ-HCH	51.84–92.76; 4.65–11.39	[27]	Sediment, river
B. Central Vietnam							
Phu Da, Hue city	1990	1	No data	*p,p'*-DDT; *p,p'*-DDE; *p,p'*-DDD; Υ-HCH, α-HCH, β-HCH	0.52; 0.43	[11]	Sediment, paddy field

Location	Year of sampling	Number of samples	Depth of sampling (cm)	Component of analyzed DDTs; HCHs	Concentration DDTs; HCHs (ng/g)	Reference	Remark
A Luoi, Hue city	1990	1	No data	p,p'-DDT; p,p'-DDE; p,p'-DDD; Υ-HCH, α-HCH, β-HCH	68; 2.4	[11]	Sediment, municipal sewage
C. Southern Vietnam							
Can Tho city, Mekong River delta	2003–2004	4	No data	p,p'-DDT; p,p'-DDE; p,p'-DDD; Υ-HCH, α-HCH, β-HCH	1.8–4.3; <0.02–0.11	[11]	Sediment, canals in Can Tho city
Duyen Hai, Mekong River delta	1998	1	–	p,p'-DDT; o,p'-DDT; p,p'-DDE; o,p'-DDE; p,p'-DDD; o,p'-DDD; Υ-HCH, α-HCH, β-HCH	0.48; 0.113	[14]	Near the mouth of Mekong, shrimp farming area
Tra Vinh, Mekong River delta	1998	1	–	p,p'-DDT; o,p'-DDT; p,p'-DDE; o,p'-DDE; p,p'-DDD; o,p'-DDD; Υ-HCH, α-HCH, β-HCH	67.49; 0.65	[14]	Sediment, canals
Saigon River, Hochiminh city	2004	5	No data	p,p'-DDT; o,p'-DDT; p,p'-DDE; o,p'-DDE; p,p'-DDD; o,p'-DDD;	37[c]	[15]	Sediment, canals, densely populated areas
	1996	11	–	p,p'-DDT; p,p'-DDE; p,p'-DDD	1.76–253.6	[8]	Sediment, canals, densely populated areas

[a]Not reported.

[b]Not detected.

[c]Mean value.

Table 3. Concentration of DDTs and HCHs (ng/g) in sediment from Vietnam.

DDT and HCH have deposited in the sediment in Vietnam in a wide range and for a long time with considerable extent. DDT and HCH residue in sediment in Vietnam is on the decreasing trend.

Monitoring surveys of DDTs and HCHs residue in sediment have been conducted during the early 1994s. In northern Vietnam, DDTs and HCHs were found in environmental sediment of Thaibinh province (Diem Dien Estuary, coast lines of Thai Binh province), Quangninh province (Halong Bay) and Hanoi city (Set, Kim Nguu, CauBay River; Yen So Lake). DDTs and HCHs have penetrated into the estuaries, urban rivers, lakes, and coastal areas. HCHs had

low residues in most of the sediment samples. Besides, high DDTs concentrations were found in the sediment of Kim Nguu River (1100 ng/g) and Set River of Hanoi city (680 ng/g) in 2006 [2]. This can be explained by the usage of DDTs in the big cities of Vietnam in the past. Both DDTs and HCHs have been used in Vietnam in considerable amounts as pesticides for crop protection and as vector control for public health purposes. DDT had been imported and used in Vietnam from 1957 up to 1994.

In Central Vietnam, DDTs and HCHs were found in the environmental sediment of Hue city (Phu Da, A Luoi). DDTs and HCHs penetrated into the canals near paddy fields or municipal sewage at medium levels. In southern Vietnam, DDTs and HCHs also found in Mekong River Delta (Duyen Hai and Tra Vinh), Can Tho city, and Hochiminh city. DDTs and HCHs are distributed in wide spaces such as drainage from rice fields, river near ferry harbor, river near the mouth of Mekong, shrimp-farming areas, and canals in the densely populated areas. Highest DDTs concentrations were found in the sediment of Saigon River, Hochiminh city (253.6 ng/g) [8].

4.3. Composition analyses of DDTs and HCHs

Composition differences of HCHs isomers or DDTs metabolites in the environment could indicate different contamination sources. DDT can be biodegraded in the environment to DDD under anaerobic conditions and DDE under aerobic conditions. Thus, p,p'-DDD was a major breakdown product of DDT in sediment from different places in Vietnam. With regards to DDT metabolites, the ratio of $(p,p'$-DDE + p,p'-DDD)/ΣDDT in the sediment samples collected in 2012 from CauBay River ranged between 0.77 and 0.89 (mean 0.80). The obtained ratios indicated that the degradation of DDT occurred significantly, and there is no recent input of DDT in the study areas [28]. This conclusion was suitable with the fact of usage of DDTs and other studies since 2006 in Vietnam. Among the isomers, β-HCH has the lowest water solubility and vapor pressure, which is the most stable and relatively resistant to microbial degradation. Besides, there is the isomerization of α- to β-HCH and of γ- via α- to the more stable β-HCH, which is energetically more favorable in the environment [28]. Therefore, the β-HCH predominance reflects an old source of input of HCH in the environment. Low ratios of α-HCH/γ-HCH may represent the use of lindane, whereas high ratios of these isomers may depict the use of technical HCH [28]. An α-HCH/γ-HCH ratio in areas where lindane has been typically used ranges from 0.2 to 1 compared to a range from 4 to 15 for technical HCH. According to Toan et al., the mean percentages of HCH isomers analyzed in sediment samples from CauBay River followed the order of β-HCH (43.2%) > α-HCH (39.3%) > γ-HCH (10.7%) > δ-HCH (6.9%) [28, 29]. Therefore, the predominance of β-HCH reflects an old source of input of HCH in the environment. Besides, the ratio of α-HCH/γ-HCH in the analyzed sediment samples of CauBay River ranged between 2.68 and 4.09 (mean 3.73). It means that the use of technical HCH is the major source and lindane is the minor source in the study areas.

4.4. Ecological risk assessment of DDTs and HCHs

To evaluate the ecotoxicological significance of DDTs and HCHs contamination in collected sediments, our data in **Table 3** were compared with the interim sediment quality guideline
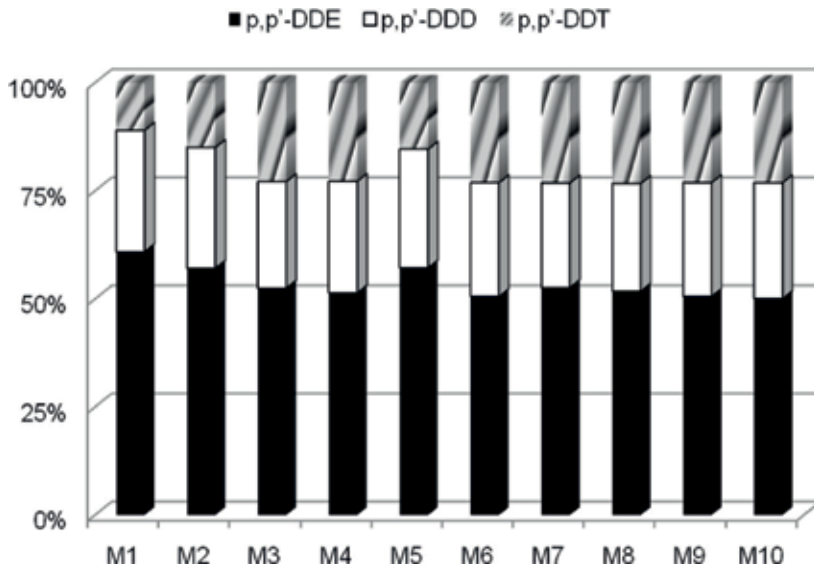
Figure 4. Mean percentages of DDT and its metabolites in sediment samples [28].

(ISQG) and the probable effective level (PEL), issued by the Canadian Council of Ministers of Environment [30]. Hoai et al. [2] reported that the concentrations of DDE, DDD, and DDT in all the Hanoi sediment samples were higher than the ISQG values (1.42, 3.54, and 1.19 ng/g, respectively). The DDE, DDD, and DDT generally exceed the PEL values (6.75 ng/g for DDE, 8.51 ng/g for DDD, and 4.77 ng/g for DDT) but vary among the sediment samples [2]. This conclusion is in agreement with DDTs residues in CauBay River and Hochiminh city [22, 28]. In general, most of the collected sediment samples in **Table 3** had DDTs at low levels as well
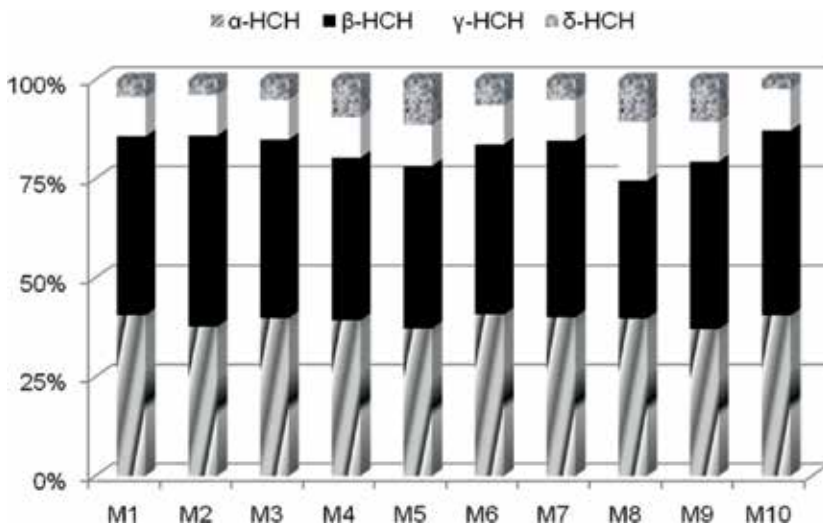
Figure 5. Mean percentages of HCH isomers in sediment samples [28].

as lower than PEL values. With regards to HCHs, no values of ISQG and PEL were reported in the international guidelines. Due to the propensity of DDTs to highly accumulate in various compartments of wildlife and human food webs, further evaluation of ecological risk assessment in Hanoi and Hochiminh city should be undertaken **Figures 4** and **5**.

5. Conclusion

This work investigated the contamination status of S-POPs in sediment of some areas in Vietnam. Wide occurrence and remarkable residue levels of S-POPs have been found in the sediment of study areas. Composition analyses show that S-POPs penetrated in the sediment for a long time. The main sources of S-POPs are from mix sources that have origin form old industrial and agricultural sources. Ecotoxicological of S-POPs is found at low levels. Due to the propensity of S-POPs to accumulate in various compartments of environment, further evaluation of ecotoxicological should be undertaken as a high priority.

Author details

Vu Duc Toan[1]* and Ngo Tra Mai[2]

*Address all correspondence to: vuductoan2001@yahoo.com

1 Thuyloi University, Hanoi, Vietnam

2 Institute of Physics, Viet Nam Academy of Science and Technology, Hanoi, Vietnam

References

[1] Agency for Toxic Substances and Disease Registry (ATSDR). Toxicological Profile for Polychlorinated Biphenyls (PCBs). ATSDR's Toxicological Profiles Web Version. 2002; Available from: https://www.atsdr.cdc.gov/toxprofiles/TP.asp?id=142&tid=26 [Accessed: 2017.07.19]

[2] Hoai PM, Giger W, Ngoc NT, Minh NH, Viet PH, Berg M, Alder C. A. Recent levels of organochlorine pesticides and polychlorinated biphenyls in sediments of the sewer system in Hanoi, Vietnam. Environmental Pollution. 2010;**158**:913-920

[3] Nhan DD, Carvalho FP, Am NM, Tuan NQ, Yen NTH, Villeuneve J-P, Cattini C. Chlorinated pesticides and PCBs in sediments and molluscs from freshwater canals in the Hanoi region. Environmental Pollution. 2001;**112**:311-320

[4] Viet PH, Hoai PM, Minh NH, Ngoc NT, Hung PT. Persistent organochlorine pesticides and polychlorinated biphenyls in some agricultural and industrial areas in northern Vietnam. Water Science and Technology. 2000;**42**:223-229

[5]   Toan VD, Quy NP. Residues of polychlorinated biphenyls (PCBs) in sediment from CauBay River and their impacts on agricultural soil, human health risk in KieuKy area, Vietnam. Bulletin of Environmental Contamination and Toxicology. 2015;**95**:177-182

[6]   Toan VD, Thao VD, Walder J, Schmutz H-R, Ha CT. Level and distribution of polychlori-nated biphenyls (PCBs) in surface soils from Hanoi, Vietnam. Bulletin of Environmental Contamination and Toxicology. 2007;**78**:211-216

[7]   Vietnam National Environment Agency (NEA), (2006) Vietnam National Plan for Treatment of Persistent Organic Pollutant (in Vietnamese). Available from: http://www.nea.gov.vn/thong-tinmt/noidung/vnn_14_08_06.htm [Accessed: 2008.12.01]

[8]   Phuong PK, Son CPN, Sauvain J, Tarradellas J. Contamination by PCB's, DDT's, and heavy metals in sediments of Ho Chi Minh City's canals, Vietnam. Bulletin of Environmental Contamination and Toxicology. 1998;**60**:347-354

[9]   Nhan DD, Am NM, Carvalho FP, Villeuneve JP, Cattini C. Organochlorine pesti-cides and PCBs along the coast of North Vietnam. Science of The Total Environment. 1999;**237**:363-371

[10] Hong SH, Kim UH, Shim WJ, Oh JR, Viet PH, Park PS. Persistent organochlorine resi-dues in estuarine and marine sediments from Ha Long Bay, Hai Phong Bay, and Ba Lat estuary, Vietnam. Chemosphere. 2008;**72**:1193-1202

[11] Iwata H, Tanabe S, Sakai N, Nishimura A, Tatsukawa R. Geographical distribution of persistent organochlorines in air, water and sediments from Asia and Oceania and their implication for global redistribution from lower latitudes. Environmental Pollution. 1994;**85**:15-33

[12] Frignani M, Piazza R, Bellucci LG, Cu NH, Zangrando R, Albertazzi S, Moret I, Romano S, Gambaro A. Polychlorinated biphenyls in sediments of the tam Giang-Cau Hai lagoon, Central Vietnam. Chemosphere. 2007;**67**:1786-1793

[13] Romano S, Piazza R, Mugnai C, Giuliani S, Bellucci LG, Huu CH, Vecchiato M, Zambon S, Hoai ND, Frignani M. PBDEs and PCBs in sediments of the Thi Nai lagoon (Central Vietnam) and soils from its mainland. Chemosphere. 2013;**90**:2396-2402

[14] Carvalho FP, Villeneuve JP, Cattini C, Tolosa I, Thuan DD, Nhan DD. Agrochemical and polychlorobyphenyl (PCB) residues in the Mekong River delta, Vietnam. Marine Pollution Bulletin. 2008;**56**:1476-1485

[15] Minh TB, Iwata H, Agusa T, Minh NH, Inoue S, Kubota R, Tu NPC, Kajiwara N, Kunisue T, Subramanian A, Viet PH, Tuyen BC, Chamnan C, Tana TS, Tanabe S. Contamination by arse-nic and persistent organic pollutants in Mekong River: Geographical distribution, patterns of accumulation and implications for environmental quality and human health. In Proceedings of the 2nd International Symposium on the Development of Water Resource Management System in Mekong Watershed. Bangkok, Thailand; 2005. pp. 15-23

[16] Kohler M, Zennegg M, Waeber R. Coplanar polychlorinated biphenyls (PCB) in indoor air. Environmental Science & Technology. 2002;**36**:4735-4740

[17] Electricity of Vietnam (EVN). Strategy and Environmental Protection Program (in Vietnamese). Electricity of Vietnam. Hanoi, Vietnam; 2003

[18] Falandysz J, Wyrzykowska B, Bochentin I, Hanari N, Orlikowska A, Yuichi H, Yamashita N. Source determination of highly chlorinated biphenyl isomers in pine needles—Comparison to several PCB preparations. Environmental Pollution. 2006;**143**:46-59

[19] Long ER, MacDonald DD, Smith SL, Calder FD. Incidence of adverse biological effects within ranges of chemical concentrations in marine and estuarine sediments. Environmental Management. 1995;**19**:81-97

[20] Hong SH, Yim UH, Shim WJ, Li DH, Oh JR. Nationwide monitoring of polychlorinated biphenyls and organochlorine pesticides in sediments from coastal environment of Korea. Chemosphere. 2006;**64**:1479-1488

[21] Toan VD, Son HV. Residue and ecological risk assessment of polybrominated diphenyl ethers (PBDEs) in sediment from CauBay River, Vietnam. World Academy of Science, Engineering and Technology International Journal of Environmental, Chemical, Ecological, Geological and Geophysical Engineering. 2014;**8**(5):292-295

[22] Minh NH, Minh TB, Isobe T, Tanabe S. Contamination of Polybrominated diphenylethers in the sewer system of Hochiminh city and estuary of Saigon – Dongnai river. Fifth International Symposium on Brominated Flame Retardants; Kyoto; April 2010. pp. 41-49

[23] Wu F, Guo J, Chang H, Liao H, Zhao X, Mai B, Xing B. Polybrominated diphenyl ethers and decabromodiphenylethane in sediments from twelve lakes in China. Environmental Pollution. 2012;**162**:262-268

[24] De Wit C. An overview of brominated flame retardants in the environment. Chemosphere. 2002;**46**:583-624

[25] Renzi M. Organic Pollutants—Monitoring, Risk and Treatment—Chapter 5—Perfluorinated Organic Compounds and Polybrominated Diphenyl Ethers Compounds—Levels and Toxicity in Aquatic Environments: A Review. Germany. Intech Publisher; 2013

[26] Agency for Toxic Substances and Disease Registry (ATSDR). Toxicological Profile for DDT, DDE and DDD, ATSDR's Toxicological Profiles Web Version, 2002. Available from: https://www.atsdr.cdc.gov/toxprofiles/tp.asp?id=81&tid=20 [Accessed: 2017.07.19]

[27] Toan VD. Chapter 14: Time trend variation of selected pesticides residues in soil from some regions in Vietnam. In: Jokanović M, editor. The Impact of Pesticide. Cheyenne, USA: Academy Publish; 2012. pp. 286-320. ISBN: 978-0-9835850-9-1

[28] Toan VD. Contamination of selected organochlorine pesticides (OCPs) in sediment from CauBay river. Bulletin of Environmental Contamination and Toxicology. 2012;**89**:516-520

[29] Toan VD. Residue of select organochlorine pesticides (OCPs) in sediment from Vietnam's CauBay River and their impact on agricultural soil and human health. Polish Journal of Environmental Studies. 2015;**24**(1):301-306

[30] Canadian Council of Minister of the Environment (CCME). Canadian Quality Guidelines for the Protection of Aquatic Life-Summary Tables. 2002. Available from: http://www.ccme.ca/assets/pdf/sedqg_summary_table.pdf [Accessed: 2010.07.19]

Spatio-Temporal Evolution of Sediments Pollution with Mobile Heavy Metals in an Abandoned Mining Area from Romania

Lidia Kim, Geanina-Gabriela Vasile,
Luoana Florentina Pascu, Bogdan Stanescu,
Alina-Maria Muresan, Adriana Cuciureanu,
Gheorghe Batrinescu and Nicolae Ionut Cristea

Additional information is available at the end of the chapter

Abstract

The present chapter focuses on spatio-temporal evolution of sediments pollution with mobile heavy metals in five sampling campaigns, in an abandoned gold-bearing mining area from Certeju de Jos, Hunedoara County. The investigated zone is situated in a region where for a long period intense activities of mining exploitation was conducted. For determination of total metals content, sediment samples were dissolved with ultra-pure nitric acid to microwave digestion. For the determination of mobile metals concentrations, it used the first step of BCR 701 sequential extraction scheme in a modified form, by reducing the extraction time from 16 hours to 20 minutes by sonication. The total and mobile concentrations of metals were determined by using ICP-MS. The concentrations of the mobile fractions of Cd, As and Cu are between 60 and 98% for Cd, 10 and 38% for As and up to 44% for Cu, indicating their presence in a bioavailable form. Due to the high mobility, these metals can pass from sediment to surface water and, implicitly, to the aquatic ecosystems. The pollution indices, calculated for the total content of As, Cd, Cu, Ni and Pb, indicate the presence of a strong environmental risk of sediment degradation in most investigated site.

Keywords: sediments, heavy metals, mining area, index pollution, spatio-temporal evolution

1. Introduction

Nowadays, aquatic sediments contamination with heavy metals is a major environmental problem at both national and global level [1–3]. One of the main sources leading to heavy-metal pollution of the aquatic environment is represented by a series of industrial activities associated with mining exploitations processes [4–7].

Due to certain conditions imposed by the legislation in force, mining companies are trying to reduce the emission of effluents resulting from operating activities, but despite all the efforts and safety procedures, accidental pollution is still common within this industry.

Also, near abandoned metal mines, high levels of heavy metals can be found as a result of the discharge and dispersion of waste tailings both the aquatic environment and the soils surrounding the mining areas [8–12].

Depending on the geochemical characteristics and the mineral waste tailing loading, the degree of heavy metals contamination recorded in mining areas varies within a large range [13]. Heavy metals concentrations exceeding the permitted limits regulated by the legislation in force are the main source of aquatic toxicity [14, 15]. The sediments coming from metallic mining areas as main feature of the acid pH value that strongly influences the transport of contaminants from sediment to surface water [16–19]. Drainage of both acid mines and also discharged sediments from abandoned metal mines represents a serious threat to the biota and human health [20].

Heavy metals accumulation in sediments occurs through five major processes: precipitation of certain compounds; binding of fine solid particles having active surface points (encountered in discharges or resuspended during turbulence); coprecipitation together with Fe or Mn oxides or in form of carbonates; association with organic molecules and incorporation into mineral crystals [20]. Therefore, these processes are represented by precipitation and adsorption processes. The balance between these two process categories depends on the metal concentrations, the size of the available surfaces and also the concentrations of the complexing agents found in the water [21]. Inorganic precipitates are formed by oxides, hydroxides, carbonates, sulfates and sulfides [22]. Within aquatic systems having high mineral loading, carbonates and hydroxides are reactive species [20]. The heavy metals as Zn, Ag, Hg, Cu, Cd, or Pb have a strong affinity for sulfide ions thus forming precipitates with very low solubility, so association as sulfide is predominant in reducing conditions as well as when sulfide is released as a result of organic matter decomposition [23].

It is important to underline that heavy metals are not biologically degradable and thus can be accumulated by plants or animals by entering in biochemical where they are transformed into various organometallic compounds [14, 24]. In recent years, more and more attention has been paid for the determination of species in which metals are found, taking in account that toxicity, bioavailability, mobility and other properties depend on the chemical forms of the metals within sample [25–27]. Due to this fact, in addition to determining the total metal

concentrations, it was proposed to determine the chemical species associated with the metal using sequential extraction schemes in order to ensure the characterization of the metals' chemical forms found in sediments, soils and muds [28–31].

In Romania, there are several areas affected by heavy metals contamination such as Baia Mare, Rosia Montana, Certej and Tara Oasului, where gold-mining activities have been carried out for a long time [32–35].

The present chapter focuses on spatio-temporal evolution of sediments pollution with mobile heavy metals as Cd, As, Cu, Ni and Pb in five sampling campaigns, in an abandoned gold-bearing mining area from Certeju de Jos, Hunedoara County. For estimation level pollution of sediments with heavy metals, pollution indexes were calculated. The investigated zone is situated in an region where for a long period intense activities of mining exploitation was conducted.

2. The study area

The analyzed sector (Bajaga River) is located on the territory of Certeju de Jos village, Hunedoara County, about 20 km north of Deva City (**Figure 1**).

In the central area of the studied perimeter, the main collector is represented by the Certej Valley. Its main tributaries are Faerag and Mures streams on the right side, and Bocsa Mica (Ciongani) and Nojag Valley streams on the left side.

After crossing the mountain area, it has a large reception basin powered by a well-developed torrential network, known as the Baiaga Valley and completed downstream by the Hondol
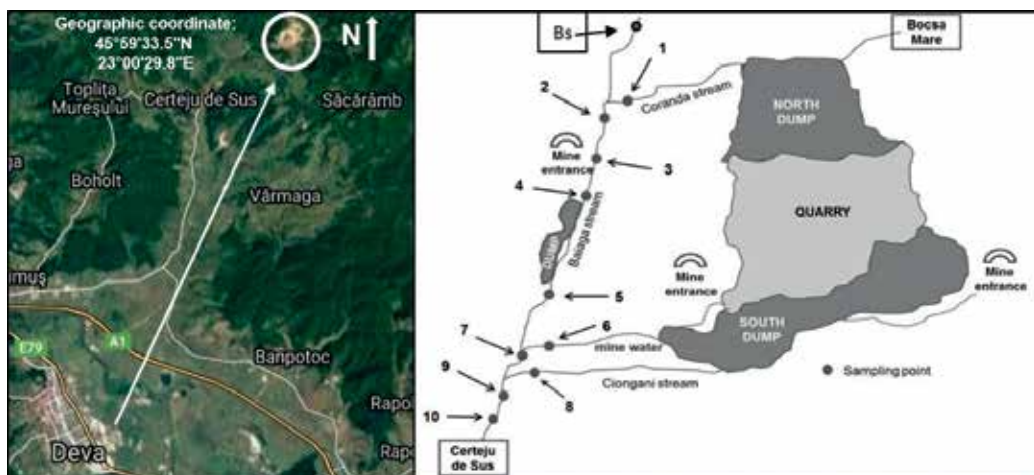
Figure 1. Sampling points location – Certej, Hunedoara County.

Valley, the Certej Valley forms a narrow meadow that gradually spreads until it flows into the Mures River.

From a topographic point of view, the studied area is part of the small mountains group, which has rounded or flat ridges with heights which do not exceed 1300 m. These kinds of mountains groups surround andesite lava beds or quaternary depressions.

Within these types of areas, the water courses are usually short, with steep slopes and insignificant average annual flows. During torrential rains, drift on the slopes occurs rapidly and facilitates the occurrence of impetuous floods, often with catastrophic effects. In these areas, the water courses are short having quick slopes and average annual flows are insignificant as values (**Figure 2**). The river flows undergo major changes during torrential rains when the slopes leakage occurs with high speeds thus facilitating the occurrence of impetuous floods, often with catastrophic effects.

In order to study the spatio-temporal evolution of heavy metal sediment pollution, five sampling campaigns were carried out over 3 years in different periods of the year. In each sampling campaign 10 samples of sediment and surface water associated with sediment within the Certej catchment were taken. In order to compare the results obtained from the polluted sediments, a blank sample was also collected. The location of the sampling points is shown in **Figure 1**, and the GPS coordinates and sample indices are shown in the **Table 1**.

Figure 2. Acid mine water – Baiaga stream.

No.	GPS coordinates	Sample type/indicative	Observations
1	45˚59′84.3″ N 23˚00′25.9″ E	S1	Sampling point situated on Coranda Stream – upstream
2	45˚59′81.9″ N 23˚00′13.1″ E	S2	Sampling point situated on Baiaga Stream, downstream of the confluence with Coranda stream
3	45˚59′80.1″ N 23˚00′06.3″ E	S3	Sampling point situated at the exit Nicodim gallery
4	45˚59′67.7″ N 22˚59′96.6″ E	S4	Sampling point situated on Baiaga Stream, downstream of the confluence with career water from Nicodim gallery
5	45˚59′41.8″ N 22˚59′74.0″ E	S5	Sampling point situated on Baiaga Stream, upstream of the confluence with career water
6	45˚59′41.7″ N 22˚59′73.9″ E	S6	Sampling point from career water, before of the confluence with Baiaga Stream
7	45˚59′39.8″ N 22˚59′74.1″ E	S7	Sampling point situated on Baiaga Stream, downstream of the confluence with career water and upstream of the confluence with Baiaga Stream
8	45˚59′41.0″ N 22˚59′72.2″ E	S8	Sampling point situated on Ciongani Stream before of the confluence with Baiaga Stream
9	45˚59′39.8″ N 22˚59′68.3″ E	S9	Sampling point situated on Baiaga Stream, downstream of the confluence with Ciongani Stream
10	45˚59′20.7″ N 22˚59′06.5″ E	S10	Sampling point situated on Baiaga Stream, in the Hondol Village
11	46˚00′29.6″ N 23˚00′51.3″ E	sediment blank sample (Bs)	Sampling point situated on Baiaga Stream – 2 kilometers away from the quarry area.

Table 1. GPS coordinates and description of sampling points.

3. Materials and methods

3.1. Sampling

The sampling techniques were used in accordance with SR ISO 5667-12/2000 – Guidance on the Sampling of Bottom Sediments the standard in force. The sediment harvested samples were taken from 0 to 5 cm depths using a Van Veen (Wagtech) scrubber. The samples were placed into polypropylene containers which were pre-washed with dilute hydrochloric acid solution.

Samples were transported to the test laboratory in refrigerated boxes and stored at 4°C until the analysis was done.

3.2. Sediment pretreatment

Total content – A part of each sediment sample collected from these sampling points was first prepared before the actual analysis by air-drying and homogenization. For evaluation of the

total content of heavy metals from each soil probe, after this pre-treatment was subjected to the final analysis, only the fraction having smaller dimensions than 63 μm. Through sieving process and using a Fritsch Analysette 3 Spartan Vibratory Sieve Shaker, the sediment samples were separated and finally 2 g of probe were digested in a microwave oven (Berghof, Germany) at 175°C in a 1:3 (v/v) ratio mixture formed by nitric acid (65%):hydrochloric acid (37%) mixture.

Mobile fraction – In order to perform mobile fraction determinations, the remaining part of each sediment sample was first sieved in wet condition using surface water from same sampling point in order to maintain the same structure existing in its natural condition. In this case, similar to total content analysis, the fraction having smaller dimensions than 63 μm was also collected.

3.3. Dry matter content

A separate portion of 1 g was taken from each sample at the same time with the experiments and was dried in an oven at 105 ± 2°C for 3–4 h until constant mass in order to measure dry matter. The results of metals were corrected according to dry matter (d.m.) content.

3.4. Mobile fraction determining methods

3.4.1. The BCR method

In order to correlate the existing analysis methods connected to metals deposition within sediments, an European researcher group conducted a collaboration with the Community Reference Materials Office (CRM). As a result of their common work and a viable alternative to the Tessier method [36], a sequential extraction scheme in three stages (BCR scheme) was proposed [37, 38]. Acetic acid (0.11 M, pH = 2.8), hydroxylamine hydrochloride (0.5 M, pH = 2) and ammonium acetate (1 M, pH = 2) were used as extraction agents. Thus three fractions were separated:

1. The changeable (mobile) fraction for metals having low adsorption rate that are released by ion exchange processes and carbonate-linked metals.

2. The fraction linked to Fe and Mn oxide, also called the "reducible fraction" due to the fact that these kinds of metals are released when this fraction is reduced.

3. The organic matter fraction, also called the "oxidizable fraction" due to the fact that these kinds of metals are released by oxidation.

Currently, this extraction procedure is being used on a large scale performing sediment, soil, muddy soil and also waste analysis [39–41].

The exchangeable (mobile) fraction for cadmium, copper, nickel and lead was determined through a modified BCR method that allowed the extraction time reduction from 16 hours to 20 minutes by using ultrasonic shaking [42] for 20 minutes at 50 KHz and 25°C (**Figure 3**).
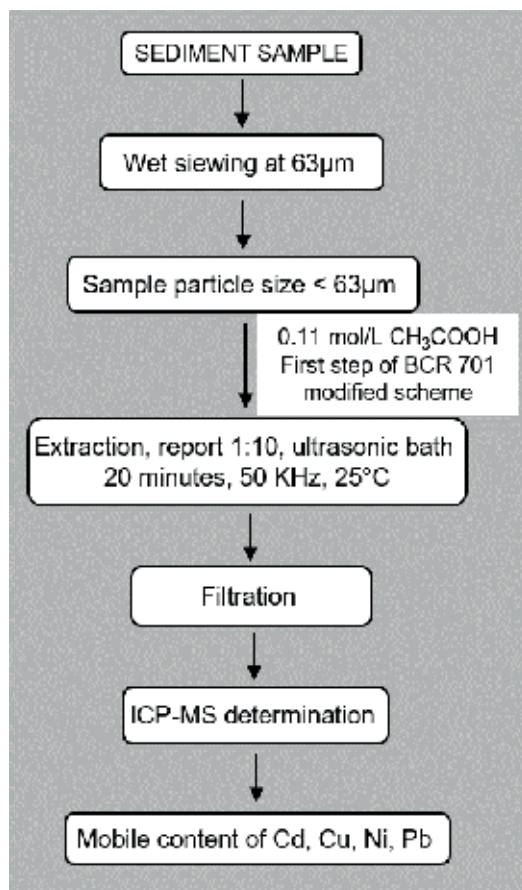
Figure 3. Scheme BCR modified.

The metals concentrations obtained by applying BCR sequential extraction scheme were verified using a certified reference material (BCR-701 – lake sediment produced by the Standards, Measurements and Testing Program – European Commission) with a recovery rate between 99.65 and 99.90%.

3.4.2. Cold extraction procedure

The mobile fraction of arsenic was determined using a cold extraction treatment (**Figure 4**). In order to verify the single chemical extraction of these two metals, this procedure was also applied on a certified reference material WQB-1: lake sediment (with a recovery rate between 99.70 and 99.88%) [43].

The BCR method and cold extraction procedures were performed three times per each sediment sample. The final results were reported as an average. To ensure the quality control of the extraction (decreasing contamination during procedure), a blank extraction (without sediment) was also used for each set of analysis.
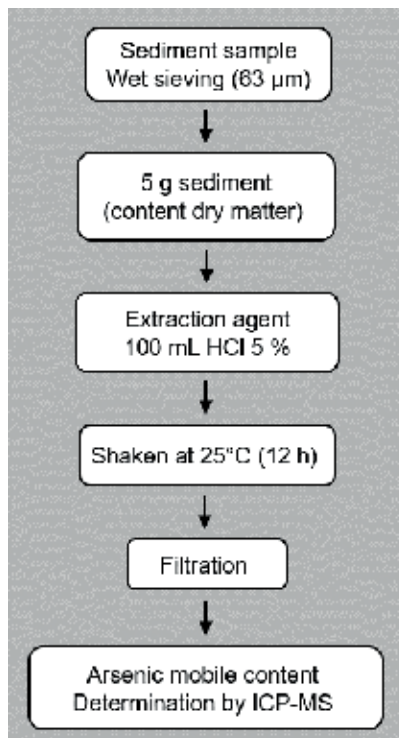
Figure 4. Cold extraction procedure scheme for arsenic mobile content.

The total and mobile content of arsenic in sediment samples were analyzed by inductively coupled plasma mass spectrometry (ICP-MS) (Bruker: Aurora M90). All the chemicals and extraction agents were analytical reagents grade provided by Merck. Calibration curve was performed using a Certified Reference Material ICP multi-element standard solution XXI for MS (Merck quality).

3.4.3. Results and discussion

For all five sampling campaigns, the entire study area indicates an acid pH, both in sediment and in surface water ranging between 3 and 4 pH units.

The results obtained in our study were correlated to the existing limits imposed by the Romanian Order no. 161/2006 on surface water quality and sediments. In **Table 2**, the results for the total and mobile concentrations of cadmium in sediments are shown. Maximum admissible value for total cadmium in sediment according to Romanian Legislation [44] is set to 0.8 mg/kg.

After analyzing the collected data, it was found that in all sampling campaigns total cadmium content exceeded the maximum admissible concentration.

The lowest points of both total and mobile cadmium concentrations were recorded in S1 sampling point located upstream of the quarry and tailings dumps. In the same line, the highest total and mobile cadmium concentrations were recorded in S3 sampling point corresponding to the Nicodim gallery.

Sampling		S1	S2	S3	S4	S5	S6	S7	S8	S9	S10
March 2013	Cd total	1.96	2.85	4.09	3.05	3.31	4.38	4.88	6.45	6.22	6.33
	Cd mobile	1.93	2.11	3.64	2.79	2.54	3.09	4.20	5.57	5.37	4.22
January 2014	Cd total	1.82	2.76	4.82	1.35	3.88	3.06	4.98	1.35	3.21	5.46
	Cd mobile	1.08	1.25	3.76	1.26	1.08	1.43	4.35	1.09	3.00	5.15
July 2014	Cd total	3.15	3.82	8.19	3.09	2.85	5.08	2.85	3.23	3.71	2.16
	Cd mobile	2.32	3.35	7.72	2.76	1.99	2.89	2.32	3.01	3.50	1.99
October 2014	Cd total	0.98	3.98	1.76	1.1	5.23	1.51	1.39	1.52	2.24	1.82
	Cd mobile	0.38	2.82	1.07	0.58	3.10	0.8	0.84	0.72	1.49	1.09
March 2015	Cd total	2.01	1.03	3.98	2.93	1.12	3.43	1.74	2.52	1.62	2.21
	Cd mobile	1.73	0.54	2.65	2.58	0.74	2.61	1.29	2.02	1.35	1.43

Table 2. Total and mobile content of CADMIUM in sediments samples (mg/kg d.m.).

The spatio-temporal evolution of the cadmium mobile content in all five sampling campaigns is given in **Figure 5**.

In all five sampling campaigns, mobile cadmium concentrations represent at least 35% of the total cadmium content recorded in the analyzed sediments. In most samples, it was observed that the mobile cadmium content ranges between 60 and 98% of total content. Also, due to the
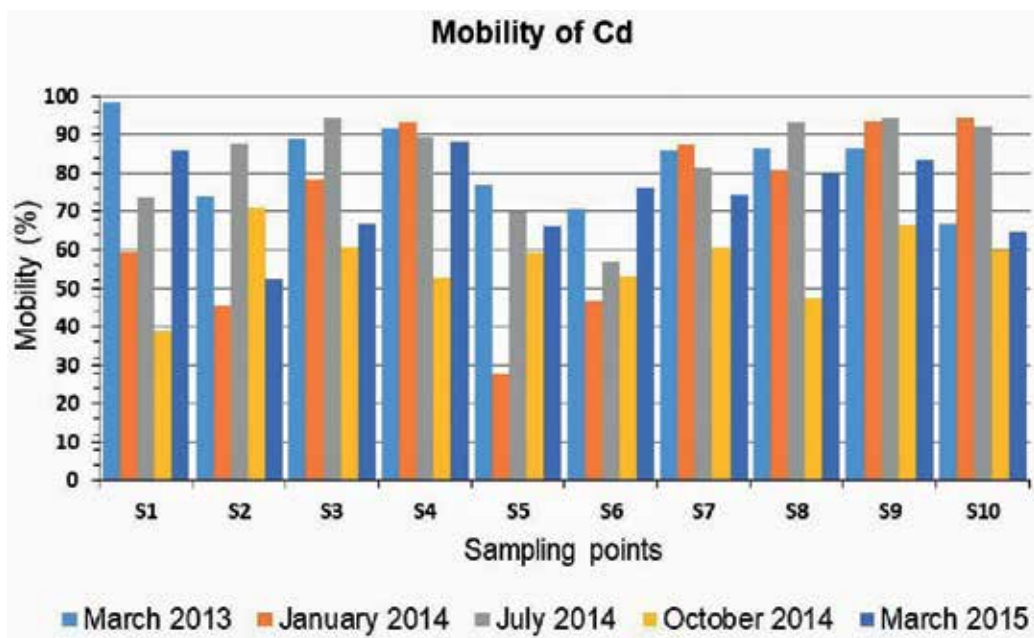
Figure 5. Spatio-temporal evolution of cadmium mobile content.

high mobility percentage, cadmium could induce strong pollution upon aquatic environment by passing from sediment within surface water.

The results obtained for total and mobile arsenic concentrations in sediments are presented in **Table 3**.

Maximum admissible value for As in sediment samples is set to 29 mg/kg, limit imposed by the Romanian legislation in force. In all sampling campaigns, total and mobile arsenic content exceeded the maximum admissible concentration. Sampling points S3 and S4 were the ones in which in all sampling campaigns, the total arsenic concentration was 10 times higher than the maximum admissible concentration.

The elevated arsenic concentrations in these points are due to the water intake from the Nicodim gallery and the water coming from the Coranda River that transports contaminants from the North Dump. It was also noted that in the spring campaigns (March 2013 and March 2015) the values obtained are comparative. This behavior confirms that metals are not biodegradable and were accumulated in aquatic systems over extended periods of time.

The spatio-temporal evolution of the mobile arsenic content in all five sampling campaigns is given in **Figure 6**.

The mobile arsenic concentrations reported to the total arsenic content varied between 10 and 38%. March 2015 sampling campaign corresponded to the highest mobile arsenic concentrations.

The average arsenic concentration obtained from all five sampling campaigns was 23%, value which represents almost a quarter of the total arsenic content. The high content of mobile arsenic induces significant sediment and aquatic ecosystem pollution.

In **Table 4** the results obtained for total and mobile copper concentrations in sediments for all five sampling campaigns are presented.

Sampling		S1	S2	S3	S4	S5	S6	S7	S8	S9	S10
March 2013	As total	282	176	658	485	386	184	312	356	331	215
	As mobil	65.4	42.1	168	89.5	74.9	57.8	56.1	98.5	88.2	55.8
January 2014	As total	202	144	588	405	289	218	222	316	209	217
	As mobil	60.9	55.1	129	105	36.1	32.6	42.8	52.4	41.6	35.6
July 2014	As total	378	285	710	512	406	173	296	411	399	381
	As mobil	71.9	51.6	145	140	93.8	59.6	43.3	91.5	94.5	92.7
October 2014	As total	198	129	775	386	276	197	189	345	277	289
	As mobil	35.6	25.8	186	81.1	52.4	49.3	29.8	75.9	49.9	46.2
March 2015	As total	274	159	614	449	298	175	294	326	246	191
	As mobil	29.7	35.4	152	110	81.1	60.3	49.2	88.6	104	56.9

Table 3. Total and mobile content of ARSENIC in sediments samples (mg/kg d.m.).
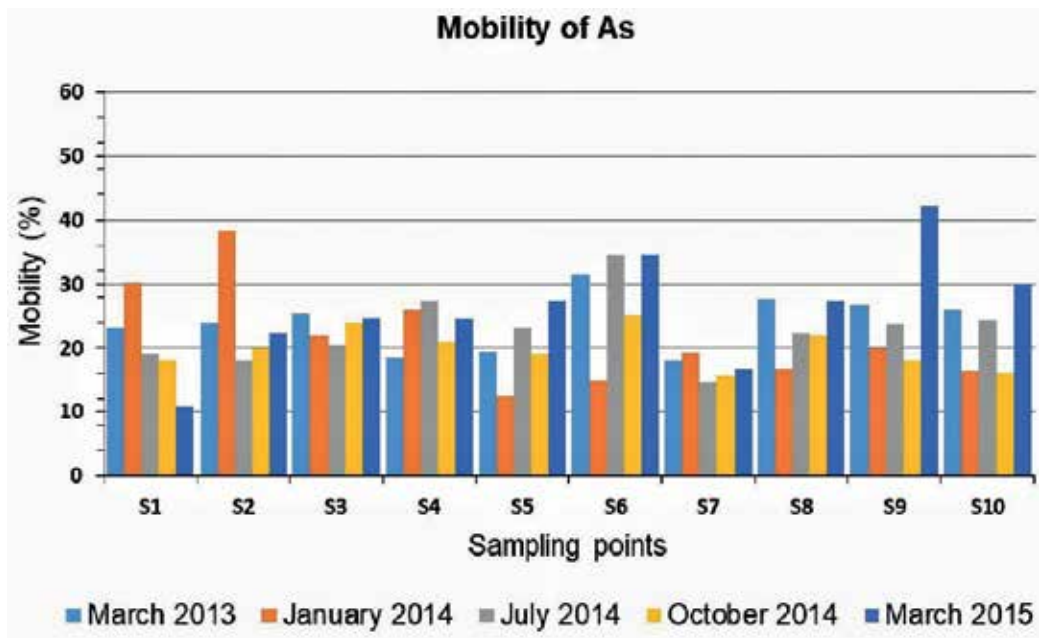
Figure 6. Spatio-temporal evolution of arsenic mobile content.

Sampling		S1	S2	S3	S4	S5	S6	S7	S8	S9	S10
March 2013	Cu total	75.2	38.9	48.2	57.6	35.4	18.8	47.1	52.6	37.5	42.1
	Cu mobil	16.9	12.8	8.27	15.6	8.91	3.56	10.44	12.35	11.9	10.8
January 2014	Cu total	28.4	32.2	43.5	70.2	29.1	48.3	35.8	36.8	26.1	25.1
	Cu mobil	6.85	14.2	9.43	18.7	4.88	19.5	6.61	5.88	7.22	5.47
July 2014	Cu total	54.2	105	57	36.4	54.9	139	29.7	54.5	35.5	32.7
	Cu mobil	11.5	25.7	13.1	8.88	12.5	30.1	5.86	12.9	8.39	8.64
October 2014	Cu total	40.4	29.6	51.4	42.8	102	64.1	44.6	109	62.2	40.3
	Cu mobil	9.6	10.8	7.8	11.4	14.7	7.37	10.5	19.2	8.6	9.6
March 2015	Cu total	66.3	15.5	40.4	25.1	48.3	20.6	37.2	33.2	20.8	50.5
	Cu mobil	6.52	4.92	7.08	2.4	4.08	7.32	1.39	1.76	1.12	1.2

Table 4. Total and mobile content of COPPER in sediments samples (mg/kg d.m.).

Regarding copper concentrations, 56% from the sediment samples has the total content above the maximum admissible concentration limit with is set to 40 mg/kg d.m. No mobile content over the limit has been recorded.

The highest concentrations exceeding twice the maximum admissible concentration are recorded at S5 and S8 (October 2014) and S2 (July 2014).

The spatio-temporal evolution of the mobile copper content in all sampling campaigns is given in **Figure 7**.

Analyzing the data presented in **Figure 7**, a decrease regarding copper content throughout the investigated route was noticed as follows: January 2014 > March 2013 > Oct 2014 > March 2015. The bioavailable content was ranged between 2 and 44%. In the same time, it was also recorded a peak in mobile copper concentration, the highest values were found in S2 (44%) and S6 (41%), corresponding to samples collected in January 2014.

All these concentrations exceeded the maximum admissible concentration according to Order 61/2006. In all the other campaigns, the mobile copper concentrations found in the investigated samples were below the maximum admissible value.

In **Table 5**, the results obtained for total and mobile nickel concentrations in sediments collected in all five sampling campaigns are presented. The data were compared with maximum admissible value, which is 35 mg/kg.
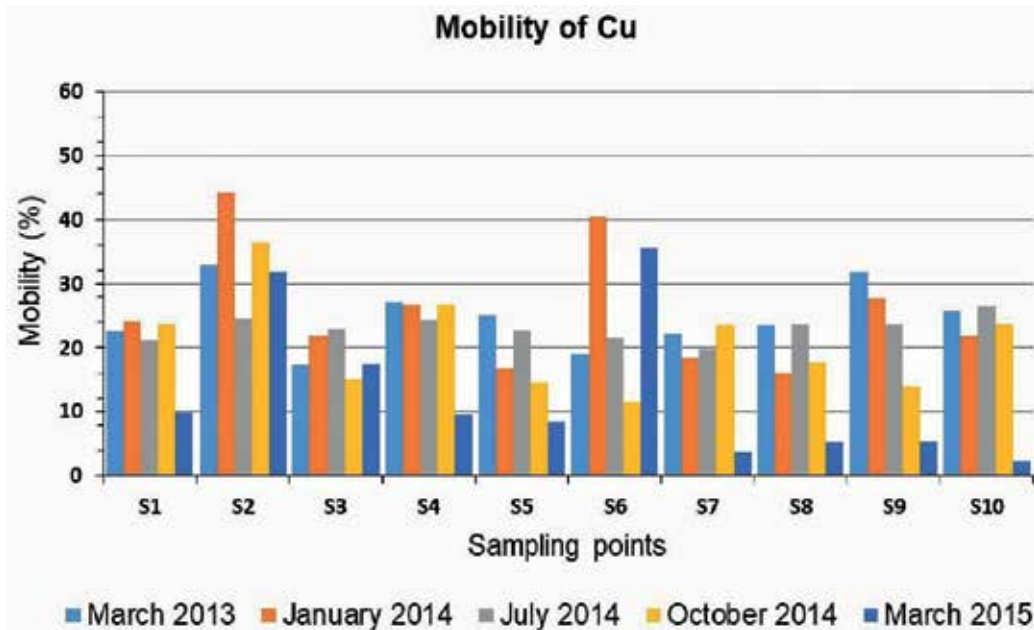
Figure 7. Spatio-temporal evolution of copper mobile content.

Sampling		S1	S2	S3	S4	S5	S6	S7	S8	S9	S10
March 2013	Ni total	32.3	16.7	62.3	18.2	33.9	16.5	8.44	43.9	30.5	30.9
	Ni mobil	8.05	6.55	14.8	8.04	19.2	8.63	2.60	8.40	9.32	10.6
January 2014	Ni total	24.3	20.5	38.6	23.1	30.8	14.2	26.2	25.2	17.6	18.6
	Ni mobil	7.35	6.28	10.7	9.84	16.5	6.82	5.86	4.79	5.88	11.7
July 2014	Ni total	34.7	25.8	75.9	29.1	40.6	24.2	19.7	38.5	32.8	27.4
	Ni mobil	7.25	8.64	17.9	5.33	11.9	9.26	3.81	4.56	7.62	6.25
October 2014	Ni total	19.1	15.2	45.1	23.4	26.9	8.03	43.9	6.58	30.1	22.9
	Ni mobil	2.83	2.60	7.94	6.83	11.9	2.17	4.56	1.79	8.28	9.71
March 2015	Ni total	27.6	22.8	65.4	25.2	30.9	12.7	15.4	25.8	22.7	31.9
	Ni mobil	5.41	6.33	20.8	7.82	6.49	4.21	8.52	10.4	13.1	16.9

Table 5. Total and mobile content of NICKEL in sediments samples (mg/kg d.m.).

The highest total nickel concentration was recorded in S3 sampling point associated with Nicodim gallery (two times higher than limit). Also nickel exceedings in S5 and S8 (July 2014), S8 (March 2013) and S7 (October 2014) were found.

At all the other sampling points, both total and mobile nickel concentrations were below the maximum admissible value.

The spatio-temporal evolution of nickel mobile content in the all sampling campaigns is given in **Figure 8**.

After the results were collected, we could conclude that in all sampling campaigns the mobile nickel concentrations varied between 10 and 63%. The highest mobile Ni concentrations were determined in the samples coming from S5, S6, S7, S9 and S10 points. In these cases, the values determined exceeded the maximum admitted concentration and represent more than 50% of the total nickel content.

The intake of contaminants accumulating in the upstream from Nicodim gallery, mine water and career water could be the main sources of these overtakings. In March 2015, the sampling campaign recorded a decrease of the Ni mobile concentrations for the majority of the investigated sediments. Sediments can change their composition, so they could be more diluted or loaded, depending on the volume of precipitation and weather conditions [43].
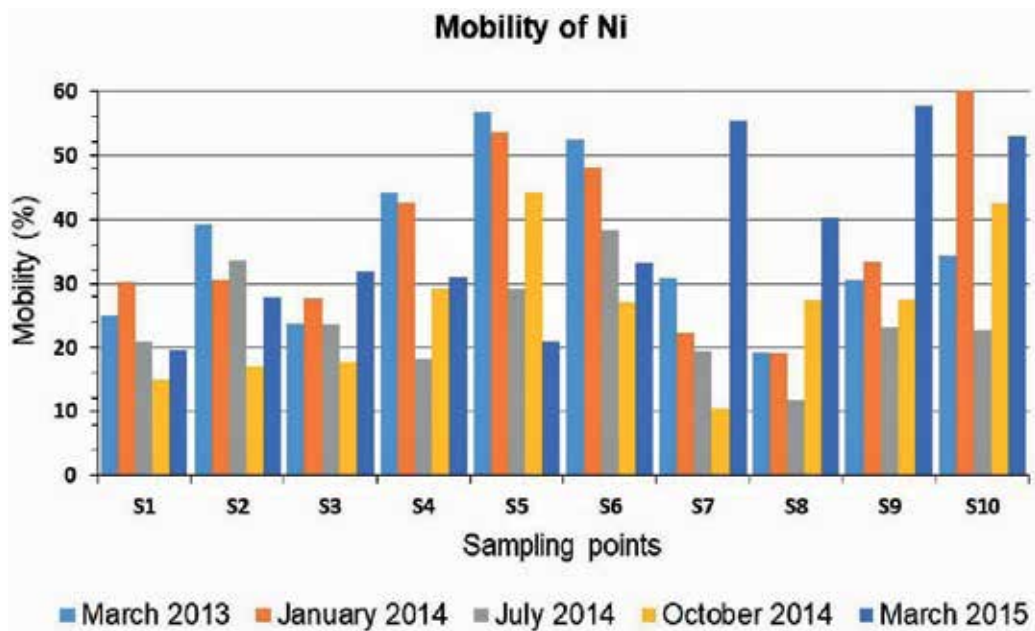
Figure 8. Spatio-temporal evolution of nickel mobile content.

In **Table 6**, the results obtained for the total and mobile lead concentrations within sediments are presented for the five sampling campaigns:

Regarding Pb content, the results obtained from the most sampling points indicate that the maximum admissible concentration, which is 85 mg/kg, was exceeded.

The highest lead concentrations were recorded at sampling point S3 where the total lead concentration ranges between 235 mg/kg d.m. (March 2013) and 539 mg/kg d.m. (October 2014).

The spatio-temporal evolution of mobile lead content in all five sampling campaigns is shown in **Figure 9**.

Although within the majority of the analyzed sediments the total lead content exceeds the maximum admissible concentration, the mobile content of Pb is below the maximum admissible value and thus in almost all investigated samples does not exceed 15 mg/kg d.m.

This behavior confirms that lead is link in a lower share within oxides, carbonates and organic matter and a greater share within residual fraction.

3.5. Estimation the pollution degree by pollution indexes

In order to assess the pollution degree of the aquatic environment with these toxic metals, we proposed the determination of two pollution indices: the contamination factor (CF) and the geoaccumulation index (I_{geo}).

Sampling		S1	S2	S3	S4	S5	S6	S7	S8	S9	S10
March 2013	Pb total	129	111	235	109	254	120	266	28.8	64.9	103
	Pb mobil	10.3	10.1	8.50	3.72	9.98	3.36	11.8	4.77	3.72	4.51
January 2014	Pb total	152	144	354	127	103	66.5	185	113	48.4	36.6
	Pb mobil	10.8	6.42	15.9	9.53	6.87	5.45	10.4	8.70	4.02	6.21
July 2014	Pb total	205	157	426	135	79.2	87.8	223	151	88.4	75.9
	Pb mobil	6.82	4.16	24.5	8.68	3.21	6.17	12.9	18.7	15.9	10.8
October 2014	Pb total	213	127	539	115	174	284	165	244	364	131
	Pb mobil	14.5	2.35	16.3	5.15	2.18	9.89	5.48	8.52	6.92	3.56
March 2015	Pb total	145	74.3	382	151	183	219	148	76.9	297	154
	Pb mobil	12.8	3.85	23.9	8.82	6.14	12.4	8.22	5.44	16.9	8.24

Table 6. Total and mobile content of LEAD in sediments samples (mg/kg d.m.).
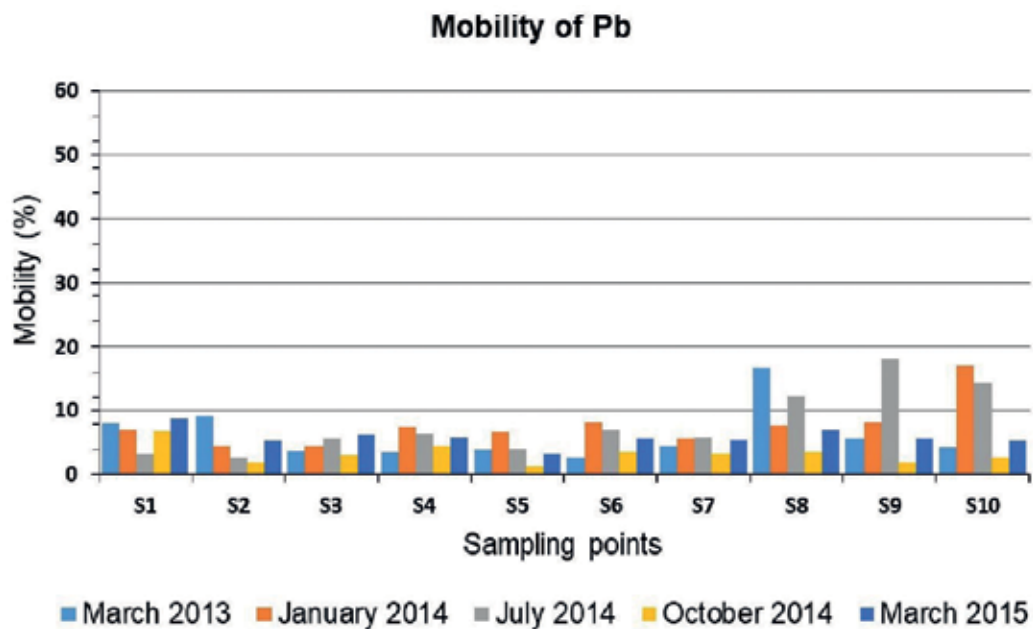

Figure 9. Spatio-temporal evolution of lead mobile content.

The contamination factor (CF) (**Table 7**)—is given by the ratio between the metal concentration within the sediment and the metal concentration in the natural background. CF is calculated according to Hakanson's formula (Eq. (1)) [45]:

$$CF = \frac{Cs}{Bs} \tag{1}$$

where *Cs* is the metal concentration within the sample and *Bs* is the metal concentration within the natural background (**Figure 1**).

The geoaccumulation index (I_{geo}) (**Table 8**) was introduced by Müller [46] and is widely used [15, 47, 48] to determine the pollution degree with heavy metal in surface sediments:

$$Igeo = \log_2\left[\left(\frac{Cs}{K \times Bs}\right)\right] \tag{2}$$

where *Cs* is the metal concentration within the sample, *Bs* is the metal concentration within the natural background and *K* is the correction factor that takes into account the variation of metal traces in the natural background as a result of the lithogenic effects (*K* = 1.5).

The geoaccumulation index provides a classification system for the pollution degree in relation to the sediment quality [46].

In **Table 9**, the concentrations of metals within the natural background are given.

The determination of contamination factor (CF) and geoaccumulation index (I_{geo}) involved assuming that each metal concentration introduced in the formulas was the average value obtained after the five sampling campaigns.

Contamination factor (CF) and geoaccumulation index (I_{geo}) values are shown in **Tables 10** and **11**.

Contamination factor (CF)	Contamination level
CF < 1	Low contamination
1 ≤ CF < 3	Medium contamination
3 ≤ CF < 6	Significant contamination
CF > 6	Very high contamination

Table 7. Contamination factor (CF) and contamination level.

I_{geo} value	Class of pollution in relation to I_{geo}	Sediment quality
≤0	0	Unpolluted level
0–1	1	Unpolluted level to moderate pollution
1–2	2	Moderate pollution level
2–3	3	Moderate pollution level to high pollution
3–4	4	High pollution level
4–5	5	High pollution level to very high pollution level
>5	6	Very high pollution level

Table 8. The relationship between I_{geo} and the pollution level.

No.	Metal	UM	Concentration within the natural background
1	Cadmium	mg/kg dm	0.43
2	Arsenic	mg/kg dm	9.34
3	Copper	mg/kg dm	23.4
4	Nickel	mg/kg dm	38.3
5	Lead	mg/kg dm	16.7

Table 9. Metal concentration within the natural background (Bs).

Concentration factor CF											
No.	Metal	S1	S2	S3	S4	S5	S6	S7	S8	S9	S10
1	Cd	4.61	6.72	10.6	5.36	7.62	8.12	7.37	7.01	7.91	8.36
2	As	28.6	19.1	71.6	47.9	35.4	20.3	28.1	37.6	31.3	27.7
3	Cu	2.26	1.89	2.06	1.98	2.31	2.49	1.66	2.45	1.56	1.63
4	Ni	0.72	0.53	1.50	0.62	0.85	0.39	0.59	0.73	0.70	0.69
5	Pb	10.1	7.34	23.2	7.63	9.50	9.31	11.8	7.35	10.3	6.00
Geoaccumulation index (I_{geo})											
No.	Metal	S1	S2	S3	S4	S5	S6	S7	S8	S9	S10
1	Cd	1.62	2.16	2.82	1.84	2.35	2.44	2.30	2.22	2.40	2.48
2	As	4.25	3.67	5.58	5.00	4.56	3.76	4.23	4.65	4.38	4.21
3	Cu	0.59	0.33	0.45	0.40	0.62	0.73	0.15	0.71	0.05	0.12
4	Ni	−1.10	−1.50	0.00	−1.30	−0.80	−1.90	−1.30	−1.00	−1.10	−1.10
5	Pb	2.75	2.29	3.95	2.35	2.66	2.63	2.98	2.29	2.78	2.00
Concentration factor CF											
No.	Metal	S1	S2	S3	S4	S5	S6	S7	S8	S9	S10
1	Cd	4.61	6.72	10.6	5.36	7.62	8.12	7.37	7.01	7.91	8.36
2	As	28.6	19.1	71.6	47.9	35.4	20.3	28.1	37.6	31.3	27.7
3	Cu	2.26	1.89	2.06	1.98	2.31	2.49	1.66	2.45	1.56	1.63
4	Ni	0.72	0.53	1.50	0.62	0.85	0.39	0.59	0.73	0.70	0.69
5	Pb	10.1	7.34	23.2	7.63	9.50	9.31	11.8	7.35	10.3	6.00
Geoaccumulation index (I_{geo})											
No.	Metal	S1	S2	S3	S4	S5	S6	S7	S8	S9	S10
1	Cd	1.62	2.16	2.82	1.84	2.35	2.44	2.30	2.22	2.40	2.48
2	As	4.25	3.67	5.58	5.00	4.56	3.76	4.23	4.65	4.38	4.21
3	Cu	0.59	0.33	0.45	0.40	0.62	0.73	0.15	0.71	0.05	0.12
4	Ni	−1.10	−1.50	0.00	−1.30	−0.80	−1.90	−1.30	−1.00	−1.10	−1.10
5	Pb	2.75	2.29	3.95	2.35	2.66	2.63	2.98	2.29	2.78	2.00

Table 10. Contamination factor (CF) and geoaccumulation index (I_{geo}) values within sediments.

Sediment	I_{geo}	Sediment	I_{geo}
S1	4	S6	4
S2	4	S7	4
S3	6	S8	5
S4	5	S9	5
S5	5	S10	5

Table 11. The quality class for each sediment according to geoaccumulation indexes.

Both arsenic and lead induce a very high contamination (CF > 6). The same behavior was also observed for cadmium, which induces very high contamination with the exception of samples S1 and S4 where the sediments exhibit only considerable contamination. In case of nickel, we could conclude that it induces low contamination in sediments, except for the S3 sediment that also enters into moderate contamination category. In all sediments that were analyzed, copper induced moderate contamination.

Taking in consideration that each of the analyzed sediments had very high concentrations of As, Cd and Pb and without taking into account the contribution that other metals could imply on the samples, the samples were introduce in very high contamination category.

According to the classification given in **Table 8**, the geoaccumulation indexes calculated for Cd in sediments classified sediments S1 and S4 into class 2 (moderate pollution level) and all the other sediments into class 3 (moderately to high polluted).

In the same time, geoaccumulation indexes calculated for As, classified sediments S2 and S6 into class 4 (highly polluted), sediments S1, S2 and S7 into class 4 (highly polluted), sediments S1, S5, S7, S8, S9, S10 into class 5 (from highly polluted to very highly polluted) and sediment S3 and S4 into class 6 (very highly polluted).

In Cu case, the geoaccumulation index values obtained classified all sediments into class 1 (from unpolluted to moderately polluted). Regarding Ni, the geoaccumulation index values obtained classified all sediments into class 0 (unpolluted level). Geoaccumulation index values obtained for Pb, classified sediment S3 into class 4 (heavily polluted) and all other sediments into class 3 (moderately to highly polluted).

Based on the results given in **Table 11**, we could conclude that the most contaminated area is at sampling point S3, the point near Nicodim gallery exit.

4. Conclusion

In all sampling campaigns, the area investigated indicates an acid pH, both in sediment and in surface water. Concerning the total of heavy metal content, from all five metals investigated, Cd, Pb and As induce high sediment contamination with concentrations exceeding the limits imposed by the legislation in force.

From the point of view of metal mobile fraction, Cd and As are predominantly present in a bioavailable form within the analyzed sediments, thus inducing a high degree of pollution upon the aquatic environment by passing from sediments within surface water.

The pollution degree of the water depends on the amount of precipitation in the area, a heavy rain implies a less dilution and also the opposite case. Therefore, all the values recorded at most sampling points may be momentary, associated with the place and time of sampling.

The pollution indexes, calculated for the total content of As, Cd, Cu, Ni and Pb, indicate the presence of a strong environmental risk of sediment degradation.

Author details

Lidia Kim*, Geanina-Gabriela Vasile, Luoana Florentina Pascu, Bogdan Stanescu, Alina-Maria Muresan, Adriana Cuciureanu, Gheorghe Batrinescu and Nicolae Ionut Cristea

*Address all correspondence to: lidiakim17@yahoo.com

National Research and Development Institute for Industrial Ecology ECOIND, Bucharest, Romania

References

[1] Lee P-K, Kang M-J, Yu S, Ko K-S, Ha K, Shin S-C, Park JH. Enrichment and geo-chemical mobility of heavy metals in bottom sediment of the Hoedong reservoir, Korea and their source apportionment. Chemosphere. 2017;**184**:74-85. DOI: 10.1016/j.chemosphere.2017.05.124

[2] El Azhari A, Rhoujjati A, Hachimi MLE. Assessment of heavy metals and arsenic con-tamination in the sediments of the Moulouya River and the Hassan II Dam downstream of the abandoned mine Zeïda (High Moulouya, Morocco). Journal of African Earth Sciences. 2016;**119**:279-288. DOI: 10.1016/j.jafrearsci.2016.04.011

[3] Kim L, Vasile GG, Stanescu B, Calinescu S, Batrinescu G. Distribution and bioavailability of mobile arsenic in sediments from a mining catchment area. Journal of Environmental Protection and Ecology. 2015;**16**:1227-1236

[4] Rieuwerts J, Mighanetara K, Braungardt C, Rollinson G, Pirrie D, Azizi F. Geochemistry and mineralogy of arsenic in mine wastes and stream sediments in a historic metal min-ing area in the UK. Science of the Total Environment. 2014;**472**:226-234. DOI: 10.1016/j.scitotenv.2013.11.029

[5] Gao Z. Evaluation of heavy metal pollution and its ecological risk in one river reach of a gold mine in Inner Mongolia, Northern China. International Biodeterioration & Biodegradation. 2017;**xxx**:1-6. DOI: 10.1016/j.ibiod.2017.01.001

[6] Chernova EN, Potikha EV, Nesterenko OE. The content of heavy metals in bottom sediments of the streams of the Sikhote-Alin biosphere reserve and the streams draining mines of the transit zone of the reserve. Achievements in the Life Sciences. 2015;**9**:9-14. DOI: 10.1016/j.als.2015.05.002

[7] Redwan M, Rammlmair D. Flood hazard assessment and heavy metal distributions around um Gheig mine area, Eastern Desert, Egypt. Journal of Geochemical Exploration. 2017;**173**:64-75. DOI: 10.1016/j.gexplo.2016.11.012

[8] Navarro M, Pérez-Sirvent C, Martínez-Sánchez M, Vidal J, Tovar P, Bech J. Abandoned mine sites as a source of contamination by heavy metals: A case study in a semi-arid zone. Journal of Geochemical Exploration. 2008;**96**:183-193. DOI: 10.1016/j.gexplo.2007.04.011

[9] Beane SJ, Comber SD, Rieuwerts J, Long P. Abandoned metal mines and their impact on receiving waters: A case study from Southwest England. Chemosphere. 2016;**153**:294-306. DOI: 10.1016/j.chemosphere.2016.03.022

[10] Antunes I, Gomes M, Neiva A, Carvalho P, Santos A. Potential risk assessment in stream sediments, soils and waters after remediation in an abandoned W>Sn mine (NE Portugal). Ecotoxicology and Environmental Safety. 2016;**133**:135-145. DOI: 10.1016/j.ecoenv.2016.06.045

[11] Neiva A, Carvalho P, Antunes I, Silva M, Santos A, Pinto MC, Cunha P. Contaminated water, stream sediments and soils close to the abandoned Pinhal do Souto uranium mine, central Portugal. Journal of Geochemical Exploration. 2014;**136**:102-117. DOI: 10.1016/j.gexplo.2013.10.014

[12] da Silva EF, Almeida SF, Nunes ML, Luís AT, Borg F, Hedlund M, de Sá CM, Patinha C, Teixeira P. Heavy metal pollution downstream the abandoned Coval da Mó mine (Portugal) and associated effects on epilithic diatom communities. Science of the Total Environment. 2009;**407**:5620-5636. DOI: 10.1016/j.scitotenv.2009.06.047

[13] Johnson R, Blowes D, Robertson W, Jambor J. The hydrogeochemistry of the Nickel Rim mine tailings impoundment, Sudbury, Ontario. Journal of Contaminant Hydrology. 2000;**41**:49-80. DOI: 10.1016/S0169-7722(99)00068-6

[14] Delgado J, Barba-Brioso C, Nieto JM, Boski T. Speciation and ecological risk of toxic elements in estuarine sediments affected by multiple anthropogenic contributions (Guadiana saltmarshes, SW Iberian Peninsula): I. Surficial sediments. Science of the Total Environment. 2011;**409**:3666-3679. DOI: 10.1016/j.scitotenv.2011.06.013

[15] Sarmiento AM, DelValls A, Nieto JM, Salamanca MJ, Caraballo MA. Toxicity and potential risk assessment of a river polluted by acid mine drainage in the Iberian Pyrite Belt (SW Spain). Science of the Total Environment. 2011;**409**:4763-4771. DOI: 10.1016/j.scitotenv.2011.07.043

[16] Zhao H, Xia B, Qin J, Zhang J. Hydrogeochemical and mineralogical characteristics related to heavy metal attenuation in a stream polluted by acid mine drainage: A case study in Dabaoshan Mine, China. Journal of Environmental Sciences. 2012;**24**:979-989. DOI: 10.1016/S1001-0742(11)60868-1

[17] Equeenuddin SM, Tripathy S, Sahoo P, Panigrahi M. Metal behavior in sediment associated with acid mine drainage stream: Role of pH. Journal of Geochemical Exploration. 2013;**124**:230-237. DOI: 10.1016/j.gexplo.2012.10.010

[18] Magyar MI, Ladson AR, Diaper C. Sediment transport in rainwater tanks and implications for water quality. In: Manning A, Editor. Sediment Transport in Aquatic Environments, InTech; Croatia. 2011. p. 65-88

[19] Zaharia L, Grecu F, Ioana-Toroimac G, Neculau G. Sediment transport and river channel dynamics in Romania–variability and control factors. In: Manning A, Editor. Sediment Transport in Aquatic Environments, InTech; Croatia. 2011. p. 293-316

[20] Peplow D, Edmonds R. The effects of mine waste contamination at multiple levels of biological organization. Ecological Engineering. 2005;**24**:101-119. DOI: 10.1016/j.ecoleng. 2004.12.011

[21] Pagenkopf GK, Cameron D. Deposition of trace metals in stream sediments. Water, Air, and Soil Pollution. 1979;**11**:429-435. DOI: 10.1007/BF00283434

[22] Ogbonna PC, Odukaesieme C, Teixeira da Silva JA. Distribution of heavy metals in soil and accumulation in plants at an agricultural area of Umudike, Nigeria. Chemistry and Ecology. 2013;**29**:595-603. DOI: 10.1080/02757540.2013.810721

[23] Al T, Blowes D, Martin C, Cabri L, Jambor J. Aqueous geochemistry and analysis of pyrite surfaces in sulfide-rich mine tailings. Geochimica et Cosmochimica Acta. 1997;**61**:2353-2366. DOI: 10.1016/S0016-7037(97)00113-0

[24] Morillo J, Usero J, Gracia I. Potential mobility of metals in polluted coastal sediments in two bays of southern Spain. Journal of Coastal Research. 2007;**23**:352-361. DOI: 10.2112/04-0246.1

[25] Castillo MA, Trujillo IS, Alonso EV, de Torres AG, Pavón JC. Bioavailability of heavy metals in water and sediments from a typical Mediterranean Bay (Málaga Bay, Region of Andalucía, Southern Spain). Marine Pollution Bulletin. 2013;**76**:427-434. DOI: 10.1016/j.marpolbul.2013.08.031

[26] Noronha-D'Mello CA, Nayak G. Assessment of metal enrichment and their bioavailability in sediment and bioaccumulation by mangrove plant pneumatophores in a tropical (Zuari) estuary, west coast of India. Marine Pollution Bulletin. 2016;**110**:221-230. DOI: 10.1016/j.marpolbul.2016.06.059

[27] Marin NM, Vasile GG, Simion M, Pascu LF, Lehr CB. Rapid method for evaluation of metallic mobile fraction from sewage sludge samples. Scientific Study & Research. Chemistry & Chemical Engineering, Biotechnology, Food Industry. 2017;**18**:43

[28] Anju M, Banerjee D. Comparison of two sequential extraction procedures for heavy metal partitioning in mine tailings. Chemosphere. 2010;**78**:1393-1402. DOI: 10.1016/j.chemosphere.2009.12.064

[29] Vasile G, Tanase IG. In-house'validation for mobile nickel in solid environment samples. Journal of Environmental Protection and Ecology. 2011;**12**:1262-1274

[30] Vasile GG, Kim L, Gheorghe S, Stanescu B. Ecological assessment of mobile cadmium in sediments from Certej mining site, Hunedoara County, Romania. In: International Multidisciplinary Scientific GeoConference: SGEM: Surveying Geology & mining Ecology Management 16-22 June 2013; Albena. Bulgaria. p. 299

[31] Vasile GG, Tanase IG. Comparative study of different extraction methods for evaluation of bioavailability of terrestrial sediment – Bound metallic elements. Revue Roumaine de Chimie. 2008;**53**:1041-1049. DOI: 10.1007/BF02484715

[32] Vasile GD, Vlădescu L. Cadmium partition in river sediments from an area affected by mining activities. Environmental Monitoring and Assessment. 2010;**167**:349-357. DOI: 10.1007/s10661-009-1054-y

[33] Vasile GG, Tanase IG, Dinu C. The influence of the air-drying pretreatment of sediment samples for metallic element mobilities. Analytical Letters. 2010;**43**:1199-1206. DOI: 10.1080/00032710903518625

[34] Vasile GD, Nicolau M, Vlădescu L. Zinc speciation in sediments from a polluted river, as an estimate of its bioaccesibility. Environmental Monitoring and Assessment. 2010;**160**: 71-81. DOI: 10.1007/s10661-008-0658-y

[35] Kim L, Vasile GG, Stanescu B, Dinu C, Ene C. Distribution of trace metals in surface water and streambed sediments in the vicinity of an abandoned gold mine from Hunedoara County, Romania. Revista de Chimie (Bucharest). 2016;**67**:1441-1446

[36] Tessier A, Campbell PG, Bisson M. Sequential extraction procedure for the speciation of particulate trace metals. Analytical Chemistry. 1979;**51**:844-851. DOI: 10.1021/ac50043a017

[37] Quevauviller P, Rauret G, López-Sánchez J-F, Rubio R, Ure A, Muntau H. Certification of trace metal extractable contents in a sediment reference material (CRM 601) following a three-step sequential extraction procedure. Science of the Total Environment. 1997;**205**:223-234. DOI: 10.1016/S0048-9697(97)00205-2

[38] Ure A, Quevauviller P, Muntau H, Griepink B. Speciation of heavy metals in soils and sediments. An account of the improvement and harmonization of extraction techniques undertaken under the auspices of the BCR of the Commission of the European Communities. International Journal of Environmental Analytical Chemistry. 1993;**51**:135-151. DOI: 10.1080/03067319308027619

[39] Pueyo M, Mateu J, Rigol A, Vidal M, López-Sánchez J, Rauret G. Use of the modified BCR three-step sequential extraction procedure for the study of trace element dynamics in contaminated soils. Environmental Pollution. 2008;**152**:330-341

[40] Sutherland RA, Tack FM. Fractionation of cu, Pb and Zn in certified reference soils SRM 2710 and SRM 2711 using the optimized BCR sequential extraction procedure. Advances in Environmental Research. 2003;**8**:37-50

[41] Rauret G, López-Sánchez J-F, Sahuquillo A, Barahona E, Lachica M, Ure A, Davidson C, Gomez A, Lück D, Bacon J. Application of a modified BCR sequential extraction (three-step) procedure for the determination of extractable trace metal contents in a sewage

sludge amended soil reference material (CRM 483), complemented by a three-year stability study of acetic acid and EDTA extractable metal content. Journal of Environmental Monitoring. 2000;**2**:228-233. DOI: 10.1039/B001496F

[42] Arain MB, Kazi TG, Jamali MK, Jalbani N, Afridi HI, Baig JA. Speciation of heavy metals in sediment by conventional, ultrasound and microwave assisted single extraction methods: A comparison with modified sequential extraction procedure. Journal of Hazardous Materials. 2008;**154**:998-1006

[43] National Laboratory for Environmental Testing – National Water Research Institute, Ontario, Canada

[44] Order no 161/2006 for the approval of the Norm concerning the reference objectives for the surface water quality classification, The Ministry of Environment and Water. Official Monitor of Romania. Part.1, no. 511 bis

[45] Hakanson L. An ecological risk index for aquatic pollution control. A sedimentological approach. Water Research. 1980;**14**:975-1001

[46] Förstner U, Müller G. Concentrations of heavy metals and polycyclic aromatic hydrocarbons in river sediments: Geochemical background, man's influence and environmental impact. GeoJournal. 1981;**5**:417-432

[47] El Azhari A, Rhoujjati A, El Hachimi ML, J-p A. Pollution and ecological risk assessment of heavy metals in the soil-plant system and the sediment-water column around a former Pb/Zn-mining area in NE Morocco. Ecotoxicology and Environmental Safety. 2017;**144**:464-474. DOI: 10.1016/j.ecoenv.2017.06.051

[48] Iordache M, Popescu LR, Pascu LF, Iordache I. Assessment of the potential ecological risk with heavy metals in surface s sediments from accumulation lakes on the sector inferior of the Olt River. In: International Symposium "The Environment and the Industry", SIMI 2015; 29-30 October 2015; Bucharest, Romania. p. 175-184

Marine Sediments as Fundamental Repository of Radioactive Contaminants in Aquatic Ecosystems

Marisé García Batlle and
Juan Manuel Navarrete Tejero

Additional information is available at the end of the chapter

Abstract

In the last three decades, the studies of artificial radionuclides concentration have attracted attention, bringing in the most significant long-term threat to the biosphere. In aquatic ecosystems, the main indicators of pollution are contaminated sediments, which are the primary repository of radionuclides and chemical elements in the marine environment. Radioactive contamination factor (RCF) has been proposed as a suitable unit to measure the magnitude of radioactive contamination at global scale, caused mainly by more than 2000 nuclear explosion tests performed during the 1945–1965 period. It is obtained as percentage of contaminant radioactivity (^{137}Cs) compared to natural radioactivity (^{40}K), both expressed in Bq/g of marine sediments conditioned in Marinelli containers and detected in both NaI(Tl) and HPGe detectors. So, in this paper, samples of marine sediments were taken up along the occidental Cuban coasts and analyzed by gamma spectrometry for the determination of gamma-emitting radioisotopes with energies between 60 and 2000 keV. The results proved that the proposed method is simple and suitable to evaluate radioactive contamination. Also, the RCF values provide an appropriate indicator to predict which will be the future pollution levels and if the rate will go down when only have passed 2,4 half-lives of ^{137}Cs.

Keywords: Cuba, gamma spectrometry, marine sediments, radioactive pollution

1. Introduction

Marine sediments constitute radionuclides and toxic elements repository in aquatic ecosystems. For many years, sediment composition has been studied with the purpose of identifying the contamination zones and to research the anthropogenic causing sources. In addition, sediments studies help to predict the pollutant effects on the ecosystem and the possible risks that can bring for human health.

The geochemical cycle of these pollutants from urban areas is largely determined by how they interact or are trapped in the sediments. Sediments act as integrators and amplifiers of the chemical elements concentrations in waters and play an important role in estuary areas and shallow waters. So, this subject becomes an interesting and important factor to diagnose the environmental quality of marine ecosystems [1]. The isotope variation concentrations in sediments happens according to the deposition rate, particle sedimentation rate, nature and particle size, as well as the presence or absence of organic matter [2, 3]. However, it is important to mention that the sediments are considered contaminated when the concentration levels are above the established limits according to the region and the type of sediment. This chapter shows how radioactive contamination can be measured by radioactive detection of marine sediments. In this type of samples, an appreciable concentration of natural radioactive isotopes such as ^{40}K can be observed. Therefore, by comparing the fission product radioactivity of ^{137}Cs with natural radioactivity from ^{40}K, this magnitude can be evaluated, and the percentage of radioactive contamination in marine sediments can be obtained (*where R_1 and R_2 are the disintegrations per second of Cs-137 and K-40, respectively*) [4].

$$RCF = \frac{R_1(Cs-137) \times 100}{R_2(K-40)} \tag{1}$$

In Cuba, from the 1990s, research starts to take place in coastal ecosystems. Dating studies of ^{210}Pb in sediments were made in the bays of Havana and Cienfuegos and in the Sagua la Grande estuary. But in contrast to the international situation, studies of radionuclide contamination in marine sediments in Cuba are very few, because research has been conducted to the study of atmospheric artificial flows of radionuclides, as reports flow of ^{137}Cs in Cienfuegos between 1994 and 2002 [5, 6].
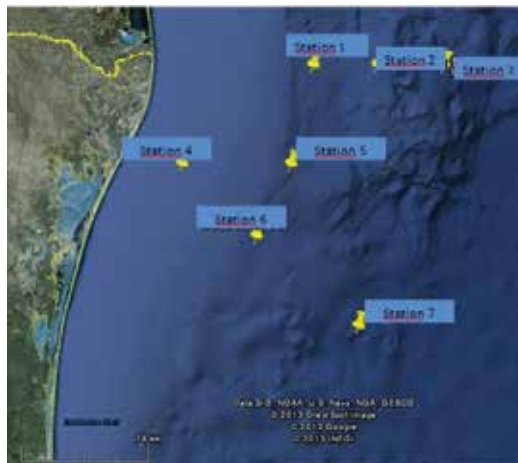
Figure 1. RCF values obtained by Navarrete et al. [4] (left). Location of the sampling sites in Mexico Gulf (right).

In 2014, minimal values of ^{137}Cs compared to natural radioactivity were found in Mexican sea waters. The researchers used Eq. (1) and estimated values of about 1% of contamination with [137]Cs. They also stated that the variations were due to the characteristics of the sample area, the sea currents and the depth of sampling. **Figure 1** shows the location of the study in Mexico Gulf [4]. So, by taking up samples of marine sediments along the occidental Cuban coasts and analyzing gamma spectrometry for the determination of gamma-emitting radioisotopes with energies between 60 and 2000 keV, it is possible to evaluate the radioactive contamination of this area.

2. Experimental

A fundamental question to be solved in sediment sampling is related to the choice of the sampling point. Logically, it is necessary that a point represents the zone conditions; however, given the unstable and seasonal character of the sedimentary deposit, especially in the case of shore sediments, this choice is not always simple and sometimes a point considered as representative for certain time, may cease to be so [7, 8].

To mitigate the possible lack of representativeness from given sample, it has been considered to take up one composite sample, being a topic of discussion the number of subsamples that must conform it. Sampling points are generally defined by their coordinates and depth, in this case, four key points were selected, two on the North coast and two on the South coast, both located in the Western part of the Cuban island.

Guanabo beach: a populated place that belongs to East Havana municipality in Havana province, located at 23.171° North latitude and −82.127° West longitude (in decimal degrees) (**Figure 2**).

Nautico beach: a populated place that belongs to Revolution square municipality, in Havana province, located at 23,097° North latitude and −82,451° West longitude (**Figure 3**).

Bibijagua beach: a populated place that belongs to Youth Island municipality, located at 21.889° North latitude and −82.727° West longitude (**Figure 4**).

Figure 2. North western coast location of Guanabo beach.

Batabano Gulf: a populated place located to the West south of the island capital, which belongs to Batabano municipality in Mayabeque province, located at 22.698° latitude and −82.293° longitude. It is the main coastal and fishing port on the southern coast of the Mayabeque province (**Figure 5**).

At sampling time, and for our purposes, it is sometimes best to analyze mixtures samples taken simultaneously, at different points, or as close as possible. This allows to evaluate the composition

Figure 3. North western coast location of Nautico beach.

Figure 4. South western coast location of Bibijagua beach.

Figure 5. South western coast location of Batabano gulf.

average of the marine sediments using a mixture of samples that represent several points. Sampling was carried out following one-star design; this method allows to obtain representative fractions of the place. Another important point is the instrument, which must be in accordance with the study that is to be carried out [8]. In this instance, the sampling was carried out at an approximately distance of 100 m from the coast and 1–1.5 m deep. Since this procedure allows the sediment surface layer sampling, the instruments are the simplest on the market. Therefore, the most appropriate would be the "picker type," which is the most affordable [8]. Samples were collected and stored in previously labeled flasks washed with distilled water.

2.1. Drying and sifting samples

For the samples drying, a conventional LAB-LINE Inc. oven was used. The sediments were dried for 3 days at 40°C until total dryness.

Subsequently, the samples were sieved in a 2000-μm sieve, to remove some remains of shells and stones that do not allow the correct Marinelli filling. Then, they were transferred to the containers and proceeded with the gamma measurement (**Figure 6**).

2.2. Gamma spectrometry analysis

The radioactive contaminants analysis of environmental samples has shown interesting results obtained both by the radiometric study of marine sediments samples from western Cuban coasts performed by Gamma Spectrometry with low background scintillation detector [NaI (Tl) crystal] as well as those obtained with one Hyperpure Germanium detector (HPGe).
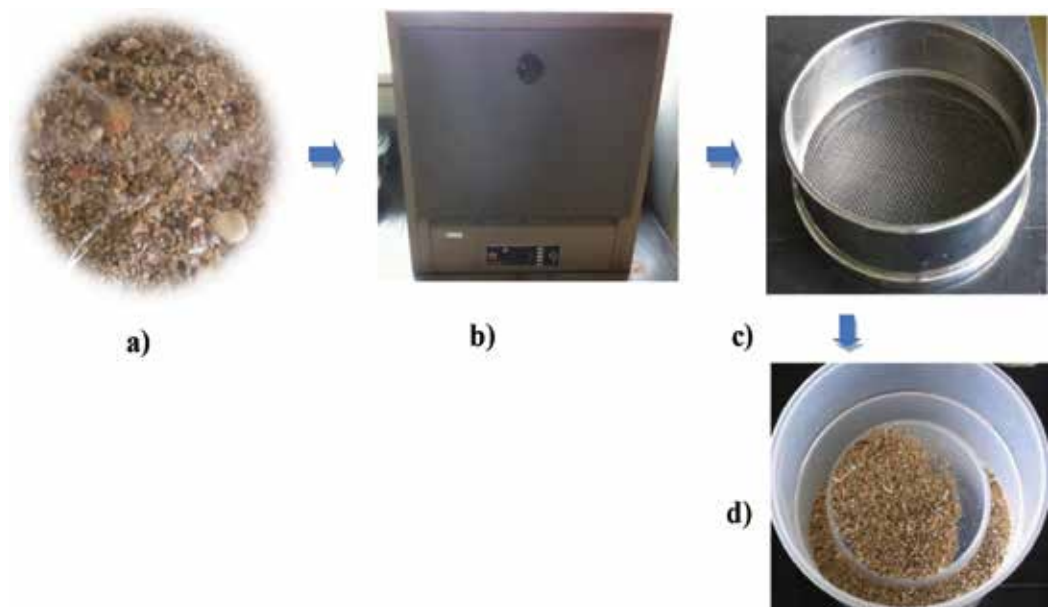
Figure 6. (a) Marine sediments, (b) drying oven, (c) 2000-μm sieve, and (d) Marinelli container.

2.2.1. Gamma spectrometry with low background scintillation detector NaI (Tl)

For scintillation system measurement, a sodium iodide scintillation equipment, Bicron 3 × 3 well Labtech brand with shielding lead distributed by Industrial and Medical Physicians S.A, was used. The results processing was done in the radioactive detection program *Maestro-32 Software Version 6.0 A65-B32 1997* distributed by ORTEC company.

A radionuclide homogeneous mixture also known as a standard certified sample (EG-ML 733-99 Isotope Products Laboratories, Burbank, CA, USA, 91504) was used for the equipment energies calibration. That is to say, an active sample containing a series of photon emitting nuclei with known activity and energy has been used. The positions (channel number) of each energy peak are determined accurately, and the efficiency is plotted as a function of the γ rays energy.

Besides, a known activity of KCl (Potassium Chloride Sigma P9541-500 g) prepared in the laboratory was used. The efficiency value for ^{40}K was 2.9% and for ^{137}Cs of 5.6%. It is important to note that the efficiency value depends on the sample geometry, size, density, and detector distance. For both detectors used in the gamma analysis, the efficiency varies significantly depending on these parameters. Therefore, each counting geometry requires an efficiency calibration, using a known standard sample, with the same geometry.

For the measurement, the samples must be dried, sieved, and weighed. They should be transferred to Marinelli containers (made of polypropylene with a cylindrical shape and an annular space to hold the sample), taking care not to exceed the filling mark and avoiding any areas with empty spaces that may affect the measurement. The detection time was 24 h.

In **Figure 7**, the system described to obtain the gamma spectra of a sample by scintillation is shown.

The spectrum allows to calculate the area under curve of the peak and therefore the net accounts value in 24 h (accounts/24 h). To obtain the counts per second (counts/seconds or cps), the obtained value in the spectrum corresponding to each selected peak area must be divided by the detection time, which in this case was 24 h (86,400 s).

Figure 7. Low background scintillation detector NaI (Tl), 325 Lab, D building, Faculty of Chemistry, UNAM.

Sample	Marinelli weight (g)	Sample weight (g)
Guanabo beach	135	561.1
Nautico beach	135	551.1
Bibijagua beach	136	558.2
Batabano gulf	138	552

Table 1. Each sample weights in the Marinelli container.

Finally, to obtain the disintegrations per second (dps = Bq), the obtained counts per second value must be divided by the detection efficiency determined for each radionuclide. That was previously determined with the certified references samples.

The activity in Bq/g, for each sample, is obtained by dividing the activity in Bq, between the weights of each sample in the Marinelli container. In **Table 1**, each sample weights are reported.

2.2.2. Gamma spectrometry with hyperpure germanium detector (HPGe)

The measurement procedure is similar. In this type of detector, there is a cryostat system that contains a double wall and a vacuum that guarantees thermal insulation. It also has an extension at the top where the detector is cooled with a liquefied gas, generally liquid nitrogen. Before performing the measurement, the liquid nitrogen system must be filled to ensure that it is at the proper working temperature.

For the HPGe detector, the energy calibration is performed using *Gamma Vision program* with radioactive sources of ^{241}Am (60 keV), ^{137}Cs (662 keV), ^{60}Co (1173, 1332 keV), and ^{40}K (1460 keV)) for 900 s (**Figure 11**).

The efficiency calibration is performed with a known specific activity of KCl standard sample (Potassium Chloride Sigma P9541-500 g). The detection efficiency for ^{40}K was 0.25% and for ^{137}Cs was 0.47%. These values are sensibly lower than those obtained with the scintillation

Figure 8. Hyperpure germanium detector (HPGe), ORTEC company. A-23 Lab, Physics Institute, UNAM.

detector. The spectra processing is performed in the Maestro-32 Software Version 6.0 program A65-B32 1997 distributed by the ORTEC company.

In this detector, each peak is better solved, which allows a better energy separation and makes it possible to analyze more complex samples, with more radionuclides and nearby energy values, which cannot be solved in scintillation detectors.

The system used can be seen in **Figure 8**. It has a high-voltage power supply, cryostat, preamplifier, amplifier, multi-channel analyzer (MCA), lead shield, and a computer (PC).

3. Results

The RCF values were calculated from the obtained counts in both detectors using the Eq. (1), and considering that the detection time was 24 h = 86,400 s. In **Tables 2** and **3**, the RCF values are reported with their respective experimental error and standard deviation. It is important to note that the considering activity for the calculation of the RCF must be in Bq/g, the sample grams were reported in **Table 1**.

The statistical percentages errors are reported in **Tables 2** and **3** and were calculated according to Eq. (2), also call, the standard deviation of the activity ratio of two radioactive sources [9, 10]:

$$\frac{a}{b} \pm \frac{x}{y}\left(\frac{1}{x}+\frac{1}{y}\right)^{1/2} \tag{2}$$

Sample	Disintegration per second ^{40}K	Disintegration per second ^{137}Cs	RCF %
Guanabo beach	14.1503	1.6110	11.4 ± 0.09
Nautico beach	8.3413	0.9403	11.3 ± 0.12
Bibijagua beach	11.5162	0.6097	5.3 ± 0.07
Batabano gulf	14.2130	0.7671	5.4 ± 0.06

Table 2. RCF values obtained with the NaI(Tl) detector from the North and South coast of Cuba.

Sample	Disintegration per second ^{40}K	Disintegration per second ^{137}Cs	RCF %
Guanabo beach	0.6091	0.0590	9.7 ± 0.42
Nautico beach	2.5806	0.2805	10.9 ± 0.22
Bibijagua beach	2.8206	0.1715	6.1 ± 0.15
Batabano gulf	3.0632	0.1785	5.8 ± 0.14

Table 3. RCF values obtained with the HPGe detector from the North and South coast of Cuba.

where a/b is the RCF value (%) in each case, x is the disintegration per second Cs-137, and y is the disintegration per second K-40.

If, in addition, the obtained RCF values for each sample in each detector are compared, several variations can be observed between them:

- For the North coast, the standard deviation is 3–15% between the two detectors. The standard deviation between both detectors of 15% in Guanabo beach and of 4% for Nautico Beach.

- In the South coast, the standard deviation is 6–13% between both detectors. The standard deviation between the two detectors was 13% in Bibijagua beach and 6% de Batabano Gulf.

These differences are expected because both detectors have several differences:

1. The detection efficiency is higher in the scintillation detector.

2. The radioactive backgrounds are different; the background is higher in the HPGe detector.

3. The peaks resolution is sensibly higher in the HPGe detector, each peak is better resolved.

Another interesting aspect that can be noticed is how the RCF values of the southern coast of the island differ from those obtained on the north coast. In all cases, the southern coast has lower RCF values than the north coast. This anomaly can be due to numerous events that they can go from the geological area characteristics and the sediment type, to the winds direction and the proximity to anthropogenic sources. **Figure 9** shows the spectrum obtained with the scintillation detector for Guanabo beach.

In *Maestro program*, it is possible to extract the information about the peaks: the FWHM (Full Width at Half Maximum), the Net and the Gross Area, the Real, Live and Dead Time with the "Peak Info" function, as shown in **Figure 10**.
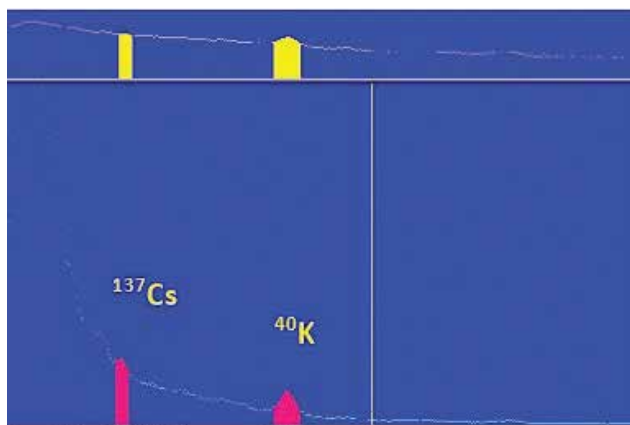
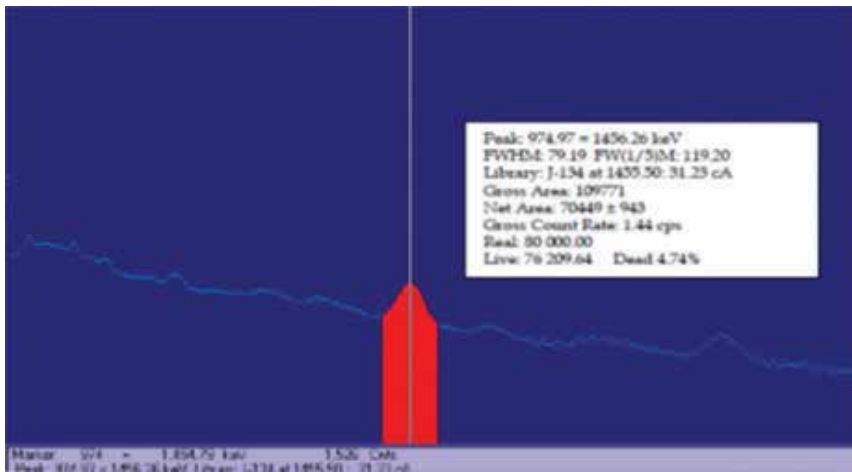**Figure 9.** Spectrum obtained with the scintillation detector for Guanabo beach.

Figure 10. Spectrum displays the peak information in Maestro program.

It is also interesting to compare the obtained RCF values in Cuba with those obtained in 2011 by Navarrete et al. in marine sediments sampling stations in the Gulf of Mexico. It can be noted that in Mexico, the highest value of RCF was 1.21%; while in Cuba, we found values up to 11% on the North coast [11–13]. **Figures 12** and **13** show the spectra obtained with the Hyperpure Germanium detector (HPGe).

Even though, these last values are not alarming because they constitute a minimum percentage of the natural radioactivity. Nevertheless, it is very interesting and exhorts us to extend this study to other geographical points to establish a global indicator of contamination of the Mexico Gulf and the Caribbean zone.

Now, the spectra obtained in the HPGe detector are shown for two marine sediment samples: one from the North (Guanabo beach) and one from the South coast (Batabano Gulf). The different peak resolutions can be noticed.
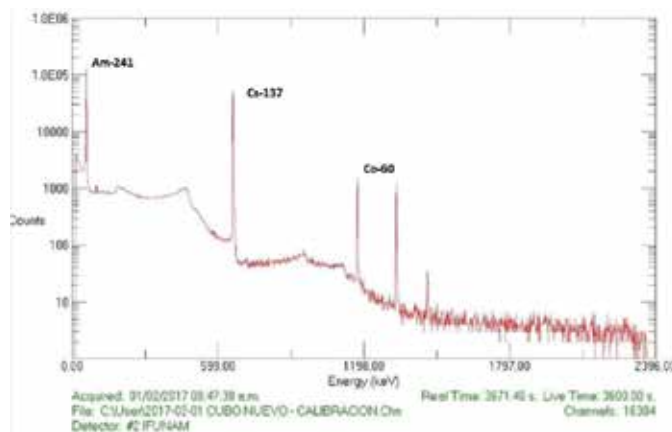

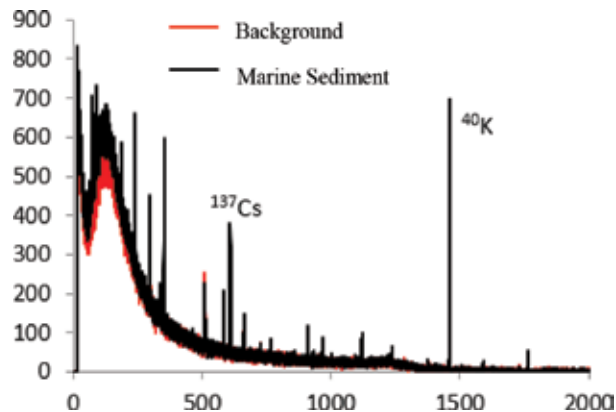**Figure 11.** Energy calibration spectra for the HPGe detector.

Figure 12. Obtained spectra from the North coast (Guanabo beach) in the HPGe detector.
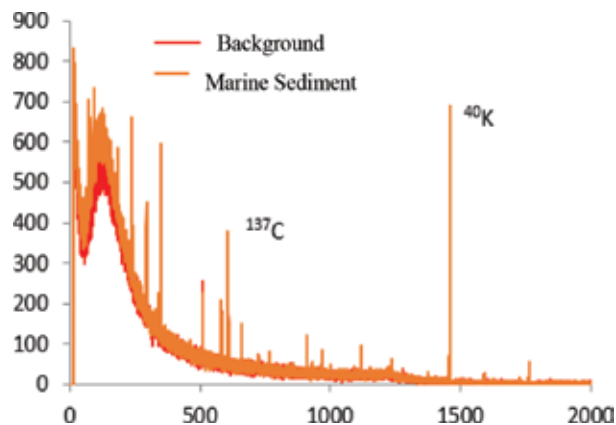

Figure 13. Obtained spectra from the South coast (Batabano gulf) in the HPGe detector.

Until now, it has been found that marine sediments are the fundamental repository of contaminants in aquatic ecosystems. The study of these materials is still necessary because if levels above sediment quality international standards are found [14], the quality of water, soils, and crops can be affected. The basic premise used to reduce the contaminants presence in waters, soils, and sediments is the constant monitoring of contaminated areas. This approach should include the long-term pollutants behavior, which is determined by the physic, chemical, and biochemical reactions in the system [15].

The obtained results for each Cuban sediment samples did not show alarming values or higher than those established, which make required remediation measures of the zone. It should be noted that for a better understanding of the radioisotopes concentrations metals in the sediments a deeper mineralogical and geochemical characterization of the sediments should be carried out.

For example, mass spectrometry methods are generally used to know the isotopic composition of an element, taking into account this premise it can be said that they could also be used

for the determination of radionuclides in a precise way, since it is possible to measure the atomic mass directly from each element (radioactive isotopes of the element).

In recent years, different articles have reported the use of mass spectrometry for the study of radionuclides with a long period of disintegration, obtaining satisfactory results [16, 17]. It is known that due to the nature of the radioactive decay, radiometric methods have a greater statistical variation in the results than those obtained by mass spectrometry. Therefore, a more precise study could be done with this attractive tool.

Finally, it is important to say that a study that allows the establishment of pollutants levels in sediments should be done frequently to regulate these levels, and thus to ensure the quality of the marine ecosystem.

4. Conclusions

1. Marine sediments are the main repository of radioactive contamination. In the Cuban sediments studied, the contents of ^{137}Cs and ^{40}K could be adequately calculated, showing that sediments are much more receptive and representative than the atmosphere and soils in the anthropogenic pollutants study.

2. The measurement of the ratio between the anthropogenic pollutant ^{137}Cs compared to the natural radionuclide ^{40}K in marine sediments (RCF) remains a suitable method for environmental radioactive contamination measuring.

3. The radioactive contamination factor (RCF) values obtained in each gamma detector, showed a 3–15% statistical variation between them.

4. It was found that there are remarkable differences in RCF values between marine sediments form the North coast and those on the South coast. The RCF values for the northern coast are higher than those obtained in samples taken on the southern coast of Cuba.

5. Comparing the RCF values of the Cuban marine sediments samples with the RCF values of the study carried out in 2011 Mexico Gulf, superior results were obtained in all cases, being approximately ten times higher the RCF values of the Cuban sediments.

Author details

Marisé García Batlle* and Juan Manuel Navarrete Tejero

*Address all correspondence to: mgarciabatlle@yahoo.com

Faculty of Chemistry, Inorganic and Nuclear Chemistry Department, National Autonomous University of Mexico, Mexico City, Mexico

References

[1] Huerta Díaz MA. Geochemistry of sediments. In: Iron Sulphides. 2006. http://www.ens.uabc.mx/iio/persogeo.htm (online course); Chapter 06

[2] Díaz Asencio M, Alonso-Hernández CM, Bolaños-Álvarez Y. One century sedimentary record of Hg and Pb pollution in the Sagua estuary (Cuba) derived from ^{210}Pb and ^{137}Cs chronology. Marine. Sciences. 2009;**40**(4):321-337

[3] Burton GA, Landrum PF. Toxicity of sediments. In: Middleton GV, Church MJ, Corigilo M, Hardie LA, Longstaffe FJ, editors. Encyclopedia of Sediments and Sedimentary Rocks. Dordrecht: Kluwer Academic Publishers; 2003. pp. 748-751

[4] Navarrete M, Zúñiga M, Espinosa G, Golzarri J. Radioactive contamination factor (RCF) obtained by comparing contaminant radioactivity (^{137}Cs) with natural radioactivity (^{40}K) in marine sediments taken up from Mexican sea waters. World Journal of Nuclear Science and Technology. 2014;**4**:158-162

[5] Alonso-Hernández CM, Cartas Águila H, Díaz-Asencio M, Muñoz-Caravaca A, Martín-Pérez J, Sibello Hernández R. Atmospheric deposition of ^{137}Cs between 1994 and 2002 at Cienfuegos, Cuba. Journal of Environmental Radioactivity. 2006;**88**(2):199-204

[6] Gelen A, Díaz O, Simón MJ, Herrera E, Soto J, Gómez J, Ródenas C, Beltrán J, Ramírez M. ^{210}Pb dating of sediments from Havana Bay. Journal of Radioanalytical and Nuclear Chemistry. 2003;**256**(3):561-564

[7] Allen BG Jr, Baudo R, Beltrami M, Rowland C. Assessing sediment contamination using six toxicity assays. Journal of Limnology. 2001;**60**(2):263-267

[8] Water quality — Sampling — Part 2: Guidance on sampling techniques. 1991. ISO 5667-2:1991

[9] Navarrete Tejero JM, Cabrera L. Introduction to the Study of Radioisotopes. Faculty of Chemistry, UNAM, 1993

[10] Maheshwar S, Madhuri S. Nuclear Chemistry. Vol. 1. Ane Books India/CRC Press; 2009. p. 173

[11] Navarrete JM, Müller G. Natural radioactivity and radioactive contamination in sea water. In: Radioactive Contamination Research Developments, Nova Science Pub., 2010;**8**:270-274

[12] Navarrete JM, Espinosa G, Müller G, Golzarri JI, Zúñiga Camacho M. Marine sediments as a radioactive pollution repository in the world. Journal of Radioanalytical and Nuclear Chemistry. 2013;**299**:843-847

[13] Navarrete JM, Müller G, Golzarri JI, Espinosa G. Establishment of a radioactive contamination index in seawater from the Gulf and Pacific coasts in Mexico. International Journal of Environment and Health. 2011;**5**:318-323

[14] Calmano W. Sediment quality assessment: Chemical and biological approaches. In: En Calmano W, Förstner U, editors. Sediments and Toxic Substances. Germany: Springer-Verlag; 1996. pp. 17-35

[15] Environmental Protection Agency. Water Quality Assessment: A Screening Procedure for Toxic and Conventional Pollutants in Surface and Ground Water—Part I and II. 1985. EPA/600/6-85/002a

[16] Becker JS, Dietze H-J. Determination of long-lived radionuclides by double focusing sector field ICP mass spectrometry. Advances in Mass Spectrometry. 1998;**14**:681-689

[17] Becker JS. Recent developments in isotope analysis by advanced mass spectrometric techniques. Plenary lecture. Journal of Analytical Atomic Spectrometry. 2005;**20**:1173-1184

Edited by Ata Amini

The lack of knowledge about sedimentation processes taking place in a watershed or a waterbody hinders practical progress in addressing problem-solving. To assist the reader in putting sediment quantity and quality issues into perspective, sedimentation engineering features the most state-of-the-art contributions from a number of researchers working in the fields of water resources and soil erosion. The book contains 10 chapters selected among a great number of submitted manuscripts. The main topics are sedimentation processes in marshes, harbor estuaries, gulf, hydraulic turbine, and volcanic area. Sediment contamination and few other topics are included as well. The case studies cover a sequence for integrated solutions where watershed management and sedimentation engineering are not decoupled. This book on sedimentation engineering is designed for researchers and professionals and for course use in environmental science.

IntechOpen